Ultrafast diffusion-ordered NMR analysis of mixtures

Ludmilla Guduff

université PARIS-SACLAY

NNT : 2018SACLS239

Ultrafast diffusion-ordered NMR analysis of mixtures

Thèse de doctorat de l'Université Paris-Saclay
préparée à l'Université Paris-Sud

École doctorale n°571 Sciences chimiques : molécules, matériaux, instrumentation et biosystèmes (2MIB)
Spécialité de doctorat: chimie

Thèse présentée et soutenue à Gif-sur-Yvette, le 11 septembre 2018, par

Ludmilla GUDUFF

Composition du Jury :

Philippe Lesot Directeur de recherche, CNRS	Président
Mathias Nilsson Associate professor, University of Manchester	Rapporteur
Bénédicte Elena-Herrmann Ingénieur de recherche, CNRS	Rapporteur
Sabine Bouguet-Bonnet Professeur des Universités, Université de Lorraine	Examinateur
Jean-Nicolas Dumez Chargé de recherche, CNRS	Directeur de thèse
Carine van Heijenoort Directeur de recherche, CNRS	Co-Directeur de thèse

Thèse de doctorat

Acknowledgments

Le travail présenté dans cette thèse a été effectué au sein du département de biologie et chimie structurale et analytique de l'ICSN à Gif-sur-Yvette. Je tiens à remercier le directeur de l'équipe RMN, Éric Guittet, dont la succession a été prise par Carine van Heijenoort, pour m'avoir accueilli dans le laboratoire.

Je souhaite ensuite remercier tous les membres de mon jury de thèse, dont particulièrement les professeurs Mathias Nilsson et Bénédicte Elena-Herrmann pour avoir accepté d'être rapporteurs de ce manuscrit. Un grand merci également à Philippe Lesot qui a suivi mon travail de près durant ces deux dernières années.

J'adresse un immense merci à Carine van Heijenoort et Jean-Nicolas Dumez, mes deux directeurs de thèse, sans qui tout ce travail n'aurait pas été possible. Merci à toi Jean-Nicolas pour ta gentillesse, ta grande disponibilité et surtout ta patience durant ces trois années. Tu as pris le temps de me réexpliquer toute la RMN, quitte à revoir les choses avec moi au moins dix fois jusqu'à ce que je comprenne, et j'ai énormément appris grâce à toi. Merci à toi Carine pour tes conseils et pour m'avoir recentrée sur mon projet à chaque fois que j'en avais besoin. Merci à tous les deux de m'avoir fait découvrir le monde de la recherche et de m'avoir donné l'opportunité de m'investir dans ce projet passionnant pendant lequel je n'ai pas eu le temps de m'ennuyer. Merci pour ces trois années qui ont été riche tant du point de vue scientifique que relationnel car au-delà du travail mené ensemble, on a bien rigolé que ce soit lors d'une bataille de boule de neige ou autour d'un verre au Val Fleury. Je n'aurai jamais cru être capable d'accomplir un tel travail et grâce à vous j'ai repoussé mes limites. Je vous dois beaucoup car vous m'avez fait confiance et énormément soutenu.

Je tiens à saluer l'ensemble des personnes de l'équipe que je j'ai eu plaisir à côtoyer quotidiennement. Merci à toi Alda pour ta bonne humeur, ta gentillesse et pour tous les bons moments qu'on a partagés que ce soit à la pause-café ou aux divers évènements organisés à l'ICSN. La bonne humeur et la bonne ambiance lors de ces moments ont également et garantis par la présence de Guillaume Loire, David, Véronique, Nelly, Christina, Nelly, François Bontems, François Giraud, Nadine, Annie, Ewen, Jean-François, Louise, Christophe, Claire-Marie, Camille, Corentin, Ghanem et Maria. Guillaume ; merci de m'avoir fait rigoler avec tes blagues et autres jeux de mots aussi inattendus les uns que les autres. Tu es venu plusieurs fois à mon secours (au secours de tout l'ICSN même !) pour résoudre mes soucis informatiques avec l'aide de ton acolyte David qui lui aussi à pas mal de bonnes blagues en réserve. Le concert d'Iron Maiden avec toi et Estelle était trop génial, je suis contente qu'on ait partagé ce moment. Merci à toi Véro pour ton côté pétillant et ta spontanéité, Nelly pour ta gentillesse, ta générosité et ta bienveillance, Christina pour ton rire communicatif et tes conseils, Nadine pour ta

gentillesse et l'attention dont tu as fait preuve à mon égard, François Bontems pour tes discussions très instructives allant de la science à la philosophie en passant par le dernier bon film sorti au cinéma; François Giraud pour m'avoir montré à faire les remplissage des spectros avec l'aide Nelly, pour ta convivialité et ta sympathie, Annie pour ta gentillesse également et tout ce que tu fais pour assurer la préparation du labo, Ewen pour m'avoir aidé à résoudre certains problèmes dans mes manipes ainsi que pour ton humour et Jean-François pour ta sympathie, tes conseils, ton aide au spectro et surtout pour m'avoir aider à faire les portrait et photos de l'équipe grâce à tes talents de photographe. Merci également à Naïma, Éric Jacquet que j'ai eu le plaisir de rencontrer ; à Louise pour ta générosité et ton grand cœur (team thé au café !), Christophe pour ta sympathie, Claire-Marie pour ta joie de vivre et ta positive attitude (you pop girl !), Camille parce tu distribue plein de câlin et pour ton franc parlé, Corentin pour ta grande gentillesse et ta bienveillance, Ghanem pour le travail qu'on a mené ensemble et pour m'avoir débloqué plus d'une fois quand j'en avais besoin ainsi que Maria pour tes conseils et ton optimisme.

Évidement la liste ne s'arrête pas là, il y a bien entendu tous les autres doctorants, post-doc et autres personnes qui ne sont plus forcément dans l'équipe mais également celles qui viennent d'arriver et que j'ai eu la chance de côtoyer à un moment donné durant ces trois ans. Merci à Arthur, Séverine, Nelsson, Safa, Marion, Seindé, Orianne Frances, Timothée, Hans, Glwadys, Ying-hui, Marie, Prishila, Anaïs, Luíza et Ndèye pour tous les instants de franche camaraderie que l'on a passé ensemble entre Arthur qui a inspiré a tous une vive sympathie, Nelsson et ses délicieux gâteaux ou encore Timothée et son franc parlé.

Je tiens également à remercier plusieurs personnes de l'ICSN notamment les étudiants et post-doc que j'ai pu rencontrer en étant au CEI et avec qui j'ai pu lier des liens d'amitié. Merci à Florent, Coralie, Gwendal et Augustin pour tous ce que l'on a partagé en étant au CEI. Merci à Julien et ses shots de sambuca, Romain pour m'avoir appris à ouvrir une bière au briquet, Alaric qui a fait sensation en Joker, Big RoRo, Charles, Valentin, Simon, Tanya, Morgane, Laure, Julie, Ali, Mélissa, Eddy, Rémy, Orianne Brel -tu m'as fait rêver à la soirée jeux ou tu t'es prise pour une œuvre d'art avec des cornflakes, Charlotte Leman-Loubière, Pauline, Morane, Mathieu, Agathe, Gwenaëlle, Guillaume Levitre, Charlotte Juillet, Laurent Laboureur, Eugénie, Yannis et Vincent notre picard national ! Un grand merci également à Alain, Laurent, Benjamin, Cécile et Sandy pour les moments de convivialité qu'on a partagé, et surtout à Philippe pour les vendredis au n°12, pour m'avoir fait apprécier le rugby et pour les blagues de l'Echo (c'est qui BOB ?).

Mes remerciements vont également aux équipes des différents laboratoires avec lesquels j'ai eu plaisir à collaborer notamment à Patrick et Gaspard du CEA, Ilya de l'université de Southampton, Geoffrey Bodenhausen, Daniel et Dennis de l'ENS. Merci à vous tous pour avoir partagé votre savoir avec moi et pour m'avoir accueillie chaleureusement dans vos équipes respectives.

Je tiens à remercier chaleureusement Valérie Fortuna responsable de la MISS, qui gère un projet formidable visant à faire partager la science aux enfants ; ce projet étant parrainé par Jamy Gourmaud

(oui oui LE Jamy de c'est pas sorcier !) et Wendelin Werner détenteur d'une médaille Fields. Merci de m'avoir donné la chance de m'investir dans un tel projet et surtout un grand merci pour ta disponibilité, ta bonne humeur et surtout la passion dont tu fais preuve et que tu nous as communiquée à moi et aux autres doctorants de la MISS. Je tiens également à tous les remercier en particulier Mickael, Kelly, Sébastien, Coralie, Sylvain, Amicie, Francesco, Ajmal, Raphaëlle, Vincent et Timothée avec qui j'ai co-encadré plusieurs ateliers dans la joie et la bonne humeur. Ces ateliers sont certes intenses mais tellement gratifiant ; ce n'est pas tous les jours qu'on a la chance d'aller enregistrer les oiseaux, écrire en cunéiforme sur de l'argile et piloter des robots ! Merci à Nicolas Graner, Séverine Martrenchard, Élisabeth Delbecq et Sylvie Sikora qui s'investissent dans ce projet quotidiennement et qui contribuent grandement à son bon déroulé et à son développement. Et puis merci à tous les enfants que j'ai pu rencontrer pendant les deux ans où j'ai participé à la MISS, leur joie, leur spontanéité, leurs petits mots ou encore les bonbons en guise de remerciements pour avoir apprécié l'atelier sont des petites attentions qui m'ont beaucoup touchées.

Merci également à toute ma famille et mes amis pour leur soutien indéfectible et leurs encouragements durant ces trois ans. Je n'y serai jamais arrivé s'ils n'avaient pas été là pour moi en particulier mes parents et mes deux sœurs. Merci à tous mes amis pour tous les super moments qu'on a vécus et pour tout ceux à venir. Mention spéciale à Alex', Vincent, Gugu, Gaby, Paul et surtout Géromine parce que vous avez toujours été présents même si moi je n'étais pas forcément disponible, merci de m'avoir encouragé, remonté le moral quand j'avais besoin et d'avoir cru en moi.

Et pour terminer, je tiens à exprimer ma plus grande gratitude à Augustin, mon pilier qui a été là à chaque instant et qui m'a donné tout le courage dont j'avais besoin pour aller jusqu'au bout de ma thèse.

"All we have to decide is what to do with the time that is given us.- Gandalf"

J.R.R Tolkien, The Fellowship of the Ring

Résumé de la thèse

Introduction

L'identification et la caractérisation des espèces moléculaires sont au cœur de la chimie. Bien que les techniques séparatives comme la chromatographie soient toujours mises en avant quand il s'agit d'analyse de mélanges, les méthodes de résonance magnétique nucléaire (RMN) sont également directement applicables avec pour objectif une séparation des composés du mélange étudié. Cet outil a la particularité d'être non destructif et surtout aucune étape préparatoire type dérivatisation n'est requise. Son utilisation pour des applications dans les domaines tels que la chimie, la biologie ou la pharmacie a confirmé son efficacité vis-à-vis de l'analyse de mélanges.

Plusieurs schémas d'expériences de type uni- ou multi-dimensionnelles sont disponibles. Grâce aux informations obtenues sur l'environnement chimique des noyaux (déplacements chimiques, couplages) et aux propriétés de relaxation ou de diffusion, les spectres RMN des mélanges peuvent être simplifiés. Nous avons choisi d'utiliser les propriétés diffusionnelle des molécules afin de séparer les spectres RMN des molécules contenues dans un mélange. La méthode DOSY (diffusion-ordered spectroscopy) exploite ces propriétés et peut être considérée comme une forme de chromatographie virtuelle. La DOSY peut être utilisée en combinaison avec des expériences 1D et 2D pour donner respectivement des expériences 2D et 3D en raison de la dimension de diffusion qui est créée par incrémentation d'un paramètre, l'aire de gradients de champ pulsés. Ceux si sont utilisés afin de pondérer le signal par la diffusion. Les méthodes multidimensionnelles requièrent de longues durées d'acquisition, jusqu'à plusieurs dizaines d'heures pour les 3D et ceci constitue un frein à l'utilisation généralisée de la DOSY pour l'analyse de mélanges. La DOSY souffre également d'un manque de sensibilité propre à la spectroscopie de RMN de manière générale.

Pour satisfaire les besoins actuels en termes d'analyse de mélanges, la DOSY se doit d'être plus rapide et plus sensible. De nouvelles stratégies visant à réduire la durée des expériences et à augmenter leur sensibilité ont émergé et peuvent être appliquées à la DOSY. On se propose donc d'exploiter ces méthodes dans le but de créer un outil inédit d'analyse de mélanges.

Plusieurs stratégies de réduction de la durée des expériences multidimensionnelles existent et nous avons choisi d'utiliser le codage spatial de la diffusion afin d'obtenir des données de 2D DOSY en moins de 1 s. Cette méthode, plus connue sous l'appellation « RMN ultrarapide », a fait ses preuves pour le suivi de réactions chimiques ou bien l'analyse métabolomique. Généralisable à plusieurs types d'expériences, elle a permis d'accélérer la COSY, la TOCSY ou encore l'HSQC.

De même, plusieurs stratégies pour amplifier le signal RMN de plusieurs ordres de grandeur ont été développées. Ces méthodes d'hyperpolarisation permettent d'étudier des échantillons peu concentrés et les signaux obtenus sont caractérisés par des durées de vie très courtes (quelques dizaines de minutes).

Dans le cas de la DOSY ces méthodes d'accélération ont été très peu utilisées mais ont tout de même montré des résultats prometteurs. Le but de ce projet est de combiner les méthodes de RMN diffusionnelle, les méthodes ultrarapides et les méthodes d'hyperpolarisation, ce qui devraient marquer une avancée significative dans le domaine de l'analyse des mélanges avec des applications pour le suivi de réaction et l'analyse de produits naturels.

Le premier axe de ce projet est centré sur le développement de méthodes de 2D DOSY rapide. Dans un deuxième temps, ces méthodes développées ont été complètement caractérisées, optimisées et étendues à la 3D. De même, des expériences de DOSY rapide qui réduisent l'effet de la convection ont été créées. La partie finale du projet est consacrée au couplage avec les méthodes d'hyperpolarisation : la polarisation dynamique nucléaire (DNP) d'une part et le SABRE (signal amplification by reversible exchange) d'autre part.

La spectroscopie RMN, un outil non destructif pour l'analyse de mélanges

Les sciences chimiques dépendent fortement de la caractérisation et de l'identification des espèces moléculaires par des méthodes analytiques. Que ce soit en recherche des produits naturels, en chimie de synthèse ou en métabolomique, l'obtention des produits purs avant de procéder à l'analyse en tant que telle est souvent considérée comme un prérequis. Pour ce qui est de l'analyse des mélanges complexes, les techniques séparatives comme la chromatographie sont devenues des méthodes incontournables afin de séparer un échantillon en ses différents éléments constitutifs. Cependant, cette étape est longue et fastidieuse et peut conduire à la dégradation des composés.

Un autre outil qui mérite une attention particulière pour l'analyse de mélanges est la spectroscopie de résonance magnétique nucléaire (RMN). Cet outil offre une grande quantité d'informations notamment sur la structure, les interactions et la dynamique des molécules. La RMN possède, en outre, des avantages qui la rendent particulièrement attractive pour l'analyse de mélanges. En effet, c'est une méthode non destructrice et qui convient pour tout type de molécules peu importe leur nature. Elle ne nécessite aucune étape préalable de type dérivatisation ou pré-concentration. Les résultats fournis par cette technique sont hautement reproductibles bien qu'un manque de résolution soit observé quand un trop grand nombre de composés est présent dans le mélange. Sa sensibilité est aussi limitée, comparée à celle de la spectrométrie de masse par exemple.

De nombreux travaux ont été effectués pour tirer parti de la RMN dans le but de caractériser les mélanges avec des applications en chimie, biologie, pharmacie, agroalimentaire ou encore en environnement. Plusieurs types d'expériences RMN existent afin d'extraire des spectres des

informations variées. Les expériences les plus simples sont les expériences 1D qui sont rapides et permettent d'obtenir des informations sur l'environnement chimique d'un noyau grâce aux déplacements chimiques, et aux couplages. Les noyaux les plus couramment observés sont les protons ^{1}H et les carbones ^{13}C. Cependant avec les méthodes 1D, pour peu que le nombre de signaux soit important, le risque de recouvrement limite sévèrement l'identification des différents composés. De façon à réduire ces recouvrements, les propriétés de relaxation, de diffusion translationnelle ou encore les couplages peuvent être utilisés pour 'filtrer' certains signaux. A titre d'exemple, les filtres type relaxation permettent de supprimer les signaux des grosses molécules tandis que les filtres de diffusion visent à supprimer les signaux des petites molécules.

Pour des spectres extrêmement encombrés, la solution est d'augmenter la dimensionnalité de l'expérience à 2 ou 3. Les signaux seront alors dispersés dans un domaine/une carte plus grande ce qui facilite leur identification. Les expériences multidimensionnelles peuvent être homonucléaires c'est-à-dire qu'elles corrèlent des noyaux identiques (^{1}H-^{1}H par exemple), hétéronucléaires c'est-à-dire qu'elles corrèlent des noyaux différents (^{1}H-^{13}C par exemple). La combinaison de ces méthodes multidimensionnelles avec les filtres type relaxation, couplage ou diffusion donne lieu à un riche panel d'expériences afin de simplifier les spectres RMN de mélanges complexes.

Comme les dimensions supplémentaires sont générées via incrémentation d'un paramètre, une expérience 2D va nécessiter plusieurs dizaines de minutes et une 3D plusieurs heures dans le cas d'un mélange concentré (~100 mM). Cette durée augmente avec la diminution de la concentration de l'échantillon. Ceci constitue le défaut majeur des expériences multidimensionnelles, ce qui tend à restreindre leur champ d'application. Le deuxième principal frein est la faible sensibilité inhérente à la RMN du fait qu'une infime fraction des spins nucléaire sont observables (par exemple, à 18.7 T et 300 K, cette fraction est d'environ 0.006 %).

Parmi les méthodes de simplification de spectre existantes, celle qui fait l'objet de ce projet de thèse est la diffusion, appelée méthode DOSY (Diffusion-Ordered SpectroscopY). Cette expérience peut être vue comme une forme de chromatographie virtuelle où les composés sont séparés sur la base de leurs coefficients de diffusion. Cette expérience qui existe depuis le milieu des années 90 a conduit à de nombreuses applications dans divers domaines de la recherche et présente un fort potentiel pour des applications innovantes sur des mélanges complexes tels que les fluides biologiques ou les produits naturels. Pour relever ce challenge d'analyse de mélanges complexes et étendre le champ d'application de la DOSY, celle-ci se doit d'être plus sensible et plus rapide. De nouvelles stratégies ont donc émergé et seront présentées dans le cas de la DOSY appliquée à l'analyse de mélange de petites molécules.

Méthodes de RMN diffusionnelle (DOSY) pour la séparation spectrale de mélanges de petites molécules

La méthode DOSY permet de trier les spectres des molécules d'un mélange en fonction de leur coefficient de diffusion. En effet, les molécules en solution sont animées d'un mouvement de diffusion translationnelle - ou mouvement Brownien- perpétuel. Celui-ci est lié à la taille et la forme des molécules mais aussi à la température et à la viscosité du solvant. Le coefficient de diffusion d'une molécule est donné par la relation de Stokes–Einstein qui fait intervenir les paramètres cités précédemment. De manière générale, les molécules de haut poids moléculaire vont diffuser plus lentement que les molécules présentant un faible poids moléculaire. Avec la DOSY, il est possible de séparer des coefficients de diffusion avec une résolution de l'ordre de 1 % .

Lors d'une expérience DOSY, les spins nucléaires vont être soumis à des gradients de champ magnétique de façon à atténuer l'intensité du signal de façon contrôlée lors de l'acquisition. De manière générale les expériences de RMN sont effectuées dans un champ magnétique statique homogène. L'application d'un gradient de champ durant une courte durée (quelques ms), qui est une variation linéaire du champ magnétique, va casser cette homogénéité et induire une perte de signal. L'utilisation de gradients d'intensité croissante au cours du temps- de 8 à 16 incréments- va entrainer une atténuation exponentielle du signal qui obéit à l'équation de Stejskal-Tanner. C'est à partir de cette équation que sont calculés les coefficients de diffusion.

Plusieurs types d'expériences de diffusion existent : d'une part, les expériences dérivés des échos de spins (SE) qui utilisent une excitation de 90° suivie de deux gradients de champ séparés par une impulsion 180°, d'autre part, les expériences dérivées des échos de spins stimulés (STE) dans lesquelles le 180° est remplacé par deux impulsions 90°. La particularité du STE est de réduire de 50% le signal observé. Cependant, cette option est favorisée par rapport à la première car elle limite les effets du couplage J et de la relaxation transverse lors du délai de diffusion. Ceux-ci induisent une perte additionnelle de signal pouvant conduire à une valeur erronée du coefficient de diffusion.

Une fois les données DOSY enregistrées, la carte DOSY peut être reconstruite à partir des valeurs de coefficient de diffusion (D) calculées. Cette carte représente les valeurs de déplacement chimique dans une dimension et les valeurs de coefficient de diffusion dans l'autre dimension dans le cas d'une expérience 2D. Si c'est une 3D, une dimension de déplacement chimique supplémentaire sera observée. Les signaux d'une même molécule seront donc alignés en face du coefficient de diffusion associé.

La qualité d'un spectre DOSY dépend fortement de la résolution car les recouvrements peuvent donner lieu à des valeurs de coefficients de diffusion erronées. D'autres facteurs comme les courants de Foucault, générés par des variations brusques et répétées de champ magnétique, peuvent entrainer des distorsions des spectres, des artéfacts qui peuvent ruiner une expérience. Les gradients de températures

ont également un effet dévastateur sur la mesure de coefficients de diffusion car ils génèrent un flux convectif, ce qui entraine une atténuation brutale du signal et des oscillation visibles sur la courbe de diffusion. Les coefficients de diffusion sont donc surestimés.

Plusieurs stratégies sont utilisées pour réduire ces effets indésirables comme l'addition de délais supplémentaires pour laisser les courants de Foucault retomber, l'utilisation de tubes de diamètres réduits, la rotation de l'échantillon, etc. Le choix des paramètres et des expériences doit se faire de façon minutieuse de manière à garantir la qualité des résultats pour une identification optimale des composés d'un mélange.

Stratégies d'accélération de l'expérience RMN DOSY

La méthode DOSY utilise des gradients de champ incrémentés au cours du temps de façon à générer des courbes d'atténuation du signal qui donnent accès aux coefficients de diffusion des molécules. De 8 à 16 incréments sont nécessaires ce qui induit des temps d'expérience longs pouvant empêcher de suivre l'évolution d'échantillons non stables au cours du temps. Plusieurs stratégies ont été employées pour tenter de réduire le temps d'acquisition des données DOSY. Celles-ci sont divisées en plusieurs catégories en fonction du type de codage utilisé.

La première stratégie fait appel à de multiples gradients pour enregistrer une série d'échos en un seul scan. La seconde stratégie fait appel à de multiples impulsions radio-fréquence (RF) combinées à un gradient de champ constant pour générer de multiples échos. La troisième stratégie fait appel au codage spatial de la diffusion en utilisant une combinaison de gradients de champ et d'impulsions balayées en fréquence qui permet une acquisition en parallèle de tous les incréments de gradients en un seul scan. D'autres alternatives sont de réduire le cyclage de phase, le délai entre scans consécutifs ou encore le nombre d'incréments en réalisant un échantillonnage partiel.

Parmi toutes ces stratégies, la troisième qui repose sur le codage spatial de la diffusion a été choisie afin d'accélérer nos expériences DOSY. En effet, les deux premières approches n'ont pas vraiment été appliquées à des mélanges et, au vu de la littérature, ont été abandonnées en raison de leur forte sensibilité au mouvement macroscopique, du manque de sensibilité du fait de l'utilisation de petits angles d'excitation, des défauts de refocalisation du signal et de l'atténuation supplémentaire due à la relaxation transverse. L'utilisation du codage spatial pour la DOSY a donné des résultats très prometteurs selon le travail de Frydman et Keeler qui sera la base de nos travaux. De manière générale, le codage spatial a fait ses preuves en matière d'accélération d'expériences diverses et variées comme la COSY, la TOCSY ou encore l'HSQC, ce qui a donné lieu à de nombreuses application en métabolomique par exemple. Cette approche semble être généralisable à tout type de séquences et je propose donc de le faire avec la DOSY, sachant que de très bons résultats ont été obtenus sans pour autant être exploités en profondeur pour l'analyse de mélange. Ces expériences sont également sensibles

à la convection et présentent une sensibilité et une résolution réduite comparée à la DOSY classique. Le gain de temps a un prix mais, pour des échantillons concentrés, le fait d'avoir une DOSY-2D en moins d'une seconde au lieu de plusieurs minute serait un avantage non négligeable. Il faut également trouver une solution au problème de sensibilité.

Augmentation de la sensibilité en RMN par des méthodes d'hyperpolarisation

Nous avons vu que la RMN de manière générale est une méthode très peu sensible en raison de la faible fraction de spins nucléaires observable, régie par la distribution de Boltzmann (polarisation de l'ordre de 10^{-5} dans des conditions standards). Traditionnellement, si on veut augmenter la sensibilité de notre expérience, on peut augmenter la concentration de l'échantillon, utiliser des molécules marquées notamment lorsque l'on étudie un noyau autre que le proton, utiliser un champ magnétique plus élevé, baisser la température mais cela n'est pas toujours possible ni pertinent. D'autres 'astuces' existent comme l'utilisation de sondes cryogéniques (cryoprobes) pour augmenter le rapport signal sur bruit (SNR), la réduction de la taille de l'échantillon, l'augmentation du nombre de scans, l'utilisation de séquence d'impulsion type INEPT, l'amélioration de l'homogénéité (shims) et de manière globale le développement instrumental et le traitement des données. Toutes ces méthodes sont utilisées en synergie et ont permis d'augmenter la sensibilité de la RMN au fil du temps. Cependant, certaines méthodes sont onéreuses, les développements prennent du temps et le gain obtenu n'est finalement pas considérable.

D'autres approches visent à augmenter le taux de polarisation jusqu'à 1 en déplaçant les populations des états de spins loin de l'équilibre thermique. On peut citer les méthodes type "Brute Force", pompage optique, polarisation induite par le para-hydrogène et sa variante SABRE ou la polarisation dynamique nucléaire (DNP). Nous nous sommes particulièrement intéressés à la DNP et au SABRE.

Avec la méthode DNP, une augmentation du signal jusqu'à un facteur 10 000 peut être obtenue. Cette stratégie repose sur le transfert de la polarisation d'électrons d'un agent polarisant, un radical paramagnétique, vers le noyau d'intérêt. Ce transfert se fait via le couplage dipolaire et est déclenché par des irradiations microondes à très basse température (1.2 K). L'échantillon est ensuite solubilisé, et transféré dans un spectromètre RMN pour pouvoir effectuer les expériences de RMN du liquide. Dans l'état liquide, le signal amplifié a une durée de vie qui dépend du temps de relaxation longitudinal T_1 du noyau. Ce T_1 est de l'ordre de 5 s pour le proton, et de 30 s pour le carbone. Cette durée pour le retour à l'équilibre du signal limite actuellement l'utilisation de la méthode à des expériences de RMN 1D. C'est également une méthode destructrice car l'échantillon ne peut être polarisé qu'une seule fois, et ne peut pas être récupéré à la fin de l'expérience.

La méthode SABRE (**S**ignal **A**mplification by **R**eversible **E**xchange) quant à elle est une méthode de polarisation réversible qui permet de polariser des substrats via le para-hydrogène.

L'hydrogène existe sous deux formes, ortho et para, et la forme para est obtenue à basse température via un catalyseur paramagnétique. C'est une source de polarisation qui peut être transférée à un substrat via le couplage scalaire J, ce qui implique que le para-hydrogène et le substrat doivent faire partie du même édifice moléculaire. Ces deux composés peuvent être associés avec un catalyseur métallique de façon à former un intermédiaire temporaire. Le transfert de polarisation se fait spontanément du para-hydrogène vers le substrat dans un champ magnétique de l'ordre de 70 G. Le signal amplifié dépend aussi du temps de relaxation longitudinal du noyau et une augmentation d'environ 300 fois le signal à l'équilibre thermique peut être obtenue. Cette méthode est limitée car seuls des composés aromatiques contenant de l'azote ont pu de nos jours être polarisés de cette manière.

Le SABRE est une option peu onéreuse comparée à la DNP mais ces deux méthodes ont été utilisées avec succès pour l'analyse de mélanges. Le problème des deux méthodes, même si les protocoles sont totalement différents, est qu'elles induisent des mouvements macroscopiques de liquide, qui perturbent fortement l'expérience DOSY. Nous sommes face au défi de mesurer des coefficients de diffusion en milieu convectif, sur un signal hyperpolarisé dont la durée de vie varie de 5 s à 1 min. La méthode ultrarapide est indispensable pour pouvoir faire une expérience 2D sur ce type de signal.

Approche pratique de la RMN DOSY ultrarapide

Plusieurs stratégies d'accélération de l'expérience DOSY ont été présentées précédemment et nous avons fait le choix de d'utiliser celle qui fait appel au codage spatial de la diffusion de façon à pouvoir enregistrer des spectres DOSY en moins de 1 s. Notre étude repose sur les travaux de Keeler et Frydman qui ont mis à profit l'utilisation du codage spatial pour la DOSY mais qui ont proposé deux approches, de type imagerie spectroscopique, afin de pouvoir décoder l'information de diffusion (lors de l'acquisition). L'objectif de cette étude est de développer une méthode rapide de séparation spectrale et d'explorer l'option du codage spatial pour des méthode RMN qui font intervenir une pondération du signal par la diffusion.

Nous savons que l'information liée au mouvement translationnel des molécules est obtenue grâce à l'utilisation de gradients de champ magnétique. Dans la version classique de la DOSY, la dimension de diffusion est générée via incrémentation de l'aire de ces gradients de champs pour induire une atténuation de l'intensité des spectres. Dans la version ultrarapide de la DOSY, le schéma classique de codage de la diffusion est modifié de sorte que l'aire des gradients dépende de la position et que l'information de diffusion soit encodée le long de l'échantillon. Cela implique que les spins localisés à différentes positions de l'échantillon vont être soumis à des valeurs d'aire de gradients différentes. De manière générale, l'échantillon peut être considéré comme divisé en plusieurs sous-ensembles, chacun étant associé à une valeur d'aire de gradient différente qui va croitre d'une extrémité à l'autre de l'échantillon. Les gradients de la version classique ont été remplacés par une combinaison de gradient

de champ et d'impulsion balayées en fréquences de sorte que l'excitation des spins se fasse de façon séquentielle le long de l'échantillon. Dans la version de Keeler, le maximum d'intensité (correspondant à l'aire de gradient minimale) est localisé à l'extrémité de l'échantillon tandis que dans la version de Frydman, celui-ci est centré sur l'échantillon. Pour notre séquence optimisée, nous avons choisi de positionner le maximum d'intensité à une extrémité de l'échantillon de façon à ce que la courbe de diffusion soit observée sur toute la région de l'échantillon observée (10 mm) et non pas la moitié.

Une autre question qui se pose est celle de la sélection de cohérence qui va permettre de sélectionner la partie du signal qui va contribuer au spectre final. Les expériences de DOSY classiques font appel à un cyclage de phase ce qui requière d'effectuer au minimum 8 scans par incrément de gradient. Ceci peut être évité par l'utilisation de gradients de sélection de cohérence de façon à ne réaliser qu'un seul scan par incrément de gradient. C'est le cas dans l'expérience Oneshot qui cependant réalise la sélection de cohérence et la pondération par la diffusion sur un unique axe de gradient z. Nous avons choisi de séparer les gradients suivant des axes orthogonaux (x et y pour la sélection de cohérence et z pour la pondération par la diffusion) ce qui permet d'éviter des compensations accidentelles des gradients entre eux et les gradients de sélections de cohérence n'ont pas besoin d'être pris en compte lors du calcul des coefficients de diffusion.

En ce qui concerne le choix du type d'acquisition, deux options sont possibles. La première repose sur l'utilisation d'un gradient de faible intensité (< 1 % de la valeur maximale) durant l'acquisition d'un spectre 1D, ce qui va donner lieu à un élargissement des signaux de ce spectre. Ces signaux élargis sont en fait des images de l'échantillon observé et elles sont centrées au niveau des déplacements chimiques correspondants. Cette stratégie qui encode l'information de déplacement chimique et de diffusion suivant la même dimension pose vite un problème de résolution car l'élargissement des signaux peut conduire à des recouvrements si de nombreuses résonances sont présentes dans le spectre.

La deuxième stratégie d'acquisition repose sur l'utilisation d'un train de gradients bipolaires de façon à générer une dimension spatiale en plus de la dimension spectroscopique. La dimension spatiale est obtenue par un gradient de lecture tandis que la dimension spectrale est générée par les N paires de gradients bipolaires. Après réarrangement des données et transformation de Fourier, les données forment un ensemble à deux dimensions dont l'une correspond à la dimension spectroscopique et l'autre la dimension spatiale. Les images de l'échantillon sont localisées au niveau des déplacements chimiques correspondants. L'intensité des gradients d'acquisition est de l'ordre de 20 à 60% de l'intensité maximale ce qui permet d'avoir des profils de diffusion moins déformés, notamment à cause de la multiplicité. De plus le risque de recouvrement est moindre comparée à la méthode précédente. Les résultats obtenus avec l'une ou l'autre des méthodes d'acquisition ont montré que l'option qui utilise des gradients bipolaires donne des valeurs de diffusion plus proches de celle de la DOSY conventionnelle.

Les caractéristiques des profils de diffusion ont été améliorées grâce à une normalisation par un profile de référence (l'effet de la diffusion étant négligeable dans ce cas-là) mais aussi grâce à une observation d'une région de 10 mm d'échantillon au lieu des 15 mm habituels ce qui permet de minimiser l'effet de la non-linéarité des gradients. La comparaison à la DOSY conventionnelle et l'évaluation des deux options d'acquisition de façon qualitative en termes de précision des coefficients de diffusion calculés, de résolution et de traitement nous ont permis d'implémenter une version de la SPEN DOSY optimisée. La séquence optimisée sera décrite plus en détails dans la section 8.

Simulations numériques et RMN spatio-temporelle

La suite de l'étude des propriétés de la SPEN DOSY s'est faite via l'utilisation de simulations numériques grâce à l'outil Spinach qui est un logiciel libre (écrit en MATLAB) principalement développé par le Dr. Ilya Kuprov. Cet outil permet d'étudier la dynamique des spins pour un ensemble varié de systèmes de spin et d'interactions. Il a la particularité de gérer simultanément les variables de spin et de diffusion en s'appuyant sur le formalisme de Fokker-Plank; ce qui permet de décrire les expériences de codage spatial de la diffusion avec exactitude. L'expérience de SPEN DOSY présentée précédemment a été simulée avec Spinach pour étudier le comportement d'un système de spins ^{1}H. Avant d'entamer la simulation, les paramètres de codage, d'acquisition, de spin, de discrétisation de l'échantillon et de diffusion ont été définis. Le résultat de la simulation est un FID qui peux être traité comme on le ferait pour une vraie expérience et les coefficients de diffusion ont été déterminés avec les mêmes fonctions d'ajustement.

Pour s'assurer que le résultat obtenu à la fin de la simulation a un réel sens physique, la première étape a été de vérifier la convergence des résultats. En effet, la dimension spatiale est décrite de manière discrète et les opérateurs utilisés dans la simulation peuvent être calculés avec exactitude par des matrices de Fourier ou bien approximés par la méthode des différences finies. La première méthode requière un temps de calcul long (36 min) contrairement à la deuxième qui nécessite moins de 2 min. Comme nous avons choisi d'utiliser la méthode des différences finies, nous devions nous assurer d'une part, que le critère spatial de Nyquist est respecté pour que les hélices créées durant le codage spatial soient bien décrites et d'autre part, que l'approximation donne un coefficient de diffusion précis, associé à un phénomène de diffusion correctement reproduit. La convergence a été obtenue pour une grille de 3000 points, des conditions aux limites périodiques et un maillage d'ordre 7. Les résultats obtenus sont comparables à ceux obtenus avec des matrices de Fourier.

Les effets des différents paramètres de codage et d'acquisition ont ensuite été étudiés pour évaluer leur effet sur le profil de diffusion. La simulation retourne des résultats attendus pour différentes valeurs d'atténuation et le gradient d'acquisition, s'il est trop faible, peut induire une distorsion du profil. Ces modifications n'ont pas d'effets indésirables sur la simulation qui est exempte de bruit, cependant

dans les expériences réelles cela peut être un problème ; notamment dans le cas du gradient d'acquisition où on est fortement limité par l'appareillage. De même, les modèles utilisés pour l'ajustement des données ont été corrigés et optimisés de façon à comprendre et réduire les erreurs systématiques sur les valeurs de coefficient de diffusion calculées. Nous avons mis en évidence que l'effet du déplacement chimique lors de l'acquisition ainsi que la durée des gradients pendant le délai de diffusion devaient être pris en compte pour obtenir un coefficient de diffusion précis. L'utilité du profil de référence a également été confirmée. Ces simulations numériques nous ont de manière générale permis d'optimiser notre modèle d'ajustement et de le corriger des erreurs potentielles qui induisent un biais sur les valeurs de coefficients de diffusion déterminées. Cet outil offre également des perspectives en termes de création de nouvelles séquences, d'étude du phénomène de convection par exemple ou encore d'étude de système de spins couplés

Méthodes avancées de RMN DOSY ultrarapide

Cette section présente plus en détails l'expérience de SPEN DOSY de même que son optimisation dans le but de réduire les erreurs systématiques sur les résultats et d'augmenter la gamme d'échantillon que l'on peut étudier. Des variantes de la SPEN DOSY basées sur des échos de spin au lieu d'échos stimulés ont été implantées et une optimisation des paramètres d'acquisition et de codage a été proposée pour obtenir des courbes de diffusion de meilleure qualité.

Nous avons ensuite montré qu'il est possible de créer une expérience tridimensionnelle de diffusion qui peut être enregistrée dans le temps d'une 2D grâce à la méthode du codage spatial. En effet, lorsque que le nombre de composés, et donc de signaux, à séparer augmente il peut être avantageux d'augmenter la dimensionnalité de l'expérience de façon à pouvoir disperser les signaux dans un plus grand domaine. Ces expériences nécessitent cependant plusieurs heures d'acquisition. Nous avons donc choisi d'accélérer l'expérience de 3D DOSY-COSY en intégrant notre séquence SPEN DOSY dans une COSY. Cette expérience peut être exécutée en 12 min au lieu de 14 h sur notre échantillon.

Nous savons que la DOSY est sensible à de nombreux facteurs expérimentaux (convection, courants de Foucault, gradient non-linéaires) ce qui peut altérer la qualité des résultats. Nous nous sommes attaqués au problème de la convection qui peut se produire dans l'échantillon à cause de gradients de température indésirables. Celle-ci induit des oscillations des courbes de diffusion ainsi qu'une atténuation supplémentaire du signal ce qui entraine généralement une surestimation des coefficients de diffusion. La solution que nous avons proposée et adaptée à la SPEN DOSY est couramment utilisée en DOSY classique et consiste à effectuer un codage de la diffusion en deux temps de manière à supprimer la composante due au flux convectif.

Un autre axe d'amélioration sur lequel nous avons travaillé est l'augmentation de la résolution car cela peu impacter la séparation des signaux. En effet, la largeur spectrale accessible dans les

expériences ultrarapides (< 5 ppm) est réduite comparée à celle accessible en RMN conventionnelle (> 10 ppm). Cela entraine que les résonances qui se trouvent hors de la fenêtre spectrale observée vont être repliées dans ladite fenêtre (par translation d'un multiple de la largeur spectrale) et vont se superposer aux signaux déjà présents. Le repliement peut être contrôlé et anticipé mais cela devient très compliqué lorsqu'un nombre trop important de résonances est présent dans le spectre. Pour éviter ce repliement, la première stratégie est d'utiliser une sélection spectrale de manière à sélectionner uniquement les résonances que l'on souhaite observer ; l'autre stratégie est d'entrelacer les spectres mais nous ne l'avons pas utilisée car elle produit des artéfacts qui peuvent compliquer la lecture de la carte DOSY. Pour terminer, toujours dans le but d'augmenter la résolution, nous avons proposé une méthode de traitement des données dans la dimension spectrale pour obtenir des spectres en absorption.

Toutes ces améliorations ont permis de rendre la SPEN DOSY applicable pour des projets de type suivi de réaction in-situ ou l'étude de mélanges hyperpolarisés.

Application de la SPEN DOSY pour les mélanges hyperpolarisés via la méthode D-DNP

La polarisation dynamique nucléaire (DNP) permet de dépasser les limites en termes de sensibilité de la RMN. En effet une amplification du signal jusqu'à un facteur 10 000 est possible. Cependant ce type de signal amplifié a une durée de vie limitée de quelques dizaines de secondes qui va dépendre du temps de relaxation longitudinal (T_1) du noyaux observé (ici ^{1}H et ^{13}C). L'utilisation de méthodes multidimensionnelles ultrarapides telles que la SPEN DOSY pour enregistrer ce type de signaux dans le temps imparti s'impose. Nous avons donc démontré que l'expérience de SPEN DOSY permet d'acquérir des données DOSY sur des échantillons hyperpolarisés.

Dans un premier temps, nous avons essayé d'obtenir des résultats en protons mais sans succès. En effet, le T_1 du signal proton hyperpolarisé est de l'ordre de 5 secondes. Sachant que la durée de transfert, à partir de la dissolution, du polariseur vers le spectromètre RMN est de au moins 6 s, nous n'avons pas réussi à enregistrer de spectre car la quasi-totalité du signal avait disparu. Pour des applications qui visent à suivre un processus qui évolue dans le temps ce n'est vraiment pas l'idéal. Nous avons tout de même appris, grâce a des expériences de dissolution sur un échantillon concentré sans étape de polarisation, que de toutes façons l'acquisition de séries de données DOSY ne donne pas des résultats stables d'une expérience SPEN DOSY à l'autre.

De là, s'en sont suivie plusieurs étapes d'optimisation de façon à améliorer la répétabilité des résultats (et la reproductibilité) mais aussi afin de préserver au maximum le signal amplifié pour pouvoir réaliser une série de SPEN DOSY. Pour ce faire nous avons décidé de polariser le ^{13}C au lieu du ^{1}H car son T_1 est de l'ordre de 30 s pour les carbones quaternaires. Cela laisse une fenêtre de l'ordre de 1 min pour enregistrer plusieurs SPEN DOSY (chaque SPEN DOSY ayant un temps d'acquisition de moins de 1s). Pour réaliser un échantillonnage multiple de l'aimantation, l'expérience de SPEN DOSY décrite

précédemment a été modifiée en un double écho de spin adiabatique avec une excitation petit angle (30°). L'usage de la version précédente basée sur un écho stimulé (STE) ne permet pas une utilisation d'un petit angle d'excitation car cette séquence utilise deux impulsions 90° centrales qui vont exciter toute l'aimantation au milieu de l'expérience.

Les problèmes de répétabilité et reproductibilité ont été identifiés comme étant dues à la convection qui est importance notamment en raison du mode de transfert de l'échantillon. L'utilisation d'une séquence qui compense la convection a permis d'obtenir des résultats stables d'une SPEN DOSY à l'autre. Jusqu'à 5 expériences ont pu être enregistrées post-dissolution sur un échantillon modèle et le gain à l'arrivée au spectromètre était de 5550. Avec un système de transfert plus efficace et une optimisation des délais de pré-acquisition nous pourrions avoir de meilleurs taux d'hyperpolarisation et réaliser plus de SPEN DOSY sur des échantillons de concentration de l'ordre du millimolaire voir moins.

Ce couplage innovant entre D-DNP et SPEN DOSY réalisé en collaboration avec l'équipe de Geoffrey Bodenhausen à l'École Normale Supérieure (ENS), en particulier avec Dennis Kurzbach et Daniel Abergel, a permis de d'établir des bases solides sur l'acquisition de données SPEN DOSY hyperpolarisées et ouvre la voix à des applications sur des mélanges peu concentrés qui évoluent dans le temps.

Application de la SPEN DOSY pour les mélanges hyperpolarisés via la méthode SABRE

En parallèle du travail sur la D-DNP présenté dans la partie précédente, nous avons étudié une autre méthode d'hyperpolarisation combinée à la SPEN DOSY. La méthode SABRE (Signal Amplification by Reversible Exchange) permet via le parahydrogène et un catalyseur métallique (ici l'iridium) d'obtenir une augmentation du signal d'un ou plusieurs substrat(s) d'un facteur allant jusqu'à 1000, par rapport au signal que l'on a normalement à l'équilibre thermique. Le gain est certes moindre par rapport à la DNP mais cette méthode est peu couteuse et facile à mettre en œuvre. De plus le même échantillon peut être hyperpolarisé plusieurs fois consécutives, ce qui n'est pas le cas avec la DNP. Cette méthode est moins 'universelle' que la DNP dans le sens où elle s'applique majoritairement à des molécules contenant des cycles aromatiques azotés bien que cette méthode tende à se généraliser pour étudier des amines, amides, acides carboxylique, alcools, phosphates, ou autres carbonates.

Nous avons démontré qu'il est possible d'obtenir des données de type SPEN DOSY sur des proton hyperpolarisés par SABRE. Comme cette expérience requière le secouage de l'échantillon contenant le catalyseur et les substrats en solution ainsi que le parahydrogène en phase gazeuse, nous avons dans un premier temps cherché à évaluer l'effet de ce secouage sur les coefficients de diffusion mesurés. Nous avons vu que cette expérience est particulièrement sensible à la convection et de manière plus générale à tout mouvement autre de celui Brownien des molécules. En secouant l'échantillon juste

avant l'acquisition, on joue un peu avec le feu. Le signal hyperpolarisé dépend du T_1 des protons qui est de 5 s ; ce qui veut dire que, entre le moment où l'échantillon est secoué et introduit dans le spectromètre, nous avons 5 s pour enregistrer la SPEN DOSY sur un échantillon qui n'a pas le temps de 'reposer'. Nous avons constaté, sur des échantillons concentrés modèles non hyperpolarisés, que dans ses conditions les coefficients de diffusion étaient trop élevés par rapport à la valeur de référence et que la séparation était compromise. Il faut attendre au moins 15 s avant acquisition pour revenir à des valeurs qui ne fluctuent plus, ce qui n'est pas envisageable dans notre cas.

Des tentatives de compensation de convection similaires à ce qui avaient été mis en place dans le cas de la DNP ont été testées mais sans grand succès. Nous avons donc changé de stratégie et procédé à une pondération par la diffusion dans le plan transverse de l'échantillon et non selon l'axe vertical de celui-ci (ce qui est la façon classique de procéder). Cette fois nous avons enfin réussi à obtenir plusieurs SPEN DOSY hyperpolarisées sur un mélange peu concentré de petites molécules. Nous avons également attesté de la répétabilité de ces expériences. Le gain obtenu est compris de 90 à 250 en fonction des substrats ce qui permet correspond aux gains relevés dans la littérature et ce qui correspond au gain maximal attendu avec notre protocole. Des tentatives pour diminuer la concentration de notre mélange sont cependant restées infructueuses. L'utilisation d'un système en flux permettrait d'élargir l'application de cet outil que nous avons mis en place en collaboration avec Gaspard Huber and Patrick Berthault au Commissariat à l'Énergie atomique et aux Énergies alternatives (CEA) à Saclay.

Conclusions et perspectives

Durant ce projet, nous avons montré que le codage spatial de la diffusion dans l'expérience DOSY permet d'obtenir un outil rapide pour la séparation de spectres 2D et 3D en fonction des coefficients de diffusion des molécules d'un mélange. La première partie du projet a donnée lieu à une séquence optimisée de 2D DOSY rapide ainsi que la création d'une nouvelle séquence de 3D DOSY rapide. Sur un échantillon modèle, nous avons pu enregistrer des données 2D DOSY en 98 ms (contrairement à 17 min en DOSY classique) et des données 3D DOSY en 12 min (contrairement à 14 h en DOSY classique). La séparation des molécules est comparable à celle obtenue en DOSY conventionnelle même si une baisse de résolution, que ce soit en dimension spectrale ou diffusionnelle, ainsi qu'une baisse de sensibilité et de précision sont à déplorer.

Le volet simulation numérique nous a permis de caractériser plus en profondeur notre séquence 2D SPEN DOSY et surtout grâce à cet outil, nous avons pu identifier des sources de biais des coefficients de diffusion calculés et les corriger. Spinach est un élément incontournable dans notre démarche d'amélioration et d'extension du panel d'expérience de SPEN DOSY telles que les expériences convection compensées. Pour aller plus loin nous pourrions envisager d'effectuer ces simulations en

présence de bruit pour mieux décrire les expériences réelles de façon à reproduire les problèmes auxquels nous avons été confrontés (notamment le problème de sensibilité).

Les expériences de 2D SPEN DOSY ont été couplées avec succès avec la méthode DNP et aussi avec la méthode SABRE. La première méthode a permis d'obtenir des séries de SPEN DOSY ^{13}C sur un mélange hyperpolarisé (20 mM) et la deuxième à permis d'obtenir des série SPEN DOSY ^{1}H sur un mélange hyperpolarisé (5 mM). Il faut savoir que la limite en termes de concentration est de 20 mM à l'équilibre thermique pour obtenir des données SPEN DOSY exploitables. Les gains sont respectivement d'un facteur 400 et 4 pour les deux méthodes. Le défi principal de ces méthodes est la convection induite lors du processus d'hyperpolarisation. Dans le premier cas une séquence qui compense la convection a permis d'obtenir des coefficients de diffusion stables d'une expérience à l'autre. Cette stratégie n'a pas fonctionné pour le SABRE et un codage spatial de la diffusion dans le plan transverse de l'échantillon a permis de régler les problèmes de convection.

Les outils DNP-SPEN DOSY et SABRE-SPEN DOSY mis en place offrent un potentiel certain pour l'analyse de mélanges de petites molécules peu concentrés et pour l'extension du champ d'application de la DOSY. Des concentrations inférieures au millimolaire pourraient être atteintes en utilisant des systèmes d'injection plus rapides dans le cas de la DNP ou des systèmes en flux dans le cas du SABRE. De tels systèmes existent et sont en constante amélioration ce qui laisse à penser que dans les années à venir de telles applications pourraient se généraliser. Nous n'avions pas encore de tels systèmes à notre disposition mais nous avons tout de même pu réaliser des développements méthodologiques très prometteurs. Les développements de séquences que nous avons proposés sont d'ailleurs utilisables sans étape de polarisation préalable et ont débouchés sur des projets de suivi de réactions au laboratoire. Nous espérons pouvoir appliquer ces méthodes d'analyse sur des échantillons complexes type produits naturels ou des problématiques d'interactions moléculaires.

Content

Notations and abbreviations

^{13}C	Carbon
^{15}N	Nitrogen
1D	One-dimensional
^{1}H	Proton
2D	Two-dimensional
^{31}P	Phorsphorus
3D	Three-dimensional
ADSE	Adiabatic Double Spin Echo
ALTADENA	Adiabatic Longitudinal Transport After Dissociation Engenders Net Alignment
ASE	Adiabatic Spin Echo
B_0	Main magnetic field
BEST	Band-selective Excitation Short-Transient
BPPSTE	Bipolar Pulse Pair Stimulated Echo
BW	BandWidth
COD	Cyclooctadiene
COSY	Correlation Ordered SpectroscopY
CP	Cross-Polarization
CPMG	Carr–Purcell–Meiboom–Gill
CSV	Coefficient Standard de Variation
CT	Constant-Time
CTP	Coherence Transfert Pathway
D	Diffusion coeffcient
D-DNP	Dissolution- Dynamic Nuclear Polarization
DANTE	Delays Alternating with Nutations for Tailored Excitation
DOSY	Diffusion-Ordered SpectroscpY
DQF	Double Quantum Filtered
DSTE	Double Stimulated Echo
EPSI	Echo-Planar Spectrocopic Imaging
FAMOUS	Fast Multi-Spin-Echo Diffusion Sequences
FID	Free induction
FOV	Field Of View
FT	Fourier Transformation
GNAT	General NMR Analysis Toolbox

HMBC	Heteronuclear Multiple Bond Coherence
HMQC	Heteronuclear Multiple Quantum Coherence
HSQC	Heteronuclear Single Quantum Coherence
HTS	High Throughput Screening
iDOSY	Internal Diffusion-Orderred SpectroscopY
IMes	1,3-bis(2,4,6-trimethylphenyl)imidazole-2-ylidene
INEPT	Insensitive Nuclei Enhanced by Polarization Transfer
ITAMED	Iterative Thresholding Algorithm for Multiexponential Decay
J-Res	J-Resolved
LED	Longitudinal Eddy current Delay
MAD	Matrix-Assisted DOSY
MMME	Multiple Modulation Multiple Echoes
MRI	Magnetic Resonance Imaging
ND	Multi-Dimensional
NMR	Nuclear Magnetic Resonance
NE	Non-Echoed
NOE	Nuclear Overhauser Effect
p-H_2	Para-Hydrogen
p-jres	Projected-J-Resolved
PASADENA	Parahydrogen And Synthesis Allow Dramatically Enhanced Nuclear Alignment
PCy_3	Tricyclohexyl phosphine,
PFG	Pulsed Field Gradient
PGMSE	Pulsed field-gradient multiple spin-echo
PHIP	Para-Hydrogen-Induced Polarization
RF	Radio Frequency
SABRE	Signal Amplification by Reversible Exchange
SE	Spin Echo
SEOP	Spin-Exchange Optical Pumping
SNR	Signal to Noise Ratio
SPEN	SPatially ENcoded
STE	STimulated Echo
T_1	Longitudinal relaxation time
T_2	Transverse relaxation time
TEMPOL	4-hydroxy-2,2,6,6-tetramethylpiperidin-1-oxyl
TOCSY	TOtal Correlation SpectroscopY

UF	UltraFast
WGA	Weak Gradient Acquisition

1. Introduction

The identification and characterization of molecular species lie at the core of chemical science, whether for natural product research or chemical synthesis [1–3]. Separative techniques such as chromatography have become a staple method when it comes to addressing one of the main concerns of chemists: retrieving the pure individual compounds of a mixture. Still, this is a tedious and long task that can lead to degradation and the loss of certain compounds.

A worthwhile tool that has demonstrated its effectiveness toward mixture analysis is nuclear magnetic resonance (NMR) spectroscopy, even though it is primarily regarded as an essential and powerful tool for structural elucidation [4–7]. As a non-destructive method that does not require any previous separation step or any derivatization and, in addition, that offers highly reproducible results, NMR spectroscopy possesses undeniable assets to address the challenge of mixture analysis. Many applications in the field of chemistry, biology, pharmacy, food and environment have taken advantages of NMR for this purpose [8–15]. A variety of schemes have been reported to unravel the spectra of mixtures, going from simple 1D experiments to more intricate multidimensional experiments [16]; They rely on information on the chemical environment of nuclei such as proton ^{1}H, carbon ^{13}C, nitrogen ^{15}N or phosphorus ^{31}P and also exploit relaxation, diffusion and coupling properties in order to simplify the NMR spectrum of a mixture [4,17–23].

Among the existing methods to separate the NMR spectra of components within mixtures, diffusion-ordered spectroscopy (DOSY) experiments are commonly used [24–27]. This method is considered as a form of virtual chromatography and the spectra of each compound are sorted according to diffusion coefficient values. Pulsed field gradients (PFG) are used to measure molecular displacement that affect the detected signal by attenuating it. DOSY data are generated via incrementation of the gradient area over time so that the detected signal is made dependent on both the gradient strength and the diffusion rate. Each spectrum generated for one gradient level is attenuated to some extent and each species will have its own decay rate. Monoexponential fitting of decaying signals yields the associated diffusion coefficient and resonances can be sorted according to these values. DOSY is commonly applicable for 1D or 2D experiments leading to pseudo-2D or pseudo-3D experiment because of the use of an incremented gradient area to create the additional diffusion dimension [28–31]. This will result in significant lengthening of the experiment but this is mandatory when the mixture contains a large number of compounds leading to a decreased resolution that complicate the identification of signals. This experiment is known since the mid 90s and DOSY has led to applications in many areas of research, and it still has a large potential for further developments and applications [29,32–34]. However, the lack of sensitivity of this method along with its duration that increases with the dimensionality of the experiment – which is also true for all multidimensional NMR experiments in general – are obstacles to its use in some important cases. To meet the current needs of complex mixture characterization and

expand its range of application, DOSY NMR must be faster and more sensitive. Overall, new innovative strategies have emerged to overcome the limitations regarding speed and sensitivity of multidimensional methods and they will be exploited in combination with diffusion NMR methods in order to create novel tools.

Attempts to reduce the duration of the DOSY experiment have resulted in several strategies that differ by their diffusion encoding strategies [35]. Some of them are meant to reduce the number of required scans to one, based on multiple gradients pulses, on multiple RF pulses, and on spatial encoding. Others, even if they require multiple scans, provide significant reduction of the duration of DOSY experiments through reduced sampling or reduced delay between scans [36][37]. The spatial encoding strategy was chosen to carry out this project. Indeed, a dramatic acceleration of multidimensional (ND) NMR experiments may be obtained with the so-called "ultrafast NMR" (UF NMR) approach, which replaces the sequential acquisition of sub-experiments by a parallel acquisition in different parts of the sample [38]. The potential of UF NMR has been demonstrated for metabolomics analysis or real-time processes monitoring [39]. Many experiments such as COSY, TOCSY or HSQC have benefited of this acceleration strategy which appear to possess a general scope of application [40]. In the case of the DOSY experiment, promising results were obtained but its full potentiality has not been fully exploited yet for mixture analysis [41,42]. Unfortunately, this gain in terms of time comes at the expense of sensitivity which is significantly reduced.

Generally speaking, NMR spectroscopy possesses a low sensitivity due to the small fraction of nuclear spins that are observable. Traditional means to increase sensitivity consist in increasing the sample concentration, using labelled compounds, going to a higher magnetic field or decreasing the temperature; which is not always possible or meaningful [43]. All of these methods used together lead to significant improvement in sensitivity but still the polarization level remains quite low as it obeys to Boltzman distribution. Solutions aiming to increase polarization level close to 1 are found in the realm of hyperpolarization. These techniques provide a considerable signal enhancement of several orders of magnitude compared to thermal equilibrium experiments. One can cite approaches such as Brute Force hyperpolarization, spin-exchange optical pumping (SEOP), polarization induced by para-hydrogen and its SABRE (Signal amplification by reversible exchange) version or dynamic nuclear polarization (DNP). The combination of conventional diffusion-based method with advanced techniques such as ultrafast NMR and hyperpolarisation should mark a significant progress for complex mixtures analysis and this particular coupling has not been fully investigated yet. Multidimensional spatially encoded (SPEN) DOSY NMR coupled with hyperpolarisation techniques would be of great interest in the case where the studied mixtures are not stable over time and could eventually find applications for real-time reaction monitoring and analysis of natural products.

In the first part of this project, we focused on the development of fast multidimensional diffusion-based NMR methods in order to separate the pure spectra of compounds within a mixture. Two types of spatially encoded DOSY experiments were studied as preliminary steps of the overall

project. Reproducing these existing sequences and performing the associated data analysis allowed us to fully understand their properties and the underlying theoretical considerations. Both approaches are similar considering the fact that they use a spatial encoding block to encode diffusion. These strategies differ from one another by their acquisition block inspired from spectroscopic imaging scheme. Indeed, the first approach is characterised by signal acquisition under a weak read gradient whereas the other one uses a train of bipolar gradient pulses. An improved sequence of SPEN DOSY was designed embedding in a distinct way all the advantageous features identified to get optimum results.

The second line of the project was dedicated to the optimization in order to reduce systematic errors and also for addressing limitations of SPEN DOSY. Since the quality of the DOSY data are sensitive to many experimental factors, we have proposed a solution to reduce the effect of one of them, sample convection, that tends to cause an overestimation of diffusion coefficients. To address the limitations of SPEN DOSY for crowded spectra, a higher dimensionality DOSY experiment that can be recorded in the time of a classic 2D DOSY was designed. The issue of resolution, caused by a reduced spectral width in spatially encoded experiments, was also addressed using spectral selection and pure-absorption spectral processing. Numerical simulations using the Spinach library [44], in partnership with Ilya Kuprov at University of Southampton, were made as well to improve the accuracy of the diffusion coefficient measured. The description of our SPEN-DOSY experiment was fully investigated in terms of convergence, effect of the parameters, effect of flow and model adjustment. All these improvements led to a SPEN DOSY experiment that was applicable to chemical reaction monitoring and the study of hyperpolarized mixtures, which constitute the last part of this thesis.

The final part of the project was dedicated to the combination of these fast methods with hyperpolarisation strategies. The first option that we explored was the coupling of SPEN DOSY with dissolution dynamic nuclear polarization (D-DNP) that provides signal enhancements of up to 10 000 [45–48]. Since the amplified signal last for few tens of seconds because of longitudinal relaxation, SPEN DOSY experiments appear to be suitable to be combined with DNP and record DOSY spectra of hyperpolarized mixtures in the imparted time-window (less than 1 min in the case of ^{13}C). As DOSY experiments are strongly impacted by convection, the pulse sequence was upgraded to compensate for convection. This innovative coupling between D-DNP and SPEN DOSY was carried in partnership with Geoffrey Bodenhausen's team at École normale supérieure (ENS), especially with Dennis Kurzbach et Daniel Abergel. The other hyperpolarization strategy studied in parallel was the signal amplification by reversible exchange (SABRE) method that consists in a transfer of polarisation from parahydrogen to the substrate [49,50]. The transfer is done via interaction between the substrate, a metal complex and parahydrogen that form a temporary intermediate. The resulting enhanced signal last for few seconds so SPEN DOSY experiments are also well indicated to record this type of signal. This approach grants high levels of polarisation at low cost as the population difference between spins states can be increased of several orders of magnitude. These experiments were done in collaboration with Gaspard Huber and Patrick Berthault in CEA Saclay.

Part 1: Literature survey

2. NMR spectroscopy, a non-destructive tool for mixture analysis

This chapter aims to give a general description on how NMR spectroscopy can be used in order to address the challenge of small-molecules mixture analysis. One-dimensional and multidimensional NMR experiments are presented as well as their applications, relevance and limitations towards mixture analysis.

2.1. The challenge of mixture analysis

Chemical sciences strongly hinge on structural characterization and identification of molecular species. Whether it is for natural product research [1,2], chemical synthesis or metabolomics studies [3], retrieving the pure compound to be analyzed is traditionally a prerequisite. Before stepping into the structural determination process, the sample should be purified in order to dispose of side compounds and isolate targeted ones from the mixture to which they belong. When it comes to complex mixture analysis, separation techniques such as chromatography have become a standard staple method in order to fractionate a sample into its individual constituents. However, this step is highly time-consuming and may results in degradation of sensitives compounds. Besides, chromatography used in conjunction with mass spectrometry provides elucidation of molecular structure even when the compound is present in small quantities (nanomolar range) and with a high resolution. As a result, it is used in routine analysis to make sure that samples are clear from unwanted compounds or for reasons of safety and quality of the products.

A valuable analytical tool for complex mixture analysis is nuclear magnetic resonance (NMR) spectroscopy [4,5]. Since its advent [6,7], NMR spectroscopy has become the preeminent methods for structural elucidation of molecules in solution as it grants access to information on the chemical environment of nuclei when placed in a static magnetic field. The measurement of parameters by NMR such as chemical shifts, relaxations rates, correlation times or diffusion coefficients provide information on molecular structure, size, binding events, and reaction kinetics [20]. It is common practice to go through extensive chromatographic fractionation before submitting the analytes to spectroscopic analysis. Nevertheless, with the recent developments of more sophisticated NMR experiments, hardware and instrument technology, the scope of applications of NMR spectroscopy has increased significantly

[16]. Its ability to provide rich information on structure, interaction and dynamics of molecules has extended to the direct analysis of mixtures.

NMR spectroscopy offers the advantages of being non-invasive and non-destructive, in contrast to chromatographic analysis that is destructive for sample since we need to either heat it (when performing gas chromatography) or dilute it (when performing liquid chromatography) with considerable amount of solvent. It is a non-biased method that is suitable for many types of samples regardless of their chemical nature. Minimal to no preparation steps are needed before proceeding to the analysis and it is not necessary to go through derivatization steps. It provides extensive structural information on analytes and is highly reproducible with accuracy and precision. In addition, a direct, separation-free analysis can also result in time savings. The main limitations of NMR are a lack of resolution when to many compounds are present and a limited sensitivity.

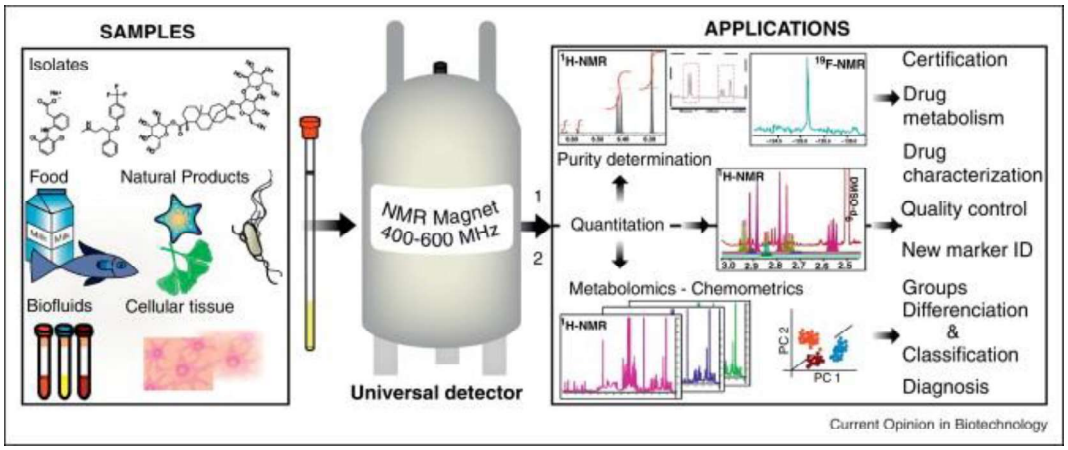

Figure 1: Sample varieties and panel of qNMR applications The current applications of qNMR can be dvided in two main groups: (1) absolute quantitation and purity determination of organic compounds (drugs, primary metabolites, natural products); and (2) metabolomics and quantitation of multiple analytes in complex natural matrices (e.g., food, botanicals, biofluids). Essentially all types of metabolites (e.g., sugars, fatty acids, organic acids, steroids) can be detected by NMR, explaining why a wide range of samples can be investigated. Therefore, qNMR applications cover the certification of purity, the identification and quantitation of drug metabolites, the quality control of food products and herbal remedies, the identification of biomarkers in complex natural matrices (e.g., herbal mixtures, biofluids), and finally clinical diagnosis. Reprinted with permission from [1] Copyright © 2013 Elsevier Ltd. All rights reserved.

Many efforts have been made to take advantages of NMR spectroscopy for the characterization of mixtures [8], not only for applications in chemical sciences, but also in biology, pharmacy [9], food industry or for environment as schematized in *Figure 1*. It is a great tool for the understanding of chemical processes through reaction monitoring as it helps to characterize intermediates. Applications are also found in natural products research, for metabolomics studies [10,11] or polymers [12] and also plant extracts. It is very useful for understanding biological processes through the analysis of biofluids,

the search for biomarkers, or the study of molecular interactions for potential medical and in-vivo applications. In pharmaceutical studies, NMR spectroscopy is used to control pharmaceutical formulations, screen new compounds, and characterize mixtures to detect unwanted compounds to ensure safety and quality of the products. In environmental studies the technique is notably used to characterize contaminant and pollutants, while in food analysis it is used to for quality control and in particular authenticity and traceability [13–15]. Overall, NMR spectroscopy is often used to certify the composition of a mixture and identify new compounds.

The analysis of mixtures by NMR often relies on 1D methods, which are however rapidly limited by signal overlap. Switching to 2D experiments instead leads to remarkable improvements in this regard. There are also many methods that provide a virtual separation of compounds, based on properties of the molecules such as relaxation, diffusion, or coupling network. The identification of components is often assisted by databases, as well as automatic methods to deal with the large quantity of data that needs to be stored and processed. Current trends in the NMR analysis of mixtures include the quest for higher sensitivity and the reduction of the time required for advanced NMR experiments. Progress on the latter over the years originates from NMR instrumentation, pulse sequence and data processing developments [51], that lead to new powerful experiments [52] as well new sampling strategies.

It should also be noted that NMR spectroscopy is often used in combination with other methods, that have complementary features. For example, mass spectrometry gives information on molecular weight and atomic composition while NMR gives information on chemical surrounding, connectivity and spatial configuration.

2.2. Mixture analysis by one-dimensional NMR

The first step of any NMR spectroscopic analysis is usually to run a simple ^{1}H 1D experiment. While many nuclei give an NMR response, protons give the highest sensitivity thanks to their high natural abundance and gyromagnetic ratio. ^{1}H 1D NMR is used in routine analysis with few parameters that need to be optimized and a quick and easy execution that gives spectra, with current limit of detection in the micromolar range. ^{1}H 1D spectra give information on the chemical environment of the nuclei via chemical shift, bonding between nuclei via J-coupling / multiplicity of the signal whose intensity reflect the associated number of nuclei [17,18]. The standard ^{1}H pulse acquire sequence is well known by organic chemists and used to check the structure of compounds at the end of a synthesis for example.

The accuracy of the information obtained with ^{1}H 1D NMR depends strongly on the complexity and purity of the sample. Unexpected compounds can modify the spectra and signal coming from the impurity can hide the signal of the compound of interest. It is also not easy to determine if signals belong to the same molecule or if they come from multiple species. In such cases, the experience of the analyst

together with NMR databases are useful. When the number of compounds to analyze increases within the sample of interest, 1D ^{1}H spectra can be quite crowded and the analysis becomes trickier. The fact that signals are spread over about 10 ppm only is unfavorable, compared to for example the ~200 ppm available for ^{13}C analysis – although the low natural abundance and gyromagnetic ratio of carbon-13 results in a 400 times lower sensitivity [17,18].

Overall, spectral overlap is a main limitation of 1D experiments for mixture analysis. In order to simplify the 1D spectrum of mixtures, spectral editing strategies based on either difference in relaxation times, molecular displacement or J-coupling network lead to selective observation of components. These methods 'filter' the NMR signals and this helps with reducing the spectral overlap that may hide the small signals present.

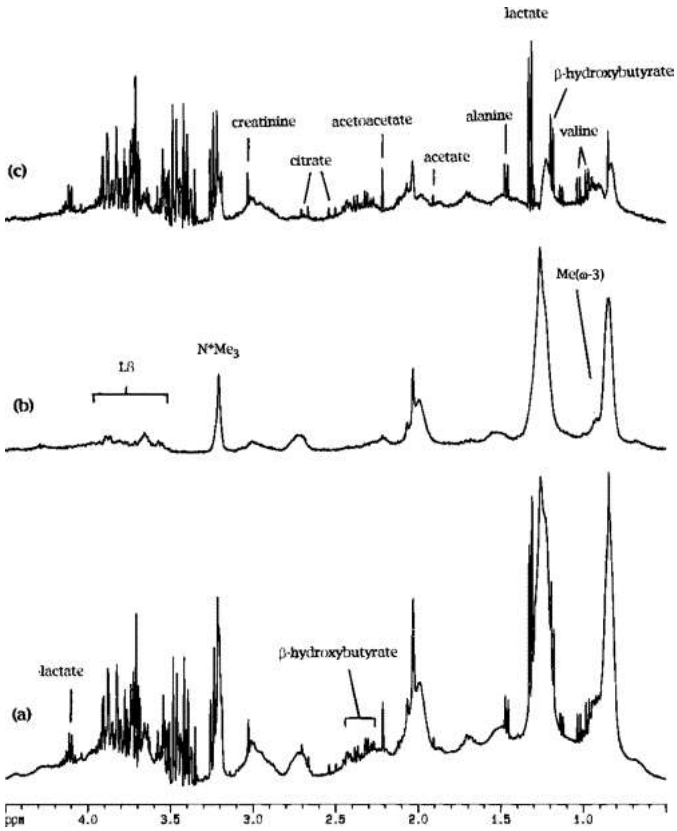

Figure 2: 400 MHz ^{1}H NMR *spectra of control human blood plasma with solvent water elimination and* edited *on the basis of differences in* diffusion *coefficients: (a) normal spectrum with application of 10 % gradient strength, (b) spectrum with gradient application at 50 %, and (c) the difference between (a) and (b). Assignments are, L8, choline and glycerol protons of phospholipids; N+Me3, N-trimethyl group of choline in phospholipids; Me(ω-3), CH3 resonance from $CH_3{\cdot}CH_2{\cdot}$ CH= containing fatty acids in lipoproteins. Reprinted with permission from* [53] *Copyright © 1996 American Chemical Society*

Filtering the signals through relaxation properties leaves the spectra free from signals coming from molecules with high molecular weight, that have a short transverse relaxation time T_2 [18,19]. The Carr-Purcell-Meiboom-Gill (CPMG) [54,55] pulse sequence element is notably used to perform spectral

editing of the spectra according to transverse relaxation properties [18]. The selective attenuation of signals from molecules with high molecular weight is useful when macromolecules signals dominate the spectra and hide smaller signals [4,19]. One interesting application of this filtering is found for the analysis of biological fluids such as plasma and blood, to remove signal from proteins and quantify low abundant analytes [53].

A complementary method to relaxation editing is to use diffusion weighting with pulsed field gradients (PFG) in one-dimensional experiments. Filtering the signals according to molecular diffusion properties now leaves the spectrum free from signals coming from molecules with low molecular weight [4,19,20]. This was successfully applied to studies on blood plasma, for biological applications and analysis of carbohydrate mixtures [53,56–58]. Another approach consists of subtracting two spectra acquired under different PFG strength, as illustrated in *Figure 2*. While this approach is not time-consuming, it required that that the observed species are well resolved in terms of size and molecular weight (MW).

Another filtering approach is 1D TOtal Correlation SpectroscopY (TOCSY), which provides a separation based on the J-coupling networks [21–23]. The purpose is to identify resonances generated by one spin system in a molecule. While there is no need of relaxation of diffusion differences in the sample, a spin multiplet need to be clearly isolated from the rest of the spectra. Also, this is a selective method that does not necessarily give access to the whole molecule, as one can only observe resonances within a given spin system. Applications of 1D TOCSY for separation of two isomers or analysis of seminal fluid have been reported [59,60]. Other applications include quantification in honey [22], balsamic vinegar [61], and urine for metabolic studies [62]. Other methods to address the issue of overlap in 1D NMR include the use of spectral deconvolution and spectral substraction [63]. Since multiplets patterns are also causing resolution issues with the 1D spectra, leading to some difficulties in signal assignment, homonuclear decoupling methods have been developed. Decoupling is usually obtained at the expense of sensitivity [64]. Solution to this issue is to extend the experiment to a second or third dimension (most effective method) [8].

2.3. Multidimensional NMR for mixture analysis

2.3.1. Principle of multidimensional experiments

When dealing with complex mixtures with a large number of compounds, we saw that the use of 1D experiments is complicated because signal overlap prevents the accurate identification and separation of molecules' signals. A way to address the overlap problem is to increase the dimensionality of the experiment to two or more [8]. Signals are then spread over a larger domain and this can help to

distinguish between two or more signals that were overlapping in the 1D spectrum. Multidimensional experiments are generated by one or more incremented dimensions in addition to the 'real-time' direct dimension. For a 2D experiment, the so-called evolution time t_1 is incremented in order to generate the indirect dimension, following this scheme:

preparation----evolution (t_1)----mixing----detection (t_2)

where the preparation and mixing events are fixed elements of a pulse sequence, t_1 is an incremented parameter and t_2 the acquisition time. The sequential repetition of this scheme gives a 2D data set $S(t_1, t_2)$. Fourier transformation in two dimensions then gives a 2D spectrum with rich structural and dynamic information. This procedure can be extended to higher-dimensional experiments, where each indirect dimension is generated scan by scan. A variety of experiments are available and they may be sorted in homonuclear and heteronuclear experiments. These experiments and their relevance for mixture analysis will be presented in this section.

2.3.2. Homonuclear experiments

Homonuclear NMR experiments involve the same type of nucleus in both dimensions. One of the oldest multidimensional pulse sequence is the ^1H–^1H correlation spectroscopy (COSY) [65]. This experiment unravels the connectivity between adjacent groups of protons that interact through J-couplings. This interaction gives rise to cross peaks in the spectrum located at the chemical shifts of the involved protons. Several variations of the COSY experiment are available such as double-quantum-filtered COSY (dqfCOSY), which is a phase-sensitive version that is very useful for mixtures when magnitude-mode COSY become two crowded. This experiment is routinely used for structural characterization of compounds, be they in a mixture or not [66]. It offers a significant separation of signals that are overlapped on the diagonal of the spectra.

The 2D version of the TOtal Correlation SpectroscopY (TOCSY) [67,68] experiment provides information of protons belonging to a given spin system in a molecule. This comes in addition to the information on directly coupled protons, thus giving a full description of the J-coupling network. TOCSY spectra tend to be trickier to analyze because of the difficulty to interpret cross peaks and because the spectra are more crowded than in COSY. Successful applications were nevertheless reported for mixture analysis with the study of insect venom [69], a chemical reaction mixture [70], a metabolic mixture [71] or amino acid mixtures [72].

Another way of simplifying spectra is to use ^1H J-resolved (J-RES) NMR experiment that consists of separating the chemical shift information from the J-coupling information [73]. This also can

be useful for the analysis of complex mixtures [74,75]; the projected version of this experiment (p-JRES) is also a possible approach to obtain homonuclear decoupled ^{1}H 1D spectra.

Last but not least, diffusion-ordered spectroscopy (DOSY) is a powerful method to separate the NMR spectra of components within a mixture [24–27]. Their differentiation is based on the measurement of translational diffusion coefficients, which depend on molecular sizes and shapes. It is possible to differentiate compounds whose diffusion coefficients differ by less than 1 %. In the classic DOSY representation, the first dimension corresponds to the 1D NMR spectrum of the sample, and the second dimension corresponds to the diffusion coefficient *D*. As a result, all the peaks from a given molecule are aligned along the corresponding value of the diffusion coefficient. This experiment is very efficient to separate NMR spectra and is considered as a form of virtual chromatography. DOSY have been used for a large of applications in mixture analysis, such as the characterization of drugs as illustrated in *Figure 3* [29], for polymer studies [32] and also for molecular weight determination [33,34].

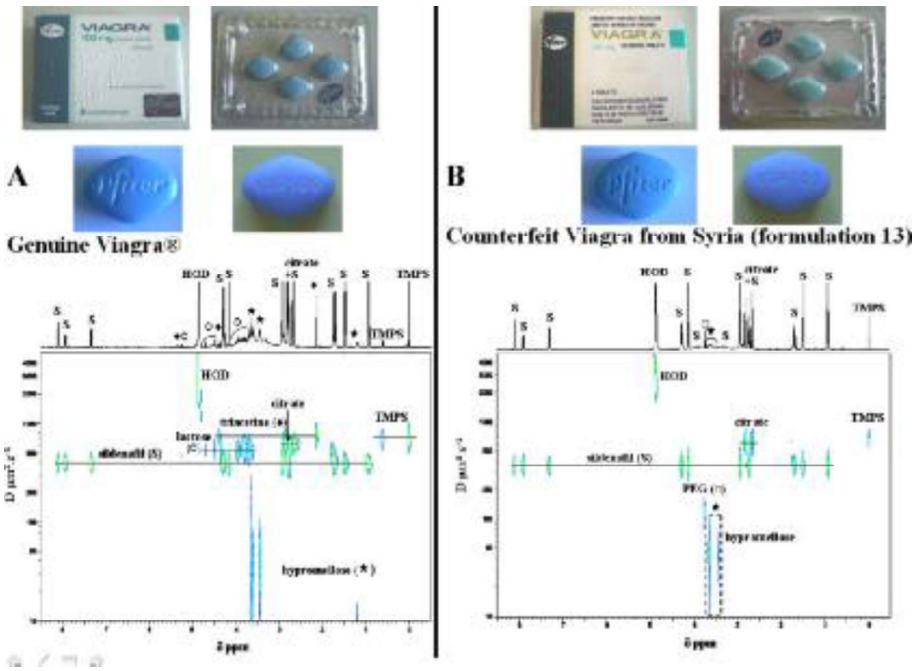

Figure 3: 2D DOSY ^{1}H NMR spectra in D_2O of tablets from (A) genuine Viagra and (B) the Syrian counterfeit formulation13. (S) sildenafil; (*) hypromellose; (♦) triacetine; (◦) lactose; (□) polyethylene glycol (PEG). TMPS (trimethylsilylpropane sulfonic acid) is the internal reference. Part B: a deeper section of the two signals of hypromellose is shown in a box. Reprinted with permission from [29] *Copyright © 2009 John Wiley & Sons, Ltd.*

2.3.3. Heteronuclear experiments

Heteronuclear NMR experiments involve different types of nuclei in the two dimensions. As ^{1}H NMR suffers from a small chemical shift range, resolution can be increased thanks to the larger chemical shift range of other nucleus, which helps to separate signals. Simultaneously this also gives precious information for structural elucidation. For example the Heteronuclear Single Quantum Coherence method (HSQC) [76] is often used to record ^{1}H-^{13}C, ^{1}H-^{31}P or ^{1}H-^{15}N correlation spectra, in which protons are correlated to their directly bonded nuclei. The sensitivity of the experiment is also enhanced by a magnetization transfer from ^{1}H to the X nucleus. This experiment is of great interest for identifying compounds in a complex mixture. The resolution is significantly increased thanks to the wide chemical shift dispersion provided by the other nuclei (ex ^{13}C) dimension. The Heteronuclear Multiple Bond Coherence method (HMBC) [77,78] can be seen as an extension of the HSQC, where not only the signal arising from the correlation of protons and their directly bonded nuclei is visible, but additional signals corresponding to correlations over 2, 3 or 4 bonds. This experiment is however seldom applied towards mixture analysis. A third type of experiment is Heteronuclear Multiple Quantum Coherence (HMQC) [79], which gives the same correlations as HSQC, but involves a multiple-quantum evolution period. The use of this pulse sequence toward mixture analysis is questionable in the way that the J-coupling effect results in loss of spectral resolution due to peak broadening. This can make the component identification more complicated than necessary [80].

2.3.4. Combined methods

Many of the pulse sequences presented above can be combined in order to define 3D experiments and extract multiple pieces of information at the same time [81]. From the point of view of mixture analysis, the most powerful approaches are obtained with combined methods that edit 2D correlation experiments with respect to diffusion, relaxation and J-coupling. The approaches discussed in section 2.2 for 1D experiments can indeed be used to create multidimensional edited experiments. This gives rise to experiments such as DOSY–COSY [28,29], DOSY–TOCSY [30,31], DOSY–HMQC [82], 2D-J-DOSY [83], COSY–iDOSY [84], constant-time-HSQC–iDOSY [85], DQF–COSY–iDOSY [86] for the diffusion case, T_2-edited COSY, TOCSY[53] and HSQC, and TOCSY-HMBC [87]. These experiments benefit at the same time from a simplification coming from differentiation in diffusion or relaxation but also from additional NMR information such a J-coupling and from the wider spectral range with heteronuclear experiments [19]. Figure 4 shows an example of DOSY-TOCSY on a mixture of methanol, ethanol, propanol, and valine.

Combinations are also possible between an NMR method and another analytical technique [88]. Such hyphenation between complementarity methods is a powerful way to analyze complex mixtures. NMR spectroscopy can for example be associated to liquid chromatography to perform mixture analysis in an online, single-shot run. The samples are pre-separated in the column and directly transferred to the spectrometer, which serves as a detector. This type of experiments were first used for plant extract analysis and also have proven to be efficient for the analysis of biofluids in real-time, high throughput screening (HTS) identification of metabolites in hypertensive rats, the analysis of carotenoid in food or the chemical profiling of marine sponge extract [2,18,89–93].

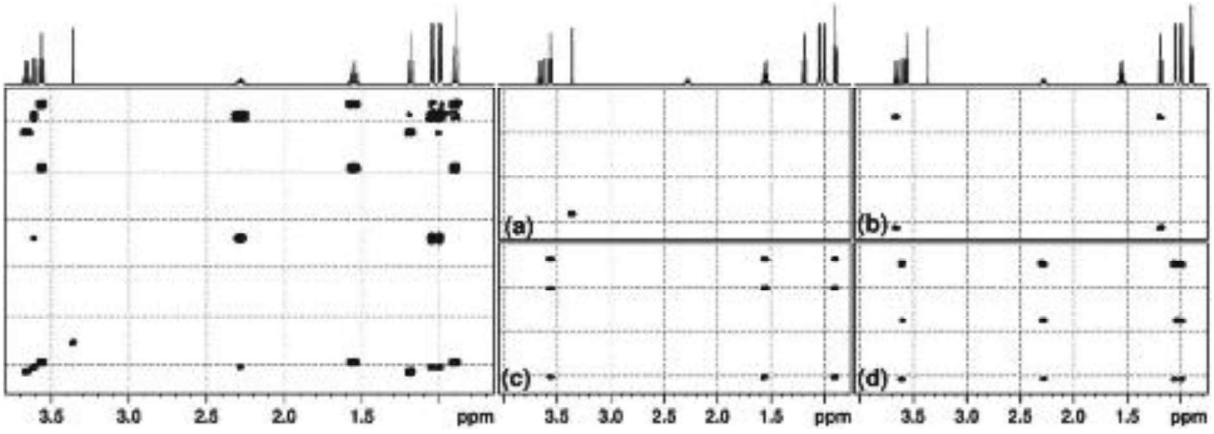

Figure 4: [Left] TOCSY spectrum of a mixture of methanol, ethanol, propanol, and valine. [Right] Sub TOCSY spectra from the 3D Hadamard- encoded DOSY-TOCSY experiment on the same mixture at (a) 1.32, (b) 1.05, (c) 0.89, and (d) 0.63 × 10^{-9} m^2 s^{-1}, corresponding to methanol, ethanol, propanol, and valine, respectively. These D values equalled within ± 2 % those determined by conventional DOSY experiments. The 1D ^{1}H spectrum is shown at the top. Reprinted with permission from [31] *Copyright © 2008 The Royal Society of Chemistry*

2.4. Limitations and perspectives of NMR towards mixture analysis

Among the methods presented in this section we have chosen to work on diffusion-ordered spectroscopy, a virtual chromatography experiment. Since it was introduced in 1992, DOSY has led to applications in many areas of research, and it still has a large potential for further developments and applications. DOSY shares the inherent drawback of multidimensional experiments, which is a duration that increases with the dimensionality of the experiment. Several hours and sometimes days may be required for the acquisition of a single spectrum. Sensitivity is also an intrinsic drawback of NMR as only a small fraction of the nuclear spins is effectively available for detection by the spectrometer,

according to the Boltzmann population of energy levels. The range of application of DOSY would expand with an increased speed and sensitivity.

An example of area that would benefit from new developments of DOSY is the analysis of counterfeit drugs. Nowadays, the need for full analysis and characterization of mixtures, the regulation toward impurities in product stress the needs for sensitive methods that can give a complete information on a sample without omitting even the smallest compounds. For example, many efforts are made for limiting frauds in the pharmaceutical industry. Mass spectrometry is a widespread technique in quality control laboratories but not all components survive the rough conditions of the detection. Sometimes it is more interesting to observe a sample in its raw state without modification and NMR can comply with this constraint.

Another area of application is the “live” monitoring of experiments, to fully characterize a reaction mixture while it is evolving. Reaction mixtures are a particular case of mixtures that are constantly changing, and this dynamic behavior can be hard to follow without an in-situ method of analysis. This also applies to unstable compounds that degrade fast, or to the formation of metabolized products in vivo. Faster experiments are needed to follow evolving mixtures, but sensitivity is also required to detect low concentrated compounds, especially in in-vivo/biological applications. For these reasons, several fast-multidimensional NMR methods are being developed for the analysis of mixtures. In the following, several fast-analytical NMR methods will be described with a focus on DOSY experiments.

3. Diffusion NMR methods for spectral separation of small molecules mixtures

Diffusion-ordered spectroscopy (DOSY) is a powerful method to separate the NMR spectra of components within a mixture [94–101]. Their differentiation is based on the measurement of translational diffusion coefficients, which are linked to the molecules size and shape [102], and with ideal conditions it is possible to differentiate compounds whose diffusion coefficients differ by less than 1 %.

3.1. Translational diffusion

Molecules in solution undergo a translational motion with random reorientations called diffusion. The diffusion behavior depends on many parameters such as temperature, the size of molecules and viscosity, and is quantified with the translational diffusion coefficient, often noted *D*. For large molecules of spherical shape, the diffusion coefficient is given by the Stokes–Einstein equation

$$D = \frac{k_B T}{6\pi\eta r} \tag{3.1}$$

where k_B is the Boltzman's constant, T is the temperature, r the hydrodynamic radius of the molecule and η is the viscosity of the solution. This implies that molecules with high molecular weight will diffuse more slowly than molecules with low molecular weight.

3.2. Diffusion encoding with pulsed field gradients

Diffusion NMR pulse sequences rely on a pair of pulsed field gradients (PFG) separated by a long delay so that translational diffusion has an effect on the detected signal intensity [103]. When using an increasing range of gradient strength, the observed signal is found to decrease exponentially and can be modeled with the so-called Stejskal-Tanner equation (see below equation 3.5) to extract the diffusion coefficient for each peak in the spectrum.

3.2.1. Gradient pulse description

High-resolution NMR spectroscopy experiments are carried out in a static magnetic field B_0 that is assumed to be homogeneous across the sample as illustrated in Figure 5a. However, a controlled

disruption of this homogeneity can be exploited to manipulate the magnetization over a short duration δ.

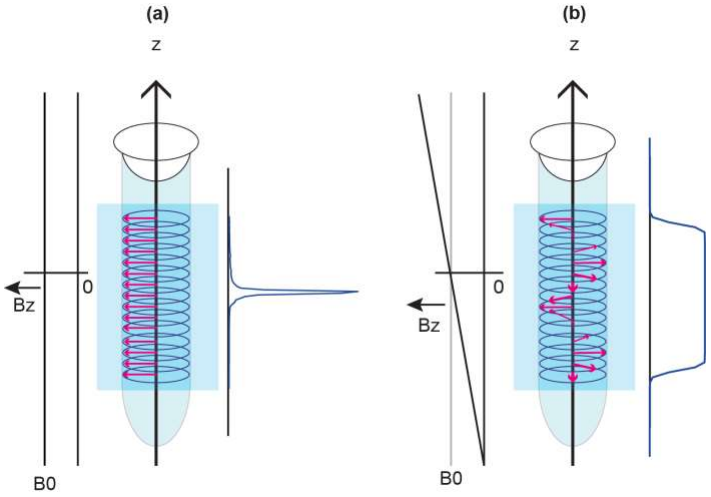

Figure 5: Effect of a magnetic field gradient on the NMR spectrum. (a) Sample in a homogeneous magnetic field and magnetization helix during acquisition. The spectrum is a peak with a narrow line. (b) Sample in a linear magnetic field and magnetization helix during acquisition. The spectrum is a broad peak corresponding to the image of the observed region of sample.

In particular, a magnetic field gradient G, which is a linear variation of the longitudinal component of the magnetic field, can be induced by a dedicated coil in the NMR probe [104]. The result is an overall field of the form:

$$B_z = B_0 + Gz \tag{3.2}$$

where z corresponds to the spatial coordinate of the spins along the B_0 axis as shown in Figure 5b. Spins with a gyromagnetic ratio γ will then have a precession frequency

$$\omega(z) = -\gamma B_0 - \gamma G z \tag{3.3}$$

that is related to their position in the sample. As a result, the phase $\phi(z)$ acquired during the gradient pulse of duration δ will also be spatially dependent:

$$\phi(z) = -\gamma G z \delta \tag{3.4}$$

The effect of a gradient pulse can be visualized by considering that the sample is divided in several slices along the z-axis, with each slice possessing its own phase, precession frequency and magnetization vector. Since a pulsed field gradient results in position-dependent precession frequency, the transverse magnetization will acquire an helix pattern represented in Figure 5b [95,105,106]. After a PFG of sufficiently large area, the magnetization vectors cancel each other and the total observable signal is zero. This is in contrast to the case shown in Figure 5a, where B_z=B_0 and all magnetization vectors are aligned since they have the same precession frequency, thus leading to full signal observation. Magnetic-field gradients are also central for imaging experiments [107] . When applied during acquisition, they reveal the sample's spatial profile Figure 5b. Indeed, the broadened signal arises from the juxtaposed

contribution of each part of the sample. Figure 5 illustrates the case of a sample with a single chemical-shift offset; cases with several chemical-shift offsets will be discussed later.

A variety of gradient-pulse usages are found in NMR experiments, depending on the desired effect on the magnetization. PFGs are also combined with radio-frequency pulses in some pulse sequence elements. Frequently encountered blocks offer the possibility to perform coherence selection with little to no phase cycling, study molecular diffusion, remove artefactual signals, perform selective excitation or perform imaging experiments [108,109].

3.2.2. Spin echo experiment

The first diffusion experiment was based on a spin echo (SE) as illustrated in Figure 6. In the SE experiment, the first 90° pulse tips the magnetization in the xy plane then the application of a gradient pulse winds this magnetization into a helix that will be reversed by the 180° pulse. The second gradient pulse unwinds the helix to form an echo that gives an observable signal. Spin-echo based diffusion NMR is however limited because of the effect of transverse relaxation during the diffusion delay, as well as J modulation that causes peak distortion. Although strategies have been introduced to mitigate the effect of J modulation, spin-echo based methods are usually not the preferred implementation of diffusion NMR [110–112].

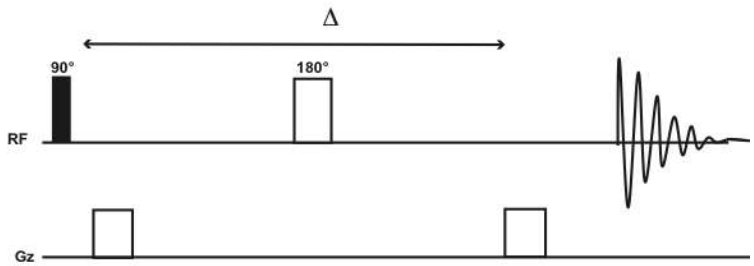

Figure 6: Conventional DOSY Spin Echo (SE) pulse sequence.

3.2.3. Stimulated echo experiment

In order to reduce the deleterious effects of J modulation and transverse relaxation, a stimulated echo-based experiment (STE) involving three 90° pulses, shown in Figure 7, is used instead of the simple spin echo. With the STE sequence, spins spend a reduced time in the transverse plane. The 180° pulse is replaced by two 90° pulses framed by the gradient pulses, which are separated by the diffusion delay Δ (often called “big delta”).

The application of the first gradient pulse, following the first 90° pulse, entails the spin's acquired phase to be of the form given in equation (3.4) The y-component of the magnetization is then stored along z-direction due to the second 90° pulse, while the x component remains in the transverse plane and is suppressed with phase cycling or a spoiler gradient. As a result, the phase modulation is converted into an amplitude modulation. The magnetization is returned into the transverse plane by the third 90° pulse. Next, a matching gradient pulse is applied and gives the same phase as before with either the same (anti-echo) or an opposite sign (echo). This results in an observable signal, which is attenuated because of the displacement that occurs during the delay Δ.

Longitudinal storage reduces the effect of J modulation. In addition, the magnetization to be subjected to longitudinal rather than transverse relaxation; as T_1 is typically significantly greater than T_2, longer diffusion delays can be used than in SE experiments. Only 50 % of the total signal is observable but it is the price to pay in order to get a spectrum with small artifacts.

Other phenomena that affect the diffusion data includes eddy currents and convection. The use of a longitudinal eddy current delay can help with minimizing the problem of eddy currents [28].

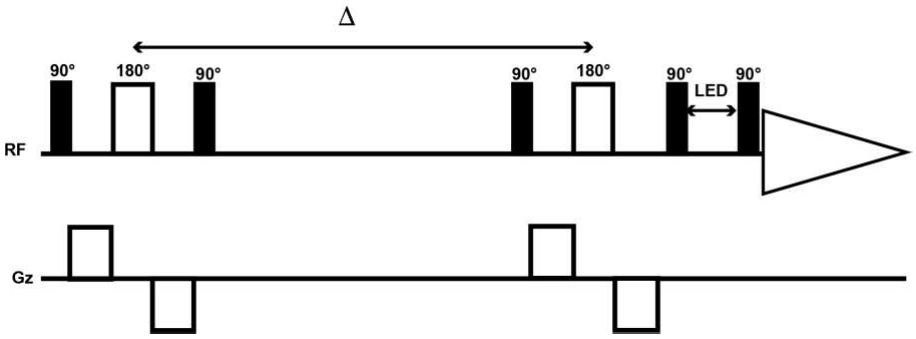

Figure 7: Conventional DOSY Stimulated Echo (STE) pulse sequence that includes bipolar gradient pulses and longitudinal eddy current delay.

3.2.4. Oneshot experiment

Most applications of DOSY rely on a STE pulse sequence using bipolar gradient pulses, and between 8 to 16 gradient increments are typically used to get a well-described diffusion curve. In addition, 8 scans or more are needed for each gradient increment, for the coherence transfer pathway (CTP) selection through phase cycling. This extensive phase cycling increases further the duration of the experiment even if it contributes to the good quality of acquired data. The Oneshot pulse sequence shown in Figure 8 offers a solution to avoid using such phase cycling while maintaining the quality of the DOSY spectra. Phase cycling is supplemented by unbalanced bipolar gradient pulses around the 180° pulses of a bipolar pulse pair stimulated echo (BPPSTE) pulse sequence [109,113]. This imbalance suppresses the non-refocused magnetization from the 180° pulses and selects the appropriate coherence transfer pathway

(CTP). Additional balancing gradient pulses are also used for maintaining lock signal stability. The Oneshot pulse sequence provides accurate diffusion measurements by using a single scan instead of sixteen per gradient increment although 4 scans may be used for clean results. The Stejskal-Tanner equation needs to be modified to take into account the effect of the coherence selection gradient on the diffusion attenuation.

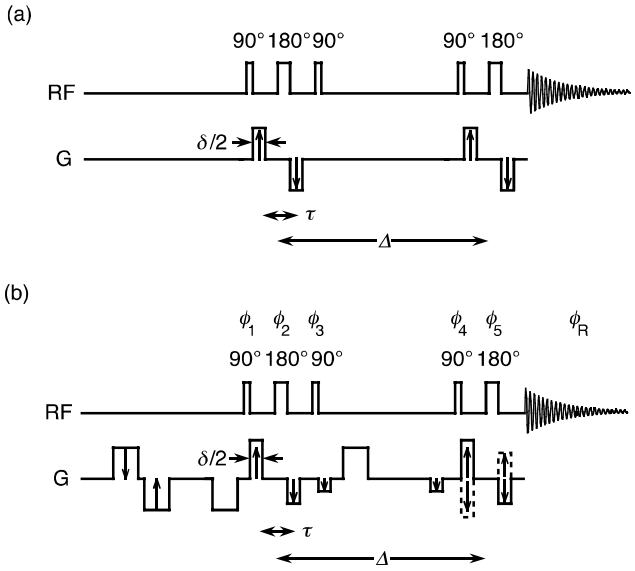

Figure 8: Radiofrequency (RF) and gradient (G) pulse sequences for DOSY. (a) Bipolar pulse pair stimulated echo (BPPSTE) sequence; (b) the proposed one-shot sequence using (solid line) the stimulated antiecho and (dotted line) the stimulated echo. The diffusion delay Δ is the time between the midpoints of the two diffusion-encoding periods and τ that between the midpoints of the antiphase field gradient pulses within a given diffusion-encoding period. The outward/inward facing arrows indicate gradient pulses which are incremented/decremented as the diffusion weighting is changed. The gradient prepulses in (b) are most conveniently given a duration of 2δ. Reprinted with permission from [113] *Copyright © 2002 John Wiley & Sons, Ltd*

3.3. Diffusion coefficient determination

DOSY data are generated via incrementation of the gradient pulse area over a series of scans, so that the detected signal is made dependent on both the gradient area and the diffusion rate. Either the intensity, G, or the duration, δ, of the gradient is increased. After Fourier transformation, each spectrum generated for one gradient level is attenuated to some extent. The attenuation shows an exponential behavior as a function of the gradient area and each resonance will have its own decay rate. The signal attenuation can be expressed by the Stejskal-Tanner equation

$$S = S_0 e^{-(DG^2\gamma^2\delta^2\Delta')} \tag{3.5}$$

where S_0 is the initial amplitude of the signal, D is the diffusion coefficient, G is the gradient intensity, γ is the gyromagnetic ratio for the appropriate nucleus, δ the gradient duration and Δ' the diffusion delay, corrected to take into account the finite nature of the gradient pulses [114]. Monoexponential fitting of the decaying signal for each peak to the Stejskal-Tanner equation yields the associated diffusion coefficient D. Resonances can then be sorted according to the value of the diffusion coefficient.

Diffusion-encoding experiments can be prepended or appended to many nD spectroscopic experiments. Appropriate data processing then gives a (n+1)D spectrum with n chemical shift axes and an additional diffusion axis. In a classic 2D DOSY display, the first dimension corresponds to the 1D NMR spectrum of the sample and the second dimension corresponds to the diffusion coefficient; peaks from the same molecule are aligned along the corresponding value of the diffusion coefficient

Data processing methods for DOSY can be sorted between univariate and multivariate methods, with many of them implemented in the open DOSYToolbox, recently extended to GNAT, which greatly facilitates the analysis of DOSY data as illustrated in Figure 9 [51,115–128].

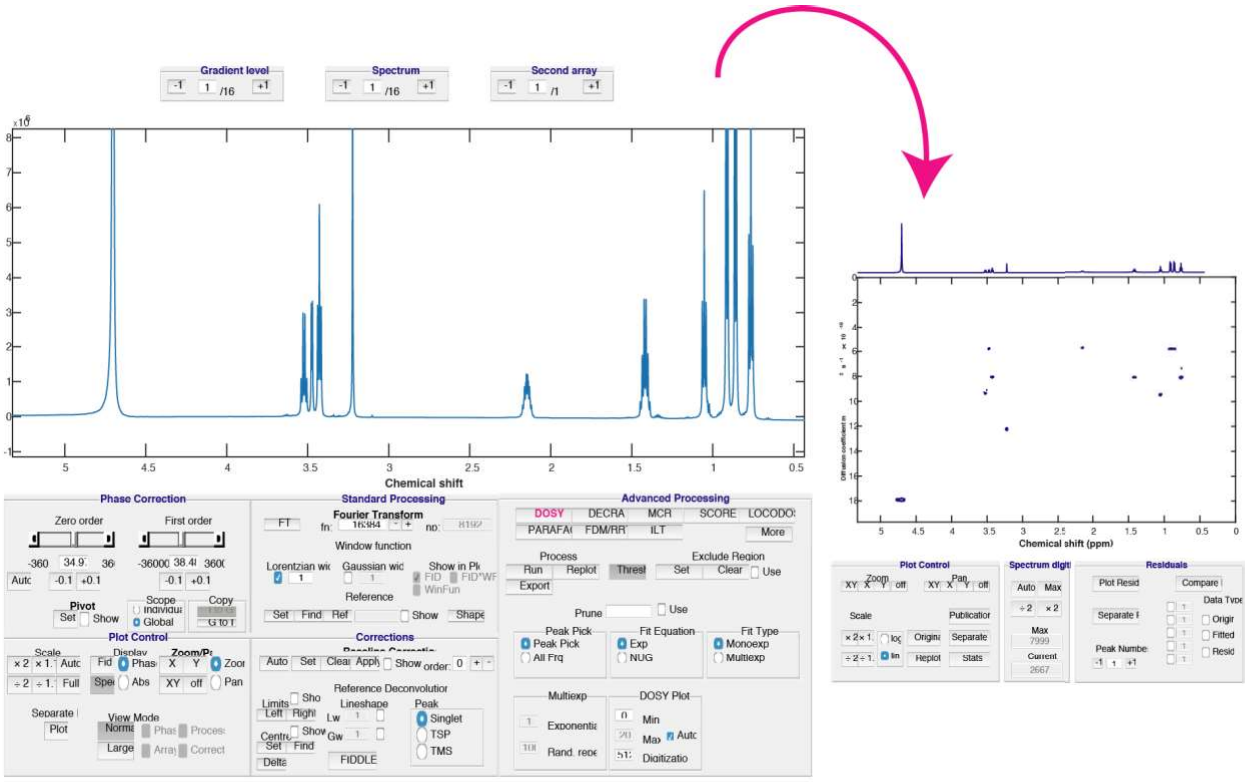

Figure 9: DOSYToolbox view to illustrate the processing of DOSY data.

Applications of the DOSY experiment are found in polymer determination of molecular weight [32–34,129–132], in a quantitative manner to quantify sucrose in beverage [133], study of reactive metal complexes [134–136], study of chemical intermediates [137], ligand identification [138] or determining chemical exchange rate [139].

3.4. Typical issues with DOSY data and how to resolve them

3.4.1. Signal overlap

DOSY data need to be acquired with the highest sensitivity and spectral resolution as possible [105,140]. The separation of compounds in the diffusion dimension depends strongly on resolution. Indeed, diffusion measurement is based on signal decay of resonances in the spectrum. In the ideal situation, the resonances are completely resolved in the spectrum and one can consider that each resonance arise from a given compound. Mono-exponential fitting of each resonance's decay can be performed and the calculated diffusion coefficients should be the same for all resonances arising from a single molecule. For very crowded mixtures, signal overlap will be an issue as it will decrease the accuracy of diffusion coefficient calculations. In this case, resonances coming from two or more compounds can be completely or partially superimposed in the spectral dimension. It entails that the decay of theses resonances can no longer be assigned to a single compound and the mono-exponential fitting won't give an accurate value but an average value of the real diffusion coefficient. This can lead to erroneous assignments of signal and a complicated DOSY display. Multi-exponential fitting can be a solution but it is only able to separate diffusion coefficients when they differ by more than 30 % [141,142], while advanced data processing can also be used [143,144] to reduce overlap or improve the separation of overlapped peaks. When spectral resolution is not sufficient with 1D NMR, using an additional dimension is another option, which however results in a longer experimental time [31,84,145–150].

Another issue is found when components are close in shape, size, molecular weight such as isomers so it can be useful to add some complementary compounds that will interact specifically with one component to help the separation. It is a sort of forced/artificial difference between molecules. Matrix assisted DOSY (MAD) relies on this principle and it has been exploited in order to distinguish between flavonoids that have similar structures [151–153]. The solvent also have an effect, which was found to help in the separation of isomers as suggested by Tessari in this study of DOSY in MeOD [154], while the use of lanthanide shift reagents was shown to increase resolution in both the spectral and the diffusion dimension [155].

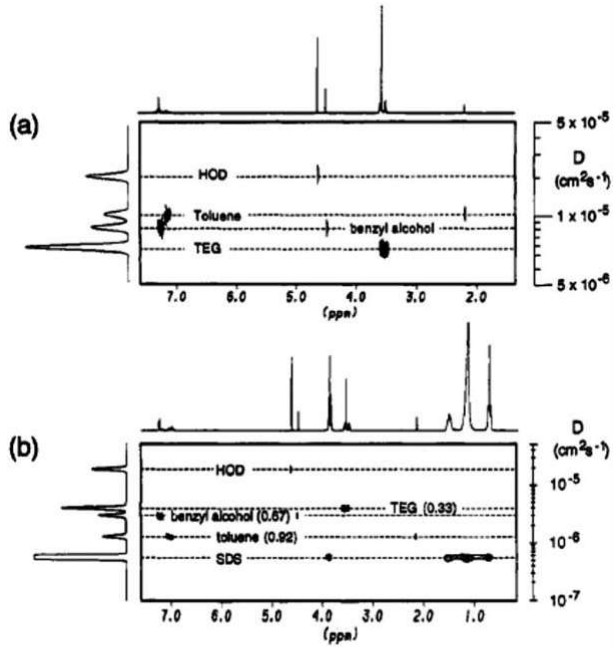

Figure 10: Fig. 2 (a) DOSY presentation of an equimolar mixture of toluene, benzyl alcohol and tetraethylene glycol in D_2O. (b) Shows the same mixture in the presence of 150 mM SDS. Reprinted with permission from Morris et al., Anal. Chem., 66 (1994) 211–215. Copyright 1994 American Chemical Society

3.4.2. Eddy currents

Eddy current originates from rapid changes in magnetic field and they depend on the gradient pulse strength. They will induce lineshape distortions, artefacts, shifts in the main magnetic field and basically everything that can ruin your experiment, especially when using many gradients pulses which is the case for DOSY [156]. Reducing the impact of eddy currents can be done by mean of RF and gradient coil design, e.g., with shaped gradient pulses that have smooth on/off switching rate, using bipolar gradient pulses or the use of a LED delay at the end of the pulse sequence to let the eddy current vanish (the magnetization is put back along z by 90° pulse, wait 5 ms and then put in the transverse plane with 90° pulse for acquisition).

3.4.3. Convection caused by temperature gradients

Temperature gradients through the sample induce convection currents, which are a serious disturbance that affects diffusion measurements [157–161]. The two main forms of convection known are the Rayleigh-Bérnard one and the Hadley flow [162]. The first form occurs when vertical temperature gradients are present, that is to say when the hotter part on the liquid moves upward while the cooler part is moving in the opposite direction. The second form occurs when transverse temperature gradients

are present. The former is present above a certain threshold that is defined according to the sample geometry, the viscosity and thermal properties of the liquid. The latter does not depend on a critical value and tends to be present in all typical liquid state NMR experiment. Temperature gradients are basically unavoidable and they come from multiple sources such as radiofrequency heating, differential heating of the outside of the probe by shim coils, but the greatest culprit of gradient temperature is the gas flow used to control the sample temperature. For this reason, temperature gradients need to be reduced as much a possible because convection can lead to significant loss of signal and overestimated diffusion coefficient values since the signal appears to decay faster than it should.

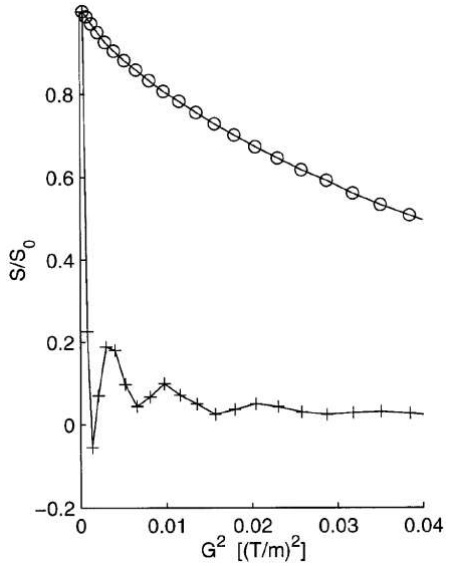

Figure 11:Echo signal attenuation as a function of the gradient strength G^2 for (+) a simple Stejskal-Tanner diffusion experiment on a sample of 0.06% polypropylene in tetratchloroethan-d_2 a 320K and (o) using a convection compensated DSTE experiment. Reprinted with permission from [163]. *Copyright © 1998 by Academic Press.*

Two perspectives against convection issue can be explored [164]. The first is related to experimental conditions adjustment. It has been shown that either reducing the NMR tube diameter, increasing the gas flow to make temperature more uniform, restraining the sample volume with Shigemi tubes or spinning the sample results in decreased convection effect.

The second approach to deal with convection is to make use of pulse sequences that are specifically designed to compensate for the convective flow as long as this flow is considered laminar during the diffusion period of the experiment [165]. In practice, as proposed by Jerschow and Muller [166,167], the diffusion weighting proceeds in two symmetrical steps rather than a single one. Since convection motion causes further phase shift of the magnetization on top of the one induced by the random Brownian motion we seek to evaluate, the aim is to impart opposite convection-induced phase shift in each half of the pulse sequence that will cancel each other out. Compensation of the velocity induced phase term is obtained in a way that the diffusion effect is cumulative at the end of the pulse

sequence. The convection compensative ability however comes at the expense of sensitivity since each STE part induce 50 % of signal loss.

3.4.4. Gradient field non-linearity

It appears that sources of error are everywhere and threaten the successful completion of the DOSY experiment. An insidious enemy is the gradient pulse itself which is key to measure diffusion coefficient but it is necessary to keep in mind that a gradient pulse is far away from being perfect [168]. It is a source of systematic error for diffusion coefficient values due to its so called "non-uniformity", especially on the edges. To deal with this non-linearity it is possible to map the position dependent gradient strength [164,169]. Another approach consists in using a restricted sample volume, e.g., with a Shigemi tube, to record data from a region over which the gradient has a more uniform value.

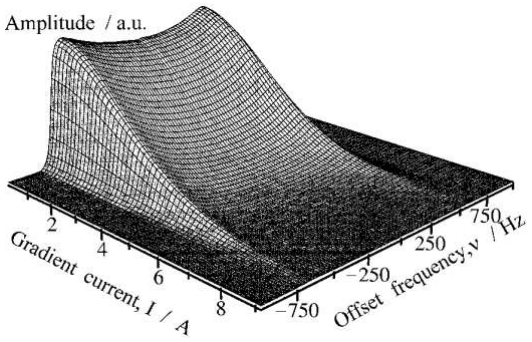

Figure 12: Results from the Stejskal–Tanner experiment using a gradient during the acquisition from a Varian standard doped water sample (1 % H_2O in D_2O ⩽ 1 mg/ml $GdCl_3$) at 600 MHz. The slope of the profile is steepest in the middle of the sample where the gradient is the strongest. The current through the gradient coil was arrayed in 60 steps between 0 and circa 10 A. Reprinted with permission from[169]. *Copyright © 2001 by Academic Press All rights of reproduction in any form reserved.*

3.5. Conclusions

From this analysis of the literature, we can see that the DOSY NMR methods was applied in many fields for mixture analysis. The main feature underlying the DOSY experiment were presented and this will serve as a basis to understand where we can modify the experiment in order to accelerate it. Various schemes were presented and will be also evaluated in order to create fast DOSY experiment. Several sources of errors were presented and it is important that we keep them in mind because chances are high that we may be confronted with them all along the project. We know the ways of correcting for these sources of errors and we will see if they are compatible with fast DOSY experiments.

4. Acceleration strategies for DOSY

Pulsed field gradient NMR is frequently used to characterize the translational motion of molecules in solution [114]. As explained in section 3, this methodology relies on a gradient incremented scheme in order to induce a diffusion-weighted signal. The recording of multiples gradient increments (at least 5 for relatively simple mixtures) over time results in a long acquisition duration, which can be detrimental for rapidly changing samples. Various strategies have been proposed to reduce the duration of diffusion experiments [35]. These approaches may be divided into different categories depending on the encoding strategy used. Here we consider three types of methods that reduce the number of required scans to one, based on multiple gradients pulses, on multiple RF pulses, and on spatial encoding. We also describe other strategies, which require multiple scans but still provide a significant reduction of the duration of DOSY experiments.

4.1. Multiple echoes induced by trains of gradients pulses

Efforts to accelerate the traditional PFG NMR experiment, which relies on a series of scans with incremented diffusion weighting, started with experiments that record series of diffusion modulated echoes in a single transient, using trains of gradient pulses.

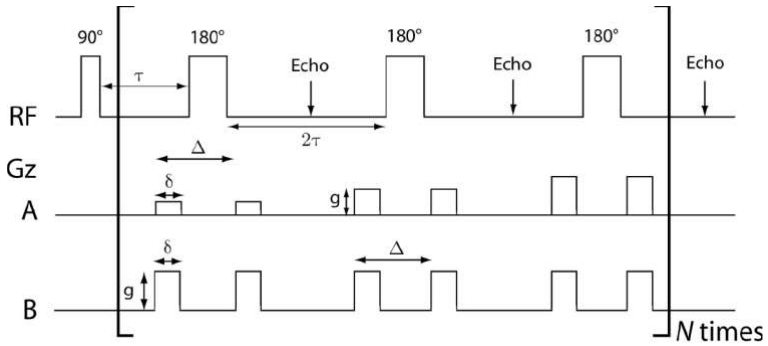

Figure 13: CPMG-based PGSE methods for measuring D in a single multiple-echo transient. A, the PGMSE method [170]*; and B, the method of Chandrakumar et al* [171]*. For A the gradient amplitude is increased systematically, while for B it is constant. Reprinted with permission from* [35] *Copyright © 2007, G. Pages*

Pulsed field-gradient multiple spin-echo (PGMSE) [170] and fast multi-spin-echo diffusion sequences (FAMOUS) [171] both derive from the Carr-Purcell-Meiboom-Gill (CPMG) experiment as shown in Figure 13. In the case of PGMSE, the amplitude of the gradient pulse pair is incremented from one echo to another. Diffusion coefficients are extracted from the amplitude ratio between two successive echoes, plotted against the gradient area. In the case of FAMOUS, the amplitude of the gradient pulse pair is

kept constant, and diffusion results in an additional line broadening of the peak obtained after Fourier transform of the signal sampled at the top of the echoes. This implies that two experiments need to be recorded, with and without diffusion encoding, to separate the contribution of relaxation and diffusion. These methods are designed for a single resonance and can be combined with a spectrally selective excitation pulse [171].

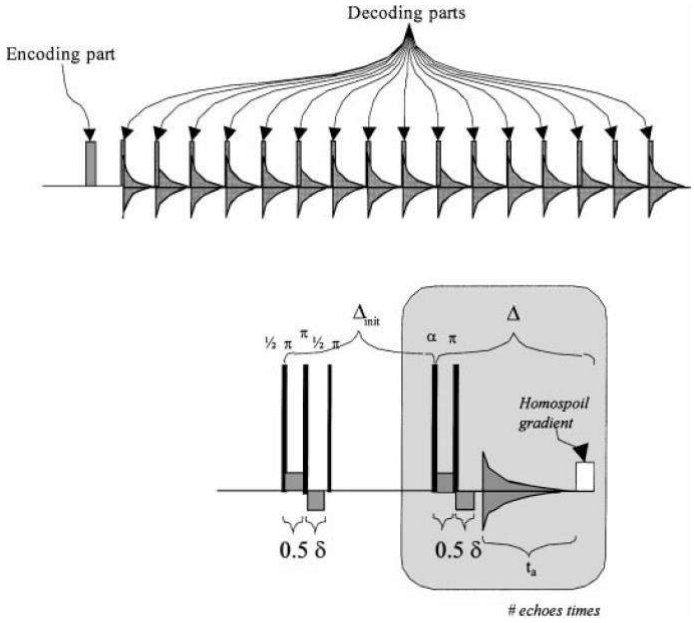

Figure 14: The proposed Difftrain pulse sequence, schematic (upper) and detailed (lower). t_a is the acquisition time and Δ is the diffusion delay. In the implementation of the Difftrain experiment, the same phase cycle as in previous BPPSTE implementations was used. Reprinted with permission from [172] *Copyright © 2001 by Academic Press*

The Difftrain pulse sequence, illustrated in Figure 14, is based on a stimulated echo and performs encoding of the spin via a bipolar gradient pulse sandwiched by 90° pulses, as in the classic STE. Multiple decoding steps are then carried out in a single scan, with the repetition of a block consisting of a small-tip-angle pulse followed by a bipolar gradient and signal acquisition [172]. Each block provides an echo signal, acquired with a diffusion time that increases from one echo to the next. After each echo, a spoiler is used to diphase any remaining transverse magnetization. As the decay of the signal is impacted by diffusion but also impacted by loss due to T_1, it is necessary to record two transients with and without diffusion gradient on. The Difftrain approach conserves chemical shift information and can in principle be used for high-resolution DOSY, although reported applications concern the analysis of unstable heterogeneous systems

Fast diffusion experiments can also be performed by measuring with a train of bipolar gradients, with a single 180° pulse between excitation and the acquisition gradient train, so that frequency offsets are refocused in the middle of the train [173]. Chemical-shift resolution is preserved to some extent, and again transverse relaxation has to be taken into account in the analysis.

To the best of our knowledge, the presented methods have not been used for applications in mixture analysis. Other applications include the use of PGMSE was used to analyse hydrated collagen [174], measurements of time dependent diffusion of laser polarized xenon gas [175] and imaging experiments [176]. These methods also have potential applications for the evaluation of macroscopic motion and the measurement of anisotropic diffusion effects, especially for in vivo applications [170]. FAMOUS was used for intercluster interaction [177] and the study of lyotropic system [178], while Difftrain was used to characterise thermodynamically unstable oil-water emulsions [179].

4.2. Multiple echoes induced by trains of RF pulses

Another family of pulse sequences relies on a train of RF pulses to generate a large number of echoes with different degrees of diffusion weighting. The DANTE (Delays Alternating with Nutations for Tailored Excitation) block, which is a selective excitation scheme, is the foundation of theses pulse sequences [180,181]. It consists in a series of low flip-angle RF pulses and is combined with a constant gradient pulse in order to induce a train of echoes. This type of RF pulse train was employed for diffusion measurement with the BURST pulse sequence shown in Figure 15 even though it was initially made for imaging experiments [182]. The acquisition is performed under a read gradient to unravel the echoes generated by the RF pulses. The RF train and echoes train are separated by a 180° pulse.

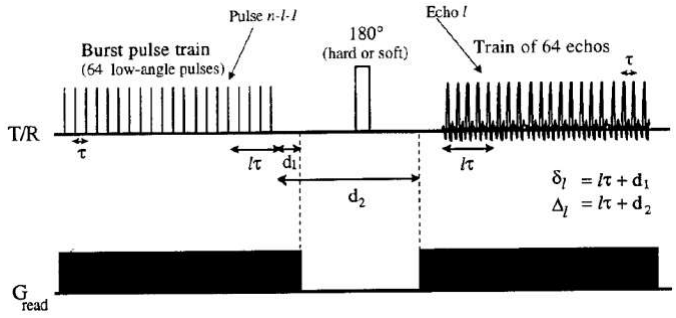

Figure 15: Pulse-sequence diagram describing the basic spin-echo Burst pulse sequence used for measuring diffusion coefficients. A read gradient is switched on and the sample excited by means of a train of very low (typically < 1°) RF pulses. The 180° pulse and the second gradient refocus a series of echoes, one corresponding to each pulse, and the delays are arranged so that the spin and gradient echoes coincide. Reprinted with permission from [182] *Copyright ©1996 by Academic Press, Inc.*

The DANTE-STE [183] sequence of Figure 16 was used for diffusion measurements of laser polarized ^{3}He and ^{129}Xe gas and the difference with the BURST previously described is found within the encoding part where 90° pulse is used to reduce T_2 effect and within the acquisition part were pulses are used to generate multiple train of stimulated echoes with different diffusion durations.

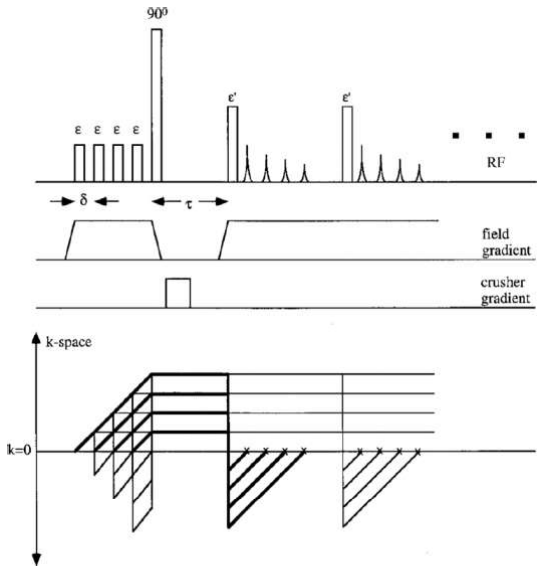

Figure 16: Pulse sequence and k-space trajectories. The principle pathways in bold are the only ones to survive in the small flip angle limit and form echoes following the readout pulse. Using this sequence, the full diffusive behavior of a sample can be read out in a single shot provided there is sufficient SNR. Reprinted with permission from [183] *Copyright © 1999 by Academic Press.*

The Multiple Modulation Multiple Echoes (MMME) [184] represented in Figure 17 also exploits a train of RF pulses but this time with varying tip angles. The gradient is maintained during the whole pulse sequence, and this generates several coherence pathways that are used to calculate diffusion coefficient. The MMME sequence has been applied for diffusion measurement in several direction at the same time, to characterise anisotropic systems [185].

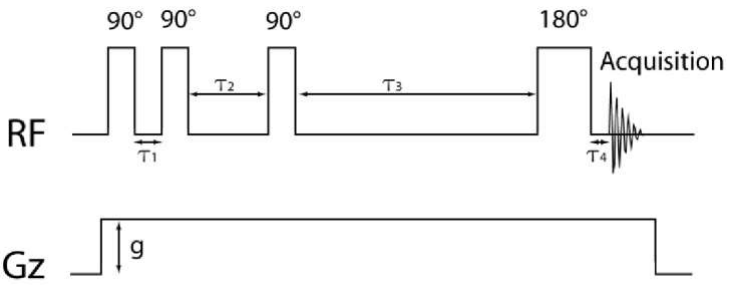

Figure 17: MMME4 pulse sequence [184] *used to measure D in a single transient. Reprinted with permission from* [35] *Copyright © 2007, G. Pages*

In these methods, as the gradient is turned on during the whole pulse sequence, hardware constraints set the maximum duration of the experiment and the gradient strength used. Also, the use of small-tip-angle pulses results in a low sensitivity. Notably, BURST and DANTE-STE require tip angles of less than 1° for accurate measurement of diffusion coefficients. Since these methods do not provide spectral resolution, few applications to the analysis of mixtures have been reported.

4.3. Spatial encoding

Another approach to accelerate diffusion NMR experiments consists of using a spatial parallelization of the gradient increments, which gives a spatial encoding of the diffusion dimension. The concept of spatial encoding was introduced in 2002 by Frydman and co-workers, with experiments where the chemical-shift information is encoded spatially [38,186–189]. Spatial encoding can be adapted for most 2D NMR pulse sequences and has led to many applications [39,40,190,191]. It relies on the partitioning of the sample in «virtual» slices, where each slice corresponds to an increment of the indirect evolution dimension of the 2D experiment. Keeler, Morris and co-workers independently introduced the spatial parallelization of gradient increments for DOSY experiments [41], a concept that was later revisited by Frydman and co-workers [42]. The spatially encoded information is read out with a spectroscopic imaging scheme, for which two options have been described. Keeler and co-workers have used a weak acquisition gradient that yields a spatial profile in the lineshape of the peaks in a 1D spectrum (hence the name of the proposed method: 1D DOSY shown in Figure 18) [41,192], while Shrot and Frydman have proposed the use of echo-planar spectroscopic imaging, which gives spatial profiles in an orthogonal dimension, which is illustrated in Figure 19 [42].

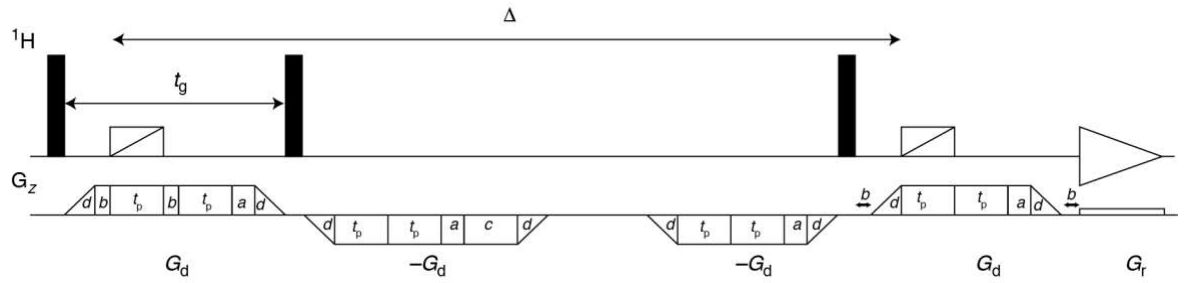

Figure 18: Detailed 1D DOSY pulse sequence. The period a ensures that all parts of the sample receive some degree of dephasing; two periods of gradient evolution ***b*** *are included before and after the frequency-swept pulses, so as to reject coherence transfer pathways that result from imperfections in the sweeps; period* ***c*** *rejects magnetization that is transverse during the longitudinal delay;* ***d*** *is a ramping period for the gradient pulses; finally, the additional gradient period of duration* $\boldsymbol{t_p}$ *ensures that every position in the sample receives a different diffusion weighting.* $\boldsymbol{G_d}$, $\boldsymbol{G_r}$ *and* $\boldsymbol{\Delta}$ *are respectively the encoding gradients, the acquisition gradient and the diffusion delay. Reprinted with permission from* [41] *Copyright © 2003 John Wiley & Sons, Ltd.*

Spatial encoding is achieved by combining chirp pulses with gradient pulses [193,194]. Chirp pulses are radio-frequency (RF) pulses, the frequency of which changes linearly as a function of time: $\omega_c(t) = O_i + Rt$ with $R = \frac{BW}{T_e}$. R is the rate of the sweep, T_e the chirp duration, O_i is the initial frequency and BW the total frequency range swept by the pulse [187]. At a given time, the pulse has a specific frequency value. Spins that have a resonance frequency close to this value will then flip under the effect

of the pulse. Since magnetic-field gradient induce a position-dependent frequency $\omega(z)$ for the spins precessing at $\omega(z)$, the chirp pulse will act $\omega(z)$ match $\omega_c(t_z)$, at a time $t_z = \frac{\gamma Gz - O_i}{R}$.

As a result, spins are flipped sequentially from one extremity of the sample to another. The flip is assumed to be instantaneous and ineffective for $\omega(z) \neq \omega(z_j)$. The phase acquired after the chirp swept is quadratic, and of the form

$$\phi_q(z) = T_e \left(\frac{z}{L}\right)^2 BW = \frac{\gamma^2 G^2 z^2}{R} \tag{4.1}$$

where L is the length of the swept region, defined by $BW = \gamma GL$.[1] To get an observable signal, the quadratic phase created needs to be fully refocused so a second, identical chirp pulse is applied under a gradient of the same sign. In diffusion experiments, the second chirp pulse combined with a gradient is incorporated at the end of Δ delay. What is left is a magnetization whose attenuation, due to spin displacement during the diffusion delay, is position-dependent. It can be described as

$$S_{(z)} = S_0 e^{-(DK(z)^2\Delta)} \tag{4.2}$$

Where $K(z) = \frac{d\phi_q}{dz} = \frac{2\gamma^2 G^2 z}{R}$. Different part of the sample experiences a different degree of attenuation during Δ' as the effective gradient strength that affect the spins increases linearly from one extremity of the sample to another. The diffusion information is encoded along the observed region of the sample.

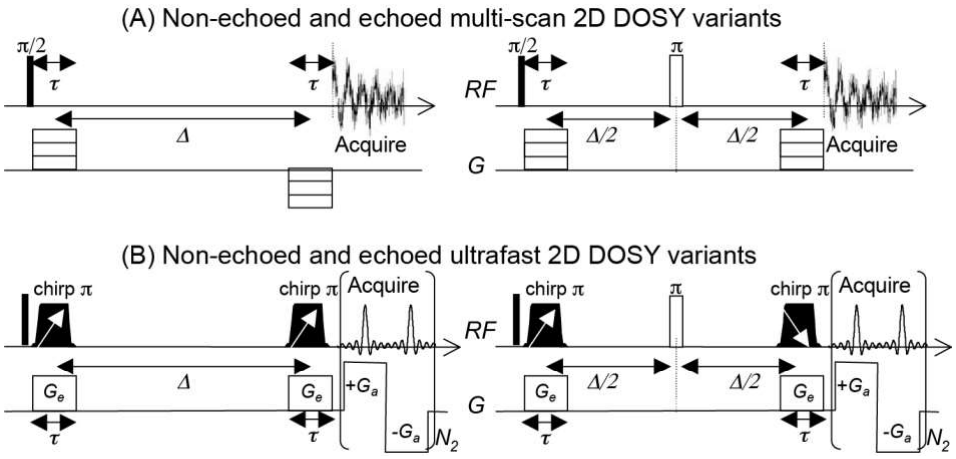

Figure 19: Comparison between conventional (A) and ultrafast (B) 2D DOSY experiments based on pulsed-gradient spin-echo sequences. Diffusion in (A) is encoded via the incrementation of G-values throughout separate scans; this can be carried out with full refocusing of coherent evolutions by applying a central p pulse and reversing the relative signs of the gradient pulses (right). In (B) this encoding proceeds by imparting spatially-dependent q-values throughout an otherwise homogeneous sample. Without a central refocusing p pulse (left) the directions of the two spatially-encoding pulses need to be identical in order to cancel each other out; if a central refocusing p pulse is employed then the senses of the two p pulses need to be reversed (right). In either case, the

[1] The quadratic phase can also be generated with a non-linear gradient pulse although it is not a practical solution

±Ga oscillating acquisition gradient enables one to read-out this indirect-domain encoding, without compromising the direct-domain spectral resolution. Reprinted with permission from [42]*Copyright © 2008 Elsevier Inc*

The methods described by the Frydman and Keeler groups are similar considering the fact that they use a spatial encoding block to encode diffusion. These strategies differ from one another by the acquisition block used to recover both spatial and spectral information in a single scan. Indeed, 1D DOSY is characterized by signal acquisition under a weak read gradient (less than 0.1 % of the maximal value) whereas single-scan 2D DOSY uses an EPSI (Echo-Planar Spectroscopic Imaging) train of bipolar gradient pulses. In the case of EPSI, the spatial dimension is obtained with one readout gradient and the spectroscopic dimension is generated by N pairs of bipolar gradients. Fourier transformation in both dimensions gives images of the sample for each chemical shift offset. The diffusion profile is observed in the spatial profile for each peak. In the case of the one-dimensional DOSY, a weak read gradient is applied during the acquisition and it will induce a broadening of the signal along the chemical shift axis. The peaks are diffusion weighted images of the observed region of the sample and reflect the effect of the gradient strength throughout the sample. These methods were successfully applied to separate compounds of a mixture even though a decrease in resolution and in SNR are a limitation. A recent development that exploits a spatial encoding of the diffusion dimension, is ultrafast Laplace NMR [195,196]. In UF LNMR, diffusion and relaxation properties are correlated, with applications in the analysis of heterogeneous samples.

4.4. Accelerated multi-scan DOSY

In this section we describe several methods that are based on an incremented gradient area across a series of independent scans, but with a reduced experiment duration compared to the standard method.

With the Oneshot experiment, phase cycling is circumvented and this significantly reduces the experiment duration, as it is no longer necessary to perform the 16 scans per gradient increment [113]. The selection of the desired coherence transfer pathway (CTP), that is to say the type of coherence order that will remain until the end of the pulse sequence and contribute to the final spectrum, is achieved using unbalanced gradients pulses. The Stejskal Tanner equation is then modified to account for the contribution of the CTP-selection gradients. The pulse sequence scheme can be seen in figure 4 of section 3.

Another approach to reduce the total experiment duration is to reduce the delay between consecutive scans, using for example the Band-selective Excitation Short-Transient (BEST) method, which for biomacromolecules yields an effective longitudinal relaxation time that can be 3 to 5 time shorter than the actual T_1 value [197]. This approach has been used in an example of 3D-BEST DOSY [37].

For 3D experiments, the total number of increments can be reduced, e.g., with a joint sparse sampling of the indirect time and diffusion dimensions as illustrated by Figure 20. This was demonstrated with a 3D CT–HSQC–iDOSY experiment [36]. Randomly selected values of t_1 and g are recorded, and the data is reconstructed with the ITAMeD algorithm. The 3D experiment can be acquired in the time required for a 2D, without sacrificing resolution. Another approach to reduce the number of increments is to co-increment the t_1 and g variables, using the Accordion strategy [198] [199].

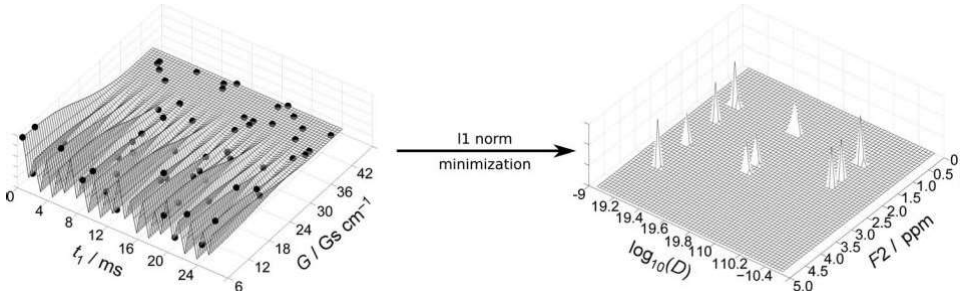

Figure 20: Joint sparse sampling of the time and gradient domains in diffusion-ordered NMR spectroscopy. Reprinted with permission from [36] *Copyright © 2014 Wiley-VCH Verlag GmbH & Co. KGaA, Weinheim.*

4.5. Conclusions

Various strategies for the acceleration of DOSY were presented and the methods involve either modification of the encoding parts of the experiment, modification of the acquisition part of the experiment or both. The methods based on multiple gradients pulses seems to be strongly impacted by additional signal loss due to relaxation so two transients are required and the method based on multiple RF pulses do not provide spectral resolution and suffer from severe sensitivity issue. Among all the methods described, the one that seems to be the most promising and compatible with our objectives is the spatial encoding strategy that provides DOSY data in less than one seconds. These methods were successfully applied to separate compounds of a mixture and will be further described, analyzed and compared in sections 6 and 8. Compared to the other ones, this strategy of acceleration was generalized for many other pulse sequences apart from DOSY so its applicability seems to be general and we want to explore it for DOSY. Perspectives for methodological development with this approach are high.

5. Addressing sensitivity limitations in liquid-state NMR of mixtures

NMR spectroscopy suffers from a low sensitivity that is due to the small population difference between nuclear spin states. Much efforts have been made in order to increase this sensitivity with novel instruments, experiments and sample preparation [43]. This section describes the origin of low sensitivity of liquid state NMR, and presents several means to address this drawback, including recent developments that provide increased levels of polarization.

5.1. The sensitivity problem of NMR

The most commonly studied nuclei in NMR spectroscopy are ^{1}H, ^{13}C, ^{15}N, ^{19}F, and ^{31}P. These nuclei possess two quantified spins states with a nuclear spin quantum number I = l/2. When immersed in a magnetic field, the spin populations will be distributed between the two states, with an excess of spin in favour of the alignment along the field. The relative number of spins in the up and down levels (respectively N_α and N_β) at thermal equilibrium are given by the Boltzmann distribution:

$$\frac{N_\alpha}{N_\beta} = e^{\frac{\gamma \hbar B_0}{kT}} \tag{5.1}$$

where γ is the gyromagnetic ratio, k is the Boltzmann's constant, T is the temperature and B_0 is the main magnetic field. This distribution is dependent on magnetic field and temperature. It is the difference between the populations of those spin states that is detectable by the NMR spectrometer. For example, for a sample placed in a 18.7 T magnetic field at room temperature (300 K) this ratio is equal to 0.999872. It means that if there are 1,000,000 nuclei in the upper energy state there are 1,000,128 nuclei in the lower energy state. This is why the sensitivity of NMR spectroscopy is limited. Indeed, only this small excess in the lower energy state is detected by the spectrometer after excitation. The remaining parts of the populations will compensate each other. The relative population difference is defined as the nuclear polarization level, which is given by:

$$P = \tanh\left(\frac{\gamma \hbar B_0}{2kT}\right) \tag{5.2}$$

This polarization level tends to be very small – in our example it would be equal to 0.006%. This is a principal reason for the limited sensitivity of NMR spectroscopy.

Many instrumental developments as well as signal processing and acquisition strategies were developed and contributed to the increase in sensitivity. A main approach to increase polarisation levels and in turn sensitivity consists in increasing the value of the static magnetic field B_0. This has led to a race for higher and higher magnetic field culminating in the upcoming release of a 28 T high-resolution

NMR spectrometer. While polarisation levels scale linearly with B_0 in the high-temperature limit, as illustrated in Figure 21, sensitivity measured as the signal-to-noise ratio (SNR), scales as:

$$S/N \sim {B_0}^{3/2}\gamma^{5/2} \tag{5.3}$$

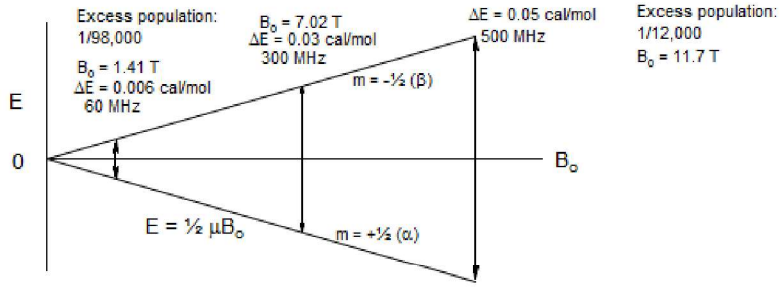

Figure 21: Effect of the magnetic field on the Boltzmann population difference in NMR. © 2010-2018 Hans J. Reich, All Rights Reserved. [200]

In terms of instruments, other developments include the design of the receiver coils, shimming technology, and the use of cryogenically cooled probes. All of these optimizations combined together led to better sensitivity and better lineshapes. Decreasing the signal linewidth lead to higher peaks hence higher signal to noise ratio since it is related to the signal peak height. Sensitivity can also be increased by appropriate sample preparation. Isotopic labelling can be performed in the case of nuclei with low natural abundance, although it is not applicable to arbitrary molecules. The use of NMR tubes with magnetic susceptibility (Shigemi tubes) matched to that of the solvent makes it possible to reduce the sample volume, and thus increase the concentration for mass-limited samples. Smaller NMR tubes, and coils with a smaller diameter can also be used to analyze very small amounts of sample. Pulse sequences have also been developed, which provide an increased sensitivity. They are commonly used to study nuclei other than ^{1}H that possess smaller abundance hence are quite insensitive. The INEPT (Insensitive Nuclei Enhanced by Polarization Transfer) pulse sequence transfers magnetization from ^{1}H to a heteronucleus, provided that a scalar coupling exists between the nuclei. The Heteronuclear NOE (Nuclear Overhauser Effect) is also used to increase the sensitivity for nuclei with close spatial proximity. Signal averaging during the course of the experiment improve the SNR of a factor $\sqrt{n}$, where n is the number of signals averaged.

Taken together, all of these improvements have led to significant increases in sensitivity, especially since they are commonly combined. However, even larger increases can be obtained by taking nuclear spin populations far from their thermal equilibrium values.

5.2. Hyperpolarization strategies

Several methods have been developed to obtain strongly polarized nuclei, with polarization level closer to 1. One can cite "brute force" hyperpolarization at ultralow temperature (mK regime) and high field (14 T) [201], Spin-Exchange Optical Pumping (SEOP), Para-Hydrogen-Induced Polarization (PHIP) method and its variation Signal Amplification By Reversible Exchange (SABRE), and Dynamic Nuclear Polarization (DNP). Here we will present the DNP and SABRE methods, that have led to the most promising results so far for mixture analysis.

5.2.1. D-DNP

Dissolution dynamic nuclear polarization (D-DNP) is a hyperpolarization method that provides signal enhancement up to 50 000 for solution-state NMR [45–48]. This popular method is based on transferring some electron polarization to the nuclei of interest. The sample needs to be prepared with a solvent mixture that will form a glass when frozen at liquid helium temperatures (between 1.2 and 4 K), and a polarizing agent that contains a paramagnetic radical. The most commonly used solvent mixture consists of glycerol and a mix of deuterated and undeuterated water. The main polarizing agents are trytil radicals, for the direct polarisation of heteronuclei, as well as TEMPOL, used to polarise protons. The polarization transfer occurs upon microwaves irradiations. The sample is then dissolved with a super-heated solvent and quickly transferred to a high field spectrometer via capillaries to perform liquid state NMR experiments.

The major downside of D-DNP experiment is that the amplified signal lasts only for short time, depending on the observed nuclei's longitudinal relaxation rate T_1. This means that, after thawing of the frozen hyperpolarized sample, the transfer time needs to be as short as possible so that not all of the signal is gone when the sample arrives in the high field spectrometer. This transfer time should be shorter that T_1 and typical apparatus provide 5 to 10 s for transfer, while fast injection methods operate in about one second [202,203]. Several methods have been developed to preserve the polarization once the sample is in the liquid state. This can be done by removing the remaining free radicals in the solution by using scavenger such as sodium ascorbate. This is because radicals, as they are paramagnetic, tend to further reduce the T_1 of nuclei thus increasing the decay rate of the amplified signal. Another strategy consists in using long-lived nuclear spin states that originate from system with nuclear spin states delocalized over two or more spins [204,205]. Pulse sequence are also designed to preserve the magnetization for a sufficient duration, notably using small tip angle excitation pulses, and refocusing pulses that are insensitive to calibration errors. The short lifetime of the polarization, together with its non-renewable nature, also has an effect on the range of experiments that can be performed and running

experiments other than 1D a real challenge [206]. Improvement of the polarization of other nuclei than ^{1}H can be done by cross polarization strategies. Indeed ^{1}H polarization level is high and reached very quickly compare to ^{13}C for example. This is because of its high magnetogyric ratio. Additional T_1 is very short so it can be better to observe ^{13}C that have a longer T_1 (especially quaternary carbons). However, they tend to have lower polarization level. By polarizing ^{1}H first then transferring this polarization to ^{13}C via CP, on can significantly increase ^{13}C polarization in a short amount of time [207,208].

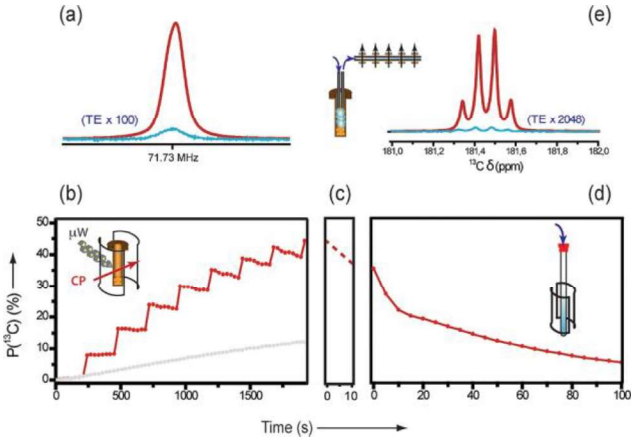

Figure 22: (a) Signals of ^{13}C NMR of 50 μL of a 3 M frozen solution of 1-^{13}C-enriched sodium acetate in a deuterated water/ethanol mixture (67:33 v/v) doped with 50 mM TEMPO measured without CP (blue) at thermal equilibrium (T = 4.2 K and B0 = 6.7 T, scaled by a factor 100) and with CP-DNP (red) (Pμw = 120 mW at fμw = 188.3 GHz). (b) ^{13}C DNP buildup with (red) and without (gray) CP measured every 30 s with β =5° pulses. CP was performed every 240 s. (c) The dissolution and transfer process require tdiss = 10.7 s. (d) Relaxation of ^{13}C in solution at ~T = 300 K after transfer to a magnetic field B0 = 7.05 T, measured with β =5° pulses at 5 s intervals. (e) Signals of 1-^{13}C sodium acetate immediately after dissolution (red) and at thermal equilibrium (blue, scaled by a factor 2048)]. Reprinted with permission from [207] *Copyright © 2012 American Chemical Society.*

5.2.2. SABRE

The **S**ignal **A**mplification by **R**eversible **E**xchange (SABRE) method consists in a transfer of spin order from parahydrogen to the substrate [49,50], mediated in a metal complex. Dihydrogen molecules exist as two spin isomers. The ortho isomer is characterized by a symmetric triplet spin state while the para isomer possesses an antisymmetric singlet spin state. At room temperature and thermal equilibrium, the ortho/para distribution is close to 75/25. Conversion from one form to another (ortho to para) is also very slow because of symmetry restrictions. The ortho/para distribution can be shifted towards the para form by taking dihydrogen gas at low temperature and using a paramagnetic catalyst. If the gas is flowed through a catalyst such as ferrous oxide at liquid nitrogen temperature (77 K), this will ensure an

approximately 50/50 distribution. Higher conversion levels can be achieved by going to lower temperatures as shown on Figure 23. The para state can be preserved for several hours or even days when returning at room temperature, provided that no paramagnetic impurity is present.

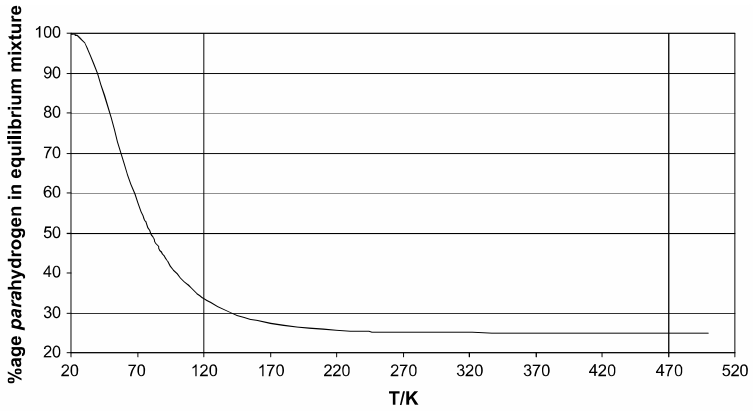

Figure 23: Calculated change with temperature of the percentage of parahydrogen in an equilibrium mixture of ortho- and parahydrogen gas. Reprinted with permission from [209] *Copyright © 2012 Elsevier B.V. All rights reserved.*

Parahydrogen can be exploited as a source of nuclear polarization in several ways [209,210]. In the original PHIP methods called ALTADENA and PASADENA, p-H_2 is added to unsaturated organic molecules via catalytic hydrogenation. This approach provides very high signal enhancements but it also transforms the substrate and requires a hydrogenable bond. The SABRE alternative [211,212] is gentler and does not alter the integrity of the substrate.

The SABRE process relies on the formation of a temporary intermediate complex formed by parahydrogen, the substrate and a metal catalyst. As the three partners belong to the same complex, the symmetry of p-H_2 is broken and spontaneous transfer of magnetization occurs. The polarization step is performed at low magnetic field outside the spectrometer [213,214]. The chemical environment experienced by the two protons upon hydrogenation breaks the singlet symmetry and renders the spin system detectable by NMR. The complex is then dissociated releasing the hyperpolarized substrates [215]. Catalyst frequently used are [Ir(COD)(IMes)Cl], **C1**, or [Ir(COD)(PCy_3)Cl], **C2**, (COD= cyclooctadiene, PCy_3= tricyclohexyl phosphine, IMes= 1,3-bis(2,4,6-trimethylphenyl)imidazole-2-ylidene) which are iridium complexes with either phosphine or carbene ligands [213,216]. It has been demonstrated that **C1** is a better catalyst than **C2** [212]. Note that the study of low concentrated mixture requires the use of a co-substrate [217]. Indeed, when the concentration of substrate, **S**, ligand decreases (**S** to **C1** ration below 3:1), the signal enhancement decreases as well because the solvent competes with the analyte for biding to the catalyst. When the solvent is bound to the catalyst, the later becomes inactivated, e.g. [Ir(IMes)$(H)_2(S)_2$MeOH]Cl is formed. The co-substrate is here to restore the catalyst activity by preventing the solvent from binding to the catalyst.

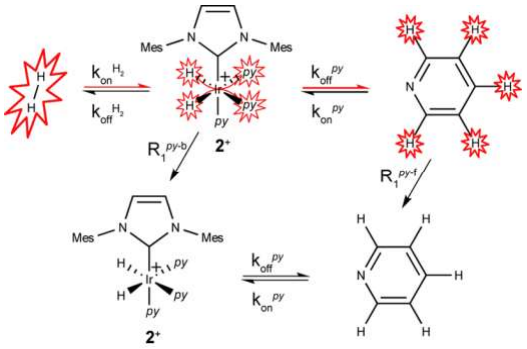

Figure 24:Schematic representation of spin order transfer from p-H_2 to py and resulting proton hyperpolarization of py both bound and free in solution. Reprinted with permission from [217] *Copyright © 2014 American Chemical Society.*

SABRE, in its most common implementation, is an ex-situ method and once in the detection magnet the enhanced signal last for few seconds depending on the longitudinal relaxation time T_1. This approach grant high level of polarization at low cost as the population difference between spins states can be increased several orders of magnitude. Polarization level strongly depends on the substrate and H_2 rate constant, the concentration of the reagents and the strength of the magnetic field where the transfer takes place.

Importantly, the SABRE process can be repeated on the same sample, provided that fresh parahydrogen is available. While the simplest implementation relies on a batch of parahydrogen and manual sample shaking, flow approaches have also been developed. These make it possible to carry out multi-scan experiments with SABRE [218].

5.2.3. Applications for mixture analysis

The main applications of hyperpolarized NMR are found for in vivo studies such as metabolic activity in tissues studied with hyperpolarized pyruvate, or real-time enzyme kinetics with hyperpolarized sugars [219,220]. The study of biosynthetic pathways, the detection of low-populated reaction intermediates and of protein–ligand interactions have also been reported [219–221]. Application of DNP strategy for mixture analysis was recently done in the case of plant extract [46] and metabolic mixture studies [222]. Diffusion experiment were performed on acetylation reaction of amino acids, however, the diffusion measurement is impacted by continuous signal loss due to T_1 [206,223]. Other diffusion measurement with DNP that use a more efficient injector system was also published [202]. SABRE is mainly used for nitrogen-based molecules but applications are also found with small molecules such as peptides [217,224,225]. Recently use of SABRE method was published for DOSY experiment using an inflow

approach [218]. The challenge is to get rid of convection effect which is always present and quite severe in this kind of experiment. Application for chemosensing in natural extracts was also published [225]. In vivo application of DNP need of non-toxic particles such a nanodiamond as a source of electron/ polarizing agent was also documented [226].

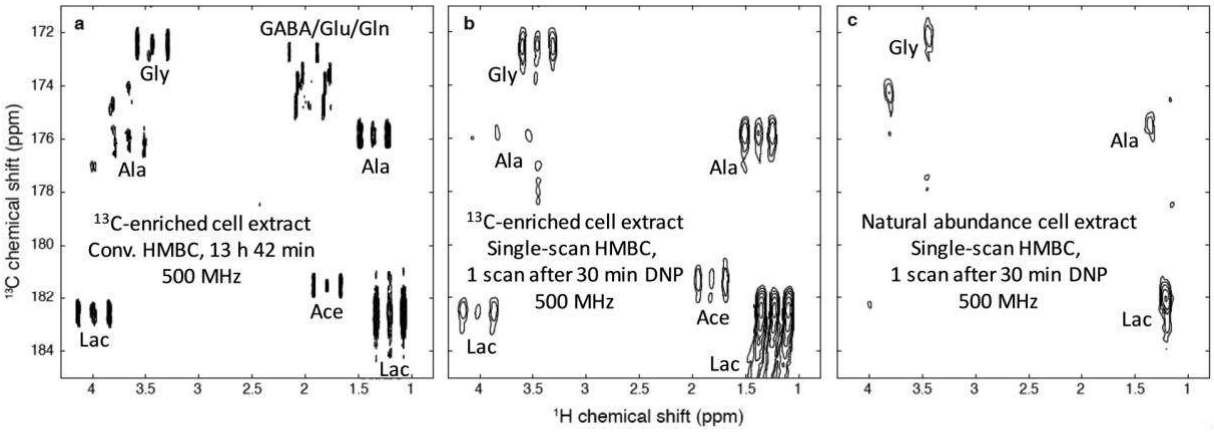

Figure 25: $^{1}H \rightarrow ^{13}C$ HMBC-type spectra of extracts of SKBR3 human breast cancer cell lines. (a) Conventional HMBC spectrum, recorded in 13 h 42 min at 500 MHz with a cryogenic probe, on a partially enriched extract (ca. 57 million extracted cells) dissolved in 700 µL D_2O. (b) Hyperpolarized single- scan spectrum. The cell extract was dissolved in 200 µL of a mixture of H_2O/D_2O/glycerol-d8 (2 : 3 : 5) with 25 mM TEMPOL and polarized for 30 min at 1.2 K and 6.7 T, and finally dissolved with 5 mL D_2O. A fraction of 700 µL of the hyperpolarized sample was injected in a 500 MHz spectrometer equipped with a cryogenic probe where the spectrum was recorded in a single scan. (c) Same as (b), but with a natural abundance extract (ca. 113 million cells) obtained from the same SKBR3 cell line. Ace: acetate; Ala: alanine; GABA: γ-aminobutyrate; Gln: glutamine; Glu: glutamate; Gly: glycine; Lac: lactate. Experimental details are given in the ESI.†]. Reprinted with permission from [46]*Copyright © The Royal Society of Chemistry 2015*

5.2.4. Limitations

Both SABRE and D-DNP provide high levels of polarization for a wide range of molecules. Protocols are quite different and are note operated over the same duration range. In terms of cost the SABRE is a relatively cheap option compared to DNP. SABRE appear to be limited since it is only possible to polarise certain classes of compounds even if progress where made to extend the substrate range [227]. Hyperpolarization of nuclei other than ^{1}H is also possible, either relayed by ^{1}H polarisation of directly [205,227]. As we said previously, T_1 is the main limiting factor that control amplified signal lifetime. With these strategies, sensitivity would no longer be a problem and low concentration level can be achieved. The short duration of the signal stress the need of faster acquisition methods in order to do

more than simple pulse acquired experiments [46,49,222,228]. This will hopefully provide access to richer information on the studied samples.

5.3. Conclusions

In conclusion, the two routes described here provide high level of polarization and depending on the application targeted, one or the other method can be favored. It seems that DNP is more oriented towards studying dynamic processes whereas SABRE seems to be well indicated for trace compounds detection. In both cases, the signal life time is really short (barely more than 1 min) and fast NMR experiments are needed to acquire these signals. 1D experiments are easy to perform but the real challenge is for multidimensional experiments. For mixture analysis this is of paramount importance because this simplify a lot the separation and identification of the signals. Continuous progress are made regarding the efficiency of polarizing agent, catalyst, substrates preparation, experimental conditions and apparatus to increase the polarization level further, to expand the range of applications and to ease the polarisation process.

Part 2: Results

6. Practical aspects of spatially encoded DOSY

6.1. Introduction

Several strategies to speed up the acquisition of DOSY data were presented in section 4. In this work, we made the choice to use spatial encoding (SPEN) in order to record DOSY spectra in less than 1 s. SPEN DOSY NMR is based on the use of a spatial dimension to encode diffusion and accelerate experiments. Decoding of the diffusion information was done by using an appropriate spectroscopic imaging scheme. As a result, the diffusion effect was observed in the lineshape of a 1D spectrum or as an additional spatial dimension. This section presents the steps that we have followed in order to implement and optimize the SPEN DOSY experiment. The two options for acquisition were evaluated in a qualitative way in terms of accuracy of diffusion coefficients, resolution and processing compared to the conventional DOSY experiment that serves as a reference. Further description on the SPEN DOSY pulse sequence will be made in section 8. The aim of this study is to develop fast methods for spectral separation and explore the option of spatial encoding for sequences that involve diffusion weighting.

6.2. Experimental section and reference experiments

All the experiments were carried on a Bruker spectrometer operating at a magnetic field of 600 MHz equipped with a triple-axis gradient probe used on the ^{1}H channel. The temperature of the sample was set at 293 K. A gradient calibration constant value along the z-axis of G_{max}=0.65 T/m was taken from constructor specifications. The diffusion gradients have a *half-sine* shape for conventional experiments. For SPEN DOSY experiments, a trapezoidal shape was used for diffusion encoding, with ramping period of 25 μs. Diffusion was encoded over a 10 mm sample range for SPEN DOSY, a 10 mm sample range for conventional experiment on Shigemi tubes and an approximately 15 mm sample range for conventional experiment using the classic tube.

6.2.1. Sample

Two types of NMR tubes were tested: classical 5 mm tubes and Shigemi tube with a fixed sample length of 10 mm. The sample was prepared mixing caffeine (5.8 mg) and ethylene glycol (2 µl) in 600 µl of D_2O. The mixture was shaken until complete dissolution of caffeine and filtered to remove any solid particles.

6.2.2. Conventional DOSY parameters

Conventional 2D spectra were recorded using a stimulated echo sequence with bipolar gradient pulses with additional LED and spoil gradients (the **ledbpgp2s** sequence in the Topspin software). The 1D version of this sequence was run for parameter optimisation. The diffusion-encoding gradient values consisted of a linear ramp ranging from 0.00325 T/m to 0.4875 T/m. The diffusion time was set to 100 ms. The duration of the bipolar gradient pulses for diffusion encoding was 1 ms. The data were acquired with 16384 points, 8 dummy scans, a spectral width of 6000 Hz, a relaxation delay of 2 s and 16 gradient steps, resulting in a total experiment duration of 19 min 41 s.

6.2.3. Processing

The data from conventional DOSY experiments were processed with the DOSY Toolbox, which is an open source program for PFG diffusion NMR data processing [122]. For all SPEN experiments, the data were processed in MATLAB (The Mathworks, Natick, U.S.A.) using home-written routines, adapted in part from the DOSY Toolbox. For SPEN 2D DOSY, the nD SPEN data was read from Bruker files, then sorted and reshaped in order to get a nD matrix. The data was multiplied by a sine function and zero-filled in the conventional dimension. Only the odd echoes were retained, and Fourier transformation was performed along both dimensions. The spectra were processed in magnitude mode. Peak maxima were selected manually and the spatial profile for each peak was obtained as a row of the (z,ω) data set. The spatial profiles were fitted with a Stejskal-Tanner equation for all resonances. In the case of the 1D DOSY experiment, the data is similar to the 1D pulse-acquire experiment so zero filling, apodization, FT and phase correction was performed. The spatial profiles were fitted with a Stejskal-Tanner equation for all resonances after peak picking and selection of the decaying part of the lineshape.

6.2.1. Reference experiment results

Figure 26 shows the reference DOSY display for the studied mixture using a conventional DOSY experiment. This model mixture was chosen because all the observed signals are non-overlapping singlets. Moreover, the molecules studied are of various sizes. Together with the limited number of species this ensures that resolving the associated diffusion coefficients will be easy using monoexponential fitting. Good resolution of the signals was obtained as expected. Notice that one of the caffeine peaks at 7.9 ppm is rather weak as it corresponds to an exchangeable proton. The diffusion coefficient values were obtained via DOSY Toolbox processing and were used as references for comparison with the proposed SPEN DOSY experiment.

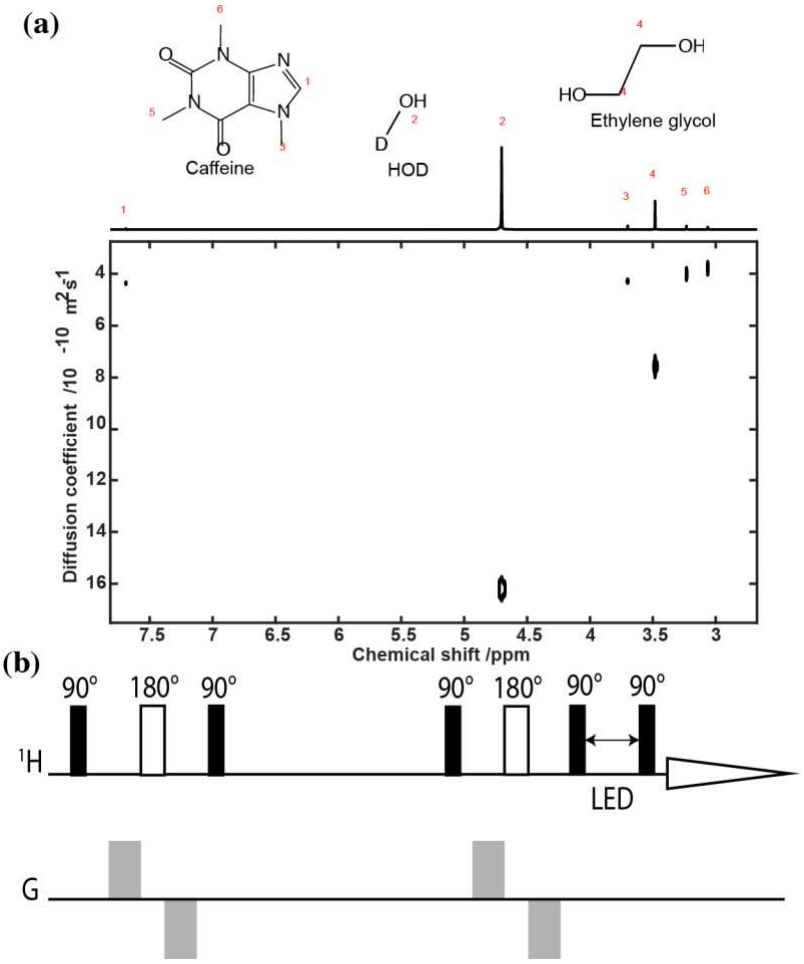

Figure 26: (a) Conventional DOSY display acquired on the mixture of caffeine and ethylene glycol in D_2O. (b) Conventional DOSY sequence used for reference measurement. Calculated values of diffusion coefficient using the DOSYToolbox were 4.12 × 10^{-10} m^2 s^{-1} for caffeine, 7.57 × 10^{-10} m^2 s^{-1} for ethylene glycol and 16.4 × 10^{-10} m^2 s^{-1} for HOD.

6.3. Spatially-encoded 2D DOSY: pulse sequences design

The design of experiments that rely on a spatial dimension to encode diffusion was initiated by Thrippleton, Loening and Keeler. They proposed a fast diffusion coefficient measurement strategy that make it possible to extract the diffusion information from a 1D spectrum of the mixture [41]. A similar approach was presented later on by Shrot and Frydman, where the diffusion effect is encoded along an additional spatial dimension [42]. Both approaches rely on the same diffusion-encoding concept considering the fact that they use a spatial encoding scheme [39]. These strategies differ from one another by their acquisition part that is inspired from spectroscopic imaging schemes. These published results were used as a basis for our experiments. The work presented here, that was a preliminary step of the overall project, consists in understanding, comparing and optimizing these existing encoding and spectroscopic imaging schemes.

6.3.1. Spatial encoding of diffusion

Gradient pulses are used to get information about the translational motion of molecules within a mixture [95,96,105]. They induce attenuation in the signal arising from each molecule. By increasing their value gradually, the signal is attenuated progressively and follows an exponential behaviour (cf. section 3) [106,114]. This creates the indirect dimension in the 2D experiment with the area of the gradient as the incremented parameter. This classic time-dependent encoding of the diffusion dimension can be modified so that the gradient area becomes spatially dependent. Figure 27 shows a comparison between the classic scheme, left, and the spatial encoding scheme, right. In the second option, the sample can be seen as virtually sliced in multiple sub-sections with an associated gradient area that increase from one extremity of the sample to another. Spins located in different slices within the sample are then submitted to different values of the gradient area. The diffusion information is hence encoded along the observed region of the sample.

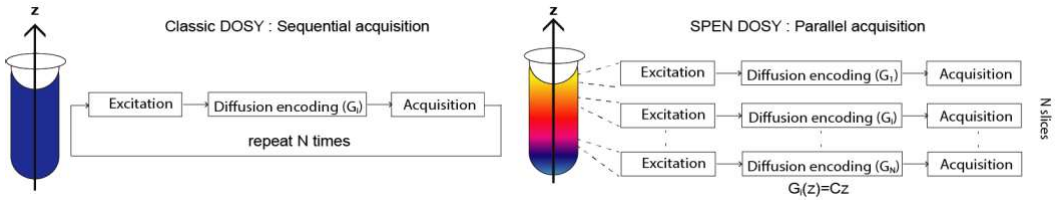

Figure 27: Classic diffusion encoding (left) versus spatial diffusion encoding (right). In the classic DOSY experiment, N spectra are acquired with increasing values of G. In the spatially encoded DOSY, the sample can be seen as sliced N times were each slice correspond to a G_i increment that will give N spectra acquired simultaneously.

In order to create such partition, linearly frequency-swept "chirp" pulses and gradients pulses are associated to perform a sequential excitation of the spins across the sample. Since two sets of bipolar gradient pulses are used in conventional DOSY, two set of gradient/ chirp pulses are needed as well so that the phase imparted by the first one is compensated by the second one, in the absence of diffusion. The SPEN DOSY pulse sequences described here are adapted from the stimulated-echo sequence (STE) with bipolar gradient pulses and the encoding part is shown in Figure 28c. 180° pulses were replaced by chirp pulses and combined with gradient pulses of same duration T_e. This combination gives a symmetric quadratic phase as illustrated in Figure 28b. This is the option proposed by Frydman and co-workers in their single-scan DOSY. The minimum of the phase corresponds to the minimum gradient strength where the signal measured will be the highest. This minimum is located in the center of the observed sample region and the diffusion range expend over half of the sample, in our case from 0 to 5 mm. The phase is calculated using

$$\phi = \frac{\gamma^2 {G_e}^2}{R}\left(\frac{z}{\mathrm{L}}\right)^2 \qquad (6.1)$$

A wider range of gradient area can be explored by adding an extra dephasing gradient period of duration T_p=T_e. The minimum of this phase will be shifted to one edge of the sample, hence the highest signal intensity as illustrated in Figure 35. Equation 6.1 will become:

$$\phi = \frac{\gamma^2 {G_e}^2}{R}\left(z + \frac{L}{2}\right)^2 - \frac{1}{4} \qquad (6.2)$$

This is the route taken by Keeler and co-workers with the One-dimensional DOSY. In this case, diffusion effect is spread over the whole observed region, in our case from –5 mm to 5 mm.

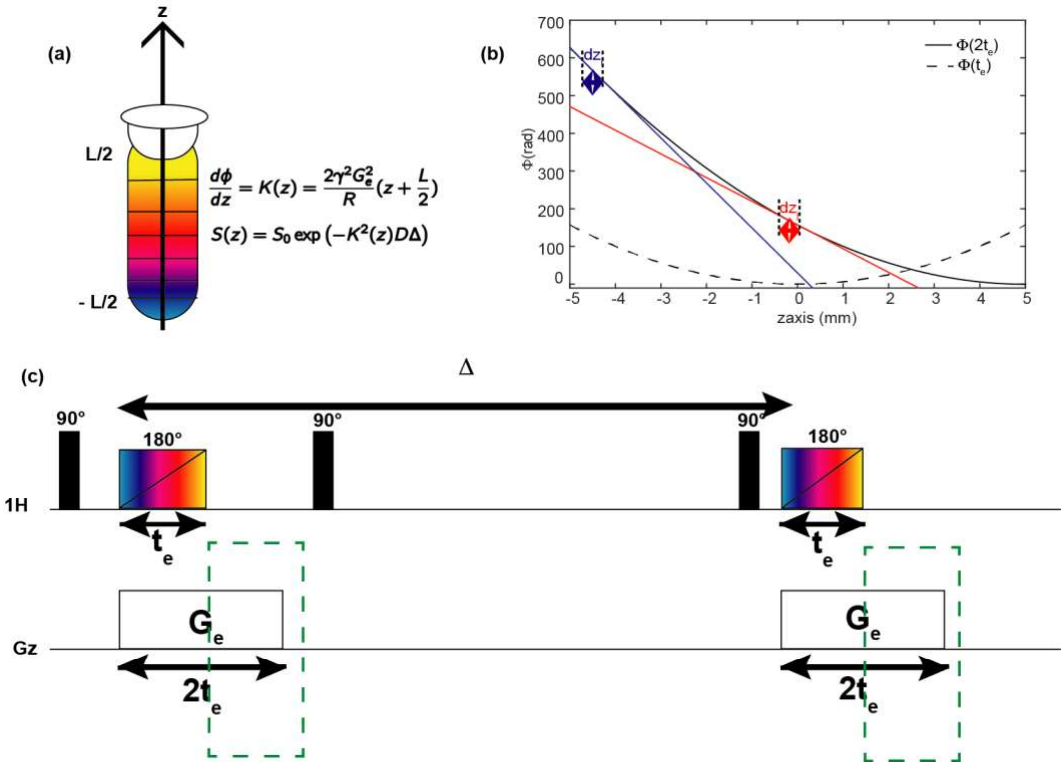

Figure 28: Phase variation during spatial encoding of the diffusion dimension. (a) Sample partitioned in several slices. (b) Phase imparted during spatial encoding with (solid black line) or without (dashed black line) post chirp gradient. (c) Excitation and diffusion encoding part of the pulse sequence. Pulse sequence is derived from the STE experiment and diffusion encoding is perform thank to pair of chirp pulses associated with gradient pulses. The phase induced by the chirp pulse is quadratic and can be shifted by using a post chirp gradient equal to T_e. This phase is locally linear.

For the data shown in this section, the diffusion-encoding parameters were chosen in order to sweep a region of 10 mm. The chirp bandwidth was set to 100 000 Hz, the encoding gradient was set to 0.2275 T/m, the chirp duration and the post-chirp gradient duration was set to 1 ms each. Diffusion delay was set to 100 ms.

6.3.2. Coherence selection

The selection of the desired coherence transfer pathway (CTP), that is to say the sequence of coherence orders that will be retained during detection and contribute to the final spectrum, can be achieved using gradient pulses. The coherence selection scheme used by our pulse sequence presented in Figure 29 was designed after the Oneshot experiment in order not to use phase cycling [113]. In the Oneshot case, a single gradient axis is used to perform both diffusion weighting and coherence selection. In our pulse sequence, the gradients were split between the three axes (x, y and z) of the probe, with the diffusion gradient along z and the others along x and y. This prevents unexpected gradient refocusing, which may

occur if all of them were on the same axis. It also avoids cross-term in the diffusion weighting. For the stimulated-echo block, consisting of two 90° pulses, the anti-echo pathway was chosen. Coherence selection involves the use of gradients to select the desired pathway and, and compensating gradients to reduce peak distortion due to lock disturbance. A spoiler gradient was placed during the longitudinal storage delay to diphase unwanted transverse magnetization and its balancing counterpart was inserted before the first 90° pulse. Unbalanced gradient pulses were used for simultaneous anti-echo pathway selection and spoiling around each chirp pulse (so that any magnetization unaffected by the chirp is rejected). Compensating counterparts of those pulses were placed between the last two 90° pulses of the stimulated echo for lock stability. In comparison with the original sequence proposed by Frydman, two spoil gradients were added to get rid of the part of the spectrum corresponding to the non-excited zone of the tube. The use of triple-axis gradients makes the implementation and analysis easier than with the original sequence since it reduces the number of gradient elements that should be taken into account during the fit of the results as it impacts its accuracy.

The gradient strength for coherence selection around the first chirp pulse were a = 0.065 T/m, $a + c$ = 0.1495 T/m with a duration of 800 µs. The gradient strength for coherence selection around the second chirp pulse were b = 0.1300 T/m, $b + c$ = 0.2145 T/m with a duration of 800 µs. The gradient strength for the spoiler during longitudinal storage was f = −0.3716 T/m and its counterpart g_1 = −f with a duration of 800 µs. Balancing pulses for lock signal retention were g_2 = (2a + c)/2 and g_3 = (2b + c)/2 with a duration of 1600 µs. The pre-phasing gradient, g_4, was set to 0.0975 T/m. The 2D experiment was recorded in a single scan of 241 ms.

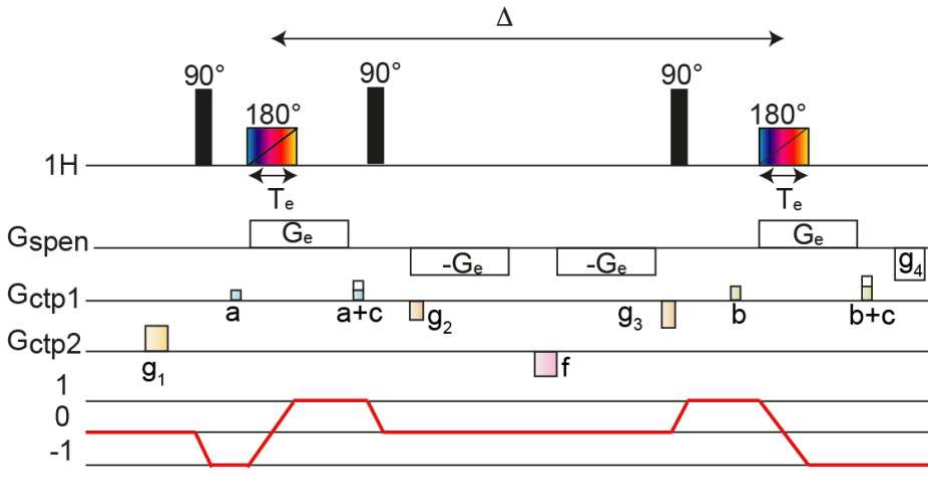

Figure 29: Coherence selection on triple axis gradients for SPEN 2D DOSY pulse sequence. The selected coherence transfer pathway is shown in red. Gradients a and b are crushers surrounding the refocusing chirp pulses; gradient c selects the anti-echo pathway for the stimulated echo; gradient f is a spoiler during longitudinal storage; g_1, g_2 and g_3 are compensating gradients; g_4 is the pre-phasing gradient used to shift the echoes in the k space.

6.3.3. Weak read Gradient Acquisition

After the position-dependent diffusion encoding, a spectroscopic imaging scheme is needed in order to reveal the diffusion weighted images of the sample. A weak readout gradient like the one illustrated in Figure 30 was then applied during the acquisition period. Values below 1 % of the maximum strength are usually required and the lower the value the better the spectral resolution. Indeed, when the acquisition is performed using a readout gradient, the precession frequency of the spins will include an additional term that varies linearly with their position in the sample. For a weak readout gradient, this leads to a broadening of each peak in the spectrum, that corresponds to an image of the sample. Provided that there are several resonances, we would obtain several images centered at the corresponding chemical shifts. This approach is however only applicable for weak values of the acquisition gradient. Suppose that we use a 0.065 T/m gradient, the dispersion induced by the gradient is 28 kHz for a 10 mm region according to $BW=\gamma GL/2\pi$. On the other hand, if it is a 0.000065 T/m gradient, the dispersion induced is of 28 Hz. Now, if we have two resonances separated by 136 Hz as in the sample caffeine and ethylene glycol, what happens is that in the first case ($BW \gg \Omega_{CS}$) the images created by the acquisition gradient will be superimposed and we will see only a single image. In the second case, however, the dispersion induced is smaller than the chemical shift difference ($BW < \Omega_{CS}$ so we are able to see two images as illustrated in Figure 31. This illustrates how using the weakest possible gradient will give the maximum spectral resolution.

Nevertheless, we said that the diffusion information is encoded in the lineshape of the image. It means that the image should be wide enough for the diffusion information to be observable. The decay should be correctly defined, that is to say well discretized to get accurate diffusion coefficient values. A compromise needs to be found between the resolution of the signals along the chemical-shift axis and the resolution within each image. As we saw, with this method, the risk of overlap is quite high. This could be limiting if too many resonances are present in the spectrum and needs to be contained in 10 ppm. With this 1D experiment, two pieces of information are encoded along the same dimension, chemical shift and diffusion property.

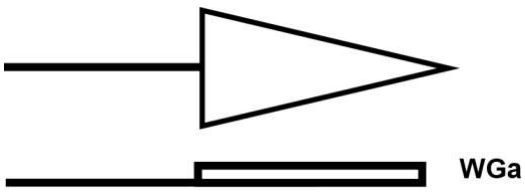

Figure 30: Spectroscopic imaging acquisition block used to recover both spatial and spectral information in SPENDOSY experiment. Acquisition is performed using a readout gradient with a weak intensity. Each peak corresponds to an image centered at the corresponding chemical shift.

Here we chose to use a 0.000195 T/m acquisition gradient strength. Since signal to noise ratio (SNR) depends on the acquisition gradient strength this value was suitable to keep balance between sensitivity and resolution. Figure 31 show the results of the variation of the acquisition gradient value and the best SNR is obtained for the smallest value of the gradient. However, the diffusion profile will be observed over a smaller range.

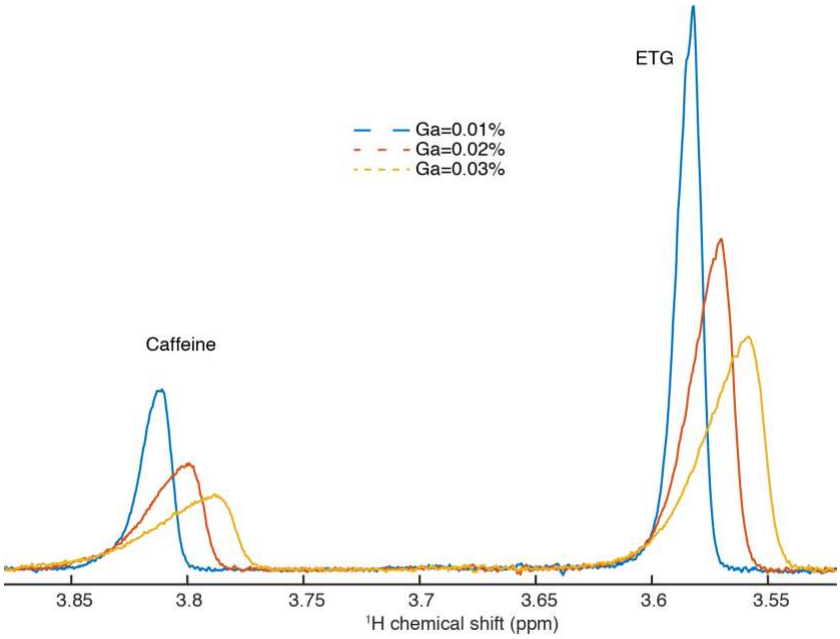

Figure 31: Comparison of spectrum acquired with different values of acquisition gradient. Section of spectrum showing the resonance of caffeine and ethylene glycol separated by 136 Hz. The acquisition gradient values in the SPENDOSY ranged from 0.000195 T/m to 0.00065 T/m.

6.3.4. Echo Planar Spectroscopic Imaging acquisition

In the approach explored by Frydman and co-workers the acquisition is performed using a train of bipolar gradient pulses in order to recover both spatial and spectral information [187]. This spectroscopic imaging acquisition block is illustrated in Figure 33. The "indirect", spatial dimension is obtained with one readout gradient, while the direct spectral dimension is generated by N pairs of bipolar gradients. The data is rearranged into a 2D matrix, and 2D Fourier transformation yields a data set in which one dimension corresponds to the chemical shift and the other one corresponds to position. The data shows one image for each peak, located at the corresponding chemical shift.

We know that gradient pulses result in a position-dependent precession frequency of the spins, which in turn creates magnetization helices. In this case, let's consider a single resonance that went through the spatial encoding process (with or without diffusion). When submitted to a single gradient, this creates a helix as illustrated in Figure 32. This helix will be refocused and will form an echo at a

time t_{cs} and be rewinding again at t_f. When the opposite signed gradient of the bipolar pair is applied, the reverse phenomenon is observed. This winding and unwinding of helices will occur during the N pairs of gradients. At the same time, the signal intensity is still evolving according to $exp(-t/T_2)$ and the chemical-shift modulation. The formed echoes will lead to a 'FID-like' signal that will decay overtime.

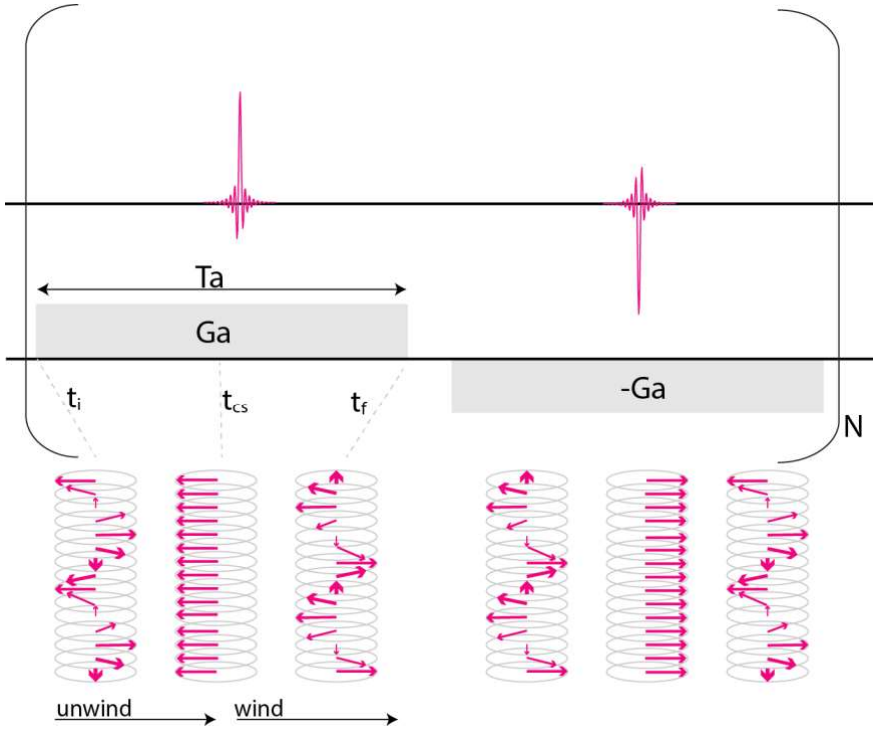

Figure 32: Acquisition in the presence of a train of bipolar gradient pulses for a sample a single resonance. The magnetization helix created at a time t_i is unwinded to form an echo at a time t_{cs} before being winded again at a time t_f for the remaining duration of the gradient. The reverse phenomenon is observed during the second part of the bipolar gradient pulse and so on during the N pair of gradients.

With this method, we can use strong acquisition gradients that give higher resolution within the lineshape of the images. The risk of overlap in the spectroscopic dimension is also significantly reduced. The diffusion lineshape is no longer distorted by multiplet splitting since $BW>>J$.

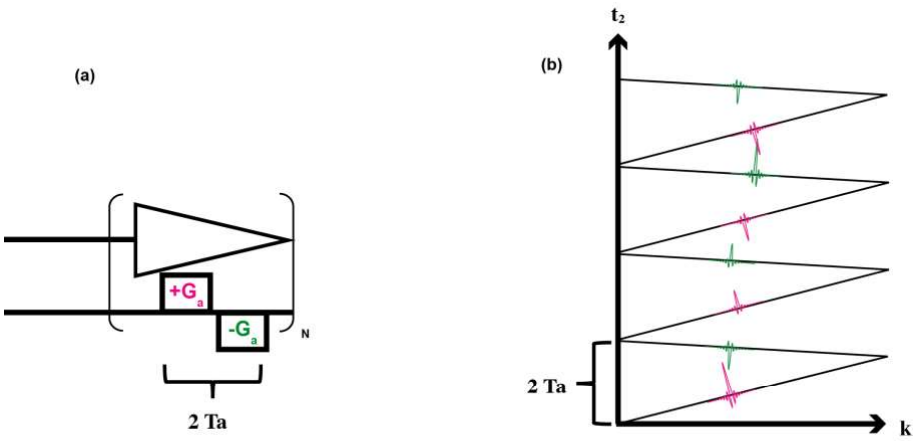

Figure 33: Spectroscopic imaging acquisition block used to recover both spatial and spectral information in SPENDOSY experiment. (a) Acquisition is performed using a train of bipolar gradient pulses. (b) Indirect dimension ,k , is obtained with one readout gradient; the direct dimension , t2, is generated by N pair of bipolar gradients.

Acquisition parameters were a 0.195 T/m acquisition gradient strength with a du ration of 384 µs, including a 25 µs ramping period, for a total number of 128 gradients loops of 128 points each. This results in a spectral width of 1300 Hz.

6.4. Diffusion coefficient determination and optimization

6.4.1. Theoretical models for diffusion curve fitting

In conventional DOSY experiment, the signal attenuation can be expressed by Stejskal-Tanner equation

$$S = S_0 e^{-(DG^2\gamma^2\delta^2(\Delta-\frac{\delta}{3})} \quad (6.3)$$

where S_0 is the initial amplitude of the signal, D is the diffusion coefficient, G is the gradient intensity, γ is the magnetogyric ratio for protons, δ the gradient duration and Δ the diffusion time. For SPEN DOSY experiments, a convenient approach to fit the data would rely on a model of a form analogous to equation 6.3:

$$S_{(z)} = S_0 e^{-(DK(z)^2\Delta')} \quad (6.4)$$

where $K_{(z)}$ is the effective gradient area at position z and Δ' a corrected diffusion delay. The initial model used by Frydman and co-workers [42] (model n°1) accounts for diffusion during the chirp so the diffusion delay is corrected as $\Delta' = \Delta + \frac{T_e}{2}$ with T_e the duration of the chirp, but with an approximate expression for $K_{(z)}$:

$$K_{(z)} = \frac{2\gamma^2 {G_e}^2 z}{R} \quad (6.5)$$

with $R = \frac{\gamma G_e L}{T_e}$, L the size of the observed region and G_e the encoding gradient. Additionally, the post chirp gradient is not taken into account in this formula. As we decided to include post chirp gradient on the basis of Keeler pulse sequence scheme we need to adjust the fitting model to suit our experiment. Analytical calculation of this equation was performed.

As described in section 4, chirp pulses are radio-frequency (RF) pulses, whose frequency changes linearly as a function of time:

$$\omega_c(t) = O_i + Rt \tag{6.6}$$

where $R = \frac{\gamma G_e L}{T_e}$ is the rate of the sweep, T_e the chirp duration, $Oi = -\frac{\gamma G_e L}{2}$ is the initial frequency and L the region swept by the pulse. At a given time, t_z, the pulse has a well-defined frequency. Spins that have a resonance frequency matching this value are assumed to flip 'instantaneously' under the effect of the pulse [42,229]. We explained earlier that linear gradient pulses induce winding of the magnetization along z-axis and spins not having the same phase and angular frequency according to their position. It is then straightforward to figure out the purpose of combining chirp and gradient pulses: while the sample is subjected to a linear magnetic field, the frequency offset of the spins is given by $\omega(z) = \Omega + \gamma G_e z$, the chirp pulse will affect spins when $\omega(z)$ match $\omega_c(t_z)$ at a time

$$t_z = \frac{\gamma G_e z + \Omega - O_i}{R} . \tag{6.7}$$

The phase acquired by the spins during the first chirp pulse can be express as

$$\Phi_1(t,z) = (\Omega + \gamma G_e z)t \qquad 0 < t < t_z \tag{6.8}$$

$$\Phi_1(t,z) = -\Phi_1(t_z,z) + 2\Phi_{rf}(t_z) + (\Omega + \gamma G_e z)(t - t_z) \qquad t_z < t < \tau \tag{6.9}$$

with $\Phi_{rf}(t) = O_i t + \frac{Rt^2}{2}$ and $\tau = T_e + T_p$.

At the end of the pulse *(t= τ)* and after substituting t_z expression, R expression in equation 6.9 the spatially dependent phase acquired after the chirp swept is quadratic of the form

$$\phi_1^{(q)}(z) = -\left(\frac{\gamma G_e T_e}{L}\right) z^2 + \left(\gamma G_e T_p - \frac{2T_e\Omega}{L}\right) z^1 + \left(\Omega T_p - \frac{\gamma G_e T_e L}{4} - \frac{T_e\Omega^2}{\gamma G_e L}\right) z^0 \tag{6.10}$$

The spatial derivative of the phase is then:

$$K_1(z,t) = \gamma G_e t \qquad 0 < t < t_z \tag{6.11}$$

$$K_1(z,t) = \gamma G_e (t - 2t_z) \qquad t_z < t < \tau \tag{6.12}$$

To get an observable signal, the quadratic phase $\phi_1^{(q)}(z)$ created needs to be fully refocussed so a second, identical chirp pulse is applied under a gradient of the same sign. In diffusion experiments, the second chirp pulse combined with a gradient is incorporated at the end of *Δ* delay. The attenuation during the diffusion delay can be expressed by the term $(\Delta - \tau)\big(K_1(z,\tau)\big)^2$ as $K_1(z,t)$ remains the same during *Δ*. The phase acquired by the spins during the second chirp pulse is written as follow

$$\Phi_2(t,z) = \Phi_1(\tau,z) + (\Omega + \gamma G_e z)t \qquad 0 < t < t_z \tag{6.13}$$

$$\Phi_2(t,z) = -\Phi_2(t_z,z) + 2\Phi_{rf}(t_z) + (\Omega + \gamma G_e z)(t - t_z) \qquad t_z < t < \tau \tag{6.14}$$

and the attenuation induced during the second chirp pulse is given by first spatial derivative of (6.13) and (6.14)

$$K_2(z,t) = \gamma G_e(t + \tau - 2t_z) \qquad 0 < t < t_z \tag{6.15}$$

$$K_2(z,t) = \gamma G_e(t - \tau) \qquad t_z < t < \tau \tag{6.16}$$

Equations (6.13), (6.14), (6.15), (6.16) and the expression of the attenuation during the diffusion delay can be substituted in equation (6.4), and we obtain

$$S(z) = \mathrm{S}_0 e^{-\left[\mathrm{D}\gamma^2 {G_e}^2 {T_e}^2\left(\frac{\tau^3}{6{T_e}^2}+\left(\frac{2z}{L}-\frac{T_p}{T_e}\right)^2(\Delta-\frac{\tau}{2})\right)\right]} \tag{6.17}$$

provided that $\gamma G_e \gg \Omega$. This is the model that we used to fit our data in the 2D SPEN DOSY. For simplification we did not take into account the z independent term like in the original paper.

The term

$$K(z) = -\gamma G_e T_e \left(\frac{2z}{L} - \frac{T_p}{T_e}\right) \tag{6.18}$$

corresponds to the effective gradient area, which is spatially dependent (instead of time dependent as in the conventional DOSY experiment) and $\Delta' = \Delta - \frac{\tau}{2}$ is the effective diffusion delay. Note that $K(z) = \frac{d\phi_1^{(q)}(z)}{dz}$ provided that $\gamma G_e \gg \Omega$.

Alternatively, as in the work of Keeler and co-workers[41] (model n°2), the effective gradient area imparted by a chirp pulse can be calculated numerically as:

$$K_{eff}(z) = \int_0^{Te} \frac{d}{dz}\sqrt{\left[\Omega_0 - \gamma G_e z - \Omega_{rf}(t)\right]^2 + \omega_{rf}(t)^2}\, dt + \gamma G_e T_p \tag{6.19}$$

where Ω_0 is the offset of the peak, $\Omega_{rf}(t)$ is frequency of the r.f sweep and $\omega_{rf}(t)$ is the strength of the r.f field. The duration of the chirp and gradient pair is assumed to be negligible

so $\Delta' = \Delta$.

Those two models were implemented in our home-written processing package and were used to process our data.

6.4.2. Diffusion profile investigations

Using the parameters determined in the previous sections we managed to obtain a "1D DOSY" spectrum that is shown in Figure 34b with WGA acquisition where the diffusion profile is observed in the lineshape of each peak along the chemical shift axis. Spectral-spatial data shown in Figure 34a were obtained using EPSI type acquisition where the diffusion profile is observed in the lineshape of each peak along z axis. For each data set, the diffusion profile was extracted for the peak of water and plotted against a reference profile in Figure 34c and Figure 34d.

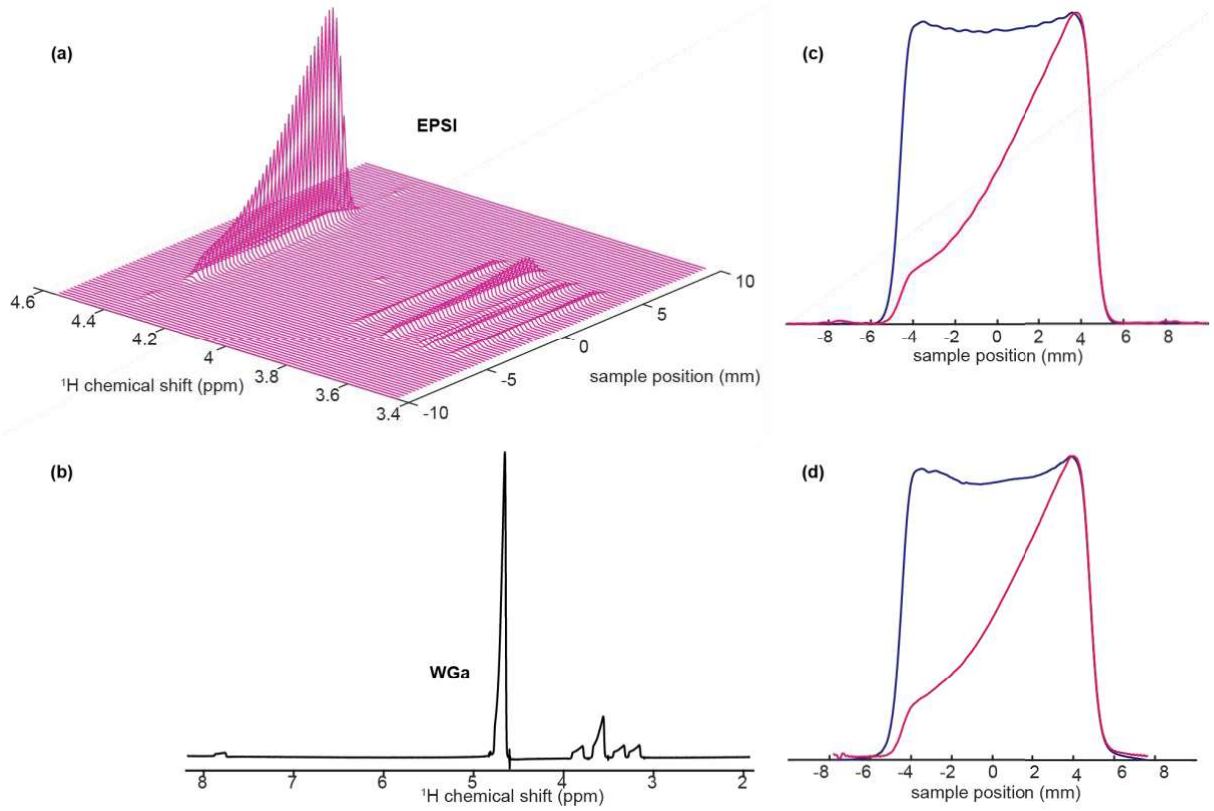

Figure 34: (a) SPEN DOSY data set acquired with EPSI type acquisition. (b) SPEN DOSY data set acquired with weak read gradient. (c) and (d) diffusion profile extracted respectively from (a) and (b) for the peak of water (magenta) and reference profile (blue) non-attenuated by diffusion.

6.4.2.1. Encoding optimization

For the encoding part of both pulse sequences, we saw that the differences between the pulse sequences lie in the spins' spatial phase. The extremum of this phase can be either shifted to one extremity of the encoded region or centered in the middle of the encoded region. Figure 35a shows a comparison that was done between the initial single-scan 2D DOSY with no post chirp gradient and a modified version that include a post chirp gradient as suggested by Keeler. In the first case, the diffusion range is wider so the diffusion curve goes from -4 mm to +4 mm (blue curve). If we take a look at the diffusion profile obtained with this method we see that the maximum signal intensity is at -4 mm. This section of the diffusion profile was fitted to equation (6.4) to calculate diffusion coefficients. This is an image extracted from the whole data set for the water signal.

In the second case (red curve), the profile was also extracted from the whole spectrum for the peak of water. We saw that this time the maximum of the intensity, corresponding to the smallest effective gradient area, was located in the center of the sample. The diffusion range is smaller as it goes from 0 to 4 mm. With respect of center of the profile, the same diffusion behavior was observed from -4 mm to 0 as the profile is symmetric. The diffusion curve can be fitted to equation (6.4) as well.

Comparable result for the diffusion coefficient was obtained in both case but the 'blue' curve tends to have a profile that is close to what we observe in conventional experiments. It is also easier to see whether the signal attenuation is appropriate, nor too fast or too slow. The option proposed by Keeler with post chirp gradient appears to be more advantageous because of the wider gradient range that is covered.

Additionally, we also tried to remove the extra dephasing part in the 1D DOSY experiment and the lineshape undergo severe distortion (Figure 35b) thus impacting the calculated values of diffusion coefficients. It seems that the use of a post chirp gradient for this experiment is mandatory. For the sake of comparison between EPSI strategy and WGA strategy we choose to keep the post chirp gradient in the encoding process.

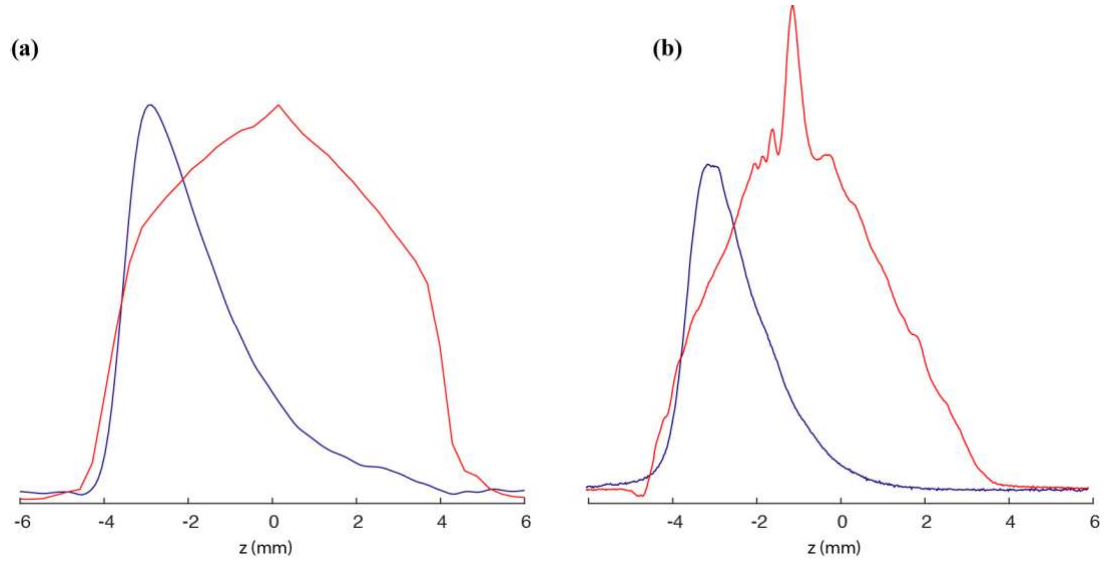

Figure 35: Effect of post chirp gradient depending on the acquisition strategy. (a) Lineshape for the water peak using EPSI acquisition with (blue) and without (red) post chirp gradient during the spatial encoding. (b) Lineshape for the water peak using weak read gradient acquisition with (blue) and without (red) post chirp gradient during the spatial encoding.

6.4.2.2. Distortion due to gradients

Another issue that can decrease the accuracy of diffusion coefficient is the non-linearity of the gradient. Although it is possible to map this non-linearity as suggested in the literature we did not go in this much details for the moment, but we know that it will induce a systematic error [164,169]. We attempted to minimize this error by reducing the size of the excited region. Indeed, if the chirp pulse sweeps the whole observed region of the tube, ca. 15 mm, on the edges the linearity of G is not respected and spins at different positions have comparable precession frequency (blue curve in Figure 36). However, by

exciting only the central part of the observed region, ca.10 mm, we no longer observe those distorted artefacts on the edges of the acquired profile. The top of the profile is almost completely 'flat'.

In practice, we used a chirp pulse smoothed at 10 % for the ramping period so if the selected region is 10 mm, the diffusion curve is observed over 8 mm. The value of the encoding gradient G_e needs to be adjusted according to $L=BW2\pi/\gamma G_e$, where BW is the bandwidth of the pulse (fixed value), L the length of the observed region, γ is the magnetogyric ration for ^{1}H and G_e is the encoding gradient strength. The higher this value is, the smaller is the observed region. Results shown in Figure 36 were obtained with a gradient echo.

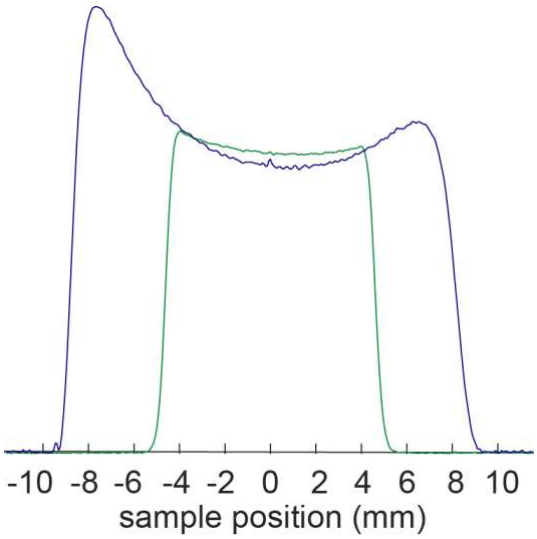

Figure 36: Profile obtained after chirped pulse application on the entire sample (blue curve) and on the selected central region of the sample (green curve).

6.4.2.3. Reference profile deconvolution

Minimizing the distortion of lineshape can also be done by normalizing the data with a reference profile, obtained without encoding. This helps to obtain more accurate values of the diffusion coefficient by improving the signal on the edges of the profile. The easiest way would be to record a 1D DOSY/WGA or a single-scan 2D DOSY/EPSI when the diffusion delay is set to 0 or lowest value as possible. However, by doing this, there were still some diffusion attenuation occurring because the diffusion delay could not be set below a minimum value of $\Delta = 17\ ms$ due to constraints in the parameter's definition in the pulse program. To obtain a reference profile with minimal diffusion weighting, a gradient echo imaging pulse sequence using the same chirp parameters as for the 2D DOSY/EPSI experiments was run. This sequence is shown in Figure 37c A version of the 1D DOSY/WGA with no diffusion delay was created as well and is shown in Figure 37b. Both of these sequences are inspired from the Bruker gradient echo pulse sequence illustrated in Figure 37a. The later was used to get the green spectrum of

Figure 36. The Results are shown in Figure 34c and Figure 34d (blue curves) using the pulse sequence presented in Figure 37. Note that for the case of EPSI acquisition, the corresponding reference experiment is a 1D, so the same profile is then used to correct for each peak in the diffusion experiment. We also created a 2D version of this experiment, which yields a specific reference profile for each peak. In practice we used the same reference profile (obtained with the 1D) for all the peaks, for simplicity and to save processing time.

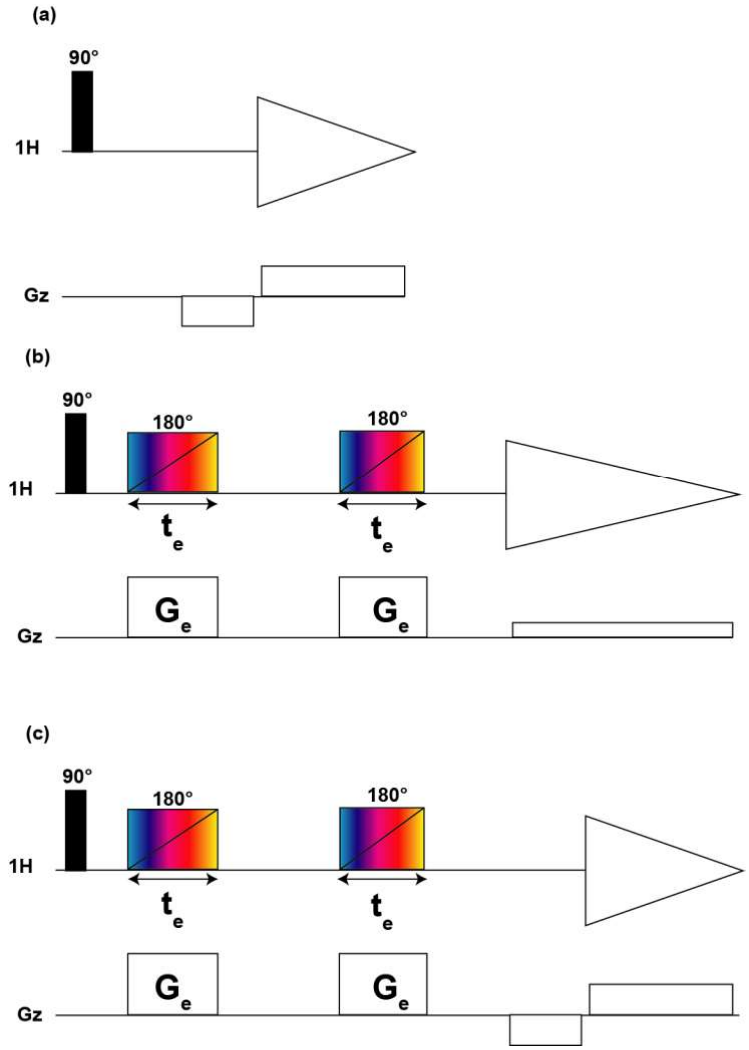

Figure 37: (a)Gradient echo from Bruker, imgegp1d. (b) Gradient echo used for the reference profile of 2D SPEN DOSY using weak read gradient acquisition. (c) Gradient echo used for the reference profile of 2D SPEN DOSY.

6.4.3. Accuracy compared to conventional DOSY

The spectra obtained with our optimized experiments are shown in Figure 34 at the beginning of the section. Now that we have explained how we found parameters that would give good estimates of diffusion coefficient, it is time to compare both models.

With the 1D DOSY/WGA strategy, we obtained the diffusion coefficients presented in Figure 38 (right). Red dots indicate the calculated values with the SPEN DOSY and dashed lines are the refences values obtained with conventional DOSY (cf. section 6.2.1). A good separation of the signals was achieved but an important systematic error was observed. With the 2D single-scan DOSY/EPSI strategy, the results shown in Figure 38 (left) are in good agreement with those of the conventional DOSY. The systematic error is reduced compared to the previous strategy using the weak read gradient during acquisition. If we take a close look at the lineshape, we noticed that it is less distorted. Indeed, the use of a weak read gradient lead to severe distortions mainly on the edges of the profiles for each peak. This is not the case when using bipolar gradient pulses whose strength is greater. Note that our signals were only singlet and we did not have issues with J couplings altering the lineshape, especially in the 1D DOSY/WGA as described by Keeler and co-workers.

In the following chapters, we chose the EPSI strategy as it provides closer results to conventional experiment and most of all because it provides a better resolution in the chemical shift dimension and a better resolution of the spatial profile itself.

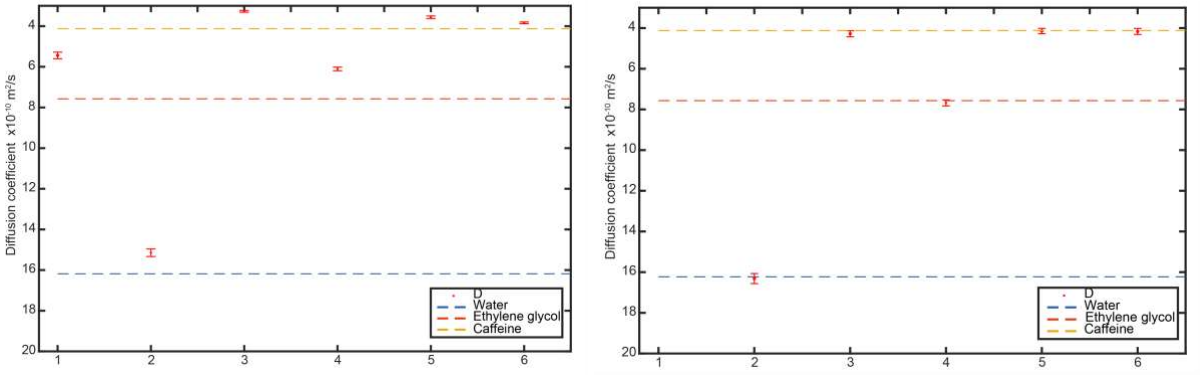

Figure 38: Left: Comparison of diffusion coefficient values for the 2D SPEN DOSY experiment using weak red gradient acquisition and the diffusion coefficient values obtained with the conventional DOSY (dashed lines).Right: comparison of diffusion coefficient values for the 2D SPEN DOSY experiment using EPSI acquisition and the diffusion coefficient values obtained with the conventional DOSY (dashed lines).

6.5. Conclusions

Using the promising results obtained by Keeler and co-workers and Frydman and co-workers as a starting point, we have presented an improved version of the SPEN DOSY pulse sequence that includes in a distinct way all the advantageous features identified to get optimum results. This helps us in our understanding of the theory behind SPEN DOSY so that we can create a spatially encoded version of more elaborate DOSY sequences. An acquisition block using bipolar gradient pulses was chosen over

the use of a weak readout gradient proposed by Keeler and co-workers because lineshape distortions are reduced. It also offers a better resolution between peaks and the risk of overlap is reduced.

The ultrafast methodology may in principle be extended to any type of diffusion experiments, eventually achieving a general, robust protocol for them. This allowed us to fully understand their characteristics and the underlying theoretical considerations. In the end we were able to choose the option that gives the most promising results for further applications. We have led here a qualitative comparison between to acquisition strategies. The full details about the pulse sequence that we chose will be further described in section 8.

7. Numerical simulations of spatiotemporal NMR

7.1. Introduction

To continue our investigation of the properties of SPEN DOSY, numerical simulation of uncoupled and coupled spin systems in the presence of translational diffusion were performed in the Spinach library. Spinach is an open source software library (written in the MATLAB language) that simulate spin dynamics for a variety of spin systems and interactions [44]. As the spatial dependence in SPEN DOSY is achieved thanks to the use of frequency-modulated pulses together with magnetic field gradients, we need a tool that can handle coexisting spin evolution and diffusion process. The computational description of spatially encoded (SPEN) experiments must simultaneously account for classical diffusion and quantum mechanical spin dynamics. In Spinach, this is achieved with the Fokker-Plank formalism that handles both spin and spatial dynamics and makes it possible to describe spatially encoded diffusion experiments with accuracy.

This section focuses on a thorough numerical description of the SPEN DOSY experiment. First, appropriate conditions and spin system description were determined. The effect of the various encoding parameters was then studied. The accuracy of the model used for fitting the SPEN DOSY data was studied as well. This numerical investigation provides ways to explore the validity of the models used as well as ways to correct it from potentials artefacts. Finally, the perspectives for numerical simulation of SPEN DOSY experiments are discussed.

7.2. Simulated pulse sequences, spin system and parameters

7.2.1. General features of Spinach and implementation

SPEN DOSY experiments were simulated using the Fokker-Planck formalism to describe spins and space dynamics according to (the equation of motion):

$$\begin{aligned} \frac{\partial \boldsymbol{\rho}(r,t)}{\partial x} &= -i\boldsymbol{L}(r,t)\boldsymbol{\rho}(r,t) + \boldsymbol{M}(r,t)\boldsymbol{\rho}(r,t) \\ \boldsymbol{L}(r,t)\boldsymbol{\rho}(r,t) &= [\boldsymbol{H}(r,t), \boldsymbol{\rho}(r,t)] + i\boldsymbol{R}\boldsymbol{\rho}(r,t) + i\boldsymbol{K}\boldsymbol{\rho}(r,t) \\ \boldsymbol{M}(r,t) &= \nabla^T . \boldsymbol{v}(r,t) + \mathbf{v}^T(r,t).\nabla + \nabla^T . \boldsymbol{D}(r,t).\nabla \end{aligned} \quad (7.1)$$

Where the term $\boldsymbol{\rho}(r,t)$ corresponds to the spin density matrix at the spatial point *r* at time *t*, **H**(r,t) corresponds to the spin Hamiltonian, *R* is the relaxation superoperator, $\boldsymbol{K}$ is the chemical kinetics superoperator, and $\boldsymbol{M}(r,t)$ is the spatial dynamics generator dealing with diffusion and flow with ∇=

$\left[\frac{\partial}{\partial x}\frac{\partial}{\partial y}\frac{\partial}{\partial z}\right]^T$ the gradient (in the mathematical sense) operator, $\boldsymbol{v}(r,t)$ the flow velocity and $\boldsymbol{D}(r,t)$ the translational diffusion tensor. The matrix representation of the superoperator is made with discretization of the spatial dimension using finite grids. Using domains with periodic boundary conditions, these superoperators can be either calculated exactly with Fourier differentiation matrices, which is computationally expensive, or approximated with finite-difference matrices that are less memory consuming [230].

The general architecture of Spinach is presented in Figure 39. Many experiments are available in this library. Main files (that are called from the MATLAB interface to start the simulations), such as *spendosy_test1*, need to be created in the section ***examples***. All the parameters, spin specifications and basis-set information are given in this file. We will see later on what parameters must be specified. Functions that handle spin system features are located in the ***kernel*** section. The actual SPEN DOSY experiment is located in ***experiments*** were the density matrix calculation is done including the acquisition part. The functions that implement pulses, gradients, delays, etc. are found in ***kernel***. The processing functions are usually located in ***experiments*** and called in the main file *spendosy_test1*. As a user, we will mostly modify files located in ***experiments*** and ***examples***. The remaining files do not necessarily need to be modified, except for more advanced considerations. The ***Interface*** and ***etc.*** sections contain functions for import, export, processing and visualization of data and were not used directly.

The following section will focus on the simulation of SPEN DOSY experiments, considering that the library is already optimized in terms of calculation speed thanks to the work of Dr. Ilya Kuprov, the main developer of Spinach. All these files in the Spinach package were operated at the time of the experiments on MATLAB version 2015a and spinach_1.8.3420. Several of the functions written during this work are now included in the distributed version of Spinach that can be found at this address: http://spindynamics.org/Spinach.php

Note that a graphical user interface is available for Spinach but since we create new functions we need to use the ‘developer version’.

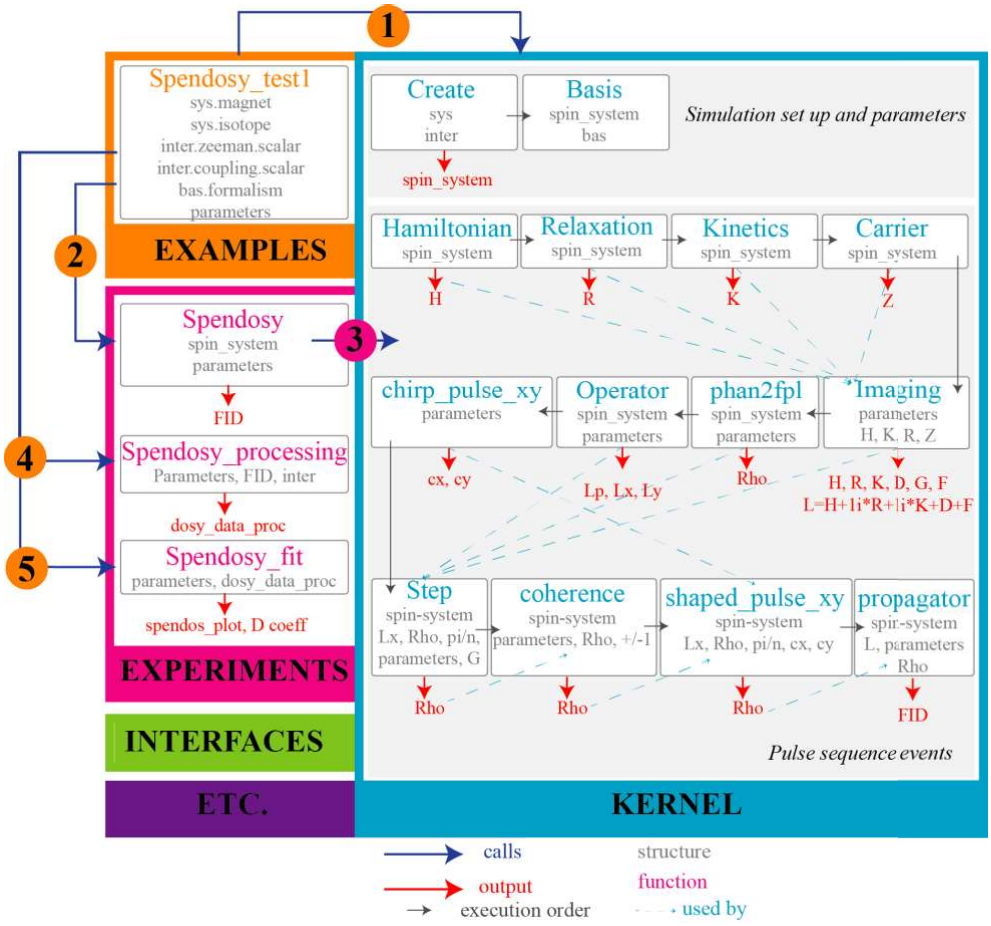

Figure 39: Spinach architecture representing the main sections of the library: Examples is used to specify the simulation parameters. Experiments is used to define the pulse sequence events and to process the simulated FID. Kernel contain the core functions of the library. Interfaces and etc are used for import, export and processing of the simulated data.

7.2.2. SPEN DOSY pulse sequence

The SPEN DOSY pulse sequence described in the previous section is illustrated in Figure 40a and was simulated to characterize the signal behaviour of a ^{1}H spin system. The simulated version corresponding to Figure 40b was built from the real experiment except that in this case the coherence selection illustrated in Figure 40c is analytical. It means that the pathways are selected by zeroing the unwanted components of the state vector instead of doing a gradient-based coherence selection.

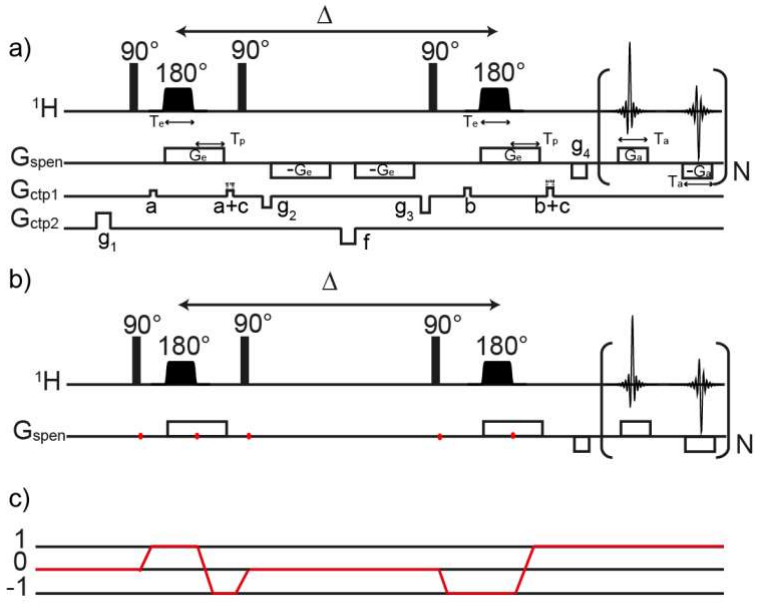

Figure 40: (a) Real pulse sequence of SPEN DOSY. (b) Simulated pulse sequence. (c) Analytical coherence transfer pathway.

Figure 39 summarises the main steps of the simulation. A main file, *spendosy_test1*, needs to be created in the section ***examples***. In step 1, the section ***kernel*** is called and the functions *create* and *basis* are run to give Spinach the necessary spin specifications, basis set and parameters. In step 2, the function *spendosy* in ***experiments*** is called by *spendosy_test1* to start the experiment with spin system and parameters. In step 3, the ***kernel*** is called for each event of the pulse sequence. In addition, to the functions shown in Fig. 1, hard pulses, evolution under a gradient pulse and evolution during the diffusion delay are generated with the function *step* and the function *coherence* is used to perform analytical coherence selection. The final result is the simulated FID (where FID refers to the acquired signal). In steps 4 and 5, the functions *spendosy_processing* and *spendosy_fit* are called to process the simulated FID obtained at the previous step.

7.2.3. Spin system specifications and input parameters

When starting a liquid state NMR simulation on Spinach, the first thing to do is to declare the function that will be used to start with a clean background. These functions are usually found in the ***examples*** set. In our case, we implemented a new function as it did not exist in the library. Other examples such as *ufcosy_test1* were present and were used as a guide to create our own function *spendosy_test1*.

The second step is to specify the spin system composition by giving the list of isotopes used. We choose to use a simple *proton* spin system, but many currently observed isotopes are available in Spinach. Next, we set the magnet magnetic field to 14.1 T as we worked on a 600 MHz in the laboratory for the real experiments, then the chemical shifts in ppm for all protons. If needed, scalar couplings can

be specified in Hz. For the moment we consider a ^{1}H uncoupled spin with no chemical shift offset. The formalism that will be used for the spin part needs to be specified as well, and in our case, we use the Liouville space description. All these information are stored in *inter*, *sys* and *bas* structures are given to Spinach through the functions create and basis during the step 1 shown in Figure 39.

Table 1: Overview of the parameters required for SPEN DOSY simulation

Sample geometry		**Acquisition parameters**		**Encoding parameters**		**Diffusion evolution**		**Equation for the fit**	
Dims (m)	0.015	spins	1 or 2	pulsenpoints	1000	Dconstant ($10^{10}m^2s^{-1}$)	0 or 8	γ ^{1}H	267524618
npts	3000	Deltat (s)	1.5e-6	Smfactor (%)	0.1	Td (s)	0.10	dscale	10^{-10}
cond	{'period',7}	npoints	256	Te (s)	0.0015			B0	
		nloops	256	Tau (s)	0.0015				
		Ga (T/m)	0.52	BW (Hz)	130000				
		Offset (ppm)	0	Ge (T/m)	0.2925				
				chirptype	smoothed				

The next stage is to specify the pulse sequence parameters that are required by Spinach to run the simulation and plot the final spectrum. These parameters are usually similar to what is used for running the real experiments at the spectrometer but they can be modified to analyze their effect, as we will see later. The parameters required by *spendosy* are listed in Table 1. For the first simulation, as we would do at the spectrometer, we indicated the values of the encoding gradients of 0.2535 T/m applied combined with a chirp pulse of 110 kHz bandwidth, with a duration of 1.5 ms. The post-chirp gradient had a duration of 1.5 ms. The acquisition was performed with a gradient amplitude of 0.52 T/m, a duration of 192 μs and 256 points. The number of points used for grid discretization, 3000, the size of the grid, 15 mm, the diffusion delay, 100ms, and also an initial input value for the diffusion coefficient, 8, needs to be provided.

Now that all the parameters, the formalism and the spin system are set, the simulation can be carried out in 'liquid state' via the *imaging* function that handle the parameters, the pulse sequence and the spin system to calculate the density matrix and render the FID. The whole simulation takes less than one minute to be completed.

7.2.4. Processing

Once the simulation has returned the FID, it is time for processing. The corresponding functions can be found in the section ***experiments*** and are called by the *spendosy_test* function for the step 4 and 5 in Figure 39. The FID obtained is shown in Figure 41a. It is a series of echoes created by the train of

gradient pulses during acquisition. In order to extract the diffusion information, the data were rearranged in the k–t space illustrated in Figure 41b where the horizontal dimension corresponds to the t_2 evolution period, and the vertical dimension to the k-space. The rearranged data were then Fourier transformed along both dimensions to give the spectrum of Figure 41c. The diffusion decay curve of Figure 41d was then obtained as a slice of the 2D matrix. The decay induced by the diffusion is observable in the spatial profile (blue curve). In Figure 41d, the dashed curves correspond to the diffusion curve when the parameter for diffusion constant was set to 0. The region of the spatial profile corresponding to the plateau of the chirp pulse can be used for diffusion coefficient determination.

The fitting functions are the same as for the actual experiment, according to the models described in section 6. As the experiments were also processed in MATLAB, we simply adapted the processing files within Spinach and used the same processing strategy that was previously described. Zero filling, apodization, and window multiplication can be performed on the simulated data, and the data were by default processed in magnitude mode.

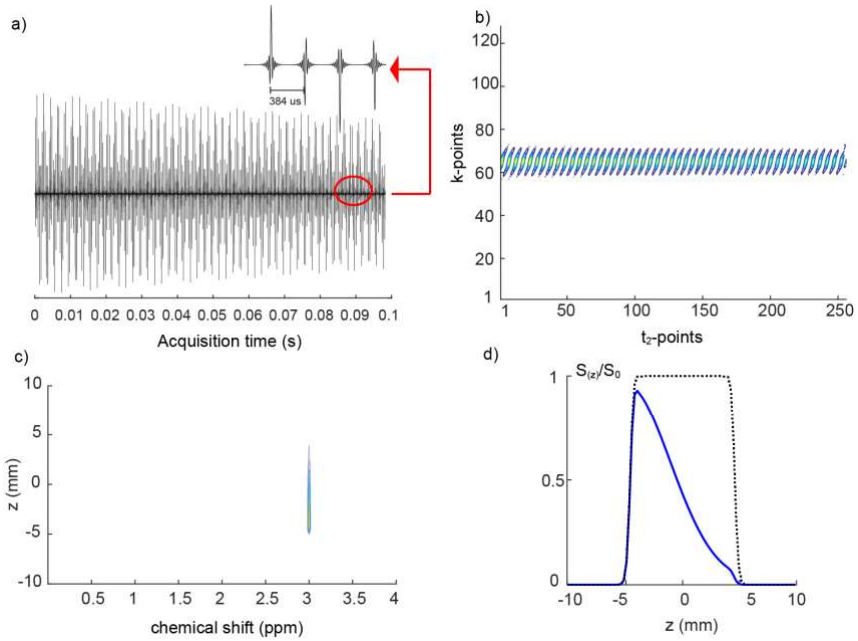

Figure 41: Processing of FID from SPEN DOSY simulation using the Fokker–Planck formalism. The free induction decay (A) is rearranged into a matrix (B) and gives the spectrum (C) after FT. The diffusion profile (D) is extracted from (B).

7.3. Convergence and accuracy considerations

Numerical simulation is a powerful way to run virtual NMR experiments that are free of sensitivity issues and many sources of experimental errors. However, when the user sets the parameters, attention must be paid to the accuracy of the results that will be obtained. Indeed, when an NMR spectrum or a

calculated result is obtained by the simulation, one must verify that it is truly meaningful from a physical/chemical point of view. In the SPEN DOSY simulation, the accuracy of the output data relies on the respect of the spatial Nyquist condition and also on the accuracy of the finite difference approximation of the diffusion operator. The first condition will ensure a proper description of the gradient helices during the diffusion encoding part and the second condition will ensure a proper behaviour of the diffusion effect.

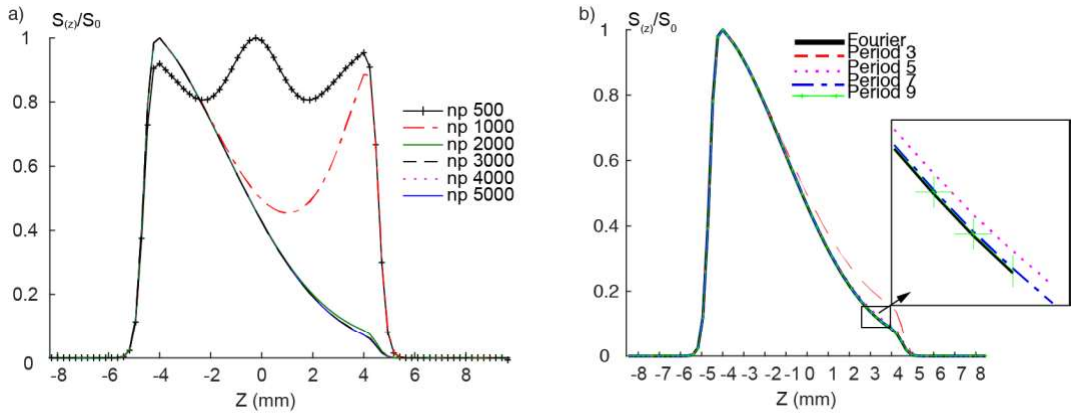

Figure 42: Effect of the grid size on the simulated signal. (a) Simulated diffusion profile using SPEN DOSY for various grid size. Below 2000 points, the profile is not meaningful. Above 2000 points Nyquist condition is satisfied leading to the expended diffusion profile. (b) Adjustment of the stencil order to achieve convergence and accuracy with sparse matrices. Fourier differentiation is formally exact.

Consider a sample that is discretized along *z* coordinate with *N* points over a length of 0.015 m, which corresponds the size of a typical NMR sample. The simulations shown above were carried out with 3000 grid points. The Nyquist condition states that the spatial discretisation grid must have at least two points per period of the fastest gradient spiral. A non-appropriate number of grid points for the sample geometry description leads to biased signal that has no physical meaning. This can be seen in Figure 42a when the grids are 500 and 1000 points. The number of points was increased until the returned answer remains stable meaning that convergence of the simulation results is achieved. Once the Nyquist condition is satisfied, which is here the case for grids with 2000 points and more, distortions disappear abruptly and accurate results were obtained. These results are reported in Table 2. On the other hand, the larger the number of points is, the larger the operators size will be, so the longer the simulation duration will be. The optimal number of points needs to be chosen in order to have reasonable simulation duration with converged output value. According to the results of in Table 2, we decided to use 3000 points for discretization to have a simulation of less than 1 min.

Table 2: Sample discretization effect on the diffusion coefficient returned by the simulation. Chirp pulse used is described by 1000 points

Number of sample points	Output value of D	Total duration (s)

	($\times 10^{10}$ m^2 s^{-1})	
500	-0.07	11.63
1000	1.1	17.62
2000	7.83	33.19
3000	7.97	52.23
4000	7.98	69.97
5000	7.98	90.26

The same considerations apply for the description of the chirp pulse. A 10% smoothed chirp pulse of 110 kHz bandwidth was used here. Its duration was 1.5 ms and it was discretized over 1000 points (which is also the typical number of points used experimentally for chirp pulses).

Table 3: Chirp pulse discretization effect on diffusion coefficient returned by the simulation. Sample is described by 3000 points

Number of chirp points	Output value of D ($\times 10^{10}$ m^2 s^{-1})	Total duration (s)
250	7.92	34.52
500	7.96	48.48
1000	7.97	54.59
1500	7.98	67.38
2000	7.98	81.91

From the results presented in Table 3, we concluded that a smaller number of points induce a loss of accuracy and a higher number of points is not necessary as it is time consuming.

Regarding the convergence of the simulations for diffusion, the accuracy of the finite difference approximation needs also to be adjusted in order to get sufficiently accurate value for the desired diffusion coefficient. As this numerical method involves a discretization of the diffusion operator, the accuracy is impacted by the space between grids points and also by the order of the stencil used for approximation. In order to evaluate the effect of the order of the stencil, we choose as a reference Fourier differentiation operator that is formally exact and very accurate, but also computationally consuming because the corresponding matrix is not sparse. The Fourier differentiation matrix (marked ‘‘exact’’ in Figure 42b) is formally exact on a given grid but has a significantly longer run time (36 minutes). For the sake of speed, we choose to approximate the operator with a much sparser finite difference matrix as it takes less than 2min to be computed. As the actual SPEN DOSY experiment takes less than 1s, a numerical simulation of 36 min would not be very convenient. Even though simulations of quantum mechanical systems are usually time consuming compared to the real experiment, the use of sparse matrices offers the possibility to have simulations that are almost as fast as the experiment while still having sufficiently accurate results. For the diffusion operator, periodic boundary conditions were used, with 7-point central finite difference operator, which gives sufficiently accurate results.

7.4. Model adjustment

7.4.1. Reference profile correction

The effect of pulse sequence parameters and instrumental imperfections can be evaluated with good quality numerical simulations, once the previously described prerequisites are validated. The gradients used in the simulation are perfectly "linear" so there is no distortion due to the gradient but a correction is needed to take into account the spatial profile induced by the chirp pulse. When the diffusion constant was set to zero, the spatial profile of the excitation region, represented as a dashed black curve in Figure 43, reflected the exact shape of the smoothed chirp pulse. Otherwise, when the diffusion constant was set to 8×10^{-10} m^2 s^{-1}, the decay induced by the diffusion, corresponding to blue curve in Figure 43, was observable in the spatial profile. Without correction, the region corresponding to the plateau of the chirp pulse can be used for diffusion coefficient determination. Since the chirp pulse is smoothed at 10 %, for an exited region of 10 mm, it implies that 1 mm on either side of the spatial profile is lost and that the remaining plateau is 8 mm. The range of attenuation for the diffusion decay is hence observed on 8 mm instead of 10 mm. One can retrieve these 2 mm with a normalization by the spatial profile of the chirp pulse, as illustrated in Figure 43 with the red curve. We also noticed that a slight improvement was made as we obtained a diffusion coefficient value of 7.98×10^{-10} m^2 s^{-1} instead of 7.97×10^{-10} m^2 s^{-1}. This improvement is more significant in real experiments as the conditions are not ideal like in the simulation and it will also account for deviations from an ideal plateau caused by B_1 field inhomogeneity for example.

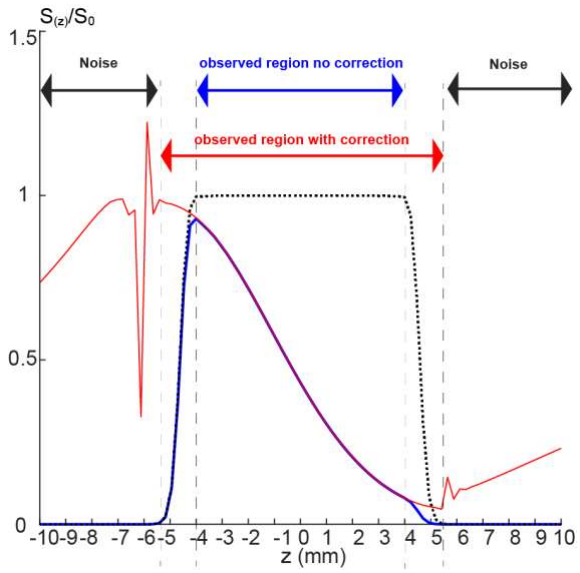

Figure 43: Reference profile correction. Diffusion-weighted DOSY lineshape obtained under a linear gradient with (red line) and without (blue line) reference profile (grey line) correction. A significant increase in the usable signal area is evident in the background- corrected signal.

7.4.2. Gradient area and diffusion time correction

Numerical simulation can be used to improve the model used to fit the data. We know that in conventional DOSY experiment, the signal attenuation can be expressed by the Stejskal-Tanner equation

$$S = S_0 e^{-\left(D G^2 \gamma^2 \delta^2 \left(\Delta - \frac{\delta}{3}\right)\right)} \quad (7.2)$$

where S_0 is the initial amplitude of the signal, D is the diffusion coefficient, G is the gradient intensity, γ is the magnetogyric ratio for protons, δ the gradient duration and Δ the diffusion time. For SPEN DOSY experiments, this equation can be generalized as:

$$S_{(z)} = S_0 e^{-(DK(z)^2 \Delta)} \quad (7.3)$$

Where $K_{(z)}$ is the effective gradient area experienced by the spins calculated from the spatial derivative of the phase $\phi_q(z) = \frac{\gamma^2 G^2 z^2}{R}$. For more details see section 4.

The first model (model n°1) that can be used would rely on a model of a form analogous to equation 7.3 as proposed by Frydman:

$$S(z) = S_0 e^{-\left[D\gamma^2 {G_e}^2 {T_e}^2 \left(\left(\frac{2z}{L} - \frac{T_p}{T_e}\right)^2 \left(\Delta - \frac{\tau}{2}\right)\right)\right]} \quad (7.4)$$

were G_e is the encoding gradient strength, T_e its duration, T_p the post chirp gradient duration, L the region swept by the pulse, z the position in the sample and $\tau = T_e + T_p$. In this case, the effective

gradient area imparted by the chirp pulse is determined in an analytical but approximate way and diffusion during the chirp pulse is accounted for. The second fitting model available (model n°2), as proposed by Keeler and co-workers [41] is:

$$S_{(z)} = S_0 e^{-\left(D K_{(z)}^{eff^2} \Delta\right)} \tag{7.5}$$

With

$$K_{eff}(z) = \int_0^{Te} \frac{d}{dz} \sqrt{\left[\Omega_0 - \gamma G_e z - \Omega_{rf}(t)\right]^2 + \omega_{rf}(t)^2}\, dt + \gamma G_e T_p \tag{7.6}$$

where Ω_0 is the offset of the peak, $\Omega_{rf}(t)$ is frequency of the r.f sweep and $\omega_{rf}(t)$ is the strength of the r.f field. Diffusion during the chirp and gradient pair is assumed to be negligible and the effective gradient area imparted by the chirp pulse is determined numerically.

The use of either model 1 or 2 results in a small but systematic error. By using a modified equation, with $K_{(z)}$ given by the exact expression, $K_{(z)}^{eff}$, and an effective diffusion time $\Delta' = \Delta - \frac{T_e + T_p}{2}$ (model n°3), the systematic error is reduced, as shown in Table 3. The former takes into account the non-instantaneous nature of the spins' flip, and the latter captures the effect of the finite duration of the chirp and gradient pair. The resulting model makes it possible to reduce systematic errors, as validated with numerical simulations.

$$S_{(z)} = S_0 e^{-\left(D K_{(z)}^{eff^2} (\Delta - \frac{\tau}{2})\right)} \tag{7.7}$$

Interestingly, numerical simulations make it possible to test the validity of model 2 (which neglects diffusion during the chirp pulses) by setting the diffusion operator to be active during the diffusion delay only. The agreement between the value obtained from the fit and the reference value is then much better. But in practice, diffusion effect takes place during the chirp pulses because of their finite duration, which is accounted for in the simulation by introducing the diffusion operator directly into the Liouvillian so that diffusion effect is acting at all steps in the pulse sequence.

Table 4: Comparison of model for diffusion coefficient determination. The model n°2 give accurate result when the diffusion effect is only active during the diffusion delay. When the diffusion operator is active during the whole pulse sequence, model n°1 and 2 are less accurate. Accuracy is restored with the model n°3 that we proposed.

Model	**Diffusion during Δ** ($\times 10^{-10}$ m^2 s^{-1})	**Diffusion during whole sequence** ($\times 10^{-10}$ m^2 s^{-1})
Model 1 (F)	-	7.81
Model 2 (K)	7.97	7.85
Model 3	-	7.97

7.4.3. Chemical shift and field of view correction

Numerical simulations are also useful in assessing the effect of chemical shift offsets in the analysis of the SPEN DOSY data. Model n°3, which is validated by the simulation, includes a correction by the chemical shift offset Ω_0 in the calculation of the effective gradient area given by equation 7.6. Chemical shift offsets induce two types of signal displacements: during encoding and during acquisition. The displacement upon encoding is accounted for in equation 7.6. Indeed, the position z along the lineshape is given by $z = \frac{\Omega_0 - \Omega}{\gamma G_e}$ with Ω the offset associated to the z position. Even if $\Omega_0 \ll \gamma G_e$ the image is displaced of a quantity $z_e = \frac{\Omega_0}{\gamma G_e}$. As $\Omega_0 \ll \gamma G_e$ for typical values of the encoding gradient, the displacement effect is quite small.

However, chemical shift displacement during acquisition has to be taken into account, as it may otherwise result in significant errors. The acquisition gradient induces also a displacement by $z_a = \frac{\Omega_0}{\gamma G_a}$. Table 5 illustrate the variation of the diffusion coefficient returned for several values of the chemical shift offset and Figure 44 shows the associated spatial diffusion profiles. Correction is performed using $z_{corr} = z - \frac{\Omega_0}{\gamma G_a}$ in equation 7.7 in order to shift the FOV. Without the correction, we observed up to 5% error in the calculated diffusion coefficient values and for an 0.52 T/m acquisition gradient.

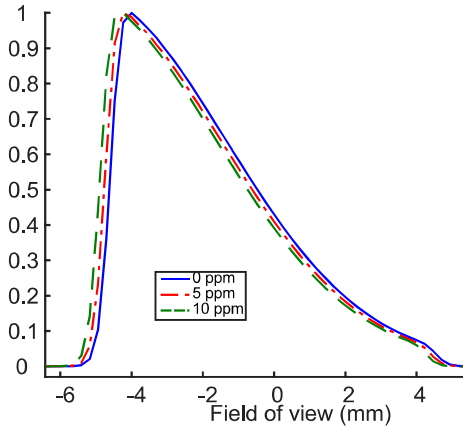

Figure 44: Image displacement according to chemical shift.

Table 5: Effect on chemical shift on the diffusion coefficient. Carrier frequency is set to 0

Chemical shift (ppm)	D non-corrected ($\times 10^{-10}$ m^2 s^{-1})	D corrected ($\times 10^{-10}$ m^2 s^{-1})
0	7.97	7.97
5	7.73	7.97
10	7.52	7.97

7.5. Influence of parameters on SPEN DOSY

The present simulations were carried out without noise and may not be used as such for the optimisation of encoding and acquisition parameters. We still verified that, in the absence of noise, modelling of the data would yield the expected value of the diffusion coefficient.

7.5.1. Encoding

In diffusion NMR experiments, the attenuation of the signal depends on the strength and duration of the gradient used to attenuate the signal and the diffusion delay. In the case of SPEN DOSY, the bandwidth of the chirp pulse and its duration need also to be chosen correctly. Using $R = \frac{BW}{T_e}$, $BW = \gamma GL$ and $z = -\frac{L}{2}$, which correspond to the position in the sample the more attenuated, equation 7.3 can be re-written as

$$S_{\left(-\frac{L}{2}\right)} = S_0 e^{-\left((D\left(-\frac{T_e BW}{L}\right)^2 \Delta\right)} \quad (7.8)$$

In analogy with the "b values" used in diffusion MRI, the maximum attenuation is characterized by the diffusion sensitivity factor given by

$$b = \Delta\left(\frac{BWT_e}{L}\right)^2 \quad (7.9)$$

Numerical simulations were performed for different values of this b factor, changing, e.g., the diffusion delay. Figure 45 and Table 6 show the variation of the spatial profile and the calculated diffusion coefficient for several value of b. In this simulation, there is essentially no difference in the estimated values even if we can see some modification of the profile attenuation. In real experiments if any variation of diffusion coefficient values were observed, this could be an indication of convection for example. Experimentally, the signal-to-noise ratio as well as the distribution of diffusion coefficient would govern which b value is more appropriate.

Table 6: Diffusion delay variation

Diffusion delay	**D calculated (model 3) ($\times 10^{10}$ m^2 s^{-1})**	**$b_{max} \times 10^6$**
50 ms	7.96	0.13
100 ms	7.97	0.25
300 ms	8.00	0.75

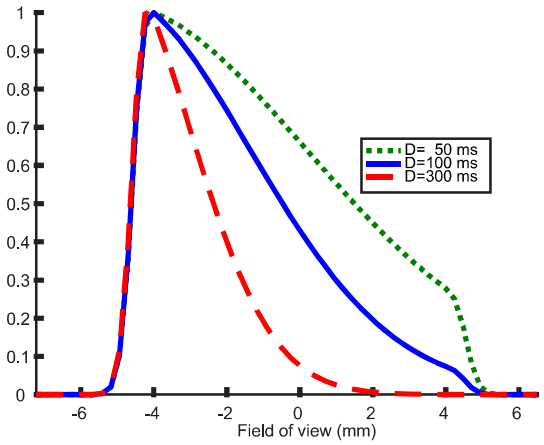

Figure 45: Effect of diffusion delay variation on lineshape decay.

Usually our molecules have diffusion coefficient ranges of 4×10^{-10} m^2 s^{-1} to 25×10^{-10} m^2 s^{-1} and we also made sure that the behavior of the simulations was correct for several values of the diffusion coefficients (data not shown).

7.5.2. Acquisition

The effect of the amplitude of the acquisition gradient G_a was studied and is presented in Figure 46. When the acquisition gradient is decreased we notice the appearance of oscillation in the profile. This oscillating behavior arises from signal truncation in k-space and can make the spatial profile difficult to analyse. This entails an over estimation of diffusion coefficient values when small values of acquisition gradient are used. These values are summed up in Table 7 and for a 0.13 T/m acquisition gradient $D=8.18 \times 10^{-10}$ m^2 s^{-1} which is higher than expected.

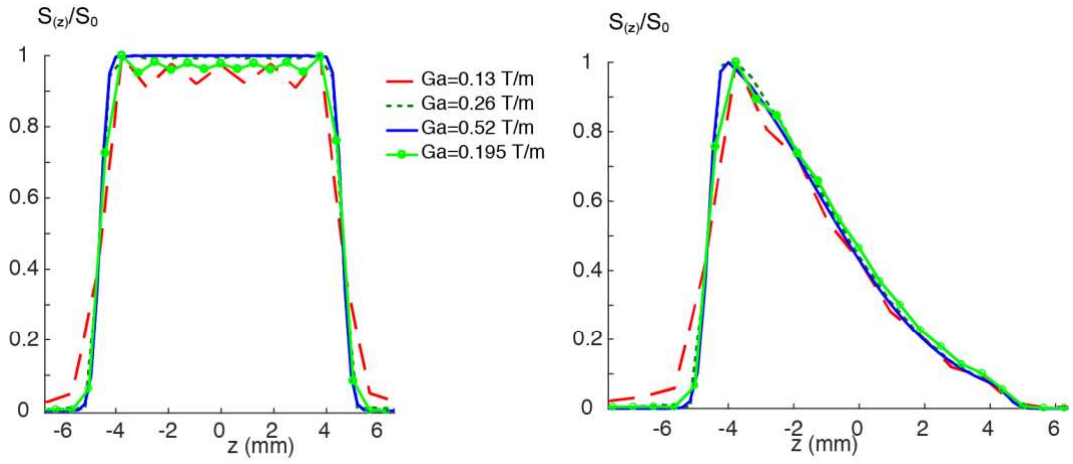

Figure 46: Gradient acquisition variation when diffusion is null (left) and when diffusion coefficient is set to 8 × 10^{-10} m^2 s^{-1} (right).

Dividing the diffusion profile by the reference profile computed with the diffusion coefficient set to zero helps to retrieve the expected value of D= 7.97 × 10^{-10} m^2 s^{-1}. This is another point in favor reference profile correction especially in the real experiment were a G_a of 0.20 T/m is used because of apparatus limitation. That is why we created a gradient echo pulse sequence by removing the evolution periods out of the pulse sequence (section 6) since it is impossible to switch the diffusion off in the SPEN DOSY experiment.

Table 7: Gradient acquisition variation

Acquisition Gradient (T/m)	D (model 3) (× 10^{10} m^2 s^{-1})	D with ref correction (× 10^{10} m^2 s^{-1})
0.52	7.97	7.98
0.26	7.97	7.98
0.195	8.06	7.98
0.13	8.18	7.97

7.6. Perspectives

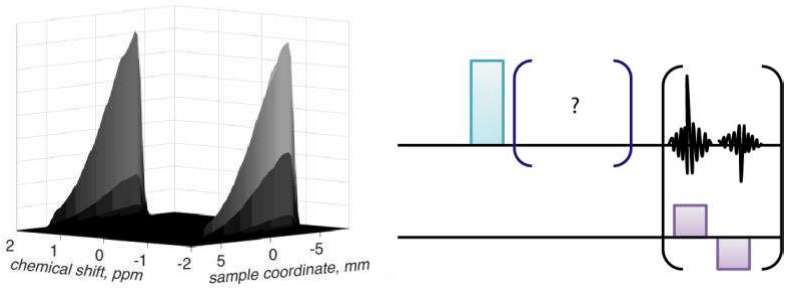

Figure 47: Insight of spinach usefulness with SPEN DOSY of multi-spin systems (left) and new pulse sequence development (right).

Now that accurate simulations of an idealized experiment are available, we can start to use the simulation framework to explore several aspects of SPEN DOSY. Beyond the initial and idealized experiment, there are many possibilities to design other diffusion-encoding, and also many sources of experimental errors. This subsection gives a brief overview of what can be done with this simulation tool, and of what was initiated during this work.

First, multi-spin systems can be easily described in spinach. Within the Fokker–Planck formalism, diffusion and imaging simulations for systems with multiple coupled spins can be carried out in exactly the same way as for uncoupled spins as equation 7.1 supports arbitrary spin Hamiltonian commutation superoperators, arbitrary relaxation theories and a host of other processes, such as chemical kinetics. Figure 47 (left) shows an example of a simulated SPEN DOSY spectrum for a two-proton spin system at 600 MHz with diffusion (8 × 10^{-10} m^2 s^{-1}), flow (0.1 mm s^{-1}), chemical shift

difference (0.5 ppm), strong J-coupling (15 Hz), full Redfield DD-CSA relaxation superoperator (2.5 Angstrom, CSA eigenvalues [-10 -10 20] ppm on both spins, with the tensor on spin 1 being collinear to the distance vector and the tensor on spin two being perpendicular to it, rotational correlation time 1.0 ns), and a non-symmetric chemical exchange process between the two spins (k+ =5 Hz, k- = 10 Hz). The calculation was set up in ten minutes and took less than five minutes to run with 3000 discretization points in the spatial grid. We noticed some sort of distortion in the lineshape when J coupling is included in the simulation. More investigations are needed at this point. Slight modification of diffusion coefficient is observed but with correction by reference profile we were able to obtained an expected value for diffusion coefficients, the same for both spins.

Second, an asset of Spinach is that in addition to trying to reproduce existing pulse sequences, it is possible to use it to design new pulse sequences and explore new possibilities. Simulations can be a good start when trying to design new experiments as we have the opportunity to assess the effects of the parameters and add pulse sequence elements without risk of damaging the spectrometer (e.g., when using experimental gradient strength that exceed the experimental limitations. In this work, and as will be described in the following, numerical simulations were used to design spin-echo-based SPEN DOSY sequences. Simulations were also used to validate the concept of the SPEN DOSY COSY experiments presented in section 8.

Third, experimental sources of errors can be included in the simulation. Convection effects are a well-known issue in diffusion NMR experiments. Since Spinach can handle dynamic processes, the effect of flow can be included in the simulation. This will be useful to understand how convection impacts our experiment but also to provide solutions to this problem. Strategies for convection compensation can be tested, and this is one of the developments for which the use of numerical simulation turns out to be the most useful.

Finally, note that the time required to simulate some pulse sequences can become a limitation, especially since complexity increases with the size of the spin system. Some improvements were implemented by Ilya Kuprov, such as a pre-calculation for the propagators that describes the acquisition, and parallel calculations were used when possible (with the *parfor* syntax of MATLAB). Also, since only echoes under positives gradients are used during data processing, the propagation corresponding to the negative echoes was implemented in a single step, which provides an acceleration by a factor of 2. We need to be careful during the processing and be sure that accuracy of the simulation is maintained.

7.7. Conclusions

Numerical simulations of the SPEN DOSY experiment for a ^{1}H spin system provided extensive information of the behavior of the pulse sequence. Extra care was taken to ensure that all our simulations converged so that we can be sure that the returned results have a physical meaning. Indeed, the finite

difference approximation of the operator make it possible to run the simulation in less than 2 min compared to the Fourier discretization that is exact but run in 36 min. We made sure that both results were equivalent. The effect of several parameters such as the encoding gradient, the acquisition gradient or chirp duration was studied to see their impact on the lineshape and the measured diffusion coefficient. Since the simulation is 'perfect' (without noise), we cannot derive real parameters from the simulation but at least we saw that the behavior of the simulation was correct for various encoding and acquisition parameters. For the later, we learn that a decreased value of acquisition entails oscillations in the diffusion profile. This can happen in our real experiments for sure because we do not work at 80 % of maximum strength. Models used for data adjustment were corrected as well in order to improve the accuracy of calculated diffusion coefficient by reducing systematics errors. We demonstrated that the chemical shift induces a displacement during acquisition and that this chemical shift must be taken into account in the processing to reduce bias. We also confirmed that the diffusion effect occurring during the encoding part must but taken account into the effective diffusion delay because of the duration of the encoding gradients are not negligible and diffusion is happening at this moment as well. This work was published in Ref. [231].

8. Advanced spatially encoded DOSY

8.1. Introduction

The ability to encode the diffusion information along a spatial dimension in NMR experiments provides an accelerated variant of the classic DOSY concept, as we described in Sections 6 and 7. In this section we will show several further developments of the SPEN DOSY approach, which aim at improving its accuracy and increasing the range of samples that can be analyzed. We will show that 3D DOSY experiments can be accelerated using spatial encoding, leading to acquisition duration that are equivalent to those needed to get a classic 2D spectrum. Since the accuracy of SPEN DOSY is also affected by convection, we will demonstrate that several solutions originally proposed for conventional DOSY can be adapted to the SPEN case. We will also describe spectral-selection schemes and a first attempt to obtain pure-absorption data with SPEN DOSY, as two other routes to better-resolved NMR peaks. In order to set the stage for these developments, we will first describe the model system that was used, the conventional data that was collected as a reference, and the optimization of the SPEN DOSY experiment described in section 6 for that particular system.

8.2. Experimental section and reference experiments

All the experiments were carried out on a Bruker spectrometer operating at a magnetic field of 600 MHz equipped with a triple-axis gradient probe used on the ^{1}H channel. The temperature of the sample was set at a nominal value of 298 K. Diffusion was observed over a 10 mm sample range for SPEN DOSY, a 10 mm sample range for conventional experiment on a Shigemi tube and a 15 mm sample range for conventional experiment using a classic tube.

8.2.1. Samples

Two sorts of NMR tubes were tested; a classic 5 mm tube and a Shigemi tube with a fixed sample length of 10 mm. Mixtures were shaken until complete dissolution of compounds and filtered to remove any solid particles.

The first mixture (**M1, M1'** for the Shigemi tube) is composed of L-valine (7.2 mg), methanol (2.4 µL), ethanol (3.4 µL) and n-propanol (4.5 µL) solubilized in 590 µL of D_2O. The concentration is near 100 mM for each compound so we have an equimolar mixture.

The second mixture (**M2**) is composed of cyclododecane (1 mg), squalene (2 mg) and adamantane (15 µL) solubilized in 600 µL of CD_2Cl_2.

The third mixture (**M3**) is a sample of pyridine, 4,4-bipyridine, 3-ethylpyridine and N,N-dimethylnicotinamide (≈ 4 × 150mM) in CD_3OD.

Note: Even though we discussed in the previous section that chemical shift dependent displacement during the acquisition needs to be corrected, the following experiments do not take this into account as they were performed before we found that this could impact our results. In the **M1** and **M3** samples the effect was barely noticeable. The phenomenon was brought to light with the work of Ghanem Hamdoun with sample **M2**.

8.2.2. Reference and signal assignment

8.2.2.1. 2D DOSY

Results are presented in Figure 48 and **Error! Reference source not found.** for 2D DOSY of mixture **M1'**. The data is acquired using a modified version of the **ledbpgp2s** Bruker sequence (stimulated echo with LED filter and two spoil gradients). Compensation gradients were added so that the lock signal is stabilized during the experiment.

For conventional 2D DOSY experiments, the gradient values were chosen so that all resonances are not completely cancelled at the last gradient level. The linear ramp is ranging from 0.013 to 0.4875 T/m. The duration of the gradient pulses was 800 µs. Theses parameters need to be carefully adjusted so that the decay is neither too fast nor too slow otherwise this lead to a less accurate estimation of diffusion coefficients. 2D spectra were acquired with 16384 points in the direct dimension, a spectral width of 6000 Hz corresponding to 10 ppm, a relaxation delay of 5 s and 16 gradient steps with 16 scans per gradient step. resulting in a total experiment duration of 17 min.

For conventional 2D DOSY experiments on the **M3** sample, the linear ramp is ranging from 0.013 to 0.4875 T/m. The duration of the gradient pulses was 1200 µs, the number of points was set to 32768 points in the direct dimension, a spectral width of 9000 Hz corresponding to 15 ppm, a relaxation delay of 5 s and 8 gradient steps with 16 scans per gradient step resulting in a total experiment duration of 15 min. The resulting DOSY display is shown in Figure 49.

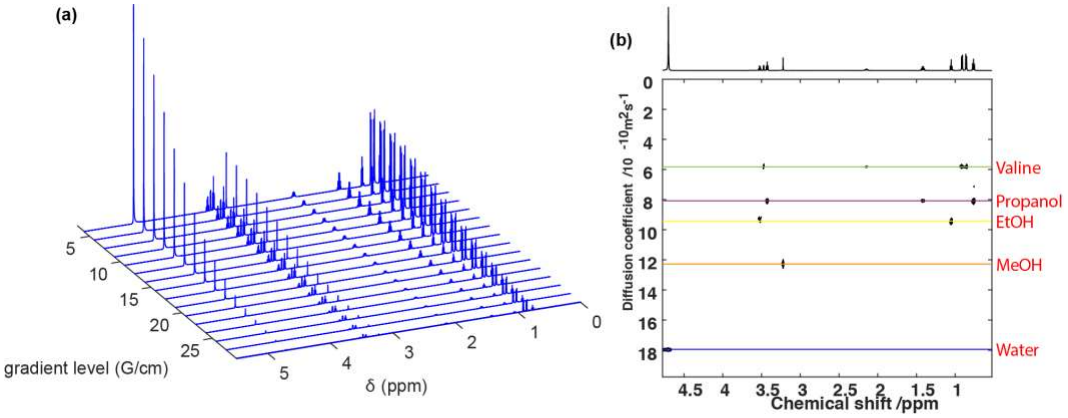

Figure 48: Conventional data for the mixture M1' of methanol, ethanol, propanol and L-valine in D_2O. (a) Stacked plot of the spectra acquired with different gradient strength. (b) Reconstructed DOSY display. The diffusion coefficients for water, methanol, ethanol, propanol, L-valine and water are respectively 18 × 10^{-10} m^2 s^{-1},12.26 × 10^{-10} m^2 s^{-1}, 9.4 ×10^{-10} m^2 s^{-1}, 8.11 × 10^{-10} m^2 s^{-1} and 5.78 × 10^{-10} m^2 s^{-1}.

The mean values of D for the molecules in the mixture, which will be considered as reference values, are 5.78 × 10-10 m² s-1 for l-valine, 8.11 × 10-10 m² s-1 for propanol, 9.4 × 10-10 m² s-1 for EtOH, 12.26 × 10-10 m² s-1 for MeOH and 18 × 10-10 m² s-1 for water.

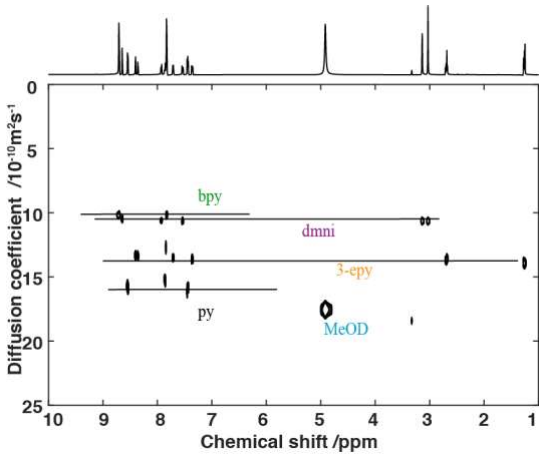

Figure 49: DOSY display of the mixture M3 of bipyridine, dimethyl nicotinamide, 3-ethylpyridine and pyridine in CD_3OD.

8.2.2.2. COSY

Results are presented in Figure 50 for COSY of mixture **M1'.** The 2D spectrum is acquired using the **cosygpqf** Bruker sequence (magnitude-mode COSY using gradients). 2D spectra were acquired with 4096 points in the direct dimension, 256 points in the indirect dimension, 8 dummy scans, 1 scan per

increment, a spectral width of 3600 Hz corresponding to 6 ppm, a relaxation delay of 5 s resulting in a total experiment duration of 11 min 33s. The signals were assigned as shown in Figure 50.

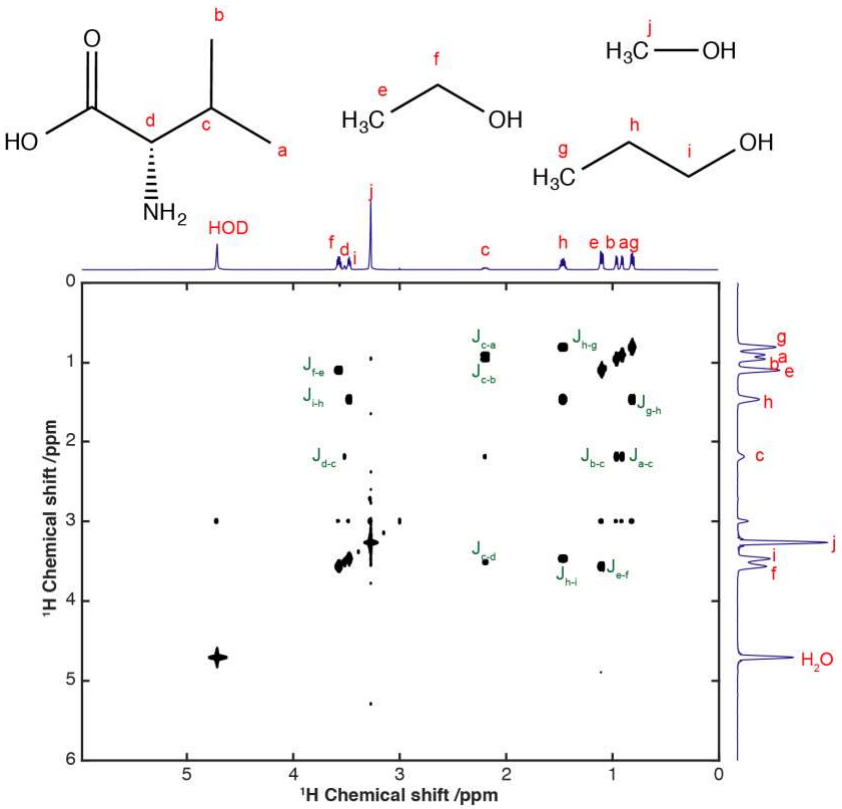

Figure 50: COSY spectrum for the mixture M1' composed of L-valine, propanol, EtOH, MeOH in D_2O.

Table 8: Results of the conventional DOSY experiment on mixture M1'.

Molecule	Signal	D × 10^{10} m² s^{-1}	Signal	D × 10^{10} m² s^{-1}	Signal	D × 10^{10} m² s^{-1}	Signal	D × 10^{10} m² s^{-1}
Water	H2O	18						
MeOH	j	12.26						
EtOH	f	9.32	e	9.47				
Propanol	i	8.08	h	8.12	g	8.12		
Valine	d	5.76	c	5.84	b	5.76	a	5.76

8.2.2.3. 3D DOSY-COSY

Results are presented in Figure 51 for 3D DOSY-COSY on mixture **M1'**. The data is acquired using a modified version of the **ledbpgpco2s3d** Bruker sequence (stimulated echo with bipolar gradient pulses for diffusion, LED filter, homonuclear shift correlation and two spoil gradients). Compensation

gradients were added to the Bruker sequence so that the lock signal be stabilized during the experiment. Going from the 2D experiment to the 3D version is done by transposing the parameters used previously and setting the COSY parameters. For the conventional DOSY-COSY, the spectrum was acquired for 14h with 4096 points, 16 gradient increments and 128 increments in the indirect dimension. The number of scans was set to 8 as well as the number of dummy scans in order to perform phase cycling.

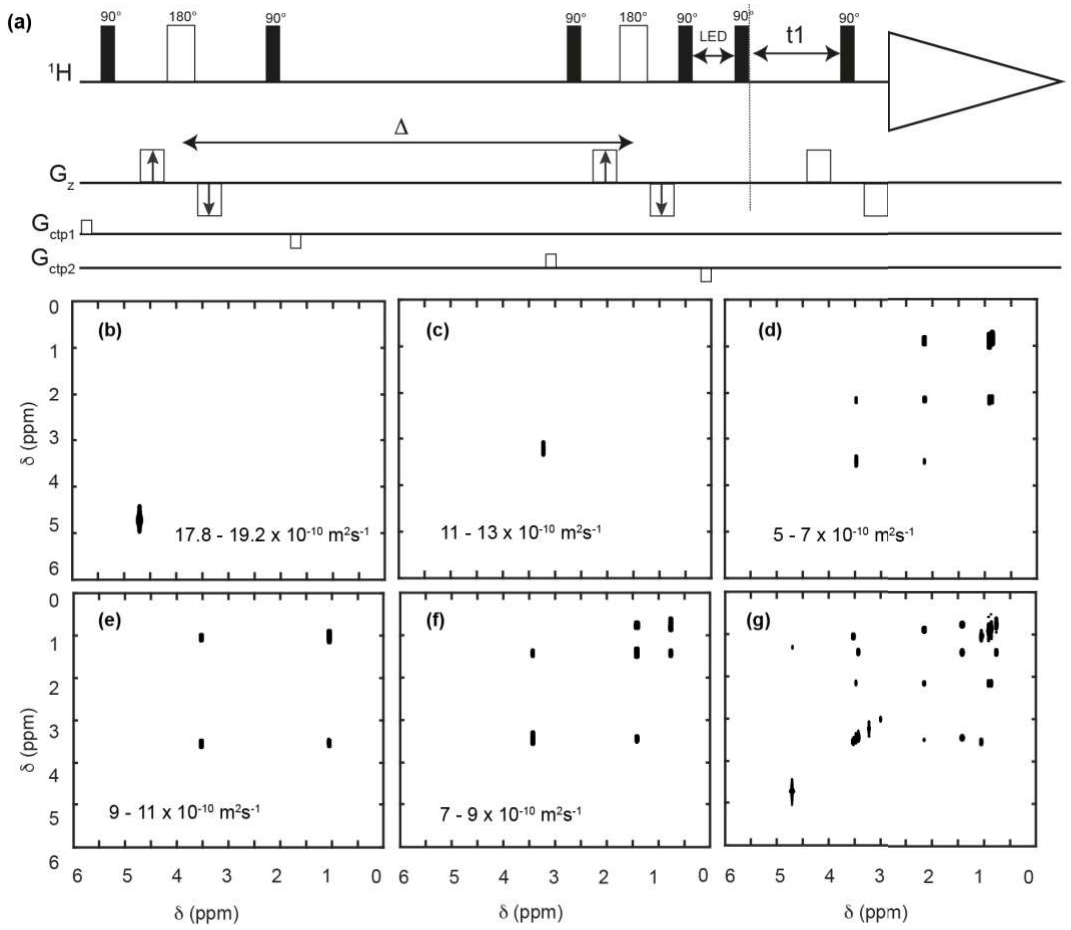

Figure 51: 3D DOSY. (a) Pulse sequence for DOSY COSY. (b-f) COSY-type spectra obtained on mixture M1' as slices of the 3D (D, δ_{direct}, $\delta_{indirect}$) dataset resulting from DOSY processing. The selected range in D is shown in each panel. The COSY spectrum with the lowest diffusion gradient area is shown in (g).

Figure 51g shows a COSY spectrum extracted from the 3D dataset, with all the signals indexed. This spectrum corresponds to the lowest gradient level that is to say the spectrum with the highest intensity. The determination of diffusion coefficients was performed by retrieving the peaks' volumes in all 16 COSY spectra associated to the 16 gradient levels, then fitting the decaying volume to equation (6.3) after DOSY Toolbox processing [82,122,148]. Diffusion coefficients obtained for the 3D experiments are close to those from the 2D experiment, as illustrated in Figure 52b, but the values are smaller of around 0.2×10^{-10} m^2 s^{-1}. Figure 52a shows the decay of all the signals against the gradient area through the experiment and the curves are separated according to their decay rate. Five 'groups' of curves appear

and each group corresponds to one compound. As expected, water (which is the smallest molecule) decays faster than the valine (which is the biggest molecule) so it will have a higher diffusion coefficient. Decaying curves coming from either correlation or diagonal peaks are well superimposed within a same compound. Extracted COSY for each compound, after the data set has been processed in the diffusion dimension, are shown in Figure 51. Each spectrum comes from a slice in the DOSY dimension. For example, ethanol spectrum was plot for D comprised between 9 and 11 $x10^{-10}$ m^2 s^{-1}.

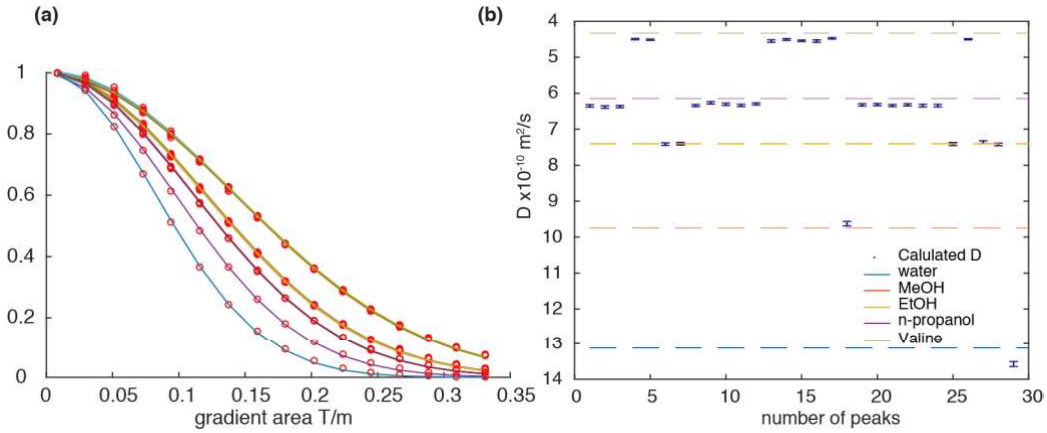

Figure 52: Diffusion coefficient determination on mixture M1'. (a) Curve fitting of the decay profile in order to determine the values of D (case using the volume of each peak. (b) Comparison between calculated diffusion coefficients (blue dots) in the DOSY-COSY and the values measures in the 2D-DOSY experiment (dashed lines).

8.2.3. Processing

Data from conventional DOSY experiments were processed with the DOSY Toolbox [122], which is an open source program for PFG diffusion NMR data processing. For the DOSY-COSY and all SPEN experiments, the data were processed in MATLAB (The Mathworks. Natick. U s.A.) using home-written routines, adapted in part from the DOSY Toolbox. In short, the SPEN data was read from Bruker files, then sorted and reshaped in order to get respectively a 2D or 3D matrix. Group delay removal, window multiplication by sine function in the t1 or (t1, t3) space and Hamming function in the k-space then zero-filling to N^n (with n=2 or n=3 and N the number of loops during acquisition) matrix size were then performed. Odd echoes were separated from even ones before Fourier transforming (FT) the data set along all dimensions. FT along the k-space gave the desired sample 'image' at corresponding spectral resonance frequency. Spectra were displayed in magnitude mode as phasing them was not possible. For 2D data set, each peak 'image' was manually selected and the observed region was fitted with equation (6.3). For 3D data set, the volume of each peak was computed to perform the fit using the same equation. Data below four times the noise level was discarded before the fit. The DOSY representation was

obtained using gaussian lineshapes with maxima corresponding to the calculated D values and linewidths set by the error of the fit.

8.3. Improved spatially-encoded 2D DOSY on mixture

8.3.1. Adjusting encoding parameters

In order to compare SPEN and conventional experiments, the effective gradient area caused by the chirp and gradient pair was adjusted to match the extremal values of the gradient levels in conventional DOSY. Figure 53a shows a comparison between the gradient area in conventional DOSY (blue diamonds), the former gradient area in SPEN DOSY (blue stars) and the matched gradient area (green circles). The effect on the lineshape can be seen on Figure 53b. The gradient area in SPEN DOSY can be expressed as

$$K(z) = \frac{2\gamma G_e T_e z}{L} + \gamma G_e T_p \tag{8.1}$$

and for conventional DOSY as

$$A_{conv}^{n} = \gamma\left(G_{n-1} + 0.637\frac{G_n - G_1}{n-1}\right)\delta \tag{8.2}$$

where γ is the magnetogyric ratio for proton, δ is the duration of the gradient, n the gradient increment, L the size of the observed region, G_e the encoding gradient, T_e the chirp duration, T_p the post chirp duration and z the position in the sample, G_1 and G_n the minimum and maximum of the gradient ramp set by the user and 0.637 is the gradient shape factor for a *sine* shape.

If z_i and z_f are respectively the positions at -4 mm and 4 mm in the encoded region and A_{conv}^{i} and A_{conv}^{f} are respectively the gradient area for the first and last gradient increment in the conventional experiment we can solve this system with G_e and T_p unknown:

$$\begin{cases} A_{conv}^{i} = \dfrac{2\gamma G_e T_e z_i}{L} + \gamma G_e T_p \\ A_{conv}^{f} = \dfrac{2\gamma G_e T_e z_f}{L} + \gamma G_e T_p \end{cases}. \tag{8.3}$$

If we express T_p as

$$T_p = \frac{A_{conv}^{i}}{\gamma G_e} - \frac{2T_e z_i}{L}, \tag{8.4}$$

after introducing (8.4) in (8.3) and solving the equation we have

$$G_e = \frac{(A_{conv}^{f} - A_{conv}^{i})\,L}{2\,\gamma T_e\left(z_f - z_i\right)}. \tag{8.5}$$

T_p can then be calculated and also the bandwidth of the pulse according to

$$BW = \frac{\gamma\, G_e\, L}{2\,\pi}\,. \tag{8.6}$$

The values of T_e and L are chosen by the user and in our case, we decided to go with a chirp duration of 2 ms, which gives a reasonable value of the maximum RF field, and a sample length of 10 mm. The diffusion delay is 100 ms for both conventional DOSY and SPEN DOSY. The corresponding encoding parameters calculated were a chirp bandwidth of 110 000 Hz, an encoding gradient of 0.26 T/m and an extra dephasing gradient duration of 1.6 ms. These parameters are found in Table 9. While these values were obtained here using the conventional DOSY as a starting point, the parameters can also be optimized directly on the mixture of interest.

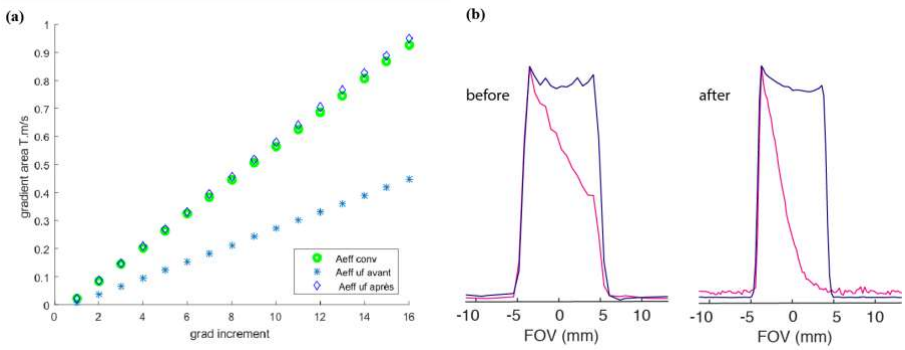

Figure 53: (a) Gradient area induced by the chirp and gradient combination before (blue star) and after (green circle) optimization to match the conventional gradient ramp (blue diamond). (b) Comparison of diffusion profile obtained with SPEN DOSY experiment (magenta curve) before and after optimization of the gradient area. The blue shape is the reference profile obtained via the dedicated pulse sequence for purpose of noise correction. Mixture M1' was used.

Table 9: Gradient area optimization parameters

Parameters	before	after
Bandwidth of the pulse (Hz)	100 000	110 000
Pulse duration (s)	0.001	0.002
Extra dephasing period (s)	0.001	0.0016
Strength for excitation (T/m)	0.2275	0.2535
Gradient area min (T s/m)	7.13×10^{-6}	2.76×10^{-5}
Gradient area max (T s/m)	4.48×10^{-4}	9.08×10^{-4}

8.3.2. Adjusting acquisition parameters

The SPEN DOSY data set of Figure 54c was acquired with an acquisition time of 241 ms with a single scan. With the echo-planar spectroscopic imaging method, the spectral width (SW) of the final spectrum

is defined by $\frac{1}{2T_a}$ where T_a is the duration of the acquisition gradient G_a. The adjustment of this parameters gives control over the folding of the peak in the spectroscopic dimension. In our experiments T_a was set to a value of 192 µs giving a SW of 4.3 ppm. Within the pulse program T_a is defined through to the total number of point (TD), the number of loops (N_L) and the dwell time of the experiments (dw) according to $T_a = \frac{TD\ dw}{4N_L}$. *TD* and *dw* can be chosen arbitrarily (as long as $\frac{1}{dw} > \frac{1}{\gamma GL}$), and N_L is chosen within the limitations of the apparatus. As SW is smaller than the one in the conventional DOSY, peaks outside the window of 4.3 ppm centered on the offset 2.4 ppm will be folded somewhere inside the observable window. Peaks out of range will undergo a translation, which is a multiple of SW. To illustrate this folding. the water peak at 4.7 ppm is folded in the ultrafast dimension at 0.4 ppm in Figure 54d.

Another limitation of EPSI is the duration of the echo-train acquisition, which is usually short (< 150 ms) because of the fragility of gradients on high-resolution probes; this leads to a truncated signal, and the resolution in the spectroscopic dimension (governed by the total acquisition time) is thus lower than for a conventional acquisition. Parameters such as the number of gradient pair oscillation (N_L), the duration of a gradient readout (T_a) and the acquisition gradient strength (G_a) were adjusted to increase resolution in the spectroscopic dimension to its maximum without overcoming the limitations of the apparatus. The acquisition time was set to 98 ms, with 256 loops and the acquisition gradient strength was set to 0.195 T/m with a duration T_a set to 192 µs. We choose to stay around 100 ms total acquisition time because it is less detrimental to the apparatus when using fast oscillations of the reading gradients. For typical values of the acquisition gradient, longer acquisition trains were not possible with our gradient units: the oscillating gradients are not effective during the whole acquisition time and there are no echoes at the end of the FID.

With EPSI, the resolution in the spatial dimension is governed by the product $\gamma G_a T_a$. The spectral width and the spatial resolution are thus not independent, and further investigation needs to be done in order to see how the value of G_a affects the diffusion coefficient measurement.

8.3.3. Diffusion coefficient determination

The SPEN DOSY experiment was run using the aforementioned optimized parameters, yielding the data set of Figure 54b after data reordering and Fourier transformation in the two dimensions. Such data set is analogous to the dataset obtained from a conventional DOSY experiment. Instead of having all of the individual spectra acquired one after another, they are obtained with just one transient. The data is processed peak by peak, as in the DOSY Toolbox. For each peak, the slice corresponding to its image is selected in the 2D dataset. The image region is plotted against position in the sample, and gives the profile in Figure 54c. Each point of the profile can be considered as analogous to a gradient level in the

conventional experiment. The gradient area experienced by the spins depends on the position in the sample and entails some degree of signal attenuation along the sample. Fitting of the decaying profile of Figure 54c was performed for a sample region ranging from -4 mm and +4 mm and results are shown on Figure 54c. The shape reflects the encoding gradient strength effect on spins throughout the observed region of the tube. The maximum of the shape corresponds to the lowest gradient area and the minimum of the shape corresponds to the highest gradient area therefore, the first and last gradient level respectively. If we look at Figure 54a, we see that the calculated values of D are close to the reference values (dashed lines) even though they are consistently higher.

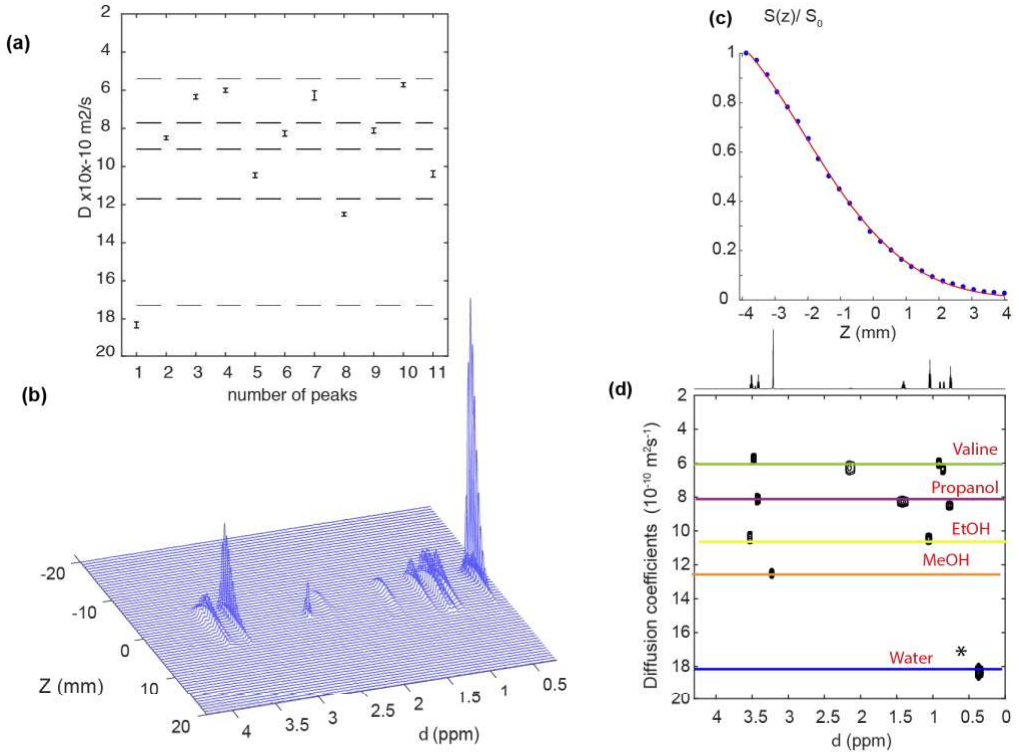

Figure 54: (a) Comparison of DOSY reference values (dashed lines) and SPEN-DOSY results for the mixture of alcohols and L-valine in D_2O. (b) SPEN DOSY dataset. (c) Diffusion curve for methanol resonance (d) SPEN DOSY display. Mixture M1 was used.

The reconstructed SPEN DOSY display is shown in Figure 54a and because of the decrease in resolution in the spectroscopic dimension, the calculated DOSY peaks are broader than those of Figure 48. A decrease of resolution is also observed in the diffusion dimension. This experiment suffers from an overall decrease in SNR as well. This time we changed the offset of our experiment so that the signal of the water peak at 4.7 ppm would be folded at 0.4 ppm in the SPEN spectrum. There is clearly a good separation of the five compounds. In the case of propanol, the three peaks give a mean value of D= 8.29 $\pm$ 0.19 $\times$ 10^{-10} m^2 s^{-1} with a RSD of 2.3 %, which means that the measured diffusion coefficients within the same molecules are consistent. In this concentrated sample no signals are lost in spite of the decreased sensitivity [232]. However, some signals, such as valine's signals at 3.54 ppm or at 2.21 ppm

are so weak that the processing was quite tricky to obtain a correct lineshape. Even if the calculated diffusion coefficients do not match very well the reference value, we demonstrated the ability of this experiment run in 241 ms to return a SPEN-DOSY spectrum comparable to the conventional spectrum. In practice, these single-scan experiments were carried-out with a recycle delay of 5 s to prevent accidental hardware damage. Stability of the SPEN-DOSY as well as reproducibility was assessed by comparing the results of 5 experiments and 4 experiments over several days. This experiment is repeatable and reproducible as there is less than 2 % of CSV for all the results. The compounds concentration in the mixture is high enough so that the decrease in sensitivity does not prevent us to recover all the peaks of the spectrum but this may not be suitable for more diluted mixtures as the SNR should be sufficient for the part of the diffusion curve the most attenuated. Scan averaging would probably be necessary but the experiment would still remain faster that the classic one.

8.3.4. Spin-echo SPEN DOSY

Several other SPEN DOSY pulse sequences were created during the course of this work. Notably, two sequences based on a spin rather than stimulated echo (STE) were implemented. Similar sequences were described, but not implemented, in the work of Shrot and Frydman[42] and are presented in Figure 55. The first one is a spin echo sequence (SE) were the chirp pulses have opposite signs and are separated with a 180° pulse [223]. The other one is a non-echoed version (NE) where the chirp pulses have the same sign and are separated by Δ. The diffusion coefficients of Table 10 obtained with those sequences were close to what we have with our own SPEN DOSY sequence. With these versions, we do not lose 50 % of the signal available compared to the stimulated echo version. However, since the magnetization remains in the transverse plane, signal loss can occur due to J-modulation and T_2 relaxation. This could explain the highest calculated values for the diffusion coefficient in Table 10.

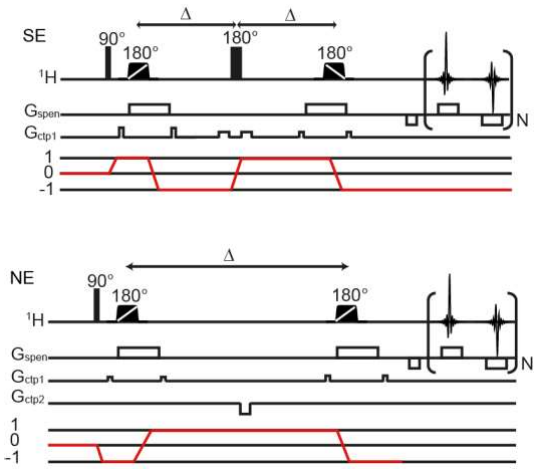

Figure 55: SPEN DOSY based on spin echo (top) and non-echoed version (bottom).

Table 10: Diffusion coefficients for SPEN DOSY STE version, SE version and NE version on caffeine and ethylene glycol in D_2O

	Diffusion coefficients ($\times 10^{10}$ m^2 s^{-1})		
Molecules	**(STE)**	**(SE)**	**(NE)**
caffeine	5.96 ± 0.15	6.10 ± 0.13	6.24 ± 0.14
caffeine	5.99 ± 0.15	6.13 ± 0.13	6.29 ± 0.14
ethylene glycol	10.40 ± 0.22	10.85 ± 0.24	11.06 ± 0.25
caffeine	5.93 ± 0.15	6.13 ± 0.14	6.30 ± 0.14
water	19.85 ± 0.57	20.62 ± 0.62	20.90 ± 0.62
caffeine	5.97 ± 0.16	6.00 ± 0.15	6.40 ± 0.16

8.4. Spatially-encoded 3D DOSY on mixture

While DOSY in its simplest form is well-suited when dealing with mixtures that contain a moderate number of compounds, it is not always suitable to separate multiple components in the case of overlapped NMR peaks. An interesting option to address this limitation of DOSY for crowded spectra is to further increase the dimensionality of the experiment by adding diffusion weighting to a given 2D experiment, such as COSY. This so-called 3D DOSY approach of course results in a lengthening of the experiment duration, from several minutes to several hours for conventional DOSY.

8.4.1. Pulse sequence design and parameters

On the basis of previously described sequences [81,84,148], a COSY encoding block was inserted within the SPEN-DOSY pulse sequence, combined with a pair of coherence selection gradient pulses flanking the mixing 90° pulse. The corresponding pulse sequence is illustrated in Figure 56. In the case of 3D DOSY pulse sequences, either one or both of the indirect domains may be spatially encoded so that experiments are performed within the timescale of a conventional 2D experiment or faster [189,233–235]. Here we choose to only spatially encode the diffusion dimension, as a doubly spatially encoded experiment would have extremely limited resolution and spectral width in the spectral dimensions.

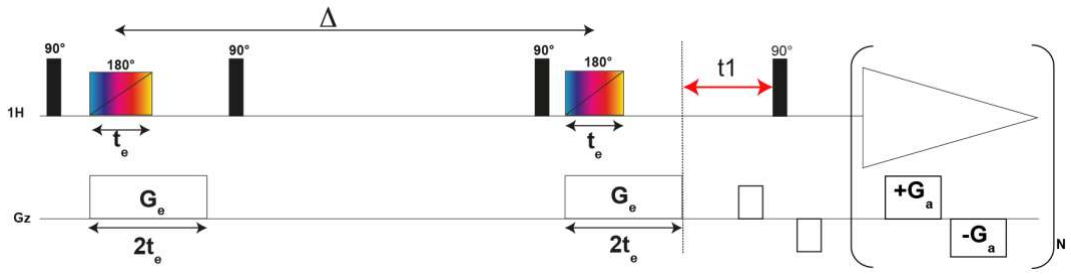

Figure 56: SPEN DOSY COSY pulse sequence using EPSI type acquisition.

The optimal encoding parameters chosen were a chirp bandwidth of 130 000 Hz, a chirp duration of 2 ms, an encoding gradient of 0.26 T/m and an extra dephasing gradient duration of 1.6 ms. The acquisition parameters were a 192 μs acquisition gradient duration, 256 gradients loops, and 4.3 ppm spectral width in the spectroscopic dimension. The SPEN DOSY COSY experiment was recorded with 128 increments in the indirect dimensions and 8 dummy scans, resulting in a total experimental time of 11 min. The data was normalized by a reference profile in the spatial dimension.

8.4.2. Results for alcohol-valine mixture

The previous results showed that it is possible to acquire a DOSY spectrum in less than one second and still have a good separation between each species in the diffusion dimension. In this part of our work we have demonstrated that the SPEN-DOSY sequence could be extended to a third dimension. As a first demonstration, the SPEN DOSY-COSY pulse sequence of Figure 56 was performed on a mixture of ethanol, methanol, propanol, L-valine in D_2O. As above, the conventional DOSY spectrum of Figure 48 was acquired for this mixture and the results from this experiment are used as reference values. Ethanol and propanol, have diffusion coefficients that differ by 10 % but they are well separated and there is no ambiguity on the peaks' assignment. The whole experiment was done in 11 min and our speed criterion is achieved. Interestingly, this experiment is run even faster than the conventional 2D DOSY.

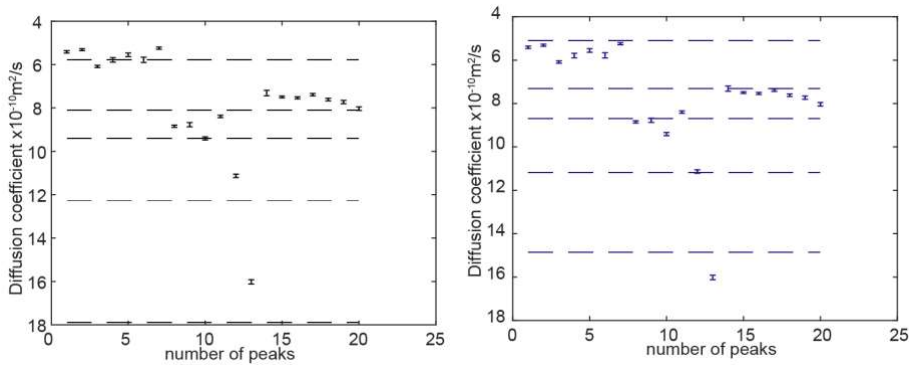

Figure 57: Results of DOSY-COSY (dashed lines) compared with results of SPEN-DOSY-COSY (left); Results of SPEN-DOSY (dashed lines) compared with results of SPEN-DOSY-COSY (right). Mixture M1 was used.

The diffusion coefficients are calculated as explained in section 8.2.3 with the volume of each signal calculated for each COSY plane of the 3D data set shown in Figure 58a. The resulting spatial profiles of Figure 58b are similar to those obtained with 2D SPEN DOSY and signals below 3 times the noise were removed. A fit to the modified Stejskal-Tanner equation then gave the diffusion coefficient. Compared to the reference diffusion coefficients values of obtained with the conventional experiment, those obtained with SPEN-DOSY-COSY were smaller, as shown in Figure 57 (left). This is consistent with earlier observations with SPEN-DOSY. However, if we compare results between the two SPEN experiment (2D and 3D) in Figure 57 (right), the values are not matching except for methanol. Note that diffusion coefficients measured for moieties of a same compounds present a variation of less than 6%. This does not prevent the extraction of the COSY of individual molecules for appropriate diffusion coefficient values in illustrated Figure 58c-g. The separation of the signals of each compound was successful as we manage to plot the expected individual COSY.

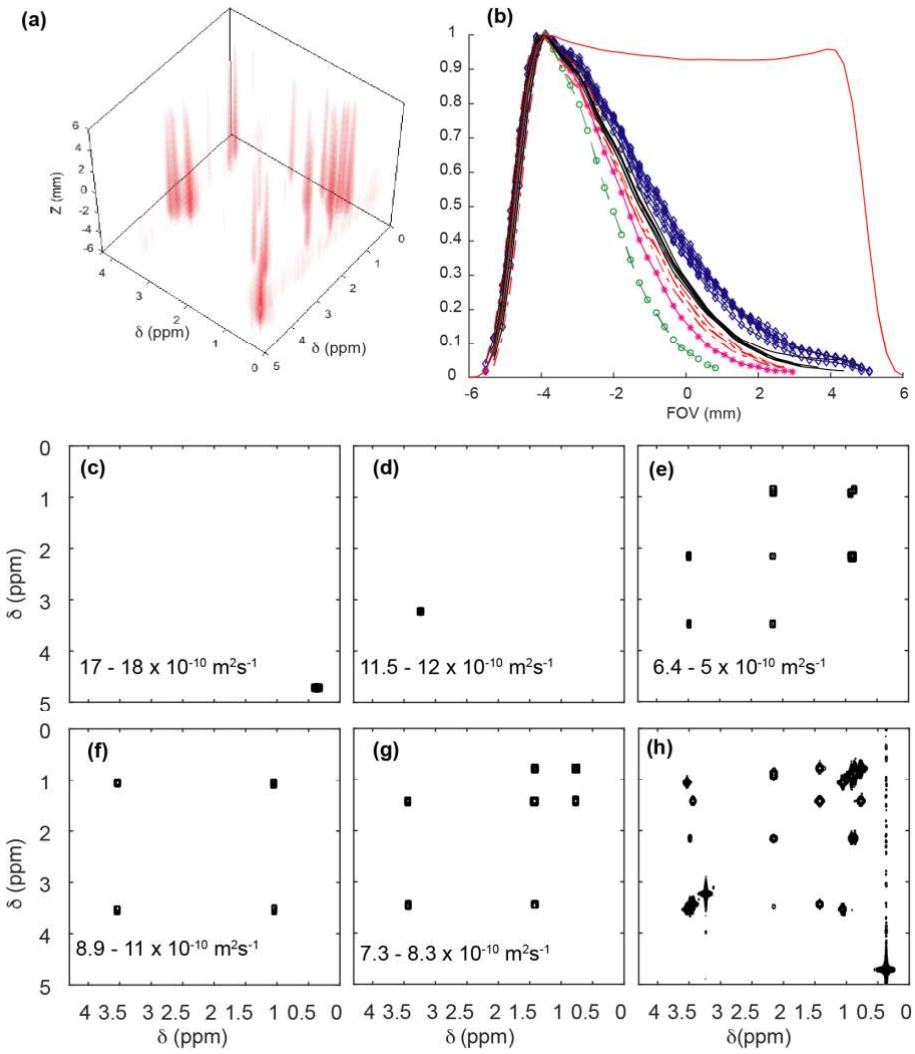

Figure 58: (a) SPEN DOSY COSY data set on mixture M1. (b) Decay profile of each signal thorough the SPEN-DOSY-COSY experiment. (c-h) Extracted COSY spectra for each molecule according to diffusion coefficients values.

For validation, the SPEN-DOSY-COSY sequence was be used on the previous model mixture of caffeine and ethylene glycol, for which it shows good results with well-aligned peaks (data not shown). The folded peak of caffeine is well separated in the COSY extracted from 3D data compared to the SPEN-DOSY spectrum where it was quite tricky to isolate from the surrounding peaks.

Note that at the time that the experiments were done, model was not corrected yet regarding the displacement due to chemical shift during the acquisition (cf. 7.3.3) so it could be interesting to reprocess the data with appropriate corrected processing. In Figure 57, peaks number 11 is between two reference and one could not conclude (without knowing the sample) that it belongs to ethanol or worse conclude that it comes from another additional compound.

8.5. Increasing the resolution in SPEN DOSY

As part of our efforts to improve the accuracy of SPEN DOSY experiments, resolution is one of the areas where we can do something to limit signal overlap, which is detrimental for retrieving diffusion coefficient via monoexponential fitting. A limitation of the proposed SPEN DOSY pulse sequence is that signal folding in the spectral dimension, due to the reduced spectral width of the EPSI acquisition, leads to more overlap. This typical feature of EPSI can be troublesome especially when the NMR spectra present many signals dispersed over a broad chemical shift range as in our mixture **M3**. We show results for a mixture of 4 molecules of bipyridine, dimethyl nicotinamide, 3-ethylpyridine and pyridine (analyzed later on in Section 10) in Figure 59. The 1D spectrum illustrated in Figure 59a reveals that in such situation, signals located outside the observed windows (red rectangle) will be folded back within the observed range (red arrows). One can attempt to find appropriate acquisition parameters so that the folded peaks can be folded where no other peaks are found. However, it is not always possible to do so and some peaks will often end up folded over the others peaks creating unwanted signal overlap; we would then be back with the problem of resolution unfavorable for DOSY. In order to avoid this limitation, a possible approach would be to increasing the spectral range of the EPSI acquisition, with an interleaved acquisition that multiplies the spectral width by n_i, with the use of n_i scans [236]. Unfortunately, this method produces several artefacts that highly affect the readability of 2D DOSY spectra as well as the measurement of diffusion coefficient when artefacts overlap with peaks of interest. The strategy we employed here to avoid signal overlap consists in suppressing signals that lay out of the observed range by applying a band-selective refocusing pulse flanked by a gradient pair after the diffusion period. The pulse sequence used for this purpose is presented in Figure 59c and the selected region corresponds to the green rectangle of Figure 59a. Only the peaks of interest are left and we no longer have to deal with the remaining ones.

While ultrafast 2D NMR experiments are generally processed in magnitude mode, pure-absorption spectra can in principle be obtained with the EPSI acquisition of SPEN DOSY, provided that the chemical shift evolution is refocused at the center of the first gradient readout [237]. Since all echoes are centered at k=0 in the (k,t2) space during the acquisition, it implies that all echoes are subjected to the same first-order phase and that phase correction can be performed to obtain absorption spectrum. This possibility will be of major importance when it comes to dealing with compounds whose NMR signals are close in chemical shift. Figure 59b shows the spectrum for the mixture without spectral selection for magnitude processed spectrum. In this case it is quite a mess and there is no clear separation of all the molecules. Some peaks as for the pyridine are not impacted too much and separated. We can see that with the spectral selection, the display of Figure 59d is cleaner but still difficult to interpret. The comparison of magnitude mode, illustrated by Figure 59d, and phased mode processing, illustrated by Figure 59e, on our mixture in methanol gives undoubted results in favor of the phased case. Separation

of the different compound in the diffusion dimension is much improved as we can see in Figure 59e. Phased DOSY display shows a better resolution and a significant improvement for the separation. Note that this was possible with the STE version of the SPEN DOSY but not with the SE nor NE version due to issues with J modulation that prevent the spectra from being phased in the conventional dimension.

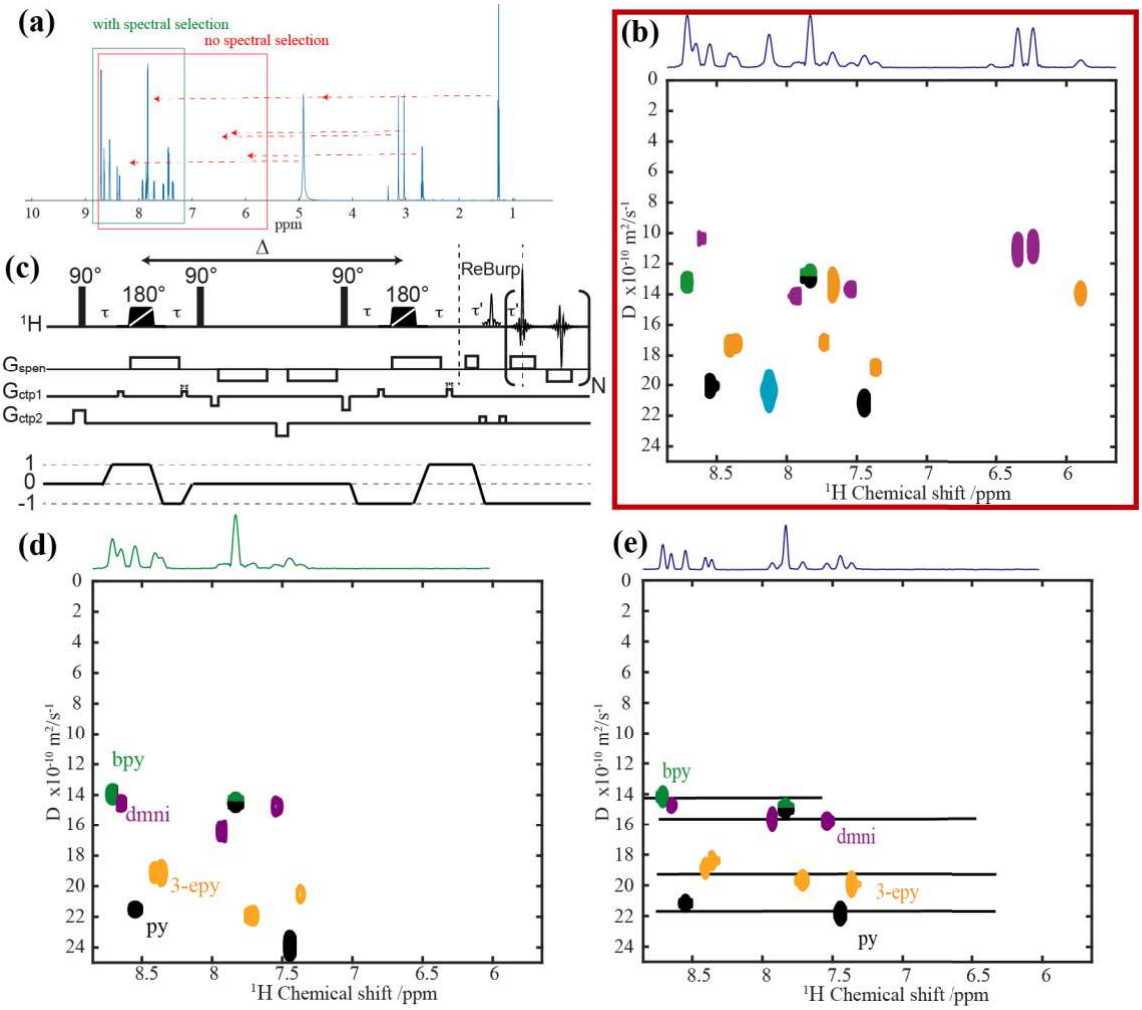

Figure 59: (a) 1D spectrum of mixture M3 which indicates folding of peaks without spectral selection (red) and the region spectrally selected (green). (b) SPEN DOSY display without spectral selection and processed in magnitude mode. (c) Phased SPEN DOSY pulse sequence that includes a band-selective shaped pulse (d) SPEN DOSY display with spectral selection processed in magnitude mode. (e) SPEN DOSY display with spectral selection processed in phased mode.

8.6. Convection compensation

A serious disturbance that affects diffusion measurement is the presence of convection currents due to temperature gradients throughout the sample [157,158,160,161]. The use of pulse sequences that are

specifically designed to compensate for the effect of convective flow can help to reduce this unwanted effect, as proposed by Jerschow and Muller [163]. In their approach, the diffusion weighting proceeds in two symmetrical steps rather than a single one. Figure 60 shows a convection compensated version of the SPEN DOSY pulse sequence that is based on a double diffusion encoding scheme. This double stimulated echo (DSTE) SPEN DOSY is inspired of what is commonly done in conventional convection compensated pulse sequence [163,165,166]. The resulting DSTE SPEN DOSY pulse sequence consists of two successive SPEN DOSY separated by a hard 180° pulse to reverse coherence transfer pathway (CTP).

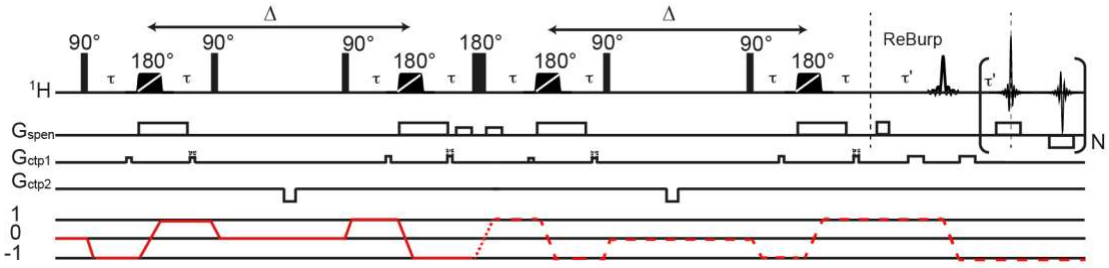

Figure 60: Convection compensated SPEN DOSY based on a double diffusion encoding scheme.

Since convection motion causes further phase shift of the magnetization on top of the one induced by the random Brownian motion we seek to evaluate, the aim is to impart opposite convection-induced phase shifts in each half of the pulse sequence that will cancel each other out. The phase error induced by a constant velocity flow is of the form

$$\Phi_v(t) = \gamma G(t) v_t \tag{26}$$

and leads to a signal modulated according to

$$S(K) = \mathrm{S}_0 e^{-\left[\mathrm{D}K^2\left(\Delta-\frac{\delta}{3}\right)\right]} e^{[iv_t K\Delta]} \tag{27}$$

In the case of SPEN DOSY Eq. 27 becomes

$$S(z) = \mathrm{S}_0 e^{-[\mathrm{D}K(z)^2(\Delta')]}\, e^{[\mathrm{i}\mathrm{D}K(z)v_t(\Delta-\tau)]} \tag{28}$$

This result is calculated from Eq (11). (12). (15). (16) in section 6 and the expression of the attenuation during the diffusion delay substituted in

$$S(t.z) = \mathrm{S}_0 e^{-\left[\mathrm{D}\int_0^t \left(K(t'.z)\right)^2 dt'\right]} e^{i\left[\mathrm{D}v_t \int_0^t K(t'.z)dt'\right]} . \tag{29}$$

If we consider p as the coherence order that change to select the desired CTP one can define

$$G^*(t) = pG(t) \tag{30}$$

and

$$K^*(z) = pK(z) \tag{31}$$

The S-T equation for the DSTE becomes

$$S(z) = \mathrm{S}_0 e^{-\left[\mathrm{D}K_1^*(z)^2\left(\Delta''-\frac{\tau}{2}\right)\right]}\, e^{[\mathrm{i}\mathrm{D}K_1^*(z)v_z(\Delta''-\tau)]}\, e^{-\left[\mathrm{D}K_2^*(z)^2\left(\Delta''-\frac{\tau}{2}\right)\right]}\, e^{[\mathrm{i}\mathrm{D}K_2^*(z)v_z(\Delta''-\tau)]}$$

with $\Delta^{"} = \frac{\Delta}{2}$ so that the result can be compared with the single STE. Compensation of the velocity induced phase term is obtained for $K_1^*(z) = -K_2^*(z)$ in a way that the diffusion effect is cumulative at the end of the pulse sequence.

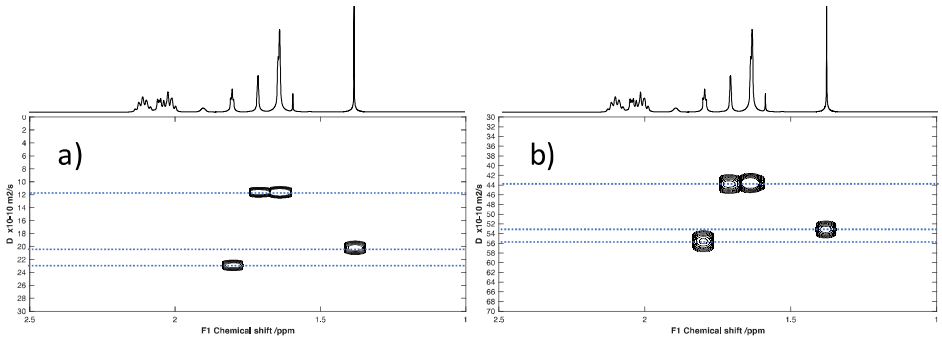

Figure 61: (a) 2D DSTE SPEN DOSY (b) 2D STE SPEN DOSY experiment on mixture M2 composed of three molecules (cyclododecane, squalene, adamantane) at a concentration of ~200 mM in CD_2Cl_2 at 295K.

The pulse sequence was tested on a model sample **M2** consisting of squalene, adamantane and cyclododecane in CD_2Cl_2. The presence of convection is expected in our model sample because of the low viscosity CD_2Cl_2, compared to D_2O for example, which can intensify convection induced by experimental conditions. Results obtained on our model sample are presented in Figure 61 and Table 11 sum up the values of diffusion coefficients measured. The following results were obtained mainly by Ghanem Hamdoun who is a post-doctoral fellow in the laboratory and he needed this pulse sequence in order to use it to perform chemical reaction monitoring in situ of an NMR tube. Results of this study were published recently [238].

Table 11: Comparison of diffusions coefficients obtained with ste SPEN DOSY, dste SPEN DOSY, conventional results for STE and DSTE experiments.

Conventional STE	**Conventional DSTE**	**SPEN STE**	**SPEN DSTE**
$\times 10^{-10}$ m^2s^{-1}	**$\times 10^{-10}$ m^2s^{-1}**	**$\times 10^{-10}$ m^2s^{-1}**	**$\times 10^{-10}$ m^2s^{-1}**
33.31	15.01	53.17	18.50
27.30	8.20	43.60	9.82
27.31	8.21	43.81	9.69
35.60	16.3	55.59	21.76

Figure 61 shows the results obtained for SPEN STE and SPEN DSTE. Diffusion coefficient values obtained are overestimated compared to the expected values. With the use of the convection compensated values, we are back to diffusion coefficient values that are consistent with the result of conventional DOSY. We must keep in mind that the convection compensative ability come at the expense of sensitivity since each STE part induce 50 % of signal loss.

Another verification that can be done to confirm the presence of convection is to plot the linear function $\left(\ln\left(S/S_0\right) = f(\Delta'.\left(K(z)\right)^2\right)$ for a given signal. This will provide information on the attenuation. In the case of a homogeneous sample 'H_2O in D_2O as reference' that do not undergo convection, the attenuation of the water signal is linear with the STE and with the DSTE and both give the same results as illustrated in Figure 62 (left). However, in the case of cyclododecane in CD_2Cl_2 shown in Figure 62 (right), the linearity is compromised with using the STE sequence. This nonlinear attenuation with respect to the applied gradient strength suggests that an additional effect other than Brownian motion contributes to the signal attenuation. The use of the DSTE sequence will restore this linearity back as the unwanted contribution from convection is removed.

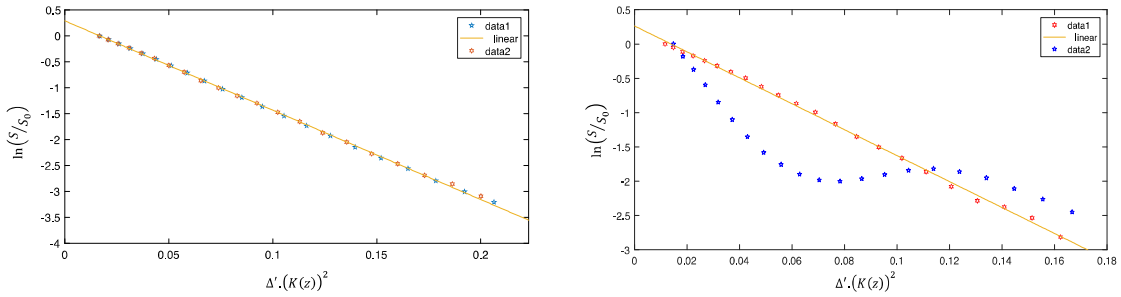

Figure 62: Left: the ln(S/S0)-attenuation of water using DSTE SPEN DOSY (red) and STE SPEN DOSY (blue) sequences. Right: the ln(S/S0)-attenuation of Cyclododecane in CD_2Cl_2 using DSTE SPEN DOSY (red) and STE SPEN DOSY (blue) sequences.

A variation of the diffusion coefficient as function of diffusion delay can be another sign of convection messing with our mixture in CD_2Cl_2. The diffusion coefficients values measured should remain the same for all the values of the diffusion delay. If not, convection will make the diffusion coefficient increase together with the diffusion delay value. In Figure 63 (left), convection causes all signals to show overestimated apparent diffusion coefficients. In Figure 63 (right) The DSTE DOSY experiment restores the signals to the correct positions in the diffusion domain.

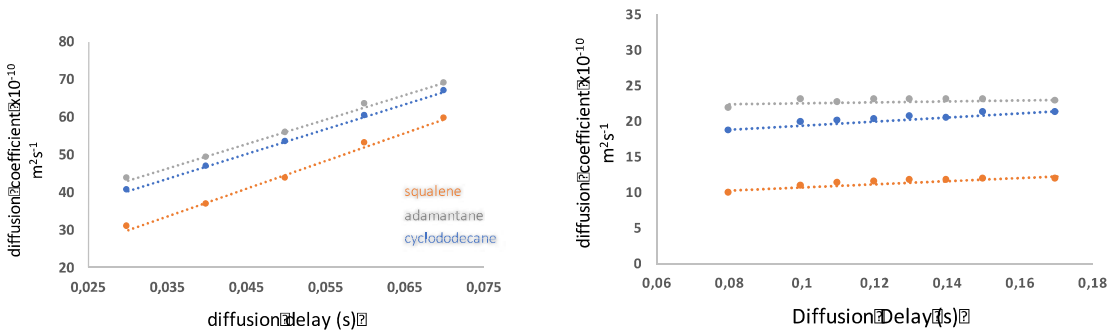

Figure 63: Diffusion coefficient from a) STE SPEN DOSY and b) DSTE SPEN DOSY experiment as function of the diffusion delay on mixture M2.

To support the ability of our new pulse sequence to compensate for convection, numerical simulations in the presence of a constant flow were performed with the Spinach library. As presented in Figure 64, in the presence of a flow, the lineshape of the signal is completely distorted in the case of simulated STE SPEN DOSY compared to simulated DSTE SPEN DOSY. Fitting of the lineshape in the first case will render a diffusion coefficient that is completely off the initial input value. Fitting the lineshape from simulated DSTE SPEN DOSY will give a diffusion coefficient that is consistent with the initial input value but slightly lower. This is because the lineshape undergo a slight displacement along the FOV and this was not accounted nor estimated.

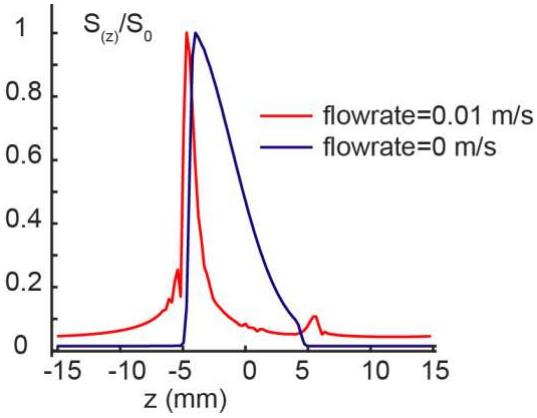

Figure 64: Effect of flow rate on simulated SPEN DOSY diffusion profile with STE (red) and DSTE (blue).

8.7. Conclusions

Our work demonstrates the ability of spatially encoded multidimensional experiments to separate mixture compounds according to their diffusion coefficient. SPEN DOSY spectra are collected in a significantly reduced amount of time, at a cost of a decreased resolution and sensitivity. Although the coefficient values present systematic errors compared to conventional results, we are still able to get

usable spectra where all compounds are sorted according to their diffusion coefficients. Moreover, our experiments suffer from gradients non-homogeneity that needs to be mapped and taken into account in order to improve the results. Three dimensional DOSY experiments can be performed following three various scheme and an interesting modification of our sequence would be to use the I-DOSY alternative to see if the experiment duration can be further decreased. We introduced a new pulse sequence that compensate for convection and that has found application for chemical reaction monitoring and determination of molecular weight. We also proposed a way of increasing the resolution that is of paramount of importance in the quality of the DOSY data. Poor resolution will entail a lack of accuracy of the calculated diffusion coefficients and this will result in a compromise separation of compounds. The work from sections 6 and 8 was published in Ref. [231,238,239].

9. SPEN DOSY of hyperpolarized mixtures using D-DNP

9.1. Introduction

The sensitivity limitations of NMR can be addressed with the use of dissolution dynamic nuclear polarization (D-DNP), which provides, in theory, signal enhancements of up to 10 000. A brief introduction to DNP and its use for the analysis of mixtures has been given in Section 5 [45], [240] In the D-DNP method, enhanced signals last for at most a few tens of seconds in solution, because of longitudinal relaxation. The SPEN DOSY experiment should thus be relevant to be combined with D-DNP and record DOSY spectra of hyperpolarized mixtures in the imparted time-window. We wanted to demonstrate the possibility to use the SPEN DOSY pulse sequence to record DOSY data from hyperpolarized substrates, which would have a significantly increased sensitivity compared to thermal equilibrium experiment, even when considering the sensitivity penalty associated with SPEN experiments. The expected signal enhancement is sufficient to compensate for the sensitivity loss that comes with ultrafast-type experiments and still be able to get a significant gain.

This section presents how we managed to record SPEN DOSY data from DNP-hyperpolarized substrates. First, we needed to implement the pulse sequence on the spectrometer used for D-DNP and adapt the parameters to the chosen model samples. We also needed to determine whether ^{1}H and/or ^{13}C data can be recorded, as the isotopes do not yield the same signal enhancements and lifetimes. As we will show, convection compensated pulse sequences turned out to be necessary to obtain stable diffusion coefficients from one experiment to another.

The experiments presented in this section were done in collaboration with the NMR group headed by Geoffrey Bodenhausen at the Ecole Normale Supérieure (ENS). The ENS hosts a unique D-DNP prototype, which is accessible through a national user platform. Specifically, we worked with Dennis Kurzbach and Daniel Abergel, who provided their expertise with D-DNP. Their knowledge and practical experience on D-DNP was a key to the successful combination of this innovative technique with SPEN DOSY.

9.2. DNP experimental settings

9.2.1. Apparatus

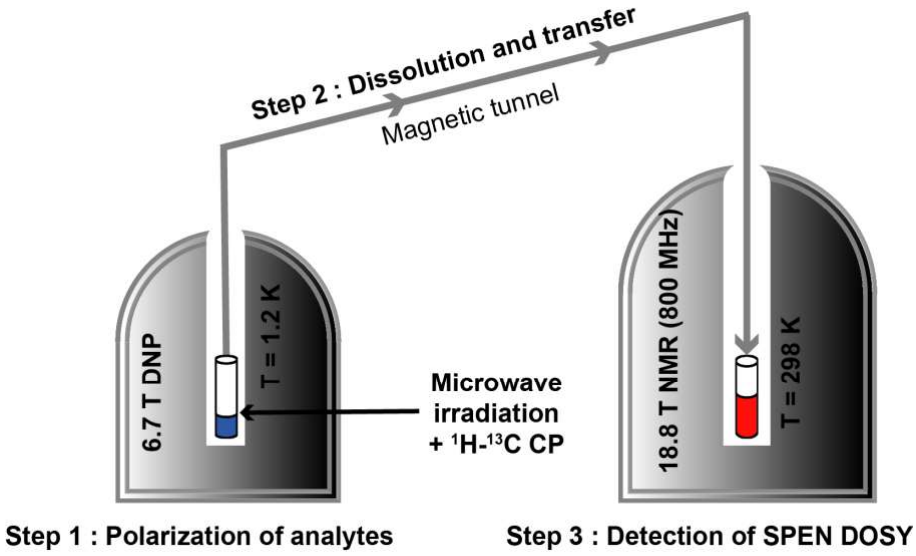

Figure 65: Dissolution DNP apparatus composed of a polarizer associated to a high field spectrometer.

Figure 65 shows a schematic description of the experimental setup for D-DNP. A prototype polarizer (Bruker) operating at 6.7 T and 1.2 K was used to perform DNP experiment. This prototype is associated with a Bruker spectrometer operating at a Larmor frequency of 800.30 MHz. A 5 mm TXI probe with triple axis gradients was used for ^{1}H experiments and a 5 mm BBO broadband probe with single z axis gradient for ^{13}C experiments (because the TXI probe was gone for repair). The temperature was set at a nominal value of 298 K. The transfer time from the polarizer to the spectrometer was set to 6 s and the magnetic field in the transfer capillaries is ca. 0.8 T. In the case of ^{13}C experiments, an additional delay of 10 s was set after injection from the separation chamber. This chamber needs to be cleaned up and dried for each experiment otherwise decrease of the signal intensity can be observed.

9.2.1. Sample preparation

A simple mixture was prepared mixing caffeine (5.8 mg) and ethylene glycol (2 µl) in 600 µl of D_2O in a 5 mm classical NMR tube. This mixture is used as to check that the SPEN DOSY experiment is implemented correctly.

The sample used for the ^{1}H D-DNP experiment was composed of 50 % ethanol and 50 % glycerol-d_8. The polarizing agent was 4-hydroxy-2,2,6,6-tetramethylpiperidin-1-oxyl (TEMPOL) at a

concentration of 50 mM. Mock dissolutions were performed on a concentrated sample at 1 M ethanol in D_2O for parameters optimization.

A mixture of 1-^{13}C-pyruvate, 1-^{13}C-acetate and ^{13}C-urea was prepared for D-DNP experiments, with a concentration of 1 M for each compound. The polarizing agent was 4-hydroxy-2,2,6,6-tetramethylpiperidin-1-oxyl (TEMPOL), at a concentration of 50 mM. All compounds were solubilized in a glass-forming solvent composed of D_2O/H_2O/glycerol-d_8 (4:1:5) (v/v). The solution was stirred until complete dissolution of all compounds and sonicated in a warm bath for 10 min.

For thermal equilibrium experiments, a mixture was prepared with a concentration of 750 mM for 1-^{13}C-pyruvate and 500 mM for 1-^{13}C-acetate and ^{13}C-urea in D_2O/H_2O/glycerol-d8 (4:1:5) (v/v), without polarizing agent. The mixture was used as is for thermal equilibrium SPEN DOSY experiments, and after dilution by a factor of 25 with D_2O for conventional DOSY experiments. We also used a solution of 1-^{13}C-pyruvate (700 mM) in D_2O and a solution of 1-^{13}C-pyruvate, 1-^{13}C-acetate, ^{13}C-urea and 1-^{13}C -methionine (100 mM each) in D_2O/H_2O for preliminary experiments.

9.2.2. Polarizing

Polarization of proton was performed on a 50 µL-sample at 1.2 K in a magnetic field of 6.7 T for 30 min under continuous microwave irradiation (187.9 GHz, ca. 12 mW at the locus of the sample). The microwave was modulated with a frequency of 2 kHz over a range of 100 MHz.

Hartmann-Hahn type cross polarization from ^{1}H to ^{13}C was performed on a 100 µL sample at 1.2 K in a magnetic field of 6.7 T for 30 min under continuous microwave irradiation (187.9 GHz, ca. 12 mW at the locus of the sample). The microwave was modulated with a frequency of 2 kHz over a range of 100 MHz.

9.2.3. Dissolution and transfer

The frozen hyperpolarized sample was then dissolved with 5 mL of superheated D_2O (10.5 bar 180 °C) and transferred in a 5 mm NMR tube placed in an 18.8 T spectrometer operating at 298 K. During the transfer, the sample arrives first in a separation chamber and is then pushed with a piston and a stepper motor into the receiving NMR tube. The sequence starts when the piston starts to move. The capillary of injection goes fully down to the bottom of the NMR tube. The total transfer duration was ca. 6 s. For the proton experiment relaxation delay d_1 was set to 2.5 s and for carbon experiment d_1 was set to 10 s.

9.3. Single-diffusion encoding: case of ^{1}H

The highest sensitivity for D-DNP experiment should be obtainable with ^{1}H spins, which have a high natural abundance and magnetogyric ratio, if they are efficiently polarized and if the polarization can be preserved until acquisition. However, since the success of the D-DNP approach is very dependent on the longitudinal relaxation time T_1 of the observed nuclei, the ^{1}H T_1 values of less typically less than 5 s can be a challenge for ^{1}H D-DNP. A first goal is to record a single SPEN DOSY spectrum that gives reliable results in less than 10 s, after dissolution. Ideally, we want to obtain multiple diffusion spectra with a single D-DNP experiment, each spectrum being recorded in less than 1 s. Here we describe our (so far unsuccessful) attempts towards the acquisition of hyperpolarized ^{1}H SPEN DOSY data, which served as a preliminary basis for the rest of the work oriented toward boosting sensitivity.

9.3.1. Transfer of methods

Since we performed the experiment on a different spectrometer and probe, preliminary experiments consisted at first of checking if the result of SPEN STE DOSY experiments gave consistent results on a new spectrometer compared to what we usually have in our laboratory. Starting with a known sample of caffeine and ethylene glycol in D_2O, the conventional DOSY sequence was tested as well as the SPEN DOSY sequence using the same settings as for the 600 MHz spectrometer. The stimulated echo sequence including bipolar gradient pulses with LED was performed and gave expected results for diffusion coefficient (data not shown). An imaging pulse sequence, presented in section 6, was also tested to get the reference profile of our sample. This is important as we can improve the accuracy of the calculated diffusion coefficient by taking the real shape of our signal that is dependent on gradient linearity. The results obtained are satisfactory compared to what we have on a 600 MHz (cf. section 6).

The various SPEN DOSY experiments that we have previously designed and implemented were run over a region of 10 mm using a chirp bandwidth of 110000 kHz for 1.5 ms, a post chirp duration of 1.5 ms, an encoding gradient of 0.2535 T/m, usual values for coherence selection, a diffusion delay of 100 ms and 0.195 T/m acquisition gradient with 256 gradients loops and a read gradient duration of 192 µs (including the 25 µs for the ramping period de the trapezoidal gradient used). This results in a spectral width of 2600 Hz. The prephasing gradient was set to 0.0975 T/m. The 2D experiments was recorded in a single scan of 241 ms.

The conventional DOSY experiment was run with the same parameters as in section 6 with a stimulated echo pulse sequence with bipolar gradient pulses, a LED delay and additional lock stabilization gradients deriving from the original **ledbpgp2s** Bruker sequence.

9.3.2. Design of spin echo based SPEN DOSY

Since we were interested in recording a time series of DOSY data, the stimulated echo pulse sequence was not suitable as it includes several 90° pulses that deplete the entire magnetization in a single can. For this reason, we designed a spin-echo pulse sequence. This in addition prevents the 50% signal loss associated with the stimulated echo. The sequence described here also relies on small tip angle excitation pulses to excite small portions of the magnetization for each scan and thus perform multiple scans with a single D-DNP run.

A version of SPEN DOSY based on a spin echo was presented in section 6 and could be used in combination with D-DNP. Our choice however was in favor of a spin-echo-based SPEN DOSY sequence, presented in Figure 66b, which involves a pair of adiabatic chirped π-pulses for refocusing (in addition to the chirp pulses that are combined with gradient pulses and responsible of diffusion encoding), which we named SPEN ASE DOSY (for adiabatic spin echo). The use of 180° adiabatic pulses help to reduce sensitivity to B_1 inhomogeneity and miscalibration [206]. A spectroscopic imaging acquisition is again used, with a train of bipolar gradient pulses. The proposed spin echo pulse sequence has the advantage of restoring the unexcited magnetization back to its initial position at the end of the pulse sequence. This is useful if we want to perform multiple sampling of the non-equilibrium magnetization as schematized in Figure 66a. However, since the excited magnetization remains in the transverse plane during the whole diffusion delay, signal losses are expected from T_2 relaxation, and distortions are expected because of J-modulation.

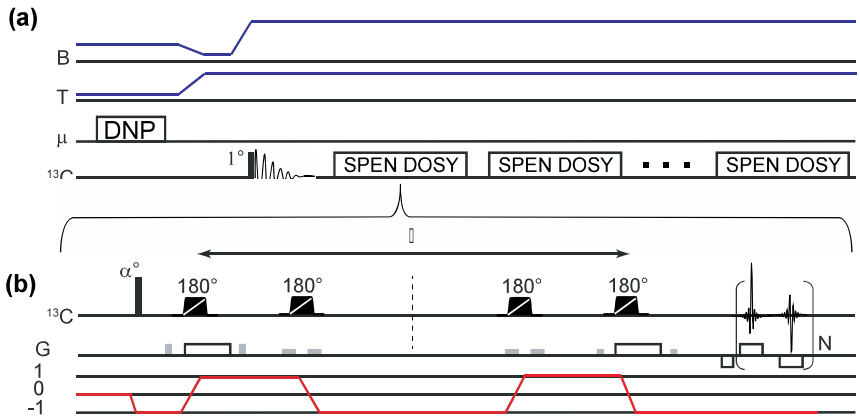

Figure 66: (a)Timing of the polarization, dissolution and acquisition steps, with the evolution of the temperature and magnetic field. (b) Adiabatic Spin Echo pulse sequence.

The use of a pair of adiabatic pulses is inspired from the work of Koelsh *et al.*, [223] and from fast spectroscopic imaging experiments for hyperpolarized ^{13}C MRI. Koelsh *et al.* demonstrated that diffusion coefficients can be determined with accuracy for ^{13}C hyperpolarized molecules with a long

longitudinal relaxation time, provided that signal losses due to T_1 relaxation and multiple excitations are taken into account. A way to avoid diffusion coefficient alteration by the hyperpolarized signal decay would be to use SPEN DOSY pulse sequence, as it offers the possibility to record a full DOSY dataset in a single scan. For coherence selection, independent pairs of gradients are placed around each chirp pulse with strength comprised between 0.0378 and 0.2538 T/m and a duration of 800 µs.

Table 12: Comparison of diffusion coefficient of SPENDOSY STE, ASE and NE on the sample of ethanol in D_2O

	Diffusion coefficients ($\times 10^{10}$ m² s^{-1})		
Molecules	**STE**	**ASE**	**NE**
Ethanol (CH3)	8.36 ± 0.08	7.89± 0.06	7.86± 0.05
Ethanol (CH2)	8.26± 0.07	7.73± 0.06	7.81± 0.05
HOD	15.63± 0.09	14.90± 0.08	14.82± 0.07

The ASE pulse sequence was first assessed with thermal equilibrium experiments on a sample of ethanol in D_2O as shown in Figure 67. The diffusion coefficients obtained, that are shown in Table 12, with this sequence were close to what we have with our STE-based SPEN DOSY sequence but a bit lower. Results are also shown for the spin-echo sequence that uses a non-echoed CTP for the sake of comparison and because we did increase gradually the complexity of the pulse sequence. This is a mean to check if the results are consistent as well. This will serve as reference values to be compared with the SPEN ASE DOSY spectra acquired with D-DNP. We can still notice that a good resolution is observed in the diffusion dimension and the results are in agreement with what we have in conventional DOSY. The error on the fit is also small.

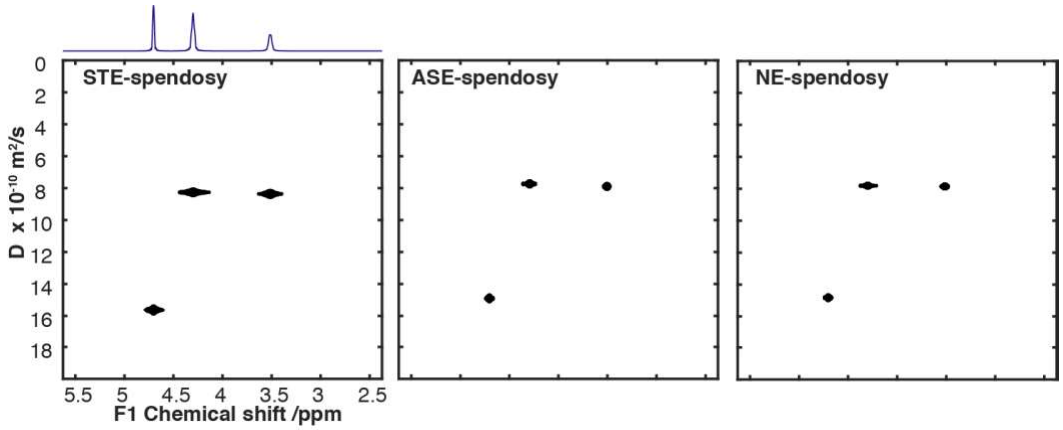

Figure 67: SPEN DOSY display acquired on a sample of ethanol in D_2O for the of SPENDOSY STE, ASE and NE experiments.

9.3.3. Dissolution experiments

In order to evaluate the stability of diffusion coefficients that could be obtained after dissolution of DNP-hyperpolarized substrates, we first performed mock dissolutions without the polarization step. The transfer and injection steps induce a lot of motion in the sample and this can strongly deteriorate the signal attenuation profile obtained with DOSY. Results of mock dissolutions are presented in Figure 68 for 4 scans acquired every 5 s.

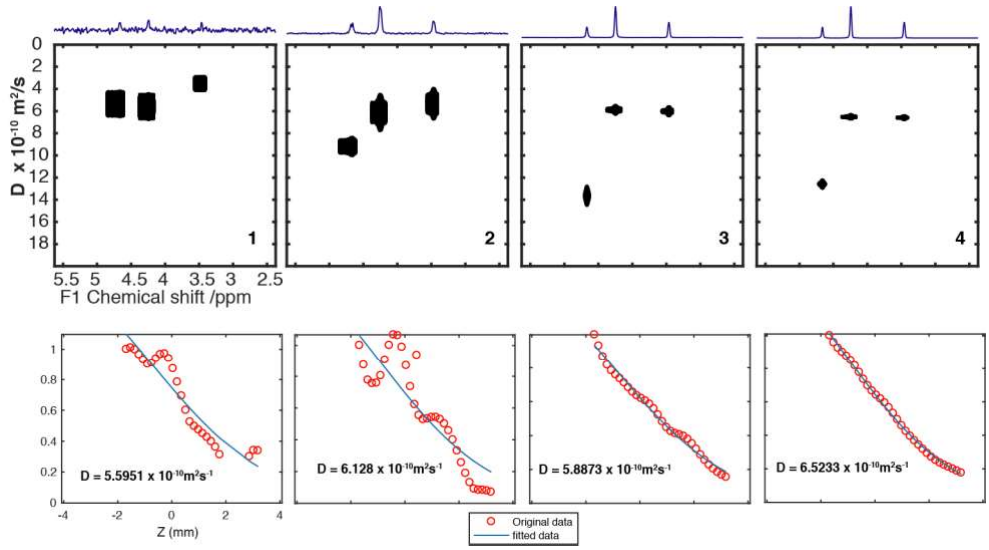

Figure 68: Mock dissolution with 4 SPEN DOSY ASE acquired on a sample of ethanol in D_2O. SPEN DOSY are acquired sequentially every ~2.5 s. Diffusion curves are shown for CH_3 resonance of ethanol at folded 4.2 ppm.

We can see that the estimated diffusion coefficients are very different from the expected values. The homogeneity for the two peaks for ethanol is not respected as well for the two first scans. The error in the fit is higher for scan 1 and 2 compared to scan 3 and 4 because the injection causes turbulences that did not have the time to settle down. Stability seems to be restored at scan 3 but the diffusion coefficients are smaller than the reference experiments shown in Figure 67. Additionally, the diffusion curves show strong oscillations that are attenuated with time. They are reduced in the 4th scan, obtained 20 s after dissolution.

Since the difficulty to acquire good quality diffusion data with DNP on ^{1}H is due to both the delay for transfer and injection and the motion caused by sample injection, we tried several methods to improve the injection step. For DNP experiments on slowly relaxing ^{13}C spins that are now routine, the sample is transferred to a separation chamber in the bore of the NMR magnet, then injected with a piston and a stepper motor in 5 s in the NMR tube that is already located in the spectrometer. Because this process is too slow for ^{1}H experiments, we tried to reduce the injection time to 3 s and also to start the acquisition earlier by using a relaxation delay d_1 of 2.5 s. A practical issue that we faced was to make

our sample arrive correctly in the tube. Indeed, the solution did not go to the bottom of the tube after injection. This was the case when the capillary was not down to the bottom of the tube. We did not want to put the capillary at the bottom of the tube to prevent distortions of the image of the sample. Indeed, we have noticed that each time the capillary was fully inside the tube, then the spatial profile was distorted as shown in Figure 69 (left). We made reference profiles and this was clear that we should not include the capillary. This is mostly due to air bubbles that entails voids in the capillary so no spin density to be observed. The profile shows gaps and decreased intensity were the bubbles are, as shown in Figure 69 (left). The downside of putting the capillary 1-2 centimeters away from the bottom of the tube is that the liquid sample will go up instead of going down. To reduce this issue, the NMR tube was inserted into the spectrometer after the heating step and few drops of ethanol were added. Hydrophobized NMR tubes were also used to further decrease this effect, but ultimately none of these methods were successful. This is because we did try to step aside from the routine protocol of D-DNP and we were constrained by apparatus limitation.

Another issue is the distortion of the signal because there is no lock or shim on during the experiments. The data set of Figure 69 (right) shows that the signals are curving in the FOV dimension instead of being straight. This will lead to errors at the fitting stage and will reduce the resolution in the diffusion dimension. Attention must be paid to shim and lock carefully on the receiving tube before the actual dissolution experiment in order to minimize this distortion.

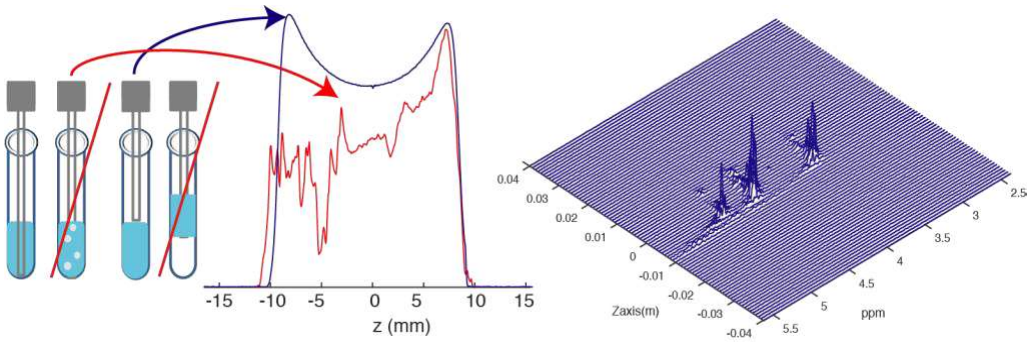

Figure 69: Sources of distortions in D-DNP experiment. Left: effect of the capillary position in the NMR tube. The capillary can be either inserted until it reaches the bottom of the tube or left 2 cm above the bottom of the tube. In the first situation the sample is correctly transferred, the second situation represents an injection that is too fast and induces bubbles, the third situation corresponds a sample that is correctly transferred and the last one shows the sample not going down properly in the NMR tube after injection. The red profile shows the effect of bubbles on the lineshape. The blue profile is a reference profile properly acquired without bubbles. (b) Effect of the lock and shim of the data set. Since the experiments are acquired without lock nor optimized shims, this can induce distortion of the signals.

9.3.4. Conclusion

From these preliminary results it appears that, even if our sequence is ultrafast, we cannot record ^{1}H SPEN DOSY data that give meaningful diffusion coefficients nor good lineshapes and diffusion curves with the D-DNP instrumentation that is currently available to us. Indeed, the T_1 is around 4 s and we saw with the mock dissolution on a concentrated sample that we need to wait until the 3rd scan (20 s after dissolution) to have acceptable diffusion coefficients. By the time we reach this scan the amplified signal would be gone. So, we cannot get a proper SPEN DOSY result and extending to multiple scans is not feasible. With our current setting and method, we are not able to perform SPEN DOSY of hyperpolarized protons. Plus, we had many issues with the samples that did not went properly down to the bottom of the tube during the transfer. All our attempts remained unsuccessful.

While these efforts were unsuccessful, they paved the way to the acquisition of SPEN DOSY data with a more established ^{13}C D-DNP approach, which exploits the long T_1 of ^{13}C spins for quaternary carbons.

9.4. Single-diffusion encoding: case of ^{13}C

Given the current limitations of hyperpolarized ^{1}H NMR with D-DNP on the system that we used, we decided to explore the feasibility of SPEN DOSY on hyperpolarized ^{13}C instead of ^{1}H.

9.4.1. Reference experiments

9.4.1.1. Conventional DOSY: ^{1}H

A sample of pyruvate, acetate, urea and methionine (100 mM each) in D_2O was used for the DOSY reference experiment shown in Figure 70 and the diffusion coefficients obtained are presented in Table 13. Conventional 2D spectra were recorded using a stimulated echo sequence with bipolar gradient pulses (LEDstebpgp2s Bruker sequence with additional lock stabilization gradients). The diffusion-encoding gradient values consisted of a linear ramp ranging from 0.0325 T/m to 0.4875 T/m. The duration of the gradient pulses was 1.2 ms. The 2D data set were acquired with 16384 points in the direct dimension, a spectral width of 8000 Hz, a relaxation delay of 2 s, 8 scans, 4 dummy scans and 16 gradient steps, resulting in a total experiment duration of 26 min.

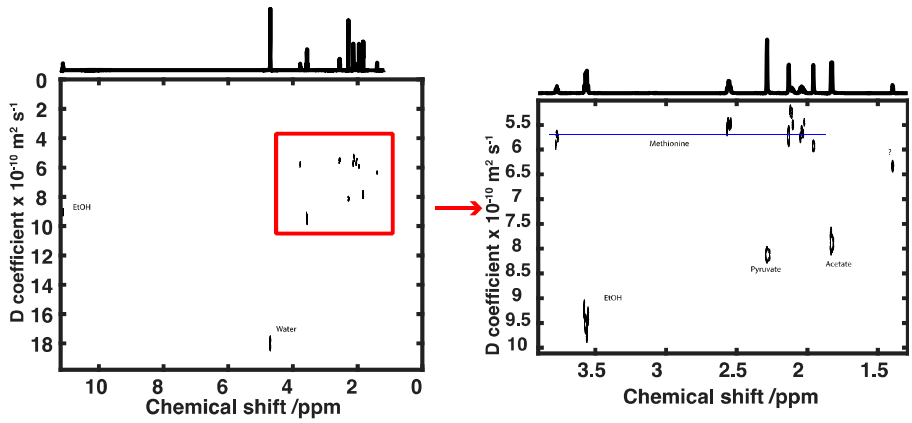

Figure 70: Conventional DOSY display for the mixture of pyruvate, acetate, urea and methionine in D_2O. Ethanol was identified in this particular sample as we used it to clean the NMR tube.

The diffusion coefficients for pyruvate and acetate are too close for these molecules to be well separated in the SPEN DOSY experiment. These results give use an idea of the behavior of the mixture in terms of diffusion coefficient except for urea that is not visible in proton du to exchange between protons of the NH_2 groups. Due to solubility issues with methionine at high level of concentration (56.6 g/L at 25° in water) we decided to continue with only pyruvate acetate and urea.

Table 13: Diffusion coefficient for the mixture of pyruvate, acetate, urea and methionine in D_2O

Compound	($D \times 10^{10} m^2/s$)
EtOH	9.51
Methionine	5.52
Pyruvate	8.12
Acetate	7.87
Urea	-
Water	18.04

9.4.1.2. Conventional DOSY: ^{13}C

We then performed a conventional ^{13}C DOSY experiment to obtain the value for urea. We did one experiment on the diluted sample that is equivalent to what we would have after D-DNP and also on the concentrated sample. The DOSY display on the diluted sample is shown in Figure 71. Conventional 2D data sets were recorded using a stimulated echo sequence with bipolar gradient pulses (LEDstebpgp1s Bruker sequence with additional lock stabilization gradients). The diffusion-encoding gradient values consisted of a linear ramp ranging from 0.0343 T/m to 0.2748 T/m. The duration of the gradient pulses was 5ms. The 2D spectra were acquired with 16384 points in the direct dimension, a spectral width of 8000 Hz, a relaxation delay of 300 s, 64 scans, 4 dummy scans and 8 gradient steps, resulting in a total experiment duration of 43 h. For the 500 mM only 8 scans were used so it took 5 h.

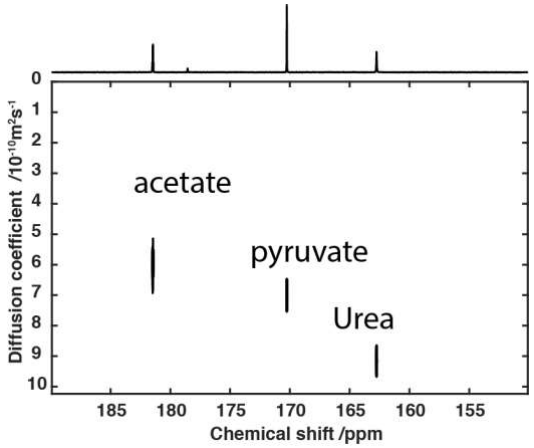

Figure 71: ^{13}C DOSY of mixture pyruvate, acetate, urea (20mM).

9.4.2. Results on hyperpolarized sample

The ASE pulse sequence was tested on a model sample composed of urea, acetate and pyruvate labelled on the carbonyl group. The advantage of working on CO groups is that the observed signals are singlets and the effect of J couplings is insignificant. A 30° excitation pulse was used for repeated sampling of the magnetization and a time series of 8 ASE experiments was recorded after a single dissolution experiment. Each ASE experiment last for a total of 278 ms and the relaxation delay was 10 s. Transfer duration, injection time and relaxation delay needed to be optimized in order to keep as much signal as possible by the time the sample reaches the receiving tube. A 1D spectrum, shown in Figure 72, was also acquired right after injection with a 1° excitation pulse, prior diffusion encoding, in order to calculate the enhancement obtained. It entails that 20 s have elapsed when the first single-scan ASE starts. It is important to understand that the spatially encoded experiment induces a reduced spectral width as we explained before so it is tricky to fold signal spanning over a 20-ppm region into a 5 ppm region. Since we only have 3 signals in the carbon spectrum, folding was achieved without overlap issues. However, for an increased number of signals this could be detrimental for spectral resolution and also for the resolution in the diffusion dimension.

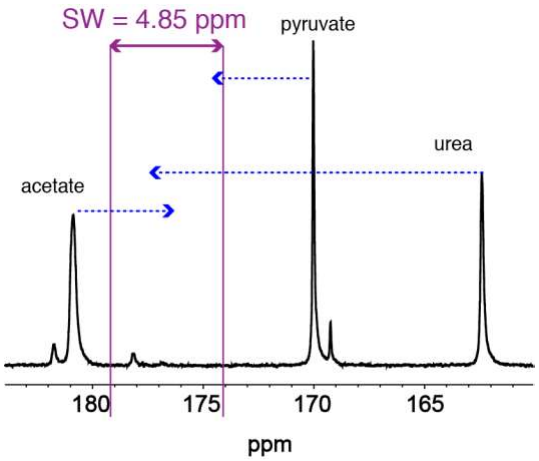

Figure 72: 1D ^{13}C spectrum of a mixture of 1-^{13}C-pyruvate, 1-^{13}C-acetate and ^{13}C-urea. The CO region is shown. The spectral window observed in the SPEN DOSY experiments is indicated. Arrows show where each peak folds into this region.

Experiments were performed using chirp pulses of duration 5 ms, a bandwidth of 40 kHz and a gradient amplitude of 0.2592 T/m. The carrier frequency was set at 176.1 ppm. The excitation flip angle was 30°. The post-chirp gradient had a duration of 5 ms. The acquisition parameters are a 0.4320 T/m acquisition gradient strength with 128 loops and a readout duration of 512 µs. This results in a spectral width of 977 Hz. For coherence selection, independent pairs of gradients are placed around each chirp pulse with strength comprised between 0.0378 and 0.2538 T/m and a duration of 800 µs. The prephasing gradient was set to 0.2160 T/m, with a duration of 487 µs. The total acquisition time was 315 ms.

Ideally, a reference profile should be recorded after each injection as shown in Figure 73 but due to the loss of signal intensity overtime, the SPEN DOSY recorded after did not give good results. We cannot do this if we want to perform multiple SPEN DOSY experiments. This could explain the distortion that may occasionally occur in our diffusion profile and to improve accuracy of the diffusion coefficient diffusion determination, we reduced our fitting region to -2 mm to 2 mm.

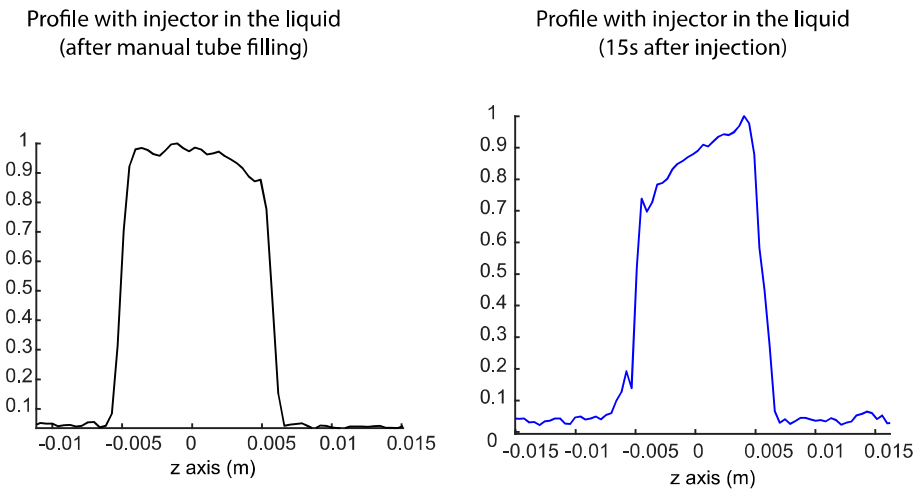

Figure 73: Reference profile of the observed region after manual tube filling (left) and right after injection (right).

Results using the ASE pulse sequence are presented in Figure 74. Only the first 3 scans were used for diffusion coefficient calculation. Up to the 5th scan, there is still some signal left but the SNR became too low and the quality of the data is compromised. After 5 scans, all signals have disappeared. The diffusion curves, extracted with our home-written processing package, show strong oscillations. The decaying signals are strongly modulated, and this modulation seems to be a convection artifact that masks the diffusion effect that we are trying to measure as described, e.g., by Jershow et al. [163] In addition, the calculated diffusion coefficients are unreliable as they show an important variability from an experiment to another and also from scans to scan of a same experiment. The results for the three compounds are summarized in Table 14. The results of scan 1 are still fluctuating and at scan 3 results seems to be correct but good part of the signal was already loss. This convection effect is possibly worsened since the sample may not be completely settled after the injection, and we did not manage to get reproducible results.

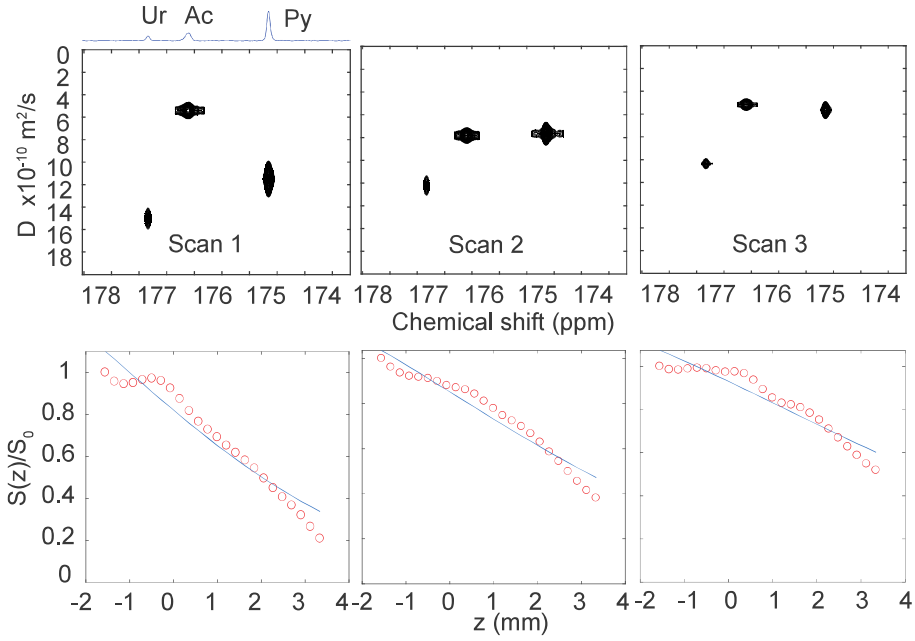

Figure 74: DOSY spectra for the mixture for 3 successive SPEN DOSY post D-DNP and diffusion curves with oscillations shown for pyruvate.

9.5. Double-diffusion encoding: solving convection issues

9.5.1. Results on hyperpolarized sample

The oscillations observed in the diffusion curves are detrimental to diffusion coefficient determination as we saw previously. We created a convection compensated version of the ASE experiment previously

described that is inspired from the work of Jershow et al.[167] To get compensation effect, the coherence transfer pathway (CTP) should be opposite for the first and the second echo. At the end, the diffusion effect is cumulated whereas the convection effect is suppressed. The pulse sequence is shown in Figure 75. We also set the timing of the pulse sequence so that the data can be processed in pure absorption, which is usually not done in ultrafast 2D NMR experiments. The principle of this approach was described in section 8. The design of the convection compensated pulse sequence was greatly helped by the use of the Spinach library [44].

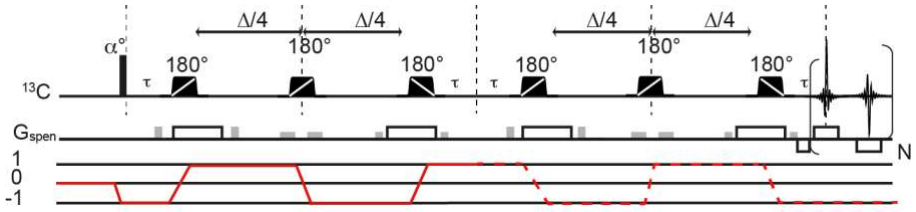

Figure 75: Adiabatic double spin echo (ADSE) pulse sequence that compensate for convection and give possibility to phase the SPEN DOSY data in the conventional dimension. Reprinted from [241] *with permission. © 2017 Wiley.*

The diffusion profile was simulated with the Spinach library for the pulse sequence used in the previous campaigns (see Figure 66). Figure 76 (left) shows the simulated diffusion lineshape for a single spin system in the presence or absence of flow for the ASE pulse sequence. The flow rate was varied from 0 to 12 mm/s. The reference profile where the flow is off is in black. The other profiles are completely distorted when the flow is on, giving an apparent faster decaying signal compared to what we expect. This leads to overestimated diffusion coefficients.

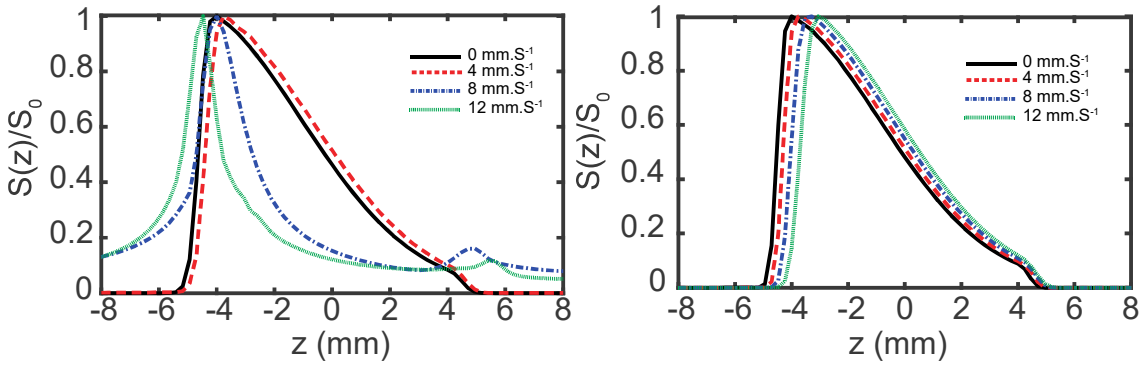

Figure 76: Simulation comparison results: left ASE and right: ADSE. left: Simulated diffusion profile with flow rate set to 0.0 (black D=8.16 × $10^{-10}m^2s^{-1}$) or 0.008 (blue D=38.02 × $10^{-10}m^2s^{-1}$) when convection is not compensated right: Simulated diffusion profile with flow rate set to 0.0 (black D=8.16 × $10^{-10}m^2s^{-1}$) or 0.008 (blue D=7.36 × $10^{-10}m^2s^{-1}$) when convection is compensated.

The diffusion profile was simulated with the Spinach library for the new pulse sequence ADSE used to compensate the convection (see Figure 75). In Figure 76 (right) results for the ADSE pulse sequence were obtained with a flow constant variation from 0 to 12mm/s. The diffusion profile is restored to what we expect with a slight shift along z-axis when the flow was not 0. The diffusion coefficients are also underestimated but this is acceptable compared to the previous situation. The diffusion coefficient is $7.97 \times 10^{-10} m^2 s^{-1}$ in the absence of flow and $7.36 \times 10^{-10} m^2 s^{-1}$ for a flow of 8 mm/s. In contrast, in the previous situation the estimated diffusion coefficient is $38 \times 10^{-10} m^2 s^{-1}$ for a flow of 8 mm/s. The value of the corrected diffusion delay Δ' diffusion delay needs to be adjusted in order to take into account the diffusion that is occurring during the chip pulse due to its finite duration nature. The ASE results were fitted using a diffusion delay equal to

$$\Delta' = 2\frac{T_e}{L}z + (\Delta - 2\tau) \quad (1)$$

and the ADSE results were fitted with

$$\Delta' = 4\frac{T_e}{L}z + (\Delta - 4\tau) \quad (1)$$

where T_e is the chirp duration, L the observed region, z the position in the sample along the FOV, Δ the diffusion delay (defined as the delay separating the middle of two successive encoding chirp) and $\tau = T_p + T_e$, T_p the post chirp duration.

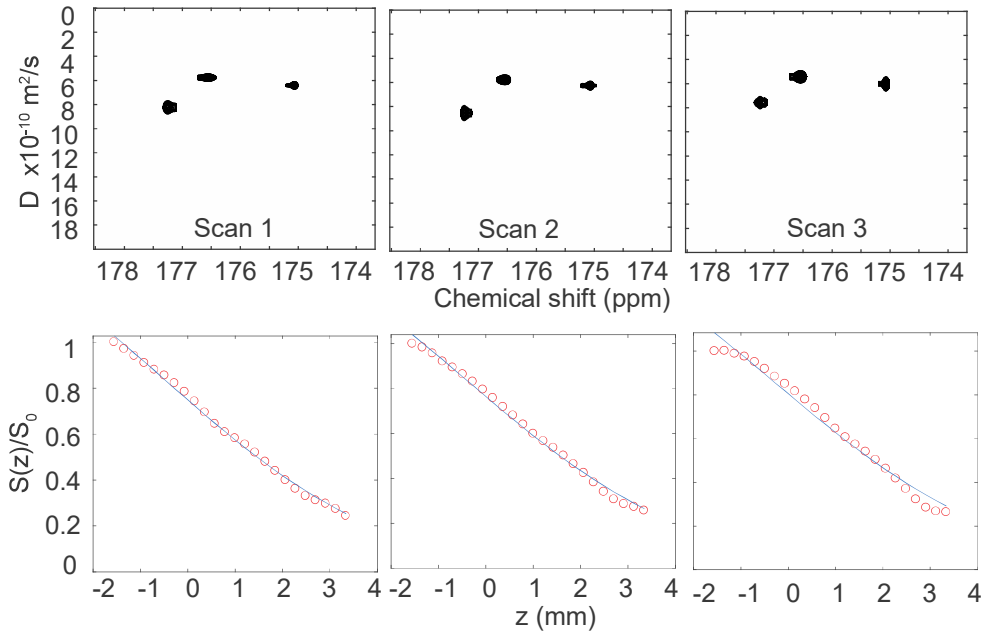

Figure 77: DOSY spectra for the mixture for three successive convection compensated SPEN DOSY post D-DNP and diffusion curves shown for pyruvate.

The result of this compensated sequence is very promising as shown in Figure 76 since distortions in the diffusion profile are no longer observed. When using this pulse sequence for real experiments in

combination with D-DNP (oscillations are no longer observed in the diffusion profile as we can see in Figure 77 and all scans give comparable results. Stability of the results from scan to scan and also from one experiment to another is observed with the new sequence as the standard variation coefficient (CSV) was less than 7 %. This includes the first scan, for which we know from previous experiments that convection is still occurring. Reproducibility of the results between several dissolutions was also assessed. CSV between three separate D-DNP experiments is below 12 % for all molecules. All the results are summarized in Table 14.

We also tried to use a 90° excitation pulse to get a single scan with the maximum signal intensity and obtained comparable values for the diffusion coefficients. The use of a small-tip-angle excitation is of potential to follow a dynamic process with DOSY data acquired in less than 1 s. In the end, the double diffusion encoding strategy is a better option compare to the single diffusion encoding strategy when it comes to monitoring a signal amplified by D-DNP with this instrumentation. Note that there are other injection methods, using a liquid or a gas to push the sample, that result in much reduced convection [203].

Table 14: Diffusion coefficients measured on the mixture of 1-^{13}C-pyruvate, 1-^{13}C-acetate and ^{13}C-urea for several experimental conditions.

		Diffusion coefficient $\times 10^{10} m^2 s^{-1}$		
Experiment	**Scan**	**Urea**	**Acetate**	**Pyruvate**
LED-STE, TE, 20 mM	-	9.2	6.9	7.1
	1	8.23	5.76	6.41
SPEN ADSE, D-DNP	2	8.54	5.78	6.26
	3	7.57	5.43	6.02
	1	15.02	5.41	11.5
SPEN ASE, D-DNP	2	12.21	7.82	7.66
	3	10.36	5.17	5.65

9.5.2. Sensitivity gain

The enhancement just after injection was determined using the 1D ^{13}C spectrum (blue), shown in Figure 78, acquired after D-DNP, compared to a thermal equilibrium spectrum (red) acquired with 16 scans after the sample has equilibrated.

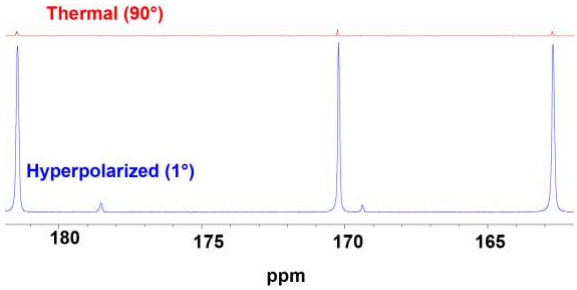

Figure 78: Hyperpolarized 1D spectrum post D-DNP (blue) and thermal spectrum (red) of the mixture of 1-^{13}C-pyruvate, 1-^{13}C-acetate and ^{13}C-urea.

A 5500-fold was calculated 10 s after dissolution with the expression

$$\varepsilon = \frac{I_{DNP}}{I_{TE}} \frac{NS_{TE}}{NS_{DNP}} \frac{\sin(\theta)_{TE}}{\sin(\theta)_{DNP}} \quad (3)$$

where I_{DNP} is the signal integral of the hyperpolarized spectrum, I_{TE} is the signal integral of the thermal equilibrium spectrum, NS_{TE} is the number of scan used to acquire of the thermal equilibrium spectrum, NS_{DNP} is the number of scan used to acquire of the hyperpolarized spectrum, $\sin(\theta)_{TE}$ is the excitation angle used to acquire the thermal equilibrium spectrum and $\sin(\theta)_{DNP}$ is the excitation angle used to acquire of the hyperpolarized spectrum.

We also calculated the decay constant of the hyperpolarized signal by plotting the enhancement against time. Figure 79 shows the enhancement measured for the initial 1D ^{13}C spectrum (green cross) as well as the time series of SPEN DOSY spectra, for pyruvate. The enhancement for the SPEN DOSY spectra was calculated by comparing each spectrum in the D-DNP experiment to a spectrum acquired at thermal equilibrium on a concentrated sample of pyruvate (750 mM).

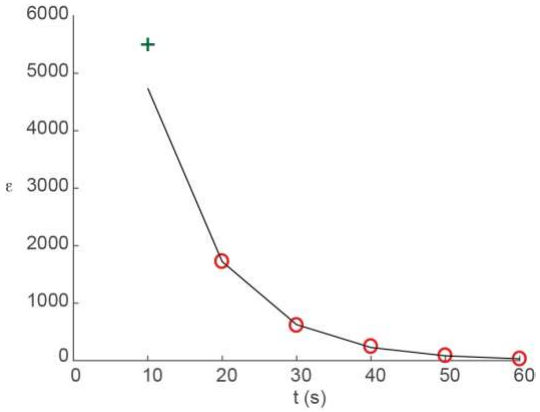

Figure 79: Signal enhancement obtained for the pyruvate signal in the D-DNP experiment where the DDE SPEN DOSY pulse sequence is used. The enhancement for the initial 1D 13C spectrum is shown with a green cross. The enhancements for the SPEN DOSY spectra are shown with red circles. The black curves correspond to the best-fit curve for the decay of the enhancement of the SPEN DOSY spectra. The time is given from sample injection.

The enhancement for the nth SPEN DOSY spectra can be modelled by an equation of the form:

$$\varepsilon(n) = \varepsilon_0 \exp(-n\,TR/T_{1\mathrm{eff}})(\cos(\alpha))^{n-1}$$

where *TR* is the repetition time, is the excitation flip angle and T_{1eff} is the fit parameter, which corresponds to an effective longitudinal relaxation rate. The resulting fit is shown in Figure 79, and a good qualitative agreement is found between the enhancement measured on the 1D spectrum and the extrapolated value of the SPEN DOSY enhancement. The fit of the decay curve gives T_{1eff}=11.5 s and ε_0=9900. The enhancement of the first ADSE experiment is E_{ADSE}=1800. This means that by the time we run the SPEN DOSY, we have already lost 80 % of the enhanced signal. There is room for improvement for the delays used between experiments in order to get as much signal as possible especially regarding the relaxation delay (d1) used. We could for example use d_1=10 s as we did for the first 1D zg and the first SPEN DOSY and then reduce it to 5 s for the remaining experiments. A compromise needs to be found between the optimal duration to get significant enhanced signal available and the duration necessary to give the sample some time to settle before acquisition. With this type of gain in sensitivity, we would be able to study sample at submillimolar concentration once it arrives into the spectrometer within a single-scan.

9.6. Conclusions

We have shown that the diffusion coefficients of hyperpolarized ^{13}C-labelled molecules can be measured in a single scan. The use of spatially encoded (SPEN) DOSY experiment together with dissolution dynamic nuclear polarization (D-DNP) provides ^{13}C DOSY data for low concentrated mixtures of small molecules. The accuracy of measured diffusion coefficients is significantly improved as the presented pulse sequence is designed for convection compensation. The combination of SPEN DOSY and D-DNP is illustrated on a model sample and numerical simulations of convection effect are discussed. Hyperpolarized ^{13}C DOSY is a promising tool for the monitoring of chemical reactions and the analysis of molecular interactions.

10. SPEN DOSY of hyperpolarized mixtures using SABRE

10.1. Introduction

In parallel to the work on dissolution-DNP [241], we studied the combination of another hyperpolarization strategy with spatially encoded DOSY. The Signal Amplification by Reversible Exchange (SABRE) method consists of a transfer of spin order from parahydrogen to the substrate [209,218]. The transfer is done via interaction between the substrate, a metal complex and parahydrogen that form a temporary intermediate. In the most common implementation of the method, the polarization step is carried out outside the detection magnet. After insertion of the sample in the magnet, the resulting enhanced signal lasts for few seconds so single-scan experiments are well indicated to record multidimensional data from this type of signal [49]. This approach grants high level of polarization with up to 1000 fold-signal enhancement [209,211,212,225,242,243]. However, it is a selective method since it is only possible to polarize certain classes of compounds this way, such as nitrogen-containing aromatic rings, but much effort has been made to extend this method to hyperpolarize a range of amines, amides, carboxylic acids, alcohols, phosphates, and carbonates [227,244].

The experiments described in this section were done in collaboration with Gaspard Huber and Patrick Berthault at CEA Saclay. We wanted to demonstrate the ability of the SPEN DOSY pulse sequence to record ^{1}H hyperpolarized spectra using SABRE. This section presents how we managed to do so. First, we needed to adapt the pulse sequence on the spectrometer and adapt the parameters to the new sample. Since the SABRE experiment requires shaking of the sample prior to acquisition, we also needed to investigate the effect of this as it creates additional movement within the liquid sample, which is detrimental for diffusion coefficient determination. We explore the use of this tool for the analysis of mixtures of several molecules commonly used with the SABRE method. Two strategies used to achieve SABRE SPEN DOSY spectra of low concentrated mixture are presented.

10.2. SABRE experimental setting

10.2.1. Parahydrogen preparation

The apparatus of Figure 80 is a device custom-made at CEA where parahydrogen is prepared by flowing hydrogen gas through a glass solenoid that is filled with a catalyst, hydrous ferric oxide, and immersed in liquid nitrogen at 77 K. The gas enriched in p-H_2 is then stored into a reservoir that is also immersed in liquid nitrogen. This helps to increase the pressure to 4 bars in the reservoir, which is then used for

the transfer step into the NMR tube (equipped with a valve) that contains the sample. The level of parahydrogen produced was found to be 52.1 % by using Raman spectroscopy. This level is maintained in the reservoir for several hours.

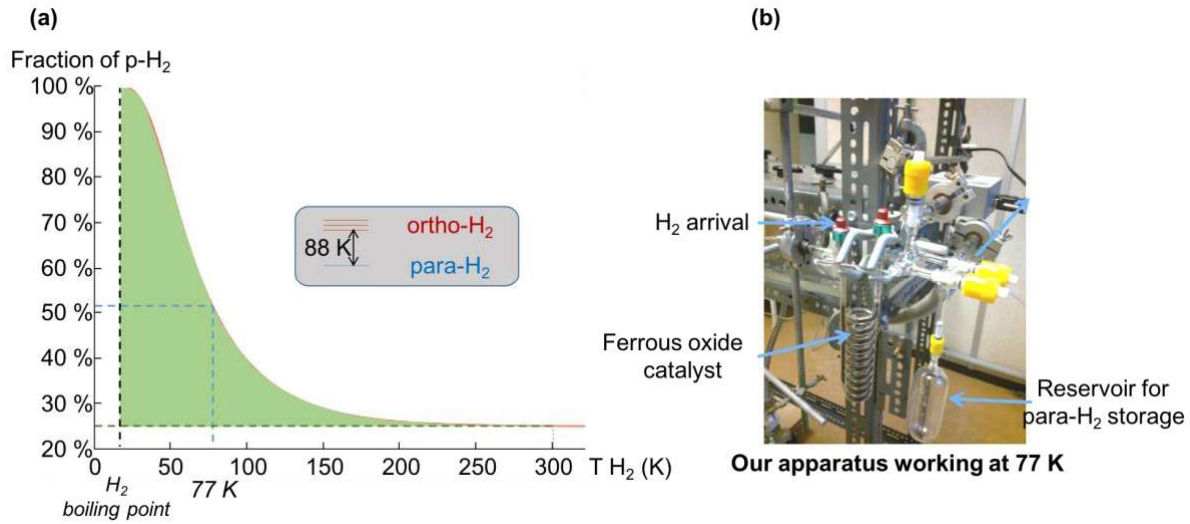

Figure 80: (a) Level of p-H_2 evolution according to temperature and (b) p-H_2 preparation apparatus.

10.2.2. SABRE set up

The NMR experiment are run on a Bruker spectrometer operating at a ^{1}H Larmor frequency of 500.13 MHz equipped with an unshielded magnet. For the first series of experiments of this study we used a 5 mm BBI broadband probe with single *z* axis gradient ($\mathbf{P}_z$); then we switched to a 5 mm TBI broadband probe with triple axis gradient ($\mathbf{P}_{xyz}$). Results presented here were acquired with one of the two probes depending on where the project status was at and this will be specified whenever necessary.

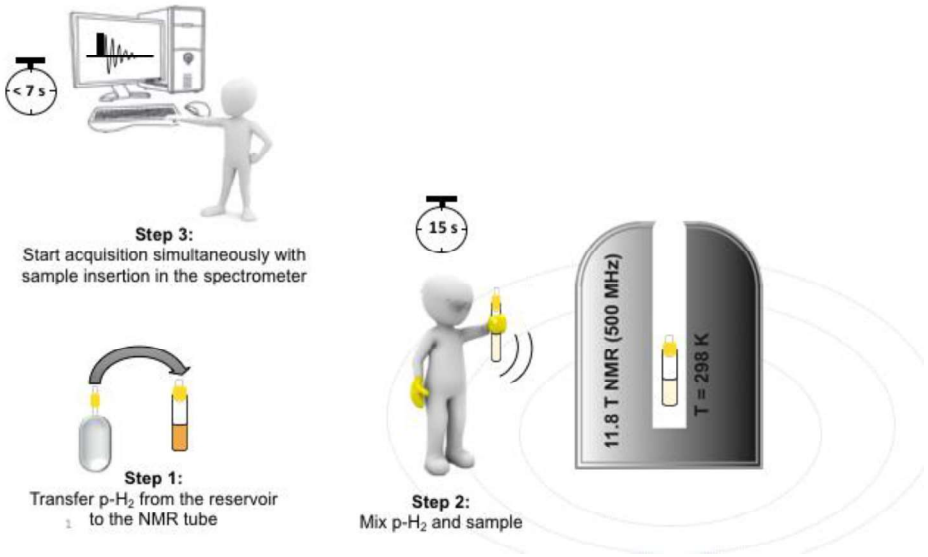

Figure 81: SABRE experiment set up.

The samples are prepared in 3.95 mm thick-walled NMR tubes equipped with a pressure valve. The experimental steps are schematized in Figure 81. The tube needs to be degassed prior introduction of p-H_2 from the storage reservoir. The sample that now contains p-H_2 is shaken vigorously for 15 s in the stray field of the spectrometer at ca. 7 mT and is quickly inserted in the spectrometer. Simultaneously the NMR experiment of choice is launched so that the hyperpolarized signal can be recorded. The recycle delay was set to at least 4 s to make sure that the sample is well set in the spectrometer before acquisition starts. The sample takes approximately 3 s to go down to the spectrometer (delay between the end of the shaking and the moment the sample is down in the spectrometer). Up to 4 consecutive shaking steps can be carried out with a single batch of p-H_2, with minimal losses of signal intensity. Also, the sample was found to be stable over more than 1 h, so that multiple experiments can be carried out without catalyst degradation.

Each sample was loaded with p-H_2 at least twice, and the results shown here correspond to the 2nd loading. This is because the first time that the catalyst is in contact with the dihydrogen there is an activation step. The catalyst used is [Ir(COD)(IMes)(Cl)] (with IMes= 1,3-bis(2,4,6-trimethylphenyl)imidazole-2-ylidene, COD= cyclooctadiene) and it will be activated to give [Ir(IMes)$(H)_2(S_i)(S_j)(S_k)$]Cl (2) (with S= substrate). [49,243] The enhancement is not the best with the first loading because the catalyst is not fully activated yet. That is why it is best to make a 2nd loading of p-H_2 to use the catalyst at its full potential and get the best results in terms of enhancement. The signal enhancement is calculated with a separate experiment, where 1D spectra are recorded after shaking and insertion. The reference, thermal equilibrium spectrum is obtained several minutes later.

The steps of locking, tuning and matching, and shimming are carried out on the sample of interest before shaking (ie., before loading of p-H_2 right after venting the sample). When we perform the SABRE experiment, once the sample is quickly introduced into the spectrometer, these steps can no

longer be done because there is not enough time. Usually the lock signal does not go back to its initial position, and field homogeneity tends to degrade after multiple shaking experiments as we do not go through the shimming procedures in between. Nevertheless, this is done whenever the sample is refilled with p-H_2.

10.2.3. Sample preparation

Several samples were studied. The first one was used to perform preliminary experiments and check that the SPEN DOSY pulse sequence performs as expected. This is important in order to adapt the processing if needed and be sure that the measured diffusion coefficients are consistent. Several reference samples were used to obtain the results and are listed below:

- **M**1 was composed of caffeine and ethylene glycol (≈ 50 mM) in D_2O.
- **M**2 is a sample of pyridine (100 mM) in CD_3OD
- **M**3 is a sample of pyridine, 4,4-bipyridine, 3-ethylpyridine and N,N-dimethylnicotinamide (≈4 × 150 mM) in CD_3OD.

The samples used for the SABRE experiments are prepared under inert atmosphere (using argon) in order to prevent any degradation of the catalyst (**C1**), [Ir(COD)(IMes)Cl] (IMes=1,3-bis(2,4,6-trimethylphenyl)imidazole-2-ylidene, COD=cyclooctadiene). Several mixtures were used to obtain the results and are listed below:

- ***M4*** is Pyridine+4,4-bipyridine + 3-ethylpyridine +N,N-dimethylnicotinamide (≈ 4 × 5 mM)+ **C1** (1 mM)+ p-H_2 in CD_3OD.
- ***M5*** is Pyridine+4,4-bipyridine + 3-ethylpyridine +N,N-dimethylnicotinamide (≈ 4 × 2.5 mM) + **C1** (1 mM) + p-H_2 in CD_3OD

10.2.4. Pulse sequences

Conventional DOSY was acquired using a modified version of the **ledbpgp2s** Bruker sequence (stimulated echo with LED filter and two spoil gradients). Compensation gradients were added so that the lock signal is stabilized during the experiment. Convection compensated conventional DOSY was also acquired using a modified version of the **dstebpgp3s** Bruker (double stimulated echo with bipolar gradient pulses for diffusion, and 3 spoil gradients). Compensation gradients were also added so that the lock signal is stabilized during the experiment.

Two SPEN DOSY experiments were used based on a stimulated echo (cf. Section 6 & 8) with either single diffusion encoding (SPEN DOSY STE) or double diffusion encoding (SPEN DOSY DSTE). The reference profiles were recorded with a double-spin echo experiment using a pair of

spatially selective refocusing chirp pulses followed by a read gradient (cf. Section 6). The hyperpolarization level was determined with 1D pulse acquire experiments, recorded separately.

10.2.5. Conventional DOSY experiments

Preliminary experiments were done using the mixtures **M1, M2 and M3** in order to assess the correct implementation behavior of the SPEN DOSY pulse sequence.

The sample **M1** (caffeine and ethylene glycol in D_2O) was first used to set up the experiments. Conventional DOSY spectra were acquired with the modified **Ledbpgp2s** pulse sequence. The linear gradient ramp was set to 10-70 % of maximum gradient value Gmax=0.65 T/m (constructor value) with a duration of 1.4 ms. The diffusion delay was set to 100 ms. Parameters are determined so that the remaining signal intensity for the last gradient is 5 % of the signal intensity for the first gradient. 8 gradients increments were used with 16 scans per increment and 4 dummy scans, 16384 points and a spectral width of 7500 Hz. The total duration of the experiment was 15 min. The data were processed with the DOSY Toolbox [122].

Conventional DOSY display of **M2** sample (pyridine in methanol) and **M3** sample (pyridine, 4,4-bipyridine, 3-ethylpyridine and N,N-dimethylnicotinamide in methanol) were obtained as previously with the same parameters but with a diffusion delay set to 75 ms and a gradient duration of 1.2 ms.

Results presented in Figure 82 are conventional experiments acquired with the modified **Ledbpgp2s** pulse sequence and they will serve as our reference spectra. Clear separation of compound is obtained for **M1** and **M2**. For **M3** good separation was obtained but bipyridine and N,N-dimethylnicotinamide have diffusion coefficients that are very close (they differ by $0.5 \times 10^{-10} m^2 s^{-1}$,ie., 1.7 %) so it is possible that we do not manage to separate them correctly with the SPEN DOSY as we approach the limit of this experiments. Note that pyridine's diffusion coefficient is 21.6×10^{-10} $m^2 s^{-1}$ in **M2** and 17.2×10^{-10} $m^2 s^{-1}$ in **M3** and at the time of writing this difference in diffusion coefficient is not fully understood.

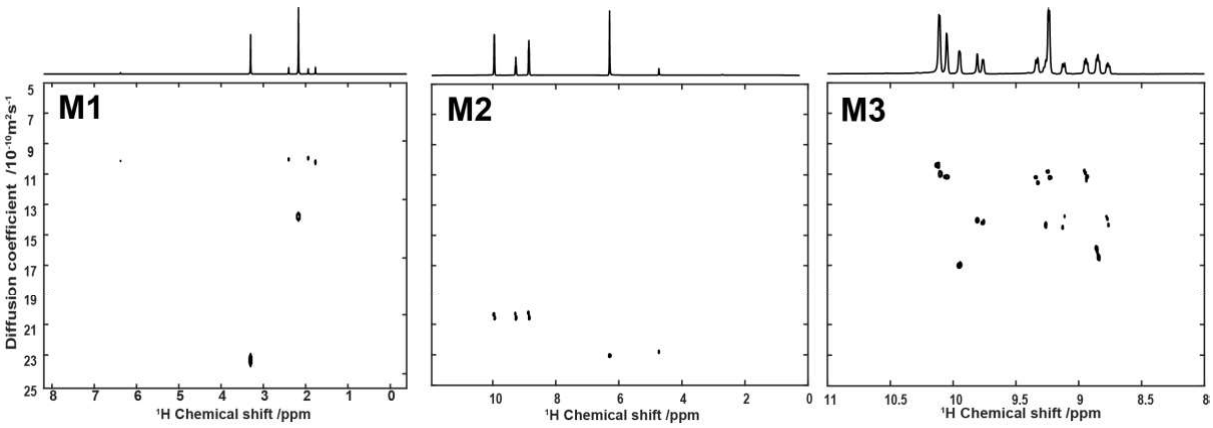

Figure 82: Conventional DOSY display of mixture M1 using $\boldsymbol{P_{xyz}}$ *probe at 298K , M2 using* $\boldsymbol{P_z}$ *probe at 298 K and M3 using* $\boldsymbol{P_{xyz}}$ *probe at 295K with the modified* ***Ledbpgp2s*** *pulse sequence.*

10.2.1. Preliminary SPEN DOSY experiments

The SPEN DOSY spectra on **M1** were acquired using SPEN DOSY STE pulse sequence using a chirp pulse with BW=110000 Hz and a duration of 1.5 ms. The post-chirp gradient had a duration of 1.5 ms, the encoding gradient strength was 0.2535 T/m and the diffusion delay was 100 ms. A selective 180° pulse was used, with a duration of 5493 us and a center frequency set at 2.7 ppm to select a spectra region. The acquisition consisted of 128 loops with gradient readout of 230 μs, resulting in an acquisition time of 59 ms, the acquisition gradient was set to 0.26 T/m and the relaxation delay was set to d_1=5 s.

SPEN DOSY spectra on **M2** and **M3** where acquired using SPEN DOSY STE pulse sequence using a chirp pulse with BW=100 000 Hz and a duration of 1.5 ms. Post chirp gradient was 1.5 ms and encoding gradient strength was 0.2535 T/m, the acquisition was set to 0.26 T/m with a duration of 256 μs for 200 loops. Diffusion delay was 75 ms. Selective 180° was used with a duration of 5714 μs centered at O_1=12.1 ppm. Total acquisition time was 102 ms. Relaxation delay was set to d_1=5s.

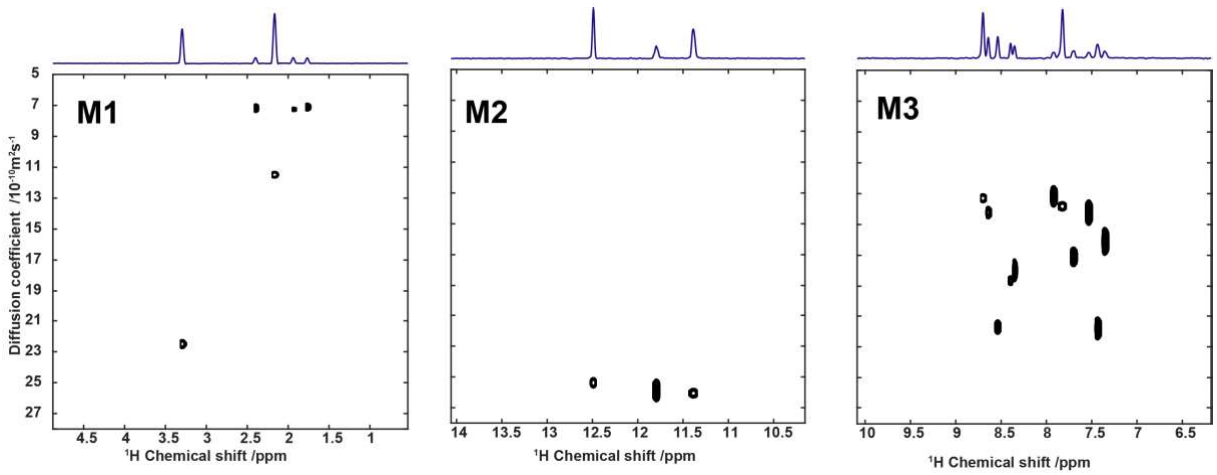

Figure 83: SPEN DOSY display of mixture M1,M2 and M3 using $\boldsymbol{P}_{xyz}$ *probe at 298K.*

Overall the SPEN DOSY experiments shown in Figure 83 give comparable results compare to the conventional DOSY experiments in term of separation, with a systematic deviation of the diffusion coefficients, which is due in part to gradient non-linearity. Indeed, the diffusion measurement is performed without region selection in the conventional DOSY whereas SPEN DOSY operates on a 10 mm region. The separation of the compounds in the mixture **M3** was a bit tricky since bipyridine and N,N-dimethylnicotinamide are close in the diffusion range. Thanks to the phasing of the data in the spectral dimension we manage to separate them. We do have some overlap going on because of the decrease resolution of SPEN DOSY and signals of the 3-ethylpyridine at 7.3 and 7.6 ppm are underestimated. Signal of bipyridine and p-pyridine at 7.8 ppm are superimposed and the diffusion value is mainly dominated by the bipyridine. This is so far the most complicated sample that we have studied as it suffers from limited resolution even with all the optimization we presented in section 8 were made to improve it.

10.3. Sources of convection in SABRE experiments

10.3.1. Convection effect due to solvent

Convection compensated experiments were acquired with the same parameters that was described in section 10.2.5. The results are shown in Figure 84 in the case of the mixture **M1** in D_2O and the observed diffusion coefficients differ by less than 2 %. We can say that the convection in D_2O is negligible as expected since the viscosity of the solvent is quite low.

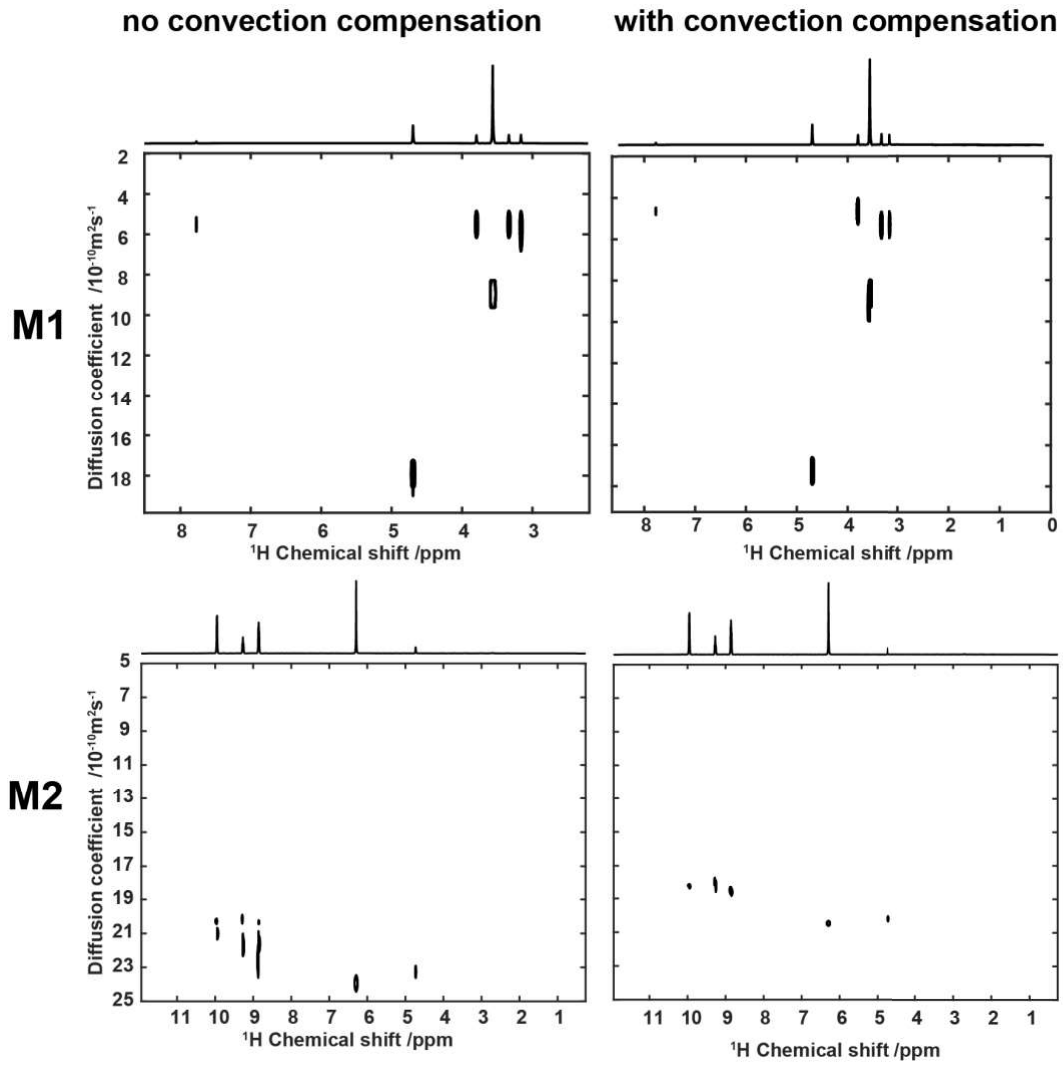

*Figure 84: Comparison of conventional convection compensated pulse sequence and non-compensated version for mixture **M1** using P_z probe at 298K and **M2** at using P_z probe at 298K.*

In the case of the sample **M2**, the results in Table 15 and in Figure 84 show that the sequence that compensates for convection gives diffusion coefficients that are 10 % smaller compared to the LED-STE sequence when working in methanol. This solvent possesses a lower viscosity than D_2O and is more prone to convection, and this will induce apparent diffusion coefficients that are greater than expected. As the SABRE samples are prepared in methanol we need to take this property into account in order to get accurate values of diffusion coefficients. The same observation was made for **M3** (data not shown).

Table 15: Results of conv DOSY of pyridine in MeOD with and without convection compensation

$D \times 10^{-10} m^2 s^{-1}$		
No convection compensation	**With convection compensation**	**Chemical shift (ppm)**
20.28	18.21	9.95
21.68	18.16	9.27
21.46	18.54	8.86
23.94	20.47	6.29
23.26	20.20	4.73

10.3.2. Effect of sample shaking in D_2O

Since the SABRE experiment requires shaking of the sample prior to acquisition, the effect of this shaking needs to be investigated as it creates sample liquid movement, which is detrimental for diffusion coefficient determination. We first investigated the effect of sample shaking on the quality of the SPEN DOSY data on non-hyperpolarized samples, starting with sample **M1** (caffeine and ethylene glycol in D_2O). The protocol consisted of shaking the sample for 15 s second, inserting it in the magnet and recording SPEN DOSY experiments (see section 10.2.2 for more details). A series of data were recorded, with increasing values of the recycle delay, ranging from 3 s to 30 s. This delay starts at the end of the shaking and 3 s is the minimum value possible otherwise the acquisition starts before the sample reach the probe. Figure 85 shows the evolution of the measured values of the diffusion coefficient, which can be used to evaluate the stabilization time.

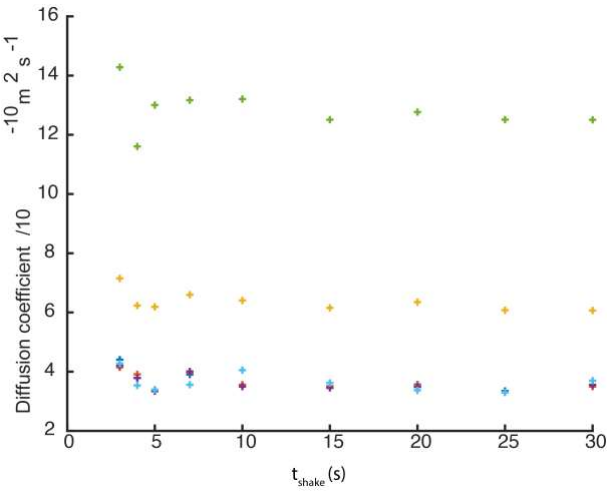

Figure 85: Evolution of diffusion coefficients as a function of the recycle delay when the sample undergoes shaking as necessary for the SABRE process. Data points corresponding to D_2O are in green, in yellow for ethylene glycol and in blue, purple and red for caffeine. Data were acquired with using $\boldsymbol{P}_z$ probe at 298K.

Stabilization of the results seems to be reached between 7 and 15 s. The shaking of the sample induces a perturbation that yields fluctuating diffusion coefficients especially during the first 10 s after the introduction of the sample in the magnet. In this case separation seems not to be too impacted but the accuracy of the diffusion coefficient is not guaranteed if the recycle delay is less than 10 s.

10.3.3. Effect of sample shaking in MeOD

The effect of sample shaking was next investigated on a sample of pyridine in CD_3OD (**M2**), which corresponds to the solvent used for our SABRE experiments. The same protocol was used as for sample **M1** and the SPEN DOSY STE was used. Unfortunately, the diffusion coefficients obtained after sample shaking stabilize only after a long recycle delay of 15 s or more, as shown in Figure 86. In addition, the values are different from those obtained on a resting, well shimmed and locked sample (dashed lines on the Figure 86). The dispersion is 1.9 % CSV when d_1=15 s and 4 % CSV when d_1=5 s compared to the reference sample that has a dispersion of 1.3 % CSV.

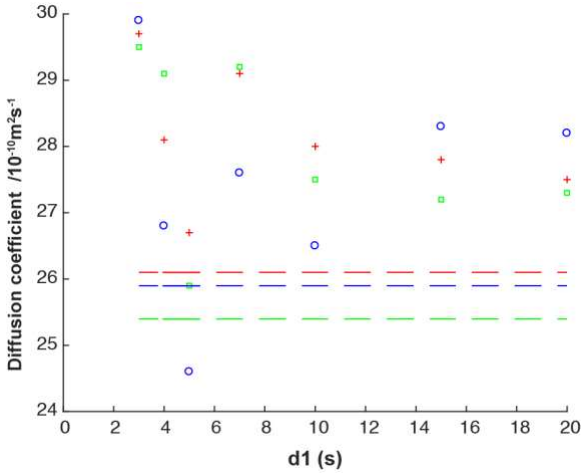

Figure 86: Evolution of diffusion coefficients according to shaking on M2 using SPEN DOSY STE. Green: signal for o-pyridine; blue: signal for p-pyridine and red: signal for m-pyridine. The dashed lines are reference. values acquired on a resting sample. Data were acquired with using $\boldsymbol{P}_{xyz}$ *probe at 298K.*

Considering the ^{1}H longitudinal relaxation rates for the compounds that are typically analyzed with SABRE, a recycle delay of 5 s or less is needed to take advantage of the SABRE-enhanced polarization. The "sample-shaking" implementation of SABRE appears at first to be completely incompatible with an accurate diffusion measurement because of the shaking that induce strong motion of the liquid. This can mask the 'real' diffusion effect and give the illusion of faster diffusion behavior. This is confirmed by looking at the diffusion curves (data not shown); signal decays faster than expected.

10.4. Convection issue: double diffusion encoding strategy

We saw that the SABRE protocol compromises the diffusion measurement and results in overestimated values for the diffusion coefficients, with a large uncertainty. In section 9 we showed that a convection compensation strategy could be used when the sample was undergoing other motion that would mask the diffusion effect. With the SABRE experiment we also tried to use this strategy, in an attempt to compensate for the unwanted convection effect induced by the shaking of the sample.

10.4.1. Case of pyridine in MeOD

First, we started by making a comparison, on sample **M2** between the conventional DSTE DOSY, that is convection compensated, the SPEN STE DOSY based on single stimulated echo and the SPEN DSTE DOSY based on a double stimulated echo that is convection compensated. The results from SPEN STE presented in Table 16 are higher than those with the conventional DSTE DOSY, while using SPEN DSTE DOSY results are closer to those with the convection compensated conventional DOSY. The correction for the diffusion effect appears to work and we no longer have overestimation with the SPEN DSTE DOSY.

Table 16: Diffusion coefficient values obtained for conventional DOSY, SPEN DSTE DOSY and SPEN STE DOSY on sample M2 at 298K

conv DOSY		**SPEN DSTE**		**SPEN STE**	
$D \times 10^{-10} m^2 s^{-1}$	**δ (ppm)**	**$D \times 10^{-10} m^2 s^{-1}$**	**δ (ppm)**	**$D \times 10^{-10} m^2 s^{-1}$**	**δ (ppm)**
24.66	11.33	24.65	11.33	26.06	11.35
24.86	11.76	24.44	11.76	25.88	11.76
24.64	12.46	25.61	12.46	25.38	12.46

To test the stability of the diffusion coefficients when the sample is submitted to shaking, we made several shakings of the sample for 15 s and ran a SPEN DSTE DOSY experiments with increasing values of the recycle delay. As shown by Figure 87, the stability of diffusion coefficient seems to occur after 15 s, but the dispersion of the measured diffusion coefficient remains quite high between the signals of the same molecule. The dispersion is 3.5 % CSV when d_1=15 s and 12 % CSV when d_1=5 s compared to the reference sample that has a dispersion of 2.5 % CSV. In addition, the values are different from those obtained on a resting, well-shimmed and locked sample (dashed lines on the Figure 86). The results seem to be worse with the DSTE strategy than with the STE which was unexpected. Nevertheless, even if the homogeneity between the diffusion coefficients values is decreased compared to what we

had with STE, we still have a slight positive effect on the overestimation of the calculated coefficient. For a d_1=15 s with STE D= 27.9 × $10^{-10}m^2s^{-1}$and with DSTE D= 26.3 × $10^{-10}m^2s^{-1}$. We have doubt that this result is significant because in the conventional experiment the difference is around 10 % between convection compensated and non-convection compensated. Here this is not the case. Maybe the reason is because of the shim and lock that degrade during the process. Notice that diffusion coefficients are still away from the refence values.

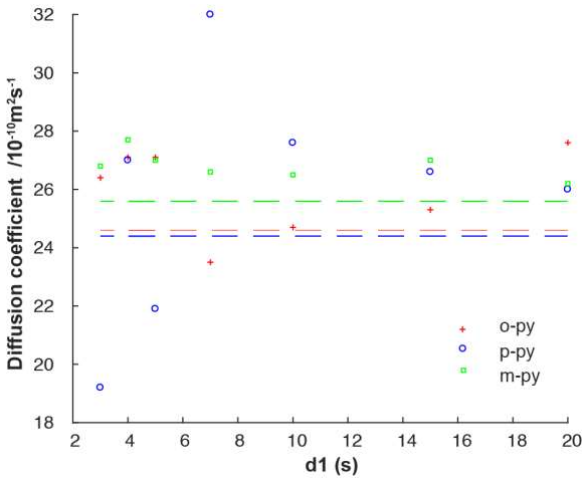

Figure 87: Evolution of diffusion coefficients according to shaking on M2 using SPEN DOSY DSTE. Green: signal for o-pyridine; blue: signal for p-pyridine and red: signal for m-pyridine. The dashed lines are reference values acquired on a resting sample. Data were acquired with using $\boldsymbol{P}_{xyz}$ *probe at 298K.*

The reproducibility of the SPEN STE and SPEN DSTE experiments was evaluated with d_1= 5 s and the results are respectively shown in Table 17 and Table 18. CVS obtained were respectively below 5 % and 3 % except for the para signal that is 19 %. The reproducibility is compromised with the SPEN DOSY DSTE pulse sequence. Since the signals acquired have an intensity two times lower than the intensity in STE, maybe this entails some sensitivity issue, especially for the signal of p-pyridine. We can say that the reproducibility of the STE experiment is assessed with the values of CSV < 5 % but this do not solve our problem of having overestimated diffusion coefficients because of convection. The results with DSTE were quite disappointing.

Table 17: STE reproducibility with shaking

Reproducibility SPEN STE								
D × $10^{-10}m^2s^{-1}$	**δ (ppm)**	**D × $10^{-10}m^2s^{-1}$**	**δ (ppm)**	**D × $10^{-10}m^2s^{-1}$**	**δ (ppm)**	**mean**	**std**	**csv (%)**
27.90	11.35	28.55	11.33	30.68	11.35	29.04	1.45	5
28.19	11.76	26.75	11.75	28.55	11.75	27.83	0.95	3
27.24	12.46	27.98	12.46	29.27	12.46	28.16	1.03	4

Table 18:DSTE reproducibility with shaking

SPEN DSTE		SPEN DSTE		SPEN DSTE				
D × $10^{-10}m^2s^{-1}$	δ (ppm)	D × $10^{-10}m^2s^{-1}$	δ (ppm)	D × $10^{-10}m^2s^{-1}$	δ (ppm)	mean	std	CSV (%)
24.70	11.33	23.38	11.34	23.28	11.33	23.78	0.79	3
23.90	11.75	22.50	11.76	31.81	11.74	26.07	5.02	19
25.43	12.46	26v88	12.46	26.58	12.45	26.30	0.77	3

10.4.2. Case mixture in MeOD

Although the results on pyridine alone were not very encouraging, we tried to use the SPEN DSTE DOSY pulse sequence on a model mixture of four SABRE-compatible molecules (**M3**). Unfortunately, we did not manage to achieve a good spectral separation with the SPEN DSTE DOSY pulse sequence, even in the absence of sample shaking, as shown in Figure 88 (right). While the STE sequence gives a good separation, the DSTE does not. We suppose that this problem is due in part to J modulation. On the samples analyzed in section 8, the SPEN DSTE DOSY sequence performed very well. This could be a limitation of this convection-compensated pulse sequence, which in the present implementation involves 20 ms in the transverse plane. An effect of sensitivity only can be excluded, as we also tried experiments with signal averaging and a more concentrated sample. We also explored a wide range of parameters, chirp pulses, selection coherence on single and triple axis but none of this strategy led to expected results.

In summary, no good results were obtained with the double-diffusion encoding strategy. Some hyperpolarization experiments were tried, but unsurprisingly they did not give a good separation of spectra. We can say that neither the STE or DSTE gave satisfactory results in terms of diffusion coefficient accuracy.

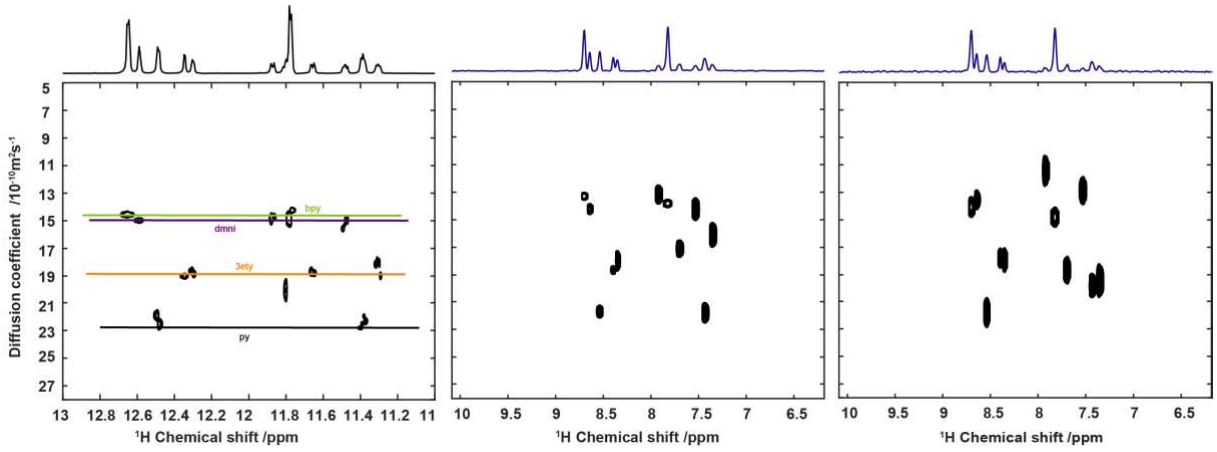

Figure 88 : Comparison between conventional DOSY display M3 (left) with SPEN DOSY STE display (middle) and SPEN DOSY DSTE display (right). Data were acquired using $\boldsymbol{P}_{xyz}$ *probe at 298K.*

10.5. Convection issue: transverse plane encoding strategy

Since the convection compensation strategy did not give good SPEN DOSY data on our selection of SABRE-compatible substrates, we decided to try a different approach. As the sample is shaken vigorously with a vertical motion, we made the assumption that convection within the coil region could mainly occur along the vertical direction of the sample, i.e., the z-axis. Additionally, convection due to temperature gradients usually operates along the z axis as well. We thus chose to perform the diffusion measurement in the horizontal direction of the sample, i.e., the x or y axis. With this method, only the diffusion effect will be measured in this direction and would not be impacted by the vertical motion. This strategy is reported in the literature to give improved results in cases where convection is significant [245].

We used the mixture of 4 SABRE-compatible molecules (**M3**) at a concentration of 150 mM each to perform the experiments. The conventional DOSY data were acquired with a double stimulated echo pulse sequence, with a LED filter and three spoil gradients, and compensating gradients for lock stabilization. Same parameters and processing as described in section 10.2.5 were used except that the number of scans was increased to 32 and that the duration the experiment was 30 min.

Conventional DOSY experiments were recorded to get reference values for the diffusion coefficient on z axis and x axis and the results are shown in Figure 89. The difference observed in diffusion coefficients is due to miscalibrated gradient. Ideally, the same diffusion coefficients values should be obtained whether the x, y or z axis is used but, in our case, lower values were obtained with the x axis. Calibration is actual work in progress and for the data presented we used the constructor values 0.65 T/m along z and 0.50 T/m along x and y.

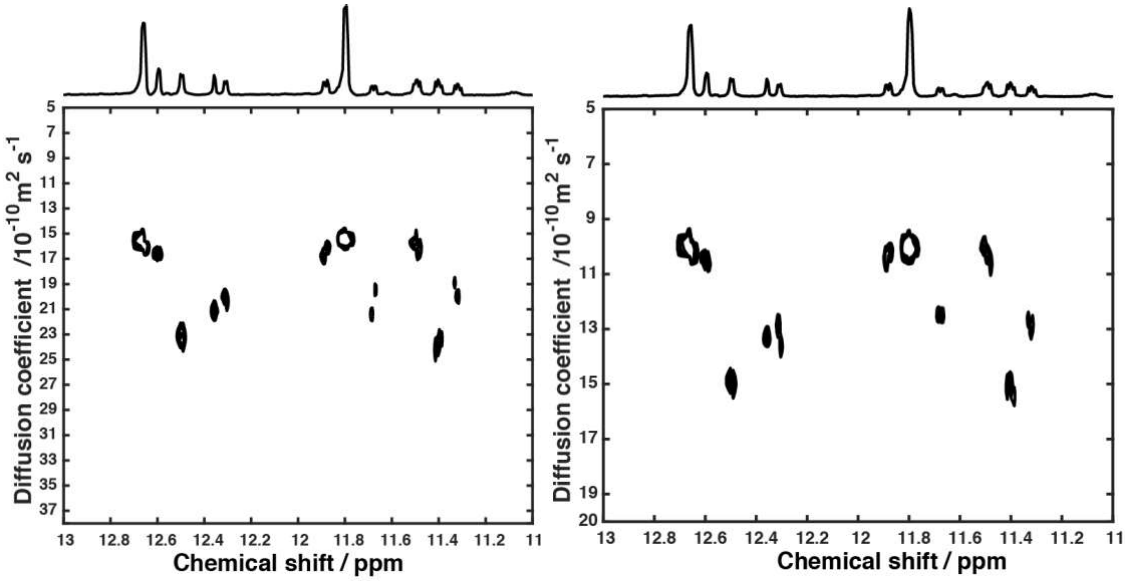

Figure 89: Conventional DOSY along z axis (left) and along x axis (right) on sample M3. Data were acquired using $\boldsymbol{P}_{xyz}$ *probe at 298K.*

10.5.1. Investigation on the transverse plane encoding

Using a transverse axis for spatial encoding requires taking into account the shape of the NMR tube: the spatial profile in the absence of diffusion is indeed round, while the profile along z is flat. A double-spin echo 1D imaging pulse sequence was used to obtain the reference spatial profile without diffusion weighting. In addition, the sample length along a transverse direction is shorter than along the z direction. For comparison, three types of experiments were carried out: along the x axis, along the z axis using a 3.95 mm region, and along the z axis using a 10 mm region as usual. The acquisition parameters for the SPEN DOSY pulse sequence were optimized for experiments that use spatial encoding along the x axis. The single stimulated echo pulse sequence using a spectrally selective refocusing pulse was used, using a timing that is compatible with a pure-absorption processing of the data.

SPEN DOSY spectra along x where acquired using SPEN STE pulse sequence using a chirp pulse with BW=70000 Hz and a duration of 1 ms. Post chirp gradient was 0.9 ms and encoding gradient strength was 0.39 T/m Acquisition gradient was set to 0.25 T/m. Diffusion delay was 100 ms. Selective 180° was used with a duration of 5915 µs centered at O_1=11.9 ppm. Total acquisition time was 66 ms for 65536 points, 128 loops, T_a=256 µs leading to a spectral width of 1953Hz. Relaxation delay was set to d_1=5 s. Observed region is 3.95 mm.

SPEN DOSY spectra along z where acquired using SPEN STE pulse sequence with the exact same parameters as before excepted for the acquisition gradient that was set to 0.325 T/m. The observed region is 3.95 mm.

SPEN DOSY spectra along z where acquired using SPEN STE pulse sequence using a chirp pulse with BW=100000 Hz and a duration of 1.5 ms. Post chirp gradient was 1.5 ms and encoding gradient strength was 0.2535 T/m. Acquisition was set to 0.26 T/m. Diffusion delay was 100 ms. Selective 180° was used with a duration of 5714 µs centered at O_1=11.9 ppm. Total acquisition time was 102 ms for 102400 points, 200 loops, T_a=256 µs. Relaxation delay was set to d_1=5 s. The observed region is 10 mm.

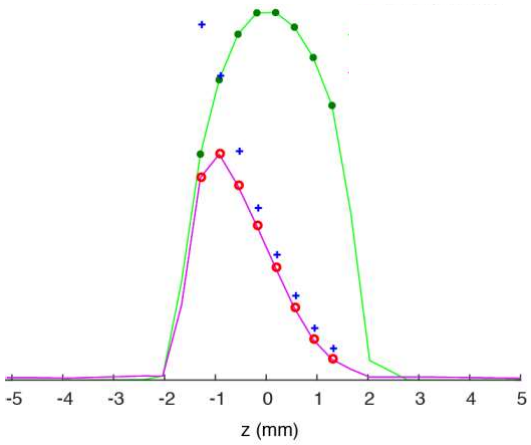

Figure 90: SPEN DOSY processing using x-axis encoding. The spatial profile obtained with SPEN DOSY is shown in pink, and points selected for the fit are shown as red circles. The reference spatial profile is shown in green, with the selected points shown as green circles. The normalized data are shown as blue crosses.

Figure 90 illustrates how the correction by the reference profile makes it possible to retrieve the diffusion decay curve from a spatial region that does not have a uniform spin density. The results shown here were obtained by exploiting the date from a region ranging from -1.3 mm to 1.5 mm. Numerical simulations were also used to validate the use of a reference profile to retrieve good diffusion curves from a non-constant initial spin density.

10.5.2. Comparison of SPEN DOSY along z-axis vs SPEN DOSY along x-axis (no shaking)

Results in the case of SPEN DOSY STE along x (observed region 3.95 mm) and z (observed region 3.95 mm and 10 mm) were obtained on a well shimmed and locked sample **M3** without prior shaking and are presented in Figure 91. These displays were used as a reference. The effect of encoding along x versus z is evaluated. When sweeping 3.95 mm the best results are obtained for the SPEN DOSY encoded along x, Figure 91a, which is less impacted by convection effect. Figure 91b is encoded along z axis over 3.95 mm this time but the separation is not good. Results are much better in term of separation for Figure 91c encoded along 10 mm but this correspond to what we observed in the previous section

where diffusion coefficients are overestimated. Diffusion coefficients of signals that belong to a same molecule are determined with accuracy (less than 3 % along x and between 2 and 10 % along z). In SPEN DOSY encoded along z diffusion coefficients appear to be higher than in SPEN DOSY encoded along x because of non-calibrated gradient constant but this is consistent with our reference conventional DOSY.

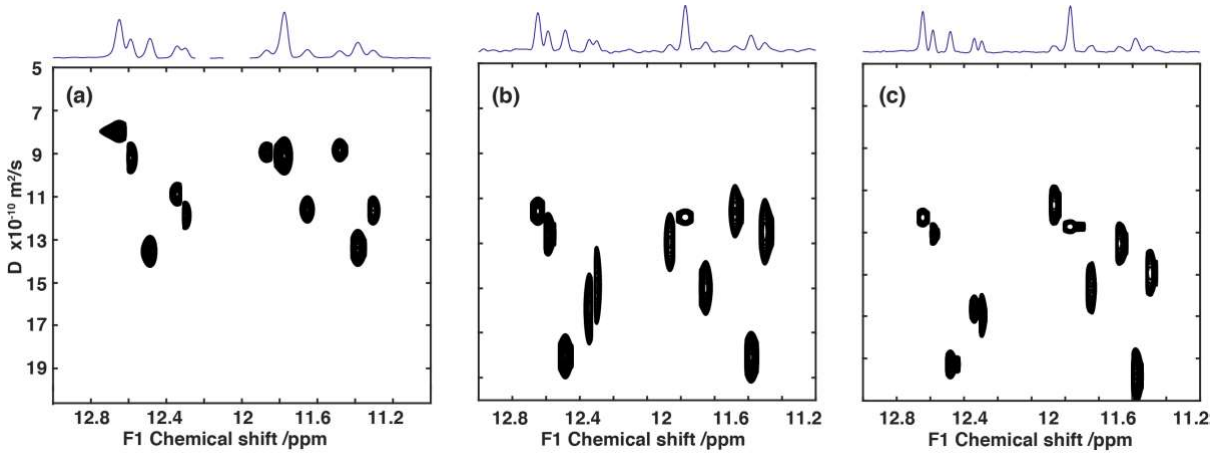

Figure 91 : (a) SPENDOSY spectra encoded along x over 3.95 mm, (b) encoded along z over 3.95 mm and (c) encoded along z over 10 mm; without shaking on sample M3. Data were acquired using $\boldsymbol{P}_{xyz}$ *probe at 298K.*

10.5.3. Comparison of SPEN DOSY along z-axis vs SPEN DOSY along x-axis (with shaking)

Figure 92 show the results obtained in order to evaluate the stability of the SPEN DOSY STE during the shaking along x and z axis on sample **M3**. They are compared with a reference SPEN DOSY display obtained without any shaking.

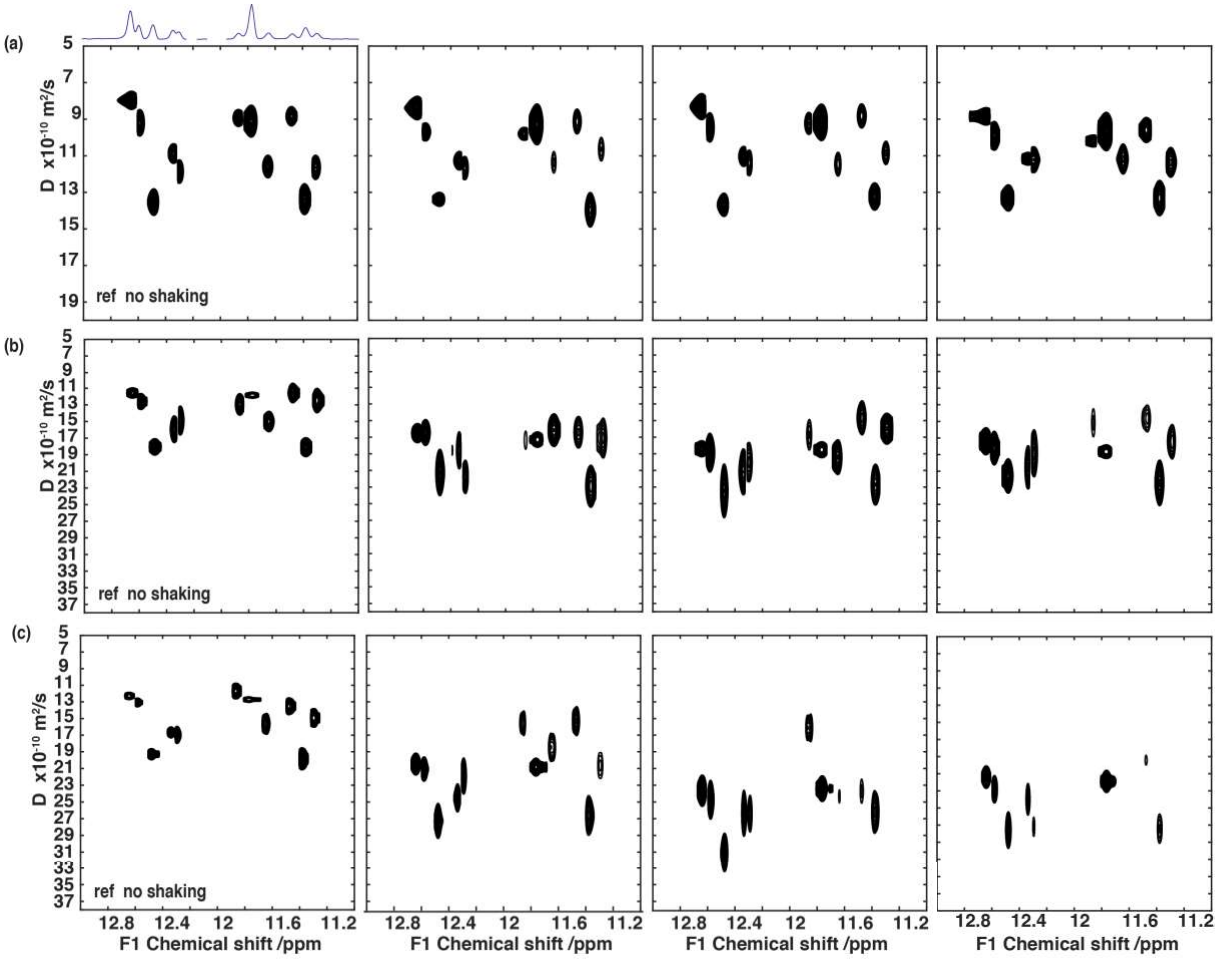

Figure 92: (a) Serie of shaken SPENDOSY spectra encoded along x over 3.95 mm compared to reference without shaking, (b) Serie of shaken SPENDOSY spectra encoded along z over 3.95 mm compared to reference without shaking and (c) Serie of shaken SPENDOSY spectra encoded along z over 10 mm compared to reference without shaking. The sample used was M3. Data were acquired using $\boldsymbol{P}_{xyz}$ *probe at 298K.*

The results obtained with the SPEN STE DOSY sequence using x-encoding remain stable even after sample shaking, as shown in Figure 92a. The variation of the diffusion coefficient within a given molecule are of less than 5 %. In addition, variation across several experiments is also below 5 %, which means that these experiments are repeatable. Compared to the reference experiment without shaking, the error is between 2 and 10 %, and the results are stable from an experiment to another.

On the contrary, the results obtained with the SPEN STE DOSY sequence using z-encoding show an unpredictable behavior of the estimated diffusion coefficients, which are not stable as seen in Figure 92b. Values vary by 12 % within a given molecule, and the CSV of D within a same molecule increase to 12 %. Compared to the reference experiment (without shaking) the error is between 22 and 50 %. This loss of accuracy in the calculation is due to convection effect after shaking, resulting in overestimated values for the diffusion coefficient. The results using a large spatial region for z encoding are even worse. Variations within a same molecule increase to 20 %, and the error compared to the reference is between 30 and 92 %.

Overall, using a transverse axis for spatial encoding seems to yield much more accurate results in cases when the sample is shaken prior to the diffusion measurement.

10.5.4. Hyperpolarized SPEN DOSY on mixture along x-axis

10.5.4.1. Diffusion coefficient calculation

Now that we have set up a strategy that provide stable diffusion coefficients after the shaking of the sample during the SABRE process it is time to put it to the test during a real SABRE experiment. Sample **M4** composed of 4 molecules SABRE-compatible was used to this purpose. Results of SPEN DOSY STE along z axis were obtained using the same parameters as described in section 10.5.1 and are shown in Figure 93. We manage to acquire a series of ^{1}H hyperpolarized SPEN DOSY display on this mixture.

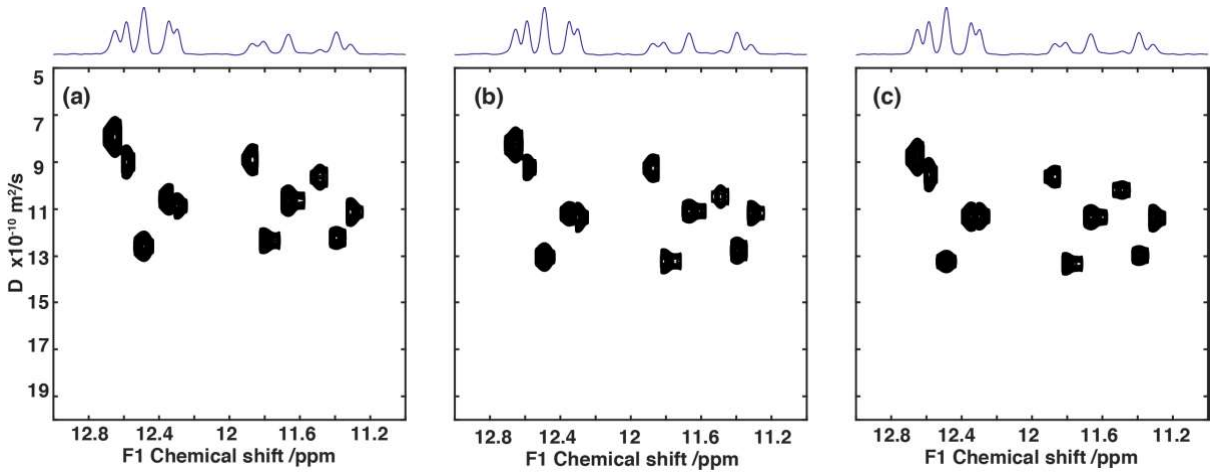

Figure 93 : SABRE SPEN DOSY on mixture M4 along x-axis , 2nd refill of p-H_2. Data were acquired using $\boldsymbol{P_{xyz}}$ *probe at 298K.*

Variation of D within a same molecule are less than 5 % and CSV is below 5 % which mean that these experiments are repeatable. A good separation is obtained and we were able to identify each molecule of our mixture. The results are no longer impacted by the unwanted convection effect and we were able to obtain stable diffusion coefficients within the 5 s delay that we have before the signal disappears. The diffusion curves are observed on 2.8 mm region because of the distortion due to the shape of the NMR tube. The correction by reference profile allows us to recover some points on the edges of the sample thus contributing to improve the resolution in the diffusion dimension. The resolution of the SPEN DOSY display is significantly decreased because of the SABRE process and because of the larger number of resonances present in the spectrum. Without all of the optimization presented in section 8 these results could not be obtained. The phasing of the data in the spectral dimension was key in order

to get those results. Since this sample is a 5 mM sample we can say that we gain a factor 4 in term of limit of detection. Usually 20 mM at least is required to get a SPEN DOSY display.

We did try to decrease the concentration of sample and the results are shown in Figure 94. The sample used is **M5** with a concentration of 2.5 mM per molecule instead of 5 mM and we see that we do not get a proper separation of the signal. Variation of D within a same molecule are less than 10 % and CSV is increased to 12 % compared to what we had previously. The separation is not achieved in this case and we probably reached the limit of this experiment. We also try to see was it would be with lower concentration (ca. 1 mM) and the use of a co-substrate but results were not much better. We did not observe all signal as the enhancement is molecules dependent and the sensitivity was too low for most of them.

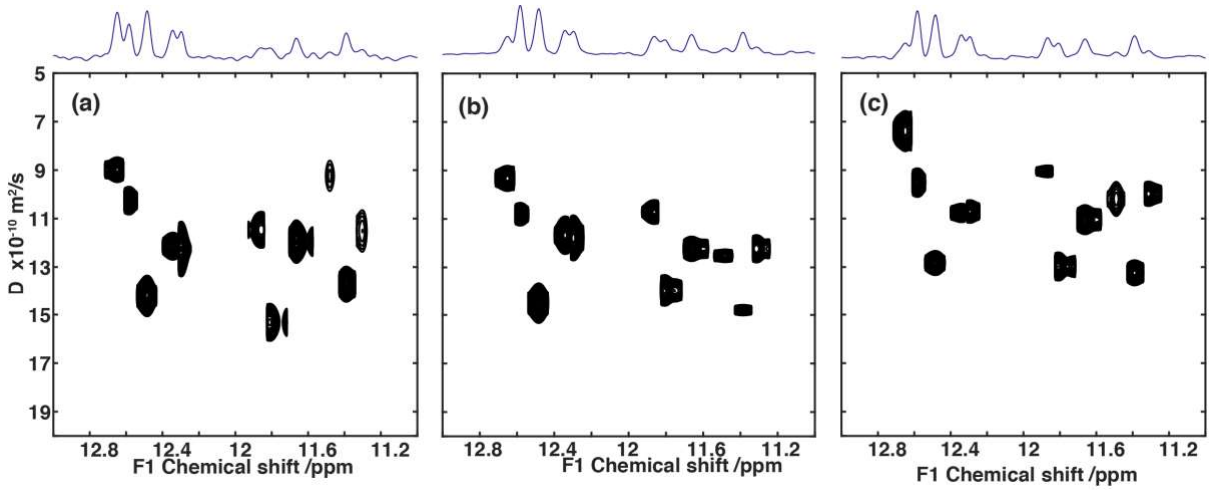

Figure 94: SABRE SPEN DOSY on mixture M5 along x-axis for a 2nd refill of p-H_2. (a), (b) and (c) were acquired after three successive shaking of the NMR tube. Data were acquired using $\mathbf{P}_{xyz}$ probe at 298K.

10.5.4.2. Signal enhancement achieved with SABRE

In this section the enhancement achieved with the SABRE method are discussed. This is important in order to see how low we can go in terms of concentration of the analytes. In thermal equilibrium experiments, the SNR required is at least 5 for the lowest gradient increment so it means that it should be 30-50 for the highest gradient increment. 20 mM is necessary to achieve this minimum SNR and get good SPEN DOSY spectra (data not shown). Ideally, we would like to go down to 1 mM. It has been demonstrated on ufCOSY coupled with SABRE at submillimolar concentrations and down to nanomolar concentrations as well [49,217].

Enhancement that we obtained in our experiment are correct compared from what is found in the literature even if they remain in the lowest side of the achievable range. Plenty of signal is obtained at 10 mM so the overall gain is a factor of 4 compared to thermal equilibrium experiments as SPEN

DOSY requires at a 20 mM sample. Results for the epsilon are found in Table 19 for all the molecules and the hyperpolarized spectrum versus the thermal equilibrium spectrum are shown in Figure 95. Enhancement was calculated by using the calculated area of the signal within topspin from a 1D spectra acquired during hyperpolarization process and after complete return to equilibrium.

Table 19: Epsilon values calculated during the SABRE experiment on a 5 mM mixture.

Molecule	Epsilon
pyridine	256
bipyridine	20
N,N-dimethylnicotinamide	85
3-ethylpyridine	256

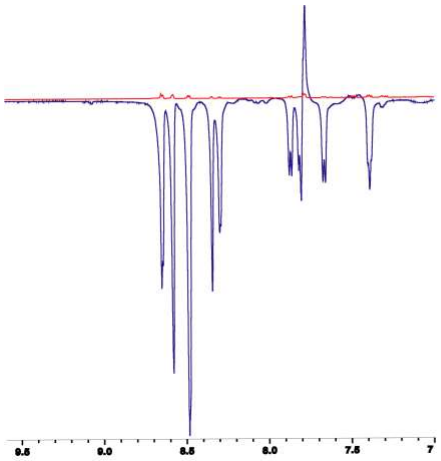

Figure 95: Comparison of thermal equilibrium 1D spectrum (red) and enhanced 1D spectrum (blue) acquired during the SABRE process on M5. Data were acquired using $\boldsymbol{P_{xyz}}$ *probe at 298K.*

The enhancement is not the same for all molecules and the highest value of ε is obtained for pyridine and 3-ethylpyridine with a 256-fold signal amplification. It is interesting to note that the epsilon for bipyridine is so low that we can recover the pyridine peak (at 11.7 ppm) that is overlapped with one of the peaks of bipyridine (see Figure 93).

Attempt to decrease the concentration and evaluate the enhancement was done only on for concentration of 1 mM and pyridine-d5 or mtz (1-methyl-1,2,3-triazole) as co-substrate (data not shown). As explained in section 5, the use of a co-substrate is mandatory to preserve the activity of the catalyst. Otherwise, an inactive complex will be formed with the solvent. The co-substrate should have the same binding properties to the catalyst than the analytes and its signals should not be overlapped with signals coming from the analytes.

At 1 mM the co-substrate mtz appear to be better than pyridine-d5 and give observable signals. No signal was observed with pyridine-d5 at this concentration and the efficacy of this co-substrate is lower compared to the mtz. The drawback of this co-substrates is its exchange with the hyperpolarized

compounds giving the impression of signal intensity over time. Overall the enhancement a 1 mM and with co-substrate is no more than 32 and this was not enough to get SPEN DOSY display with SABRE.

10.6. Conclusions

Convection compensated pulse sequences were used but led to no accurate results. We finally managed to get successful results by encoding to diffusion encoding along a transverse direction. We were able to record SPEN DOSY data from SABRE hyperpolarized substrates. The signal enhancements were comprised between 20 for bipyridine and 256 for pyridine. With a single batch of parahydrogen, 3 to 5 consecutive sample shaking can be carried out. The use of a reference profile is mandatory for the processing of data obtained with spatial encoding along a transverse axis, and this approach provides a measurement that is more robust against sample convection. The gain is a factor 4 compare to what we usually have with thermal equilibrium SPEN DOSY. Nevertheless, our attempt of SABRE-DOSY on a lower concentration (2.5 mM and 1 mM) failed since the enhancement was not sufficient. With in-flow system maybe lower concentration could be achieved.

The SABRE SPEN DOSY method that we have proposed is an innovative way of performing DOSY experiments in a fast and sensitive way.

Conclusions and perspectives

During this project, we have shown that spatially encoded diffusion-ordered NMR spectroscopy (SPEN DOSY) is a general tool that can be used to address the challenge of separating 1D and 2D spectra of components in a mixture. Regarding the first part of the project, we focused on the development of fast multidimensional diffusion-based NMR methods in order to separate the pure spectra of compounds within a complex mixture. Starting from the initially proposed NMR sequences by Keeler and Frydman [41,42], two types of fast DOSY experiments were studied as preliminary steps of the overall project. Using these results as a basis, an improved sequence for SPEN DOSY was designed, embedding in a distinct way all the advantageous features identified to get optimum results [239]. Using a model sample, it was demonstrated that it is possible to perform a diffusion experiment in 241 ms compared to conventional experiments that require 17 min to be completed. The SPEN DOSY display, in which signals are sorted according to their diffusion coefficient value, is comparable to the conventional one. The SPEN DOSY approach provides a fast separation of components in mixtures. Although the accuracy of SPEN DOSY is not equivalent to that of the conventional approach, the separation of the components is still good.

To address the limitations of SPEN DOSY for crowded spectra, a higher dimensionality DOSY experiment was then created by appending a COSY encoding block to the SPEN-DOSY pulse sequence [239]. In the case of 3D pulse sequences, either one or both of the indirect domains may be spatially encoded so that experiments are performed within the timescale of a conventional 2D experiment or faster. We choose to only spatially encode the diffusion dimension for the sake of greater resolution and maximized spectral width. This is a novel sequence that improves significantly the speed of the existing DOSY COSY experiment [148]. Using a model sample, we demonstrated that it is possible to perform a 3D diffusion experiment in 12 min compared to conventional experiments that require 14h to be completed. The SPEN DOSY COSY experiment was successful in returning the individual COSY of each molecule in the studied mixture

Numerical simulations of the SPEN DOSY experiment using Spinach software [44], in partnership with Ilya Kuprov, were used as a support to improve those results. With this package, the SPEN DOSY-like diffusion lineshape was simulated on a ^{1}H spin system. Extra care was taken to ensure that all our simulations converged so that we can be sure that the returned results have a physical meaning. The finite difference approximation of the operator was used to run the simulation in less than 2 min. The effect of several parameters such as the encoding gradient, the acquisition gradient or chirp duration was also studied to see their impact on the lineshape and the measured diffusion coefficient. Models used for data adjustment were corrected as well in order to improve the accuracy of calculated diffusion coefficient by reducing systematic errors.

SPEN DOSY spectra were collected from samples hyperpolarized with D-DNP. A new pulse sequence was designed so that several SPEN-DOSY data set could be recorded after a single dissolution step. Instead of using a STE based pulse sequence, this version is based on a double spin echo that uses an even number of adiabatic pulses as it helps to preserve magnetization from scan to scan. [206], [223] A small tip angle (30°) is also used to excite part of the magnetization at each scan. As DOSY experiments are strongly impacted by convection, the pulse sequence was upgraded to compensate for convection. Jershow and Muller proposed, in the case of conventional DOSY experiments, to use double diffusion encoding steps instead of a single diffusion encoding step [163]. The strategy was successfully exploited for SPEN DOSY experiments and supported by numerical simulations. Using a model sample composed of acetate, pyruvate and urea labelled on the carbonyl, we demonstrated that it is possible to record DOSY data of hyperpolarized compounds in a single-scan. We are able to perform up to 5 SPEN DOSY after a single DNP step and this is promising to monitor dynamic processes. The results we obtained are repeatable and reproducible even though systematic error is still present and need to be corrected.

The Signal Amplification by Reversible Exchange (SABRE) method that consists in a transfer of polarization from parahydrogen to the substrate was studied in parallel [49]. Compared to DNP this method is relatively cheap and easy to implement. This method is less 'universal' than DNP as only molecules that possess nitrogen aromatic ring can be efficiently polarised although current development make it possible to polarise compounds such as amines, amides, carboxylic acids, alcohols, phosphates or carbonates. We demonstrated that it was possible to obtain SPEN DOSY display of SABRE hyperpolarized compounds. Since the SABRE experiment requires shaking of the sample that contain the catalyst and the substrate in solution as well as the para-hydrogen in the gaseous phase, we first evaluated the shaking effect on the calculated diffusion coefficients. By shaking the sample, we create additional movement other that Brownian motion which is detrimental for DOSY experiments. We observed that it takes 15s after shaking to get stable results so it means that the amplified signal would have disappeared before we can get proper values for diffusion coefficient. Attempts of convection compensation like the one used for the DNP case were unsuccessful. Performing the spatial encoding of the diffusion in the transverse plane was the strategy that gave successful results, and we were able to get SABRE hyperpolarized SPEN DOSY data.

DNP and SABRE together with SPEN-DOSY are of great potential use for the analysis of low concentrated mixtures of small molecules thus broadening the range of mixtures that may be analysed with diffusion NMR. Promising results were obtained for DNP-DOSY and SABRE-DOSY and despite the good separation achieved, the measured diffusion coefficients suffer from a systematic error. This strategy may be applied for chemical reaction monitoring. In the meantime, the use of a double diffusion-encoding step makes it possible to attenuate convection effects, which is also supported by numerical simulations that did play an important role to reach our goal. This was a key strategy in our experiments. Systems undergoing chemical reactions or molecular interactions may benefit from this approach. H

igher enhancements are expected with the use of faster transfer systems or shorter recycle delay and this, in the case of DNP, would allow for studies of low concentrated mixtures down to sub-millimolar concentrations. Our attempt to decrease the concentration with SABRE remained vain but with in-flow systems we should be able to do it. Some work has still to be done in order to reduce the systematics errors on diffusion coefficients values.

In conclusion, this project has provided solid ground for SPEN DOSY experiments thank to the introduction of a powerful numerical tool for the simulation, understanding and improvement of SPEN DOSY experiments but also thank to the robust implementation of the SPEN 2D DOSY approach. The methodological developments around ND DOSY is expending especially in the field of chemical reaction monitoring and we hope that it will lead to application on real complex mixtures.

Bibliography

[1] C. Simmler, J.G. Napolitano, J.B. McAlpine, S.N. Chen, G.F. Pauli, Universal quantitative NMR analysis of complex natural samples, *Curr. Opin. Biotechnol.* **2014**, 25, 51–59.

[2] A. Marston, K. Hostettmann, Natural product analysis over the last decades, *Planta Med.* **2009**, 75, 672–682.

[3] J. Kruk, M. Doskocz, E. Jodłowska, A. Zacharzewska, J. Łakomiec, K. Czaja, J. Kujawski, NMR Techniques in Metabolomic Studies: A Quick Overview on Examples of Utilization, *Appl. Magn. Reson.* **2017**, 48, 1–21.

[4] J. Van Duynhoven, E. van Velzen, D.M. Jacobs, Quantification of complex mixtures by NMR, *Annu. Reports NMR Spectrosc.* **2013**, 80, 181–236.

[5] P. Giraudeau, Quantitative 2D liquid-state NMR, *Magn. Reson. Chem.* **2014**, 52, 259–272.

[6] E.M. Purcell, H.C. Torrey, R. V. Pound, Resonance absorption by nuclear magnetic moments in a solid, *Phys. Rev.* **1946**, 69, 37–38.

[7] F. Bloch, W.W. Hansen, M. Packard, The nuclear induction experiment, *Phys. Rev.* **1946**, 70, 474–485.

[8] D. Jeannerat, J. Furrer, NMR experiments for the analysis of mixtures: Beyond 1D 1H spectra, *Comb. Chem. High Throughput Screen.* **2012**, 15, 15–35.

[9] M. Malet-Martino, U. Holzgrabe, NMR techniques in biomedical and pharmaceutical analysis, *J. Pharm. Biomed. Anal.* **2011**, 55, 1–15.

[10] R.R. Forseth, F.C. Schroeder, NMR-spectroscopic analysis of mixtures: From structure to function, *Curr. Opin. Chem. Biol.* **2011**, 15, 38–47.

[11] S. Wei, J. Zhang, L. Liu, T. Ye, G.A.N. Gowda, F. Tayyari, D. Raftery, Ratio Analysis NMR Spectroscopy (RANSY) for Selective Metabolite Identification in Complex Samples, *Anal. Chem.* **2011**, 83, 7616–7623.

[12] P.L. Rinaldi, Three-dimensional solution NMR spectroscopy of complex structures and mixtures., *Analyst*. **2004**, 129, 687–99.

[13] M. Spraul, B. Schütz, E. Humpfer, M. Mörtter, H. Schäfer, S. Koswig, P. Rinke, Mixture analysis by NMR as applied to fruit juice quality control, *Magn. Reson. Chem.* **2009**, 47,.

[14] R. Lamanna, A. Braca, E. Di Paolo, G. Imparato, Identification of milk mixtures by 1H NMR profiling, *Magn. Reson. Chem.* **2011**, 49, S22–S26.

[15] F. Wei, K. Furihata, F. Hu, T. Miyakawa, M. Tanokura, Complex mixture analysis of organic compounds in green coffee bean extract by two-dimensional NMR spectroscopy, *Magn. Reson. Chem.* **2010**, 48, 857–865.

[16] J.W. Emsley, J. Feeney, Forty years of Progress in Nuclear Magnetic Resonance Spectroscopy, *Prog. Nucl. Magn. Reson. Spectrosc.* **2007**, 50, 179–198.

[17] A.S. Edison, F.C. Schroeder, NMR – Small Molecules and Analysis of Complex Mixtures, *Compr. Nat. Prod. II*. **2010**, 9, 169–196.

[18] J.S. McKenzie, J.A. Donarski, J.C. Wilson, A.J. Charlton, Analysis of complex mixtures using high-resolution nuclear magnetic resonance spectroscopy and chemometrics, *Prog. Nucl. Magn. Reson. Spectrosc.* **2011**, 59, 336–359.

[19] R. Novoa-Carballal, E. Fernandez-Megia, C. Jimenez, R. Riguera, NMR methods for unravelling the spectra of complex mixtures, *Nat. Prod. Rep.* **2011**, 28, 78–98.

[20] A.M. Dixon, C.K. Larive, NMR spectroscopy with spectral editing for the analysis of complex mixtures, *Appl. Spectrosc.* **1999**, 53, 426A–440A.

[21] K. Skidmore, D. Hewitt, Y.H. Kao, Quantitation and characterization of process impurities and extractables in protein-containing solutions using proton NMR as a general tool, *Biotechnol. Prog.* **2012**, 28, 1526–1533.

[22] P. Sandusky, D. Raftery, Use of Selective TOCSY NMR Experiments for Quantifying Minor Components in Complex Mixtures: Application to the Metabonomics of Amino Acids in Honey, *Anal. Chem.* **2005**, 77, 2455–2463.

[23] P. Sandusky, E. Appiah-Amponsah, D. Raftery, Use of optimized 1D TOCSY NMR for improved quantitation and metabolomic analysis of biofluids, *J. Biomol. NMR*. **2011**, 49, 281–290.

[24] H. Barjat, G.A. Morris, S. Smart, A.G. Swanson, S.C.R. Williams, High-Resolution Diffusion-Ordered 2D Spectroscopy (HR-DOSY) - A New Tool for the Analysis of Complex Mixtures, *J. Magn. Reson. Ser. B*. **1995**, 108, 170–172.

[25] R.E. Hoffman, H. Arzuan, C. Pemberton, A. Aserin, N. Garti, High-resolution NMR "chromatography" using a liquids spectrometer, *J. Magn. Reson.* **2008**, 194, 295–299.

[26] S. Caldarelli, Chromatographic NMR: a tool for the analysis of mixtures of small molecules, *Magn. Reson. Chem.* **2007**, 45, S48–S55.

[27] K.A. Heisel, J.J. Goto, V. V. Krishnan, NMR Chromatography: Molecular Diffusion in the Presence of Pulsed Field Gradients in Analytical Chemistry Applications, *Am. J. Anal. Chem.* **2012**, 03, 401–409.

[28] D.H. Wu, A. Chen, C.S. Johnson, An Improved Diffusion-Ordered Spectroscopy Experiment Incorporating Bipolar-Gradient Pulses, *J. Magn. Reson. Ser. A*. **1995**, 115, 260–264.

[29] S. Trefi, V. Gilard, S. Balayssac, M. Malet-Martino, R. Martino, The usefulness of 2D DOSY and 3D DOSY-COSY 1H NMR formixture analysis: Application to genuine and fake formulations of sildenafil (Viagra), *Magn. Reson. Chem.* **2009**, 47,.

[30] A. Jerschow, N. Müller, 3D diffusion-ordered TOCSY for slowly diffusing molecules, *J. Magn. Reson. - Ser. A*. **1996**, 123, 222–225.

[31] S. Viel, S. Caldarelli, Improved 3D DOSY-TOCSY experiment for mixture analysis, *Chem. Commun.* **2008**, 0, 2013–2015.

[32] A. Jerschow, N. Müller, Diffusion-separated nuclear magnetic resonance spectroscopy of polymer mixtures, *Macromolecules*. **1998**, 31, 6573–6578.

[33] J. Aidi Chen, Donghui Wu, and Charles S. Johnson, Determination of Molecular Weight Distributions for Polymers by Diffusion-Ordered NMR, *J. Am. Chem. Soc.* **1995**, 117, 7965–7970.

[34] S. Viel, D. Capitani, L. Mannina, A. Segre, Diffusion-Ordered NMR Spectroscopy A Versatile Tool for the MW determination of uncharged polysaccharides, *Biomacromolecules*. **2003**, 4, 1843–1847.

[35] G. Pages, P.W. Kuchel, NMR Methods for the Fast Recording of Diffusion, *Diffus. Fundam.* **2007**, 6, 3.1-3.17.

[36] M. Urbańczyk, W. Koźmiński, K. Kazimierczuk, Accelerating diffusion-ordered NMR spectroscopy by joint sparse sampling of diffusion and time dimensions, *Angew. Chemie - Int. Ed.* **2014**, 53, 6464–6467.

[37] M. Shukla, K. Dorai, Resolving overlaps in diffusion encoded spectra using band-selective pulses in a 3D BEST-DOSY experiment, *J. Magn. Reson.* **2011**, 213, 69–75.

[38] L. Frydman, T. Scherf, A. Lupulescu, The acquisition of multidimensional NMR spectra within a single scan., *Proc. Natl. Acad. Sci. U. S. A.* **2002**, 99, 15858–15862.

[39] P. Giraudeau, L. Frydman, Ultrafast 2D NMR: An Emerging Tool in Analytical Spectroscopy, *Annu. Rev. Anal. Chem.* **2014**, 7, 129–161.

[40] B. Gouilleux, L. Rouger, P. Giraudeau, Ultrafast multi-dimensional NMR: Principles and recent applications, *EMagRes*. **2016**, 5, 913–922.

[41] M.J. Thrippleton, N.M. Loening, J. Keeler, A fast method for the measurement of diffusion coefficients: One-dimensional DOSY, *Magn. Reson. Chem.* **2003**, 41, 441–447.

[42] Y. Shrot, L. Frydman, Single-scan 2D DOSY NMR spectroscopy, *J. Magn. Reson.* **2008**, 195, 226–231.

[43] J.H. Lee, Y. Okuno, S. Cavagnero, Sensitivity enhancement in solution NMR: Emerging ideas and new frontiers, *J. Magn. Reson.* **2014**, 241, 18–31.

[44] H.J. Hogben, M. Krzystyniak, G.T.P. Charnock, P.J. Hore, I. Kuprov, Spinach - A software library for simulation of spin dynamics in large spin systems, *J. Magn. Reson.* **2011**, 208, 179–194.

[45] J.H. Ardenkjaer-Larsen, B. Fridlund, A. Gram, G. Hansson, L. Hansson, M.H. Lerche, R. Servin, M. Thaning, K. Golman, Increase in signal-to-noise ratio of > 10,000 times in liquid-state NMR, *Proc. Natl. Acad. Sci.* **2003**, 100, 10158–10163.

[46] J.-N. Dumez, J. Milani, B. Vuichoud, A. Bornet, J. Lalande-Martin, I. Tea, M. Yon, M. Maucourt, C. Deborde, A. Moing, L. Frydman, G. Bodenhausen, S. Jannin, P. Giraudeau, Hyperpolarized NMR of plant and cancer cell extracts at natural abundance, *Analyst*. **2015**, 140, 5860–5863.

[47] L. Lumata, A.K. Jindal, M.E. Merritt, C.R. Malloy, A.D. Sherry, Z. Kovacs, DNP by thermal mixing under optimized conditions yields >60 000-fold enhancement of 89Y NMR signal, *J. Am. Chem. Soc.* **2011**, 133, 8673–8680.

[48] B. Plainchont, P. Berruyer, J.-N. Dumez, S. Jannin, P. Giraudeau, Dynamic Nuclear Polarization Opens New Perspectives for NMR Spectroscopy in Analytical Chemistry, *Anal. Chem.* **2018**, 90, 3639–3650.

[49] V. Daniele, F.X. Legrand, P. Berthault, J.N. Dumez, G. Huber, Single-Scan Multidimensional NMR Analysis of Mixtures at Sub-Millimolar Concentrations by using SABRE Hyperpolarization, *ChemPhysChem*. **2015**, 16, 3413–3417.

[50] R.W. Adams, S.B. Duckett, R.A. Green, D.C. Williamson, G.G.R. Green, A theoretical basis for spontaneous polarization transfer in non-hydrogenative parahydrogen-induced polarization, *J. Chem. Phys.* **2009**, 131, 194505.

[51] I. Toumi, B. Torre, S. Caldarelli, E ff ective Processing of Pulse Field Gradient NMR of Mixtures by Blind Source Separation, *Anal. Chem.* **2013**, 85, 11344–11351.

[52] J. Wist, Complex mixtures by NMR and complex NMR for mixtures: experimental and publication challenges, *Magn. Reson. Chem.* **2017**, 55, 22–28.

[53] M. Liu, J.K. Nicholson, J.C. Lindon, High-Resolution Diffusion and Relaxation Edited One- and Two- Dimensional 1H NMR Spectroscopy of Biological Fluids, *Anal. Chem.* **1996**, 68, 3370–3376.

[54] H.Y. Carr, E.M. Purcell, Effects of Diffusion on Free Precession in Nuclear Magnetic Resonance Experiments, *Phys. Rev.* **1954**, 94, 630–638.

[55] S. Meiboom, D. Gill, Modified spin echo method for measuring nuclear relaxation times., *Rev Sci Instr*. **1958**, 29, 688–691.

[56] G. Graça, I.F. Duarte, B.J. Goodfellow, A.S. Barros, I.M. Carreira, A.B. Couceiro, M. Spraul, A.M. Gil, Potential of NMR Spectroscopy for the study of human amniotic fluid, *Anal. Chem.* **2007**, 79, 8367–8375.

[57] H. Kählig, K. Dietrich, S. Dorner, Analysis of carbohydrate mixtures by diffusion difference NMR spectroscopy, *Monatshefte Fur Chemie*. **2002**, 133, 589–598.

[58] J.F.K. Limtiaco, C.J. Jones, C.K. Larive, Diffusion-edited NMR spectra of heparin contaminants, *Anal. Methods*. **2012**, 4, 1168–1172.

[59] S.S. T. Kanthimathi, Y. V. S. Narayana Moorthy, C. N. Pillai, N. Moorthy, Spectral Separation of Two Very Closely Related Organic Compounds by 1D TOCSY, **1994**, 32, 452–457.

[60] M.J. Lynch, J. Masters, J.P. Pryor, J.C. Lindon, M. Spraul, P.J. Foxall, J.K. Nicholson, Ultra high field NMR spectroscopic studies on human seminal fluid, seminal vesicle and prostatic secretions, *J Pharm Biomed Anal*. **1994**, 12, 5–19.

[61] R. Consonni, L.R. Cagliani, F. Benevelli, M. Spraul, E. Humpfer, M. Stocchero, NMR and Chemometric methods: A powerful combination for characterization of Balsamic and

Traditional Balsamic Vinegar of Modena, *Anal. Chim. Acta*. **2008**, 611, 31–40.

[62] P. Sandusky, D. Raftery, Use of semiselective TOCSY and the Pearson correlation for the metabonomic analysis of biofluid mixtures: Application to urine, *Anal. Chem.* **2005**, 77, 7717–7723.

[63] K.L.B. Robin A. de Graaf, Golam M. I. Chowdhury, Quantification of High-Resolution 1H NMR Spectra from Rat Brain Extracts, *Anal. Chem.* **2011**, 83, 216–224.

[64] K. Takegoshi, K. Ogura, K. Hikichi, A perfect spin echo in a weakly homonuclear J-coupled two spin- 1 2 system, *J. Magn. Reson.* **1989**, 84, 611–615.

[65] W.P. Aue, E. Bartholdi, R.R. Ernst, Two-dimensional spectroscopy. Application to nuclear magnetic resonance, *J. Chem. Phys.* **1976**, 64, 2229–2246.

[66] T.A. Carpenter, L.D. Colebrook, L.D. Hall, G.K. Pierens, Applications of gradient-selective COSY and DQCOSY to brucine and gibberellic acid, *Magn. Reson. Chem.* **1992**, 30, 768–773.

[67] A. BAX, Homonuclear Hartmann-Hahn Experiments, **1989**, 176, 151–168.

[68] L. Braunschweiler, R.R. Ernst, Coherence transfer by isotropic mixing: Application to proton correlation spectroscopy, *J. Magn. Reson.* **1983**, 53, 521–528.

[69] F. Zhang, A.T. Dossey, C. Zachariah, A.S. Edison, R. Brüschweiler, Strategy for automated analysis of dynamic metabolic mixtures by NMR. Application to an insect venom, *Anal. Chem.* **2007**, 79, 7748–7752.

[70] A.K. Galande, J.O. Trent, A.F. Spatola, Understanding Base-Assisted Desulfurization Using a Variety of Disulfide-Bridged Peptides, *Biopolym. - Pept. Sci. Sect.* **2003**, 71, 534–551.

[71] K. Bingol, F. Zhang, L. Bruschweiler-Li, R. Brüschweiler, Quantitative analysis of metabolic mixtures by two-dimensional 13C constant-time TOCSY NMR spectroscopy, *Anal. Chem.* **2013**, 85, 6414–6420.

[72] F. Zhang, R. Brüschweiler, Robust deconvolution of complex mixtures by covariance TOCSY spectroscopy, *Angew. Chemie - Int. Ed.* **2007**, 46, 2639–2642.

[73] W.P. Aue, J. Karhan, R.R. Ernst, Homonuclear broad band decoupling and two-dimensional J-resolved NMR spectroscopy, *J. Chem. Phys.* **1976**, 64, 4226–4227.

[74] Y.L. Wang, M.E. Bollard, H. Keun, H. Antti, O. Beckonert, T.M. Ebbels, J.C. Lindon, E. Holmes, H.R. Tang, J.K. Nicholson, Spectral editing and pattern recognition methods applied to high-resolution magic-angle spinning 1H nuclear magnetic resonance spectroscopy of liver tissues, *Anal. Biochem.* **2003**, 323, 26–32.

[75] M.R. Viant, Improved methods for the acquisition and interpretation of NMR metabolomic data, *Biochem. Biophys. Res. Commun.* **2003**, 310, 943–948.

[76] G. Bodenhausen, D.J. Ruben, Natural abundance nitrogen-15 NMR by enhanced heteronuclear spectroscopy, *Chem. Phys. Lett.* **1980**, 69, 185–189.

[77] A. Bax, Z. Dinya, Structure Elucidation of the Antibiotic Desertomycin through the Use of New Two-Dimensional NMR Techniques, **1986**, 108, 8056–8063.

[78] M.F. Summers, L.G. Marzilli, A. Bax, Complete proton and carbon-13 assignments of coenzyme B12 through the use of new two-dimensional NMR experiments, *J. Am. Chem. Soc.* **1986**, 108, 4285–4294.

[79] A. Bax, S. Subramanian, Sensitivity-enhanced two-dimensional heteronuclear shift correlation NMR spectroscopy, *J. Magn. Reson.* **1986**, 67, 565–569.

[80] A. Bax, S.S. Pochapsky, Optimized Recording of Heteronuclear Multidimensional NMR Spectra Using Pulsed Field Gradients, *J. Magn. Reson.* **1992**, 99, 638–643.

[81] S. Davies, A. Freeman, Three-Dimensional Correlation Spectroscopy . + COSY-3D, *J. Magn. Reson.* **1988**, 76, 555–560.

[82] H. Barjat, G.A. Morris, A.G. Swanson, A Three-Dimensional DOSY-HMQC Experiment for the High-Resolution Analysis of Complex Mixtures, *J. Magn. Reson.* **1998**, 131, 131–138.

[83] J.C. Cobas, M. Martín-Pastor, A homodecoupled diffusion experiment for the analysis of complex mixtures by NMR, *J. Magn. Reson.* **2004**, 171, 20–24.

[84] M. Nilsson, A.M. Gil, I. Delgadillo, G.A. Morris, Improving pulse sequences for 3D DOSY: COSY-IDOSY, *Anal. Chem.* **2004**, 76, 5418–5422.

[85] A.S. McLachlan, J.J. Richards, A.R. Bilia, G.A. Morris, Constant time gradient HSQC-iDOSY: Practical aspects, *Magn. Reson. Chem.* **2009**, 47, 1081–1085.

[86] J.M. Newman, A. Jerschow, Improvements in complex mixture analysis by NMR: DQF-COSY iDOSY, *Anal. Chem.* **2007**, 79, 2957–2960.

[87] M. Lin, M.J. Shapiro, Mixture Analysis by NMR Spectroscopy, *Anal. Chem.* **1997**, 69, 4731–4733.

[88] Z. Zhou, W. Lan, W. Zhang, X. Zhang, S. Xia, H. Zhu, C. Ye, M. Liu, Implementation of real-time two-dimensional nuclear magnetic resonance spectroscopy for on-flow high-performance liquid chromatography, *J. Chromatogr. A*. **2007**, 1154, 464–468.

[89] K. Akira, H. Mitome, M. Imachi, Y. Shida, H. Miyaoka, T. Hashimoto, LC-NMR identification of a novel taurine-related metabolite observed in1H NMR-based metabonomics of genetically hypertensive rats, *J. Pharm. Biomed. Anal.* **2010**, 51, 1091–1096.

[90] I.D. Wilson, U.A.T. Brinkman, Hype and hypernation: multiple hyphenation of column liquid chromatography and spectroscopy, *TrAC - Trends Anal. Chem.* **2007**, 26, 847–854.

[91] C. Tode, T. Maoka, M. Sugiura, Application of LC-NMR to analysis of carotenoids in foods, *J. Sep. Sci.* **2009**, 32, 3659–3663.

[92] G. Graça, I. Duarte, B.J. Goodfellow, Metabolite profiling of human amniotic fluid by hyphenated nuclear magnetic resonance spectroscopy, *Analytical*. **2008**, 80, 6085–6092.

[93] D.A. Dias, S. Urban, Application of HPLC-NMR for the rapid chemical profiling of a Southern Australian Sponge, Dactylospongia sp, *J. Sep. Sci.* **2009**, 32, 542–548.

[94] P. Stilbs, Fourier Pulsed-Gradient Studies of Molecular Diffusion, *Prog. NMR Spectrosc.* **1987**, 19, 1–45.

[95] C.S. Johnson, Diffusion ordered nuclear magnetic resonance spectroscopy: principles and applications, *Prog. Nucl. Magn. Reson. Spectrosc.* **1999**, 34, 203–256.

[96] W.S. Price, Pulsed-field gradient nuclear magnetic resonance as a tool for studying translational diffusion: Part II. Experimental aspects, *Concepts Magn. Reson.* **1998**, 10, 197–237.

[97] G. Pagès, V. Gilard, R. Martino, M. Malet-Martino, Pulsed-field gradient nuclear magnetic resonance measurements (PFG NMR) for diffusion ordered spectroscopy (DOSY) mapping, *Analyst*. **2017**, 3771–3796.

[98] B. Geil, Measurement of translational molecular diffusion using ultrahigh magnetic field gradient NMR, *Conc.Magn.Reson.* **1998**, 10, 299–321.

[99] N. Birlirakis, E. Guittet, A new approach in the use of gradients for size-resolved 2D-NMR experiments, *J. Am. Chem. Soc*. **1996**, 118, 13083–13084.

[100] T.L. James, G.G. McDonald, Measurement of the self-diffusion coefficient of each component in a complex system using pulsed-gradient fourier transform NMR, *J. Magn. Reson.* **1973**, 11, 58–61.

[101] W.S. PRICE, Pulsed-Field Gradient Nuclear Magnetic Resonance as a Tool for Studying Translational Diffusion. Part 1. Basic Theory, *Concepts Magn Reson*. **1997**, 9, 299–336.

[102] R. Evans, G.D. Poggetto, M. Nilsson, G.A. Morris, Improving the Interpretation of Small Molecule Diffusion Coefficients, *Anal. Chem.* **2018**, 90, 3987–3994.

[103] D.C. Edelman, Branding in the digital age: You're spending your money in all the wrong places, *Harv. Bus. Rev.* **2010**, 88, 39–65.

[104] J. Keeler, Understanding NMR Spectroscopy, *John Wiley Sons*. **2010**, 409–416.

[105] B. Antalek, Using pulsed gradient spin echo NMR for chemical mixture analysis: How to obtain optimum results, *Concepts Magn. Reson. Part A Bridg. Educ. Res.* **2002**, 14, 225–258.

[106] D. Sinnaeve, The Stejskal – Tanner Equation Generalized for Any Gradient Shape — An Overview of Most Pulse Sequences Measuring Free Diffusion, **2012**, 40, 39–65.

[107] P. Mansfield, Multi-planar image formation using NMR spin echoes, *J. Phys. C Solid State Phys.* **1977**, 10, 55–58.

[108] T. Parella, Pulsed field gradients: A new tool for routine NMR, *Magn. Reson. Chem.* **1998**, 36, 467–495.

[109] J. Keeler, R.T. Clowes, A.L. Lewis, E.D. Laue, Pulsed-Field Gradients : Theory and Practice, *Methods Enzymol.* **1994**, 239, 145–207.

[110] J.A. Aguilar, M. Nilsson, G. Bodenhausen, G.A. Morris, Spin echo NMR spectra without J modulation, *Chem. Commun.* **2012**, 48, 811–813.

[111] A.M. Torres, R. Dela Cruz, W.S. Price, Removal of J-coupling peak distortion in PGSE experiments, *J. Magn. Reson.* **2008**, 193, 311–316.

[112] J.A. Aguilar, R.W. Adams, M. Nilsson, G.A. Morris, Suppressing exchange effects in diffusion-ordered NMR spectroscopy, *J. Magn. Reson.* **2014**, 238, 16–19.

[113] M.D. Pelta, G.A. Morris, M.J. Stchedroff, S.J. Hammond, A one-shot sequence for high-resolution diffusion-ordered spectroscopy, *Magn. Reson. Chem.* **2002**, 40, 147–152.

[114] E.O. Stejskal, J.E. Tanner, Spin diffusion measurements: Spin echoes in the presence of a time-dependent field gradient, *J. Chem. Phys.* **1965**, 42, 288–292.

[115] R. Huo, R. Wehrens, J. Van Duynhoven, L.M.C. Buydens, Assessment of techniques for DOSY NMR data processing, *Anal. Chim. Acta*. **2003**, 490, 231–251.

[116] B.R. Martini, V.A. Mandelshtam, G.A. Morris, A.A. Colbourne, M. Nilsson, Filter diagonalization method for processing PFG NMR data, *J. Magn. Reson.* **2013**, 234, 125–134.

[117] R. Huo, R.A. Van De Molengraaf, J.A. Pikkemaat, R. Wehrens, L.M.C. Buydens, Diagnostic analysis of experimental artefacts in DOSY NMR data by covariance matrix of the residuals, *J. Magn. Reson.* **2005**, 172, 346–358.

[118] J. Björnerås, A. Botana, G.A. Morris, M. Nilsson, Resolving complex mixtures: Trilinear diffusion data, *J. Biomol. NMR*. **2014**, 58, 251–257.

[119] R. Bro, N. Viereck, M. Toft, H. Toft, P.I. Hansen, S.B. Engelsen, Mathematical chromatography solves the cocktail party effect in mixtures using 2D spectra and PARAFAC, *TrAC - Trends Anal. Chem.* **2010**, 29, 281–284.

[120] A. Cherni, E. Chouzenoux, M.-A. Delsuc, PALMA, an improved algorithm for DOSY signal processing, *Analyst*. **2017**, 142, 772–779.

[121] R. Huo, R. Wehrens, L.M.C. Buydens, Robust DOSY NMR data analysis, *Chemom. Intell. Lab. Syst.* **2007**, 85, 9–19.

[122] M. Nilsson, The DOSY Toolbox: A new tool for processing PFG NMR diffusion data, *J. Magn. Reson.* **2009**, 200, 296–302.

[123] L. Castañar, G.D. Poggetto, A. Colbourne, G.A. Morris, M. Nilsson, The GNAT: a new tool for processing NMR data, *Magn. Reson. Chem.* **2018**, 56, 546–558.

[124] J.C. Cobas, P. Groves, M. Martin-Pastor, A. De Capua, New applications, processing methods and pulse sequences using diffusion NMR, *Curr. Anal. Chem.* **2005**, 1, 289–305.

[125] M. Nilsson, G.A. Morris, Speedy component resolution: An improved tool for processing diffusion-ordered spectroscopy data, *Anal. Chem.* **2008**, 80, 3777–3782.

[126] M. Nilsson, G.A. Morris, Correction of systematic errors in CORE processing of DOSY data, *Magn. Reson. Chem.* **2006**, 44, 655–660.

[127] B. Antalek, Accounting for spin relaxation in quantitative pulse gradient spin echo NMR mixture analysis, *J. Am. Chem. Soc.* **2006**, 128, 8402–8403.

[128] B.T. Ichrak Toumi, Stefano Caldarelli, A review of blind source separation in NMR spectroscopy, *Prog. Nucl. Magn. Reson. Spectrosc.* **2014**, 81, 37–64.

[129] S. Augé, P. Schmit, C. a Crutchfield, M.T. Islam, D.J. Harris, E. Durand, M. Clemancey, A.-A. Quoineaud, J. Lancelin, Y. Prigent, F. Taulelle, M.-A. Delsuc, NMR Measure of Translational Diffusion and Fractal Dimension. Application to Molecular Mass Measurement, *J. Phys. Chem.*

B. **2009**, 113, 1914–1918.

[130] P. Groves, Diffusion ordered spectroscopy (DOSY) as applied to polymers, *Polym. Chem.* **2017**, 8, 6700–6708.

[131] R. Neufeld, D. Stalke, Accurate molecular weight determination of small molecules *via* DOSY-NMR by using external calibration curves with normalized diffusion coefficients, *Chem. Sci.* **2015**, 6, 3354–3364.

[132] M.J. Stchedroff, A.M. Kenwright, G. a. Morris, M. Nilsson, R.K. Harris, 2D and 3D DOSY methods for studying mixtures of oligomeric dimethylsiloxanes, *Phys. Chem. Chem. Phys.* **2004**, 6, 3221–3227.

[133] R. Cao, A. Nonaka, F. Komura, T. Matsui, Application of diffusion ordered-1H-nuclear magnetic resonance spectroscopy to quantify sucrose in beverages, *Food Chem.* **2015**, 171, 8–12.

[134] R. Neufeld, T.L. Teuteberg, R. Herbst-Irmer, R.A. Mata, D. Stalke, Solution Structures of Hauser Base iPr2NMgCl and Turbo-Hauser Base iPr2NMgCl.LiCl in THF and the Influence of LiCl on the Schlenk-Equilibrium, *J. Am. Chem. Soc.* **2016**, 138, 4796–4806.

[135] S. Denis-Quanquin, F. Riobé, M.A. Delsuc, O. Maury, N. Giraud, Paramagnetic DOSY: An Accurate Tool for the Analysis of the Supramolecular Interactions between Lanthanide Complexes and Proteins, *Chem. - A Eur. J.* **2016**, 22, 18123–18131.

[136] S. Bachmann, B. Gernert, D. Stalke, Solution structures of alkali metal cyclopentadienides in THF estimated by ECC-DOSY NMR-spectroscopy (incl. software), *Chem. Commun.* **2016**, 52, 12861–12864.

[137] D. Li, I. Keresztes, R. Hopson, P.G. Williard, Characterization of reactive intermediates by multinuclear diffusion-ordered NMR spectroscopy (DOSY)., *Acc. Chem. Res.* **2009**, 42, 270–80.

[138] J.S. Gounarides, A. Chen, M.J. Shapiro, Nuclear magnetic resonance chromatography: Applications of pulse field gradient diffusion NMR to mixture analysis and ligand-receptor interactions, *J. Chromatogr. B Biomed. Sci. Appl.* **1999**, 725, 79–90.

[139] P. Thureau, B. Ancian, S. Viel, A. Thévand, Determining chemical exchange rates of the uracil labile protons by NMR diffusion experiments, *Chem. Commun.* **2006**, 0, 200–202.

[140] B. Antalek, Using PGSE NMR for chemical mixture analysis: quantitative aspects, *Concepts Magn. Reson.* **2007**, 30A, 219–235.

[141] M. Nilsson, M.A. Connell, A.L. Davis, G.A. Morris, Biexponential fitting of diffusion-ordered NMR data: Practicalities and limitations, *Anal. Chem.* **2006**, 78, 3040–3045.

[142] A.A. Colbourne, G.A. Morris, M. Nilsson, Local covariance order diffusion-ordered spectroscopy: A powerful tool for mixture analysis, *J. Am. Chem. Soc.* **2011**, 133, 7640–7643.

[143] A.A. Colbourne, S. Meier, G.A. Morris, M. Nilsson, Unmixing the NMR spectra of similar species – vive la différence, *Chem. Commun.* **2013**, 49, 10510–10512.

[144] G.S. Armstrong, N.M. Loening, J.E. Curtis, A.J. Shaka, V.A. Mandelshtam, Processing DOSY spectra using the regularized resolvent transform, *J. Magn. Reson.* **2003**, 163, 139–148.

[145] M. Nilsson, A.M. Gil, G.A. Morris, Improving Pulse Sequences for 3D Diffusion-Ordered NMR Sp e c t r o scopy : 2 D J - I DOSY, **2004**, 76, 88–91.

[146] M. Shukla, K. Dorai, Disentangling diffusion information of individual components in a mixture with a 3D COMPACT-IDOSY NMR experiment, *Magn. Reson. Chem.* **2012**, 50, 341–346.

[147] G.N. Manjunatha Reddy, M. Yemloul, S. Caldarelli, Combined maximum-quantum and DOSY 3D experiments provide enhanced resolution for small molecules in mixtures, *Magn. Reson. Chem.* **2017**, 55, 492–497.

[148] D. Wu, A. Chen, C.S. Johnson, Three-dimensional diffusion-ordered nmr spectroscopy: The homonuclear COSY-DOSY experiment, *J. Magn. Reson. - Ser. A*. **1996**, 121, 88–91.

[149] M. Shukla, K. Dorai, A Novel Multiple-Quantum Correlation NMR Scheme to Separate Components of a Mixture According to Their Diffusion Coefficients, *Appl. Magn. Reson.* **2012**, 43, 485–497.

[150] L.H. Lucas, W.H. Otto, C.K. Larive, The 2D-J-DOSY experiment: Resolving diffusion coefficients in mixtures, *J. Magn. Reson.* **2002**, 156, 138–145.

[151] J. Cassani, M. Nilsson, G.A. Morris, Flavonoid mixture analysis by matrix-assisted diffusion-ordered spectroscopy, *J. Nat. Prod.* **2012**, 75, 131–134.

[152] C.F. Tormena, R. Evans, S. Haiber, M. Nilsson, G.A. Morris, Matrix-assisted diffusion-ordered spectroscopy: Application of surfactant solutions to the resolution of isomer spectra, *Magn. Reson. Chem.* **2012**, 50, 458–465.

[153] R. Evans, I.J. Day, Matrix-assisted diffusion-ordered spectroscopy, *RSC Adv.* **2016**, 6, 47010–47022.

[154] I. Reile, R.L.E.G. Aspers, M.C. Feiters, F.P.J.T. Rutjes, M. Tessari, Resolving DOSY spectra of isomers by methanol-d4solvent effects, *Magn. Reson. Chem.* **2017**, 55, 759–762.

[155] A.K. Rogerson, J.A. Aguilar, M. Nilsson, G.A. Morris, Simultaneous enhancement of chemical shift dispersion and diffusion resolution in mixture analysis by diffusion-ordered NMR spectroscopy, *Chem Commun*. **2011**, 47, 7063–7064.

[156] W.M. Spees, N. Buhl, P. Sun, J.J.H. Ackerman, J.J. Niel, J.R. Garbow, Quantification and Compensation of Eddy-Current-Induced Magnetic Field Gradients, *J. Magn. Reson.* **2012**, 212, 116–123.

[157] N.M. Loening, J. Keeler, Measurement of Convection and Temperature Profiles in Liquid Samples, *J. Magn. Reson.* **1999**, 139, 334–341.

[158] A. Jerschow, Thermal Convection Currents in NMR: Flow Profiles and Implications for Coherence Pathway Selection, *J. Magn. Reson.* **2000**, 145, 125–131.

[159] Y.Q. Song, U.M. Scheven, An NMR technique for rapid measurement of flow, *J. Magn. Reson.* **2005**, 172, 31–35.

[160] K.C. Chung, H.Y. Yu, S. Ahn, Convection effects on PGSE-NMR self-diffusion measurements at low temperature: Investigation into sources of induced convective flows, *Bull. Korean Chem.*

Soc. **2011**, 32, 1970–1974.

[161] I. Swan, M. Reid, P.W.A. Howe, M.A. Connell, M. Nilsson, M.A. Moore, G.A. Morris, Sample convection in liquid-state NMR: Why it is always with us, and what we can do about it, *J. Magn. Reson.* **2015**, 252, 120–129.

[162] T.M. Barbosa, R. Rittner, C.F. Tormena, G.A. Morris, M. Nilsson, Convection in liquid-state NMR: expect the unexpected, *RSC Adv.* **2016**, 6, 95173–95176.

[163] A. Jerschow, N. Müller, Convection Compensation in Gradient Enhanced Nuclear Magnetic Resonance Spectroscopy, *J. Magn. Reson.* **1998**, 132, 13–18.

[164] M.A. Connell, P.J. Bowyer, P. Adam Bone, A.L. Davis, A.G. Swanson, M. Nilsson, G.A. Morris, Improving the accuracy of pulsed field gradient NMR diffusion experiments: Correction for gradient non-uniformity, *J. Magn. Reson.* **2009**, 198, 121–131.

[165] M. Nilsson, G.A. Morris, Improving pulse sequences for 3D DOSY: Convection compensation, *J. Magn. Reson.* **2005**, 177, 203–211.

[166] A. Jerschow, N. Müller, Convection Compensation in Gradient Enhanced Nuclear Magnetic Resonance Spectroscopy, *J. Magn. Reson.* **1998**, 132, 13–18.

[167] A. Jerschow, N. Müller, Suppression of Convection Artifacts in Stimulated-Echo Diffusion Experiments. Double-Stimulated-Echo Experiments, *J. Magn. Reson.* **1997**, 125, 372–375.

[168] R.F. Karlicek, I.J. Lowe, A modified pulsed gradient technique for measuring diffusion in the presence of large background gradients, *J. Magn. Reson.* **1980**, 37, 75–91.

[169] P. Damberg, J. Jarvet, A. Gräslund, Accurate measurement of translational diffusion coefficients: A practical method to account for nonlinear gradients, *J. Magn. Reson.* **2001**, 148, 343–348.

[170] L. Li, C.H. Sotak, Diffusion measurements by pulsed field-gradient multiple spin echoes, *J. Magn. Reson.* **1991**, 92, 411–420.

[171] S. Velan, N. Chandrakumar, High-Resolution NMR Measurement of Molecular Self-Diffusion by Fast Multi-Spin-Echo Diffusion Sequences, *J. Magn. Reson. A*. **1996**, 123, 122–125.

[172] J.P. Stamps, B. Ottink, J.M. Visser, J.P.M. Van Duynhoven, R. Hulst, Difftrain: A novel approach to a true spectroscopic single-scan diffusion measurement, *J. Magn. Reson.* **2001**, 151, 28–31.

[173] P. Vangelderen, A. Olson, C.T.W. Moonen, A single-shot diffusion experiment, *J. Magn. Reson. - Ser. A*. **1993**, 103, 105–108.

[174] A. Traore, L. Foucat, J.P. Renou, 1H-NMR study of water dynamics in hydrated collagen: Transverse relaxation-time and diffusion analysis, *Biopolymers*. **2000**, 53, 476–483.

[175] R.W. Mair, D.G. Cory, S. Peled, C.H. Tseng, S. Patz, R.L. Walsworth, Pulsed-Field-Gradient Measurements of Time-Dependent Gas Diffusion, *J. Magn. Reson.* **1998**, 135, 478–486.

[176] L. Li, C.H. Sotak, Self-Diffusion Measurements by Pulsed-Gradient Multiple-Spin-Echo Imaging, *J. Magn. Reson. Ser. B*. **1993**, 101, 8–16.

[177] N. Sandhyarani, M.R. Resmi, R. Unnikrishnan, K. Vidyasagar, S. Ma, M.P. Antony, G. Panneer

Selvam, V. Visalakshi, N. Chandrakumar, K. Pandian, Y.T. Tao, T. Pradeep, Monolayer-protected cluster superlattices: Structural, spectroscopic, calorimetric, and conductivity studies, *Chem. Mater.* **2000**, 12, 104–113.

[178] S. V Raman, V. Vijayaragavan, V. Krishnan, S. Nadakatti, K. V Babu, N. Chandrakumar, NMR measurements on model lyotropic systems, *Struct. Dyn. Mater. MESOSCOPIC DOMAIN*. **1999**, 11–25.

[179] C. Buckley, K.G. Hollingsworth, A.J. Sederman, D.J. Holland, M.L. Johns, L.F. Gladden, Applications of fast diffusion measurement using Difftrain, *J. Magn. Reson.* **2003**, 161, 112–117.

[180] G. Bodenhausen, R. Freeman, G.A. Morris, A Simple Pulse Sequence for Selective Excitation in Fourier-Transform Nmr, *J. Magn. Reson.* **1976**, 23, 171–175.

[181] G.A. Morris, R. Freeman, Selective excitation in Fourier transform nuclear magnetic resonance, *J. Magn. Reson.* **1978**, 29, 433–462.

[182] S.J. Doran, M. Decorps, A Robust, Single-Shot Method for Measuring Diffusion Coefficients Using the Sequence, *J. Magn. Reson. Ser. A*. **1995**, 117, 311–316.

[183] S. Peled, C.-H. Tseng, A.A. Sodickson, R.W. Mair, R.L. Walsworth, D.G. Cory, Single-Shot Diffusion Measurement in Laser-Polarized Gas, *J. Magn. Reson.* **1999**, 140, 320–324.

[184] Y.Q. Song, X. Tang, A one-shot method for measurement of diffusion, *J. Magn. Reson.* **2004**, 170, 136–148.

[185] X.P. Tang, E.E. Sigmund, Y.Q. Song, Simultaneous measurement of diffusion along multiple directions, *J. Am. Chem. Soc.* **2004**, 126, 16336–16337.

[186] L. Frydman, A. Lupulescu, T. Scherf, Principles and Features of Single-Scan Two Dimensional NMR Spectroscopy, *J. Am. Chem. Soc.* **2003**, 125, 9204–9217.

[187] A. Tal, L. Frydman, Single-scan multidimensional magnetic resonance, *Prog. Nucl. Magn. Reson. Spectrosc.* **2010**, 57, 241–292.

[188] L. Frydman, Single-scan multidimensional NMR, *Comptes Rendus Chim.* **2006**, 9, 336–345.

[189] Y. Shrot, L. Frydman, Sigle-Scan NMR Spectroscopy at Abitrara Dimensions, *Jacs*. **2003**, 125, 12.

[190] M. André, M. Piotto, S. Caldarelli, J.-N. Dumez, Ultrafast high-resolution magic-angle-spinning NMR spectroscopy, *Analyst*. **2015**, 140, 3942–3946.

[191] M. Gal, L. Frydman, Multidimensional NMR spectroscopy in a single scan, *Magn. Reson. Chem.* **2015**, 53, 971–985.

[192] N.M. Loening, J. Keeler, G.A. Morris, One-dimensional DOSY, *J. Magn. Reson.* **2001**, 153, 103–112.

[193] A. Tannús, M. Garwood, Adiabatic pulses, *NMR Biomed.* **1997**, 10, 423–434.

[194] J.M. Böhlen, G. Bodenhausen, Experimental aspects of chirp NMR spectroscopy, *J. Magn. Reson. - Ser. A*. **1993**, 102, 293–301.

[195] S. Ahola, V. V. Zhivonitko, O. Mankinen, G. Zhang, A.M. Kantola, H.Y. Chen, C. Hilty, I. V. Koptyug, V.V. Telkki, Ultrafast multidimensional Laplace NMR for a rapid and sensitive chemical analysis, *Nat. Commun.* **2015**, 6, 1–7.

[196] J.N. King, V.J. Lee, S. Ahola, V.V. Telkki, T. Meldrum, Ultrafast Multidimensional Laplace NMR Using a Single-Sided Magnet, *Angew. Chemie - Int. Ed.* **2016**, 55, 5040–5043.

[197] P. Schanda, H. Van Melckebeke, B. Brutscher, Speeding Up Three-Dimensional Protein NMR Experiments to a Few Minutes Speeding Up Three-Dimensional Protein NMR Experiments to a Few Minutes, *Society*. **2006**, 128, 9042–9043.

[198] S.M. Pudakalakatti, K. Chandra, R. Thirupathi, H.S. Atreya, Rapid Characterization of Molecular Diffusion by NMR Spectroscopy, *Chem. - A Eur. J.* **2014**, 20, 15719–15722.

[199] G. Bodenhausen, R.R. Ernst, The Accordion Experiment, A Simple Approach to Three-Dimensional Spectroscopy, *J. Magn. Reson.* **1981**, 45, 367.

[200] H.J. Reich, 5-HMR-0 The NMR Experiment, **2010**, online, http://www.chem.wisc.edu/areas/reich/nmr/index.htm.

[201] M.L. Hirsch, N. Kalechofsky, A. Belzer, M. Rosay, J.G. Kempf, Brute-Force Hyperpolarization for NMR and MRI, *J. Am. Chem. Soc.* **2015**, 137, 8428–8434.

[202] H.-Y. Chen, C. Hilty, Implementation and Characterization of Flow Injection in Dissolution Dynamic Nuclear Polarization NMR Spectroscopy, *ChemPhysChem*. **2015**, 16, 2646–2652.

[203] S. Bowen, C. Hilty, Rapid sample injection for hyperpolarized NMR spectroscopy, *Phys. Chem. Chem. Phys.* **2010**, 12, 5766–5770.

[204] D. Kurzbach, E.M.M. Weber, A. Jhajharia, S.F. Cousin, A. Sadet, S. Marhabaie, E. Canet, N. Birlirakis, J. Milani, S. Jannin, D. Eshchenko, A. Hassan, R. Melzi, S. Luetolf, M. Sacher, M. Rossire, J. Kempf, J.A.B. Lohman, M. Weller, G. Bodenhausen, D. Abergel, Dissolution dynamic nuclear polarization of deuterated molecules enhanced by cross- polarization, *J. Chem. Phys.* **2016**, 145, 194203.

[205] H. Nonaka, M. Hirano, Y. Imakura, Y. Takakusagi, K. Ichikawa, S. Sando, Design of a 15 N Molecular Unit to Achieve Long Retention of Hyperpolarized Spin State, *Sci. Rep.* **2017**, 7, 9–14.

[206] C.H. Cunningham, A.P. Chen, M.J. Albers, J. Kurhanewicz, R.E. Hurd, Y.F. Yen, J.M. Pauly, S.J. Nelson, D.B. Vigneron, Double spin-echo sequence for rapid spectroscopic imaging of hyperpolarized13C, *J. Magn. Reson.* **2007**, 187, 357–362.

[207] A. Bornet, R. Melzi, A.J. Perez Linde, P. Hautle, B. Van Den Brandt, S. Jannin, G. Bodenhausen, Boosting dissolution dynamic nuclear polarization by cross polarization, *J. Phys. Chem. Lett.* **2013**, 4, 111–114.

[208] A. Bornet, J. Milani, B. Vuichoud, A.J. Perez Linde, G. Bodenhausen, S. Jannin, Microwave frequency modulation to enhance Dissolution Dynamic Nuclear Polarization Dedicated to To Martial Rey, as a token of appreciation., *Chem. Phys. Lett.* **2014**, 602, 63–67.

[209] R.A. Green, R.W. Adams, S.B. Duckett, R.E. Mewis, D.C. Williamson, G.G.R. Green, The theory and practice of hyperpolarization in magnetic resonance using parahydrogen, *Prog. Nucl. Magn. Reson. Spectrosc.* **2012**, 67, 1–48.

[210] C.R. Bowers, D.P. Weitekamp, Parahydrogen and Synthesis Allow Dramatically Enhanced Nuclear Alignment, *J. Am. Chem. Soc.* **1987**, 109, 5541–5542.

[211] K.D. Atkinson, M.J. Cowley, P.I.P. Elliott, S.B. Duckett, G.G.R. Green, J. López-Serrano, A.C. Whitwood, Spontaneous transfer of Parahydrogen derived spin order to pyridine at low magnetic field, *J. Am. Chem. Soc.* **2009**, 131, 13362–13368.

[212] M.J. Cowley, R.W. Adams, K.D. Atkinson, M.C.R. Cockett, S.B. Duckett, G.G.R. Green, J.A.B. Lohman, R. Kerssebaum, D. Kilgour, R.E. Mewis, Iridium N-heterocyclic carbene complexes as efficient catalysts for magnetization transfer from para -hydrogen, *J. Am. Chem. Soc.* **2011**, 133, 6134–6137.

[213] E.B. Dücker, L.T. Kuhn, K. Münnemann, C. Griesinger, Similarity of SABRE field dependence in chemically different substrates, *J. Magn. Reson.* **2012**, 214, 159–165.

[214] S. Knecht, A.N. Pravdivtsev, J.-B. Hövener, A. V. Yurkovskaya, K.L. Ivanov, Quantitative description of the SABRE process: rigorous consideration of spin dynamics and chemical exchange, *RSC Adv.* **2016**, 6, 24470–24477.

[215] N.K.J. Hermkens, M.C. Feiters, F.P.J.T. Rutjes, S.S. Wijmenga, M. Tessari, High field hyperpolarization-EXSY experiment for fast determination of dissociation rates in SABRE complexes, *J. Magn. Reson.* **2017**, 276, 122–127.

[216] B.J.A. van Weerdenburg, N. Eshuis, M. Tessari, F.P.J.T. Rutjes, M.C. Feiters, Application of the π-accepting ability parameter of N-heterocyclic carbene ligands in iridium complexes for signal amplification by reversible exchange (SABRE), *Dalt. Trans.* **2015**, 44, 15387–15390.

[217] N. Eshuis, N. Hermkens, B.J.A. Van Weerdenburg, M.C. Feiters, F.P.J.T. Rutjes, S.S. Wijmenga, M. Tessari, Toward nanomolar detection by NMR through SABRE hyperpolarization, *J. Am. Chem. Soc.* **2014**, 136, 2695–2698.

[218] I. Reile, R.L.E.G. Aspers, J.M. Tyburn, J.G. Kempf, M.C. Feiters, F.P.J.T. Rutjes, M. Tessari, DOSY Analysis of Micromolar Analytes: Resolving Dilute Mixtures by SABRE Hyperpolarization, *Angew. Chemie - Int. Ed.* **2017**, 56, 9174–9177.

[219] S. Bowen, C. Hilty, Time-Resolved Dynamic Nuclear Polarization Enhanced NMR Spectroscopy, *Angew. Chemie*. **2008**, 120, 5313–5315.

[220] E. Miclet, D. Abergel, A. Bornet, J. Milani, S. Jannin, G. Bodenhausen, Toward Quantitative Measurements of Enzyme Kinetics by Dissolution Dynamic Nuclear Polarization, *J. Phys. Chem. Lett.* **2014**, 5, 3290–3295.

[221] J. Svensson, S. Månsson, E. Johansson, J.S. Petersson, L.E. Olsson, Hyperpolarized 13C MR angiography using trueFISP, *Magn. Reson. Med.* **2003**, 50, 256–262.

[222] M. Yon, J. Lalande-Martin, T. Harris, I. Tea, P. Giraudeau, L. Frydman, 13C NMR detection of

metabolic mixtures enhanced by dynamic nuclear polarization, *Sci. Lett.* **2015**, 4, 82.

[223] B.L. Koelsch, K.R. Keshari, T.H. Peeters, P.E.Z. Larson, D.M. Wilson, J. Kurhanewicz, Diffusion MR of hyperpolarized 13C molecules in solution (SI), *Analyst*. **2013**, 138, 1011.

[224] M.T. Niels K. J. Hermkens, Nan Eshuis, Bram J. A. van Weerdenburg, Martin C. Feiters, Floris P. J. T. Rutjes, Sybren S. Wijmenga, NMR-based Chemosensing via p-H2 Hyperpolarization: Application to Natural Extracts Niels (SI), *Acta Crystallogr. Sect. E Struct. Reports Online*. **2009**, 65, 2396–2407.

[225] N.K.J. Hermkens, N. Eshuis, B.J.A. Van Weerdenburg, M.C. Feiters, F.P.J.T. Rutjes, S.S. Wijmenga, M. Tessari, NMR-Based Chemosensing via p -H2Hyperpolarization: Application to Natural Extracts, *Anal. Chem.* **2016**, 88, 3406–3412.

[226] P. Dutta, G. V. Martinez, R.J. Gillies, Nanodiamond as a new hyperpolarizing agent and its13C MRS, *J. Phys. Chem. Lett.* **2014**, 5, 597–600.

[227] J.F.P. Colell, A.W.J. Logan, Z. Zhou, R. V. Shchepin, D.A. Barskiy, G.X. Ortiz, Q. Wang, S.J. Malcolmson, E.Y. Chekmenev, W.S. Warren, T. Theis, Generalizing, Extending, and Maximizing Nitrogen-15 Hyperpolarization Induced by Parahydrogen in Reversible Exchange, *J. Phys. Chem. C*. **2017**, 121, 6626–6634.

[228] M. Mishkovsky, L. Frydman, Progress in hyperpolarized ultrafast 2D NMR spectroscopy, *ChemPhysChem*. **2008**, 9, 2340–2348.

[229] J. Valette, F. Lethimonnier, V. Lebon, About the origins of NMR diffusion-weighting induced by frequency-swept pulses, *J. Magn. Reson.* **2010**, 205, 255–259.

[230] I. Kuprov, Fokker-Planck formalism in magnetic resonance simulations, *J. Magn. Reson.* **2016**, 270, 124–135.

[231] L. Guduff, A.J. Allami, C. van Heijenoort, J.-N. Dumez, I. Kuprov, Efficient simulation of ultrafast magnetic resonance experiments, *Phys. Chem. Chem. Phys.* **2017**, 19, 17577–17586.

[232] P. Giraudeau, S. Akoka, Sources of sensitivity losses in ultrafast 2D NMR, *J. Magn. Reson.* **2008**, 192, 151–158.

[233] P. Giraudeau, E. Cahoreau, S. Massou, M. Pathan, J.C. Portais, S. Akoka, UFJCOSY: A fast 3D NMR method for measuring isotopic enrichments in complex samples, *ChemPhysChem*. **2012**, 13, 3098–3101.

[234] R. Boisseau, B. Charrier, S. Massou, J.C. Portais, S. Akoka, P. Giraudeau, Fast spatially encoded 3D NMR strategies for 13C-based metabolic flux analysis, *Anal. Chem.* **2013**, 85, 9751–9757.

[235] S. Akoka, P. Giraudeau, Fast hybrid multi-dimensional NMR methods based on ultrafast 2D NMR, *Magn. Reson. Chem.* **2015**, 53, 986–994.

[236] L. Rouger, B. Charrier, M. Pathan, S. Akoka, P. Giraudeau, Processing strategies to obtain clean interleaved ultrafast 2D NMR spectra, *J. Magn. Reson.* **2014**, 238, 87–93.

[237] B. Shapira, A. Lupulescu, Y. Shrot, L. Frydman, Line shape considerations in ultrafast 2D NMR, *J. Magn. Reson.* **2004**, 166, 152–163.

[238] G. Hamdoun, L. Guduff, C. van Heijenoort, C. Bour, V. Gandon, J.-N. Dumez, Spatially encoded diffusion-ordered NMR spectroscopy of reaction mixtures in organic solvents, *Analyst.* **2018**, 143, 3458–3464.

[239] L. Guduff, I. Kuprov, C. van Heijenoort, J.-N. Dumez, Spatially encoded 2D and 3D diffusion-ordered NMR spectroscopy, *Chem. Commun.* **2017**, 53, 701–704.

[240] J.-N. Dumez, J. Milani, B. Vuichoud, A. Bornet, J. Lalande-Martin, I. Tea, M. Yon, M. Maucourt, C. Deborde, A. Moing, L. Frydman, G. Bodenhausen, S. Jannin, P. Giraudeau, Hyperpolarized NMR of plant and cancer cell extracts at natural abundance., *Analyst*. **2015**, 140, 5860–3.

[241] L. Guduff, D. Kurzbach, C. van Heijenoort, D. Abergel, J.N. Dumez, Single-Scan 13C Diffusion-Ordered NMR Spectroscopy of DNP-Hyperpolarised Substrates, *Chem. - A Eur. J.* **2017**, 23, 16722–16727.

[242] W. Iali, A.M. Olaru, G.G.R. Green, S.B. Duckett, Achieving High Levels of NMR-Hyperpolarization in Aqueous Media With Minimal Catalyst Contamination Using SABRE, *Chem. - A Eur. J.* **2017**, 23, 10491–10495.

[243] P.J. Rayner, S.B. Duckett, Signal Amplification by Reversible Exchange (SABRE): From Discovery to Diagnosis Peter, *Angew. Chemie Int. Ed.* **2018**, 57, 6742–6753.

[244] W. Iali, P.J. Rayner, S.B. Duckett, Using *para* hydrogen to hyperpolarize amines, amides, carboxylic acids, alcohols, phosphates, and carbonates, *Sci. Adv.* **2018**, 4, eaao6250.

[245] P. Kiraly, I. Swan, M. Nilsson, G.A. Morris, Improving accuracy in DOSY and diffusion measurements using triaxial field gradients, *J. Magn. Reson.* **2016**, 270, 24–30.

Appendices

Publications

- **Spatially encoded 2D and 3D diffusion-ordered NMR spectroscopy**

  L. Guduff, I. Kuprov, C. van Heijenoort, J.-N. Dumez, Chem. Commun. 2017, 53, 701–704.

- **Efficient simulation of ultrafast magnetic resonance experiments**

  L. Guduff, A.J. Allami, C. van Heijenoort, J.-N. Dumez, I. Kuprov, Phys. Chem. Chem. Phys. 2017, 19, 17577–17586.

- **Single-Scan 13C Diffusion-Ordered NMR Spectroscopy of DNP-Hyperpolarised Substrates**

  L. Guduff, D. Kurzbach, C. van Heijenoort, D. Abergel, J.N. Dumez, Chem. - A Eur. J. 2017, 23, 16722–16727.

- **Spatially encoded diffusion-ordered NMR spectroscopy of reaction mixtures in organic solvents**

  G. Hamdoun, L. Guduff, C. van Heijenoort, C. Bour, V. Gandon, J.-N. Dumez, Analyst. 2018, 143, 3458–3464.

Titre : Analyse de mélanges par RMN diffusionnelle ultrarapide

Mots clés : RMN ultrarapide, RMN diffusionnelle (DOSY), hyperpolarisation, mélanges, simulations numériques

Résumé : La spectroscopie de résonance magnétique nucléaire (RMN) est un outil puissant qui permet l'étude directe de mélanges de manière non destructive. Les spectres RMN de petites molécules en solution peuvent être différenciés grâce à la stratégie DOSY (diffusion-ordered spectroscopy), une méthode de 'chromatographie virtuelle' qui s'appuie sur la mesure de coefficients de diffusion translationnelle. Les principaux obstacles à l'utilisation de la DOSY sont liés à la piètre sensibilité de la RMN de manière générale mais aussi à la nécessité d'introduire une dimension temporelle supplémentaire d'acquisition, ce qui va augmenter de manière significative la durée de l'expérience. Ce travail de thèse a pour objectif de mettre au point des outils inédits de RMN plus rapides et plus adaptés à la caractérisation de mélanges peu concentrés de petites molécules. Dans un premier temps, le concept de codage spatial de la diffusion dans l'expérience DOSY a été généralisé. Mis à profit dans les méthodes RMN dites 'ultrarapides', l'utilisation d'une dimension spatiale plutôt que temporelle pour encoder le phénomène de diffusion permet une accélération des expériences de RMN multidimensionnelles de plusieurs ordres de grandeur. L'acquisition séquentielle de spectres est remplacée par une acquisition parallèle de ces spectres dans différentes parties de l'échantillon. L'étude poussée des méthodes de DOSY rapides s'est appuyée sur des outils de simulation numérique dans le but d'améliorer la résolution des spectres et la précision des résultats. Les problèmes de sensibilité ont été abordés via le couplage des méthodes DOSY rapides avec des méthodes d'hyperpolarisation qui permettent d'augmenter l'intensité du signal. La combinaison des méthodes de diffusion conventionnelles avec les méthodes avancées de RMN ultrarapide et d'hyperpolarisation permettront des avancées significatives pour l'analyse de mélanges, en particulier les mélanges dynamiques.

Title : Ultrafast diffusion-ordered NMR analysis of mixtures

Keywords : Ultrafast NMR, diffusion-ordered spectroscopy (DOSY), hyperpolarization, mixtures, numerical simulations

Abstract : NMR spectroscopy is a powerful tool that allows a direct study of mixtures in a non-invasive manner. The NMR spectra of molecular species in mixtures can be separated with diffusion-ordered spectroscopy (DOSY), a 'virtual chromatography' approach based on the measurement of translational diffusion coefficients. Major limitation of DOSY comes from the time-dependent diffusion dimension, which results in long experiment durations, and also from the low sensitivity of NMR. The present work aims to build an innovative tool for mixtures characterization that will be faster and more efficient for low concentrated samples. We first generalized the concept of nD spatially encoded (SPEN) DOSY experiments for the analysis of complex mixtures. As bring forward by the so-called "ultrafast NMR" (UF NMR), the use of a spatial dimension to encode diffusion can accelerate experiments by several orders of magnitude since it replaces the sequential acquisition of sub-experiments by a parallel acquisition in different slices of the sample. More advanced exploration of SPENDOSY were carried out using numerical simulations for purpose of resolution and accuracy improvement. To address sensitivity issues, we then demonstrated that SPENDOSY data can be collected for hyperpolarized substrates. This particular coupling between conventional diffusion-based method with advanced techniques such as ultrafast NMR and hyperpolarization should mark a significant progress for complex mixtures analysis especially for time-evolving processes.